The Development of Hydrogels and Nanoparticles for Drug and Cell Delivery to the Distal Airways

AUTHOR(S)

Christina Payne

CITATION

Payne, Christina (2018): The Development of Hydrogels and Nanoparticles for Drug and Cell Delivery to the Distal Airways. Royal College of Surgeons in Ireland. Thesis. https://doi.org/10.25419/rcsi.10802090.v1

DOI

10.25419/rcsi.10802090.v1

URL

https://repository.rcsi.com/articles/thesis/The_Development_of_Hydrogels_and_Nanoparticles_for_Drug_and_Cell_Delivery_to_the_Distal_Airways/10802090/1

The Development of Hydrogels and Nanoparticles for Drug and Cell Delivery to the Distal Airways

Submitted to the Royal College of Surgeons in Ireland in partial fulfilment of the requirements for the degree of

Doctor of Philosophy

September 15th 2017

RCSI

Christina M Payne MPharm MPSI

Supervisors:

Dr. Helena Kelly

Prof. Sally Ann Cryan

External Examiner:

Dr. Helen McCarthy

Queen's University, Belfast

Internal Examiner:

Dr. Fiona O'Brien

RCSI

Declaration

I declare that this thesis, which I submit to RCSI for examination in consideration of the award of a higher degree of Doctor of Philosophy, is my own personal effort. Where any of the content presented is the result of input or data from a related collaborative research programme this is duly acknowledged in the text such that it is possible to ascertain how much of the work is my own. I have not already obtained a degree in RCSI or elsewhere on the basis of this work. Furthermore, I took reasonable care to ensure that the work is original, and, to the best of my knowledge, does not breach copyright law, and has not been taken from other sources except where such work has been cited and acknowledged within the text.

Signed _____

Student Number _____

Date _____

Abstract

Chronic Obstructive Pulmonary Disease (COPD) is a major public health issue, affecting 64 million people globally. COPD is defined as a lung disease characterised by chronic obstruction of lung airflow that interferes with normal breathing and is not fully reversible. This obstruction is due to a combination of airway and parenchymal damage, associated with an enhanced chronic inflammatory response to noxious particles present in tobacco smoke. Despite the significant evolution of medical treatment options for COPD in the last two decades, it is still an incurable disease. Current interventions include pharmacological agents, which primarily aim for symptomatic control, and lung transplantation for those in end-stage disease. However, neither of these options treat or address the underlying disease state or progressive damage being caused, meaning there is an unmet clinical need for the investigation of novel strategies that can achieve this at a much earlier stage in disease development.

The overall objective of this research was to develop novel delivery systems suitable for minimally invasive drug and cell delivery that could have potential applications in the treatment of COPD. Our central hypothesis was that hydrogels and solid lipid nanoparticles can be used as drug and cell delivery vectors, which are then capable of exerting an anti-inflammatory effect on the local environment present in COPD. It was hypothesised that Human Mesenchymal Stem Cells (hMSCs) could be utilised to exert an anti-inflammatory effect via paracrine actions, and all trans-Retinoic Acid (atRA) as an anti-inflammatory signalling molecule. Strategies such as these may provide alternatives to current therapies which have suboptimal effects and also enable loco-regional delivery of therapeutics, which could significantly enhance clinical outcomes.

This thesis initially investigated a methylcellulose, collagen and beta-glycerophosphate hydrogel for its thermoresponsive properties and ability to maintain viability of encapsulated stem cells. This hydrogel (“Respiragel”) underwent sol-gel transition at

37^{o}C and was physically robust in nature. Respiragel could be delivered through a range of common clinical devices, facilitated encapsulation of hMSCs and also maintained their survival and proliferation. Respiragel could be sterilised using gamma irradiation, which did not adversely affect either its thermogelation properties or cell encapsulation ability, establishing it as a highly suitable delivery vector for this cell type.

In order to assess further hydrogel biomaterials for their ability to support cell encapsulation, novel self-assembling co-polypeptides, Star-PLL-PLT and Linear-PLL-PLT, were developed. Both polymers were capable of forming hydrogels spontaneously on addition of aqueous media. The Star-PLL-PLT showed superior rheological properties and physical robustness than the Linear-PLL-PLT. Both hydrogels could be pushed through a range of clinical devices, indicating promise for minimally invasive delivery. However, both hydrogels were cytotoxic on encapsulation of hMSCs, demonstrating their lack of suitability as a cell delivery vector in their current form.

Solid lipid nanoparticles (SLNs) were formulated which were capable of a high degree of encapsulation of all trans-Retinoic Acid (atRA). SLNs were biocompatible and enabled sustained release of atRA. Suspension of atRA SLNs within the previously developed Respiragel was possible with no resulting negative effects on thermoresponse or atRA release. Thus, atRA SLNs suspended in Respiragel forms a promising combinatorial drug delivery system which has the potential to enable loco-regional delivery of atRA to the lung using minimally invasive delivery device technology.

Evaluation of atRA SLNs and atRA SLN/Respiragel formulations in an *in vitro* model of inflammation in COPD was performed, with both formulations demonstrating an anti-inflammatory effect through a reduction in IL-6 and IL-8 concentrations. This data has shown that atRA could modulate the inflammatory environment in COPD, which may result in a potential reduction in airway destruction. The hMSC/Respiragel formulation

however, resulted in an increase in IL-6 and IL-8 – possibly indicating a pro-inflammatory reaction of MSCs when placed in an already inflammatory environment.

Collectively, the research presented in this thesis has resulted in the investigation of multiple formulations as potential cell or drug carriers which can be delivered in a minimally invasive manner. This thesis has highlighted potential shortcomings of the use of MSCs in the treatment of chronic inflammatory conditions, which need to be verified in further detailed studies. However, both atRA SLNs and a thermoresponsive hydrogel (Respiragel), when used in combination, provide unique potential for the loco-regional delivery of anti-inflammatory therapeutic agents in COPD.

Contents

Acknowledgements

Throughout my (very long) time in RCSI I have met so many wonderful people that it will difficult to name them all, so bear with me…!

Firstly, I would like to express my sincere thanks to my two supervisors, Dr Helena Kelly and Prof. Sally-Ann Cryan. I cannot thank you enough for all of the meetings, support, advice and guidance over the past 4 years. Thanks in particular to Helena for the many thesis corrections over the past couple of weeks, and especially in light of me throwing everything into a panic by booking flights! I appreciate your time and patience so much.

I would like to thank everyone in the School of Pharmacy (academic staff, support staff and operations) for all of the encouragement and assistance over the past four years, particularly in relation to my role as a Senior Demonstrator. On the lab side of things, I would also like to extend my thanks to the technical team – Danielle, Colin, Jim, Peter and Eoin. Thank you for all of your help in the lab, and for putting up with me when I broke the HPLC!

To all of the staff and PhD students in Anatomy and TERG – the group has spanned so many people since I started that I can't even begin to name everyone – but thank you so much to everyone who I have ever worked with. You have been an excellent group of people to be around every day, which definitely lessened the PhD related pain somewhat! Particular shout outs in TERG to Johnny and Vinny for the all of lab related assistance over the years.

Some more science related acknowledgements – thanks to Brenton Cavanagh for all of your help with the confocal, Clodagh and Neal in TCD for SEM and also Ruth Levey in NUIG for SEM. Thanks to Dr Cian O'Leary and Dr Gemma O'Connor in the School of Pharmacy and TERG for all of the help with atRA/HPLC/calculations. Thanks to Prof. Garry Duffy for allowing me to send samples to you! Thanks to Janice O'Sullivan for

isolation of hMSCs used in this thesis. Thanks also to Dr Eimear Dolan for such patience attempting to teach me the Zwick (and also for being the best post-doc we could ask for ☺). Thanks to the TREND group in RCSI, especially Robert Murphy for synthesis of polymers used in Chapter 3 of this thesis. In particular, I would like to extend sincere thanks to Dr Daniel O'Toole in NUIG for the help, advice and suggestions in relation in Chapter 5 of this thesis, and to Dr Shahd Horie also for Chapter 5 assistance.

A few personal mentions are also in order… To the best group of friends I have been so lucky to have made over the past few years: Laura, Seóna, Joanne, Gemma and Dave. Thank you for all the lunchtimes, laughs and being amazing people to have a great rant to (and also apologies for you all having to listen to me)! Special thanks to Seóna and Joanne for proof-reading this thesis. Thanks to Rachel for being such a fantastic desk buddy. Also to the group who I started with on Day 1 – Laura, Nicola, Amy, Tati, Rukmani and last but definitely not least, Will. You're all fabulous, and I am so glad I got to start and finish my PhD with such a brilliant bunch of people.

Finally, thanks to the people who still don't know what I spent my last 4 years doing or why but put up with me anyway: my friends and family, for their support and encouragement. In particular, thanks to my parents – I promise I'll get a "real" job soon. Thanks to my sister Claire, for her endless belief in me. Finally, thank you to Michael, for making me dinner and knowing when to give me a glass of wine.

Funding Sources

I gratefully acknowledge my funding sources which allowed me to complete my PhD – specifically, Science Foundation Ireland (SFI) under Investigator Award 13/IA/1840 and also a bursary provided by the School of Pharmacy, Royal College of Surgeons in Ireland.

Publications, Prizes and Presentations

Journal Publications

R. Murphy, T. Borase, **C. Payne**, J. O'Dwyer, S.A. Cryan, A. Heise. Hydrogels from amphiphilic star block co-polypeptides. RSC Advances 2016; 6: 23370–6

H.S. O' Neill, L. Gallagher, C. Curley, E. Dolan, J. O'Sullivan, W. Whyte, A. Hameed, J. O'Dwyer, **C. Payne**, D. O'Reilly, E.T. Roche, F.J. O'Brien, S.A. Cryan, H.M. Kelly, B. Murphy, G.P. Duffy. Biomaterial-Enhanced Cell and Drug Delivery: Lessons Learned in the Cardiac Field and Future Perspectives. 2016; 28(27): 5648-61

C. Payne, E. Dolan, J. O'Sullivan, S.A. Cryan, H.M. Kelly. A methylcellulose and collagen based temperature responsive hydrogel promotes encapsulated stem cell viability and proliferation *in vitro*. Drug Delivery and Translational Research 2017; 7(1): 132-146

Prizes

2017 – Travel Prize to the value of £1000.00 awarded by the UK and Ireland Controlled Release Society (UKICRS) to travel to the Controlled Release Society (CRS) 2017 Annual Meeting and Exposition

Presentations

C. Payne, D. O'Toole, S.A. Cryan, H.M. Kelly. A site specific delivery platform for all trans-Retinoic Acid in pulmonary regeneration applications; In: *44th Annual Meeting and Exposition of the Controlled Release Society,* Boston, 2017. Poster presentation

C. Payne, D. O'Toole, S.A. Cryan, H.M. Kelly. A site specific delivery platform for all trans-Retinoic Acid in pulmonary regeneration applications; In: *TERMIS (Tissue*

Engineering and Regenerative Medicine International Society) European Chapter Meeting, Davos, 2017. Oral presentation

C. Payne, D. O'Toole, S.A. Cryan, H.M. Kelly. A temperature responsive hydrogel for delivery of all trans-Retinoic Acid and stem cells to the distal airways for pulmonary regeneration applications; In: *Royal College of Surgeons in Ireland Annual Research Day*, Dublin, 2017. Poster presentation

C. Payne, S.A. Cryan, H.M. Kelly. A temperature responsive hydrogel for the delivery of lipophilic molecules and stem cells to the distal airways; In: *UK and Ireland Controlled Release Society (UKICRS) Symposium*, Cardiff, 2017. Poster presentation

C. Payne, S.A. Cryan, H.M. Kelly. A temperature responsive hydrogel for the delivery of lipophilic molecules and stem cells to the distal airways; In: *38th All Ireland Schools of Pharmacy Conference*, Dublin, 2016. Oral presentation

C. Payne, S.A. Cryan, H.M. Kelly. A temperature responsive hydrogel for the delivery of lipophilic molecules and stem cells to the distal airways; In: *Royal College of Surgeons in Ireland Annual Research Day*, Dublin, 2016. Poster presentation

C. Payne, S.A. Cryan, H.M. Kelly. Development of hydrogels for drug and cell delivery to the distal airways; In: *22nd Annual Conference of the Section of Bioengineering of the Royal Academy of Medicine in Ireland (RAMI)*, Galway, 2016. Oral presentation

C. Payne, S.A. Cryan, H.M. Kelly. The development of hydrogels for drug and cell delivery to the distal airways; In: *42nd Annual Meeting and Exposition of the Controlled Release Society,* Edinburgh, 2015. Poster presentation

C. Payne, S.A. Cryan, H.M. Kelly. The development of hydrogels for drug delivery and tissue engineering applications; In: *21st Annual Conference of the Section of Bioengineering of the Royal Academy of Medicine in Ireland (RAMI)*, Kildare, 2015. Oral Presentation

Abbreviations

AEPC	Alveolar Epithelial Progenitor Cells
ALI	Acute Lung Injury
ANOVA	Analysis of Variance
AQP	Aquaporin
ARDS	Acute Respiratory Distress Syndrome
ASC	Adipose Stromal Cells
ATI	Alveolar Type I Cells (Type I Pneumocytes)
ATII	Alveolar Type II Cells (Type II Pneumocytes)
ATCC	American Type Culture Collection
atRA	all trans Retinoic Acid
BAL	Bronchoalveolar Lavage
βGP	Beta Glycerophosphate
BMP	Bone Morphogenetic Protein
bSLN	Blank Solid Lipid Nanoparticles
CCK-8	Cell Counting Kit 8
cm	centimetre
COPD	Chronic Obstructive Pulmonary Disease
CO_2	Carbon Dioxide
^oC	Degrees Celsius
cP	Centipoise
CRP	C Reactive Protein
CXCL8	Chemokine C-X-C Motif Ligand 8 (IL-8)
DC	Decellularised
dH_2O	Deionised Water
DL	Drug Loading
DLS	Dynamic Light Scattering
DMEM	Dulbecco's Modified Eagles Medium
DMSO	Dimethyl Sulfoxide
EBV	Endobronchial Valve
EDTA	Ethylenediaminetetraacetic Acid
EE	Encapsulation Efficiency
ELISA	Enzyme Linked Immunosorbent Assay
ELVR	Endoscopic Lung Volume Reduction
$ERK_{1/2}$	Extracellularly Regulated Kinase 1/2
FBS	Foetal Bovine Serum

FEV_1	Forced Expiratory Volume in 1 second
FGF	Fibroblast Growth Factor
FVC	Forced Vital Capacity
G	Gauge
G	Relative Centrifugal Force
G’	Storage Modulus
G”	Loss Modulus
GF	Growth Factor
GM-CSF	Granulocyte-Macrophage Colony- Stimulating Factor
GOLD	Global Initiative for Chronic Obstructive Lung Disease
h	Hour
hAEpCs	human Alveolar Epithelial Cells
HCl	Hydrochloric Acid
HGF	Hepatocyte Growth Factor
hMSCs	human Mesenchymal Stem Cells
HPLC	High Performance Liquid Chromatography
HT	Homogenisation Time
Hz	Hertz
ICG	Indocyanine Green
ICS	Inhaled Corticosteroid
IBV	Intrabronchial Valve
IL-1α	Interleukin 1 alpha
IL-1β	Interleukin 1 beta
IL-6	Interleukin 6
IL-8	Interleukin 8 (CXCL8)
Irr	Irradiated
KGF	Keratinocyte Growth Factor
kGy	Kilo Gray
kV	Kilo volts
L	Litre
LABA	Long Acting Beta Agonist
LAMA	Long Acting Muscarinic Antagonist
LVRS	Lung Volume Reduction Surgery
M	Molar
MCP-1	Monocyte Chemoattractant Protein-1
MC	Methylcellulose
min	minute
µg	microgram

mL	millilitre
µL	microlitre
µm	microns
mV	Millivolts
mW	Milliwatt
NaCl	Sodium Chloride
Na_3PO_4	Trisodium Phosphate
NFκB	Nuclear Factor [Kappa] B
ng	nanogram
NHTBE	Normal Human Tracheobronchial Epithelial cells
NICE	National Institute of Health and Care Excellence
nm	nanometres
non-Irr	Non Irradiated
NTA	Nanoparticle Tracking Analysis
ODTI	Organ Donation and Transplant Ireland
Pa	Pascal
PBS	Phosphate Buffered Saline
PCL	Poly-ε-caprolactone
PCS	Photon Correlation Spectroscopy
PDI	Polydispersity Index
PFT	Pulmonary Function Test
pg	picogram
PGA	Polyglycolic Acid
PLVR	Polymeric Lung Volume Reduction
RAR	Retinoic Acid Receptor
RARE	Retinoic Acid Responsive Elements
RCT	Randomised Controlled Trial
RM	Regenerative Medicine
RPM	Revolutions Per Minute
RXR	Retinoid X Receptor
SABA	Short Acting Beta Agonist
SAMA	Short Acting Muscarinic Antagonist
SE	Standard Error of the Mean
SEM	Scanning Electron Microscopy
SLN	Solid Lipid Nanoparticle
ST	Sonication Time
t	Time
TE	Tissue Engineering

TEM	Transmission Electron Microscopy
TGF-β	Transforming Growth Factor beta
TNF-α	Tumour Necrosis Factor alpha
VEGF	Vascular Endothelial Growth Factor
VILI	Ventilator Induced Lung Injury
v/v	Volume/Volume
w/v	Weight/Volume
W	Watt
WHO	World Health Organisation
X	Magnification
Z-ave	Nanoparticle Average Size
ZP	Zeta Potential

List of Tables, Figures and Equations

Tables

Figures

Equations

1. Chapter 1; Introduction and Literature Review

1.1.Anatomy, physiology and pathophysiology of the lung and COPD

1.1.1. Anatomy of the lung

The lungs are the essential organs of the respiratory tract that enable us to exchange oxygen and carbon dioxide with the environment, to facilitate respiration within cells and tissue. The human respiratory tract contains nearly 50 different cell types along its hierarchical structure [1], which can be subdivided into two distinct sections; the proximal (or conducting) airways, and the distal airways. Air is inhaled through the nose and mouth, passing through the larynx and trachea and then into a rapidly dividing series of bronchi and bronchioles – this section is referred to as the proximal or conducting airway (Figure 1.1) [2]. The distal airways then (or respiratory airways), comprise the non-cartilaginous section of terminal bronchioles and alveoli, which are responsible for gas exchange. The diverse range of cell types spread across the airways is primarily separated into these defined regions as a reflection of their functionality.

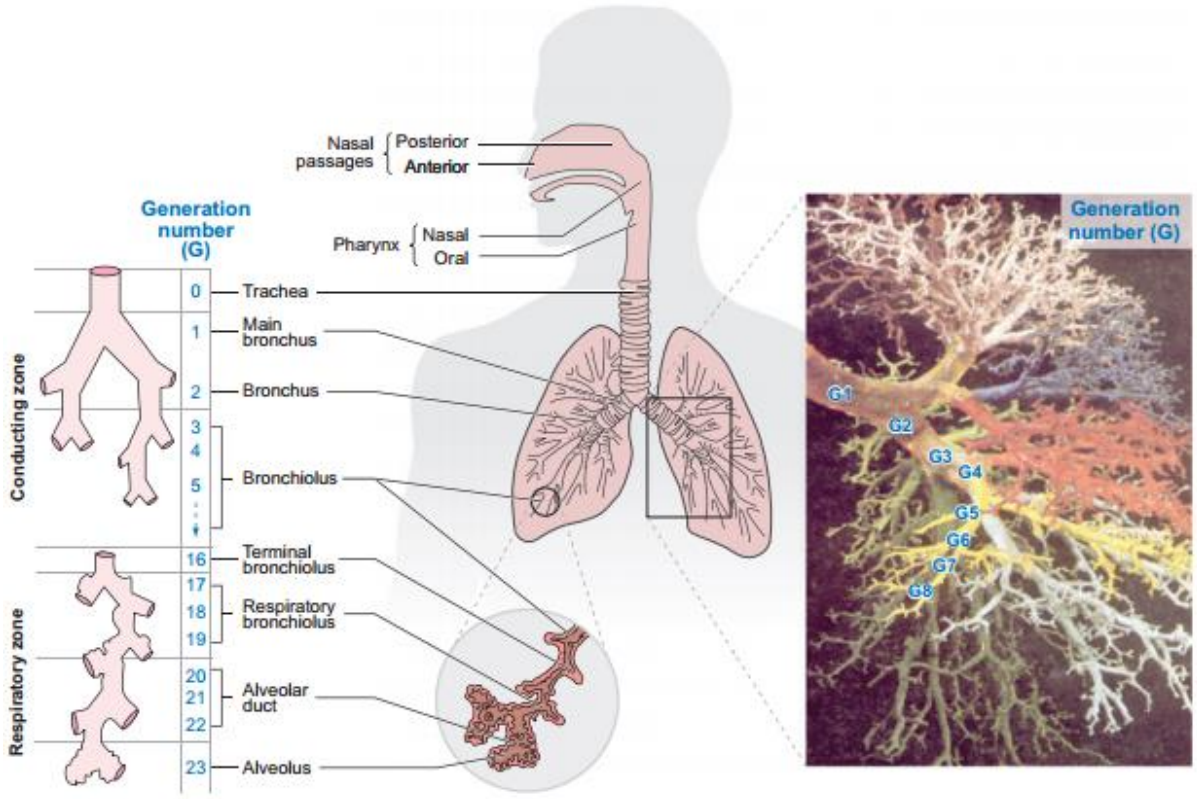

Figure 1.1. The respiratory tract, subdivided into conducting (proximal) and respiratory (distal) zones. Adapted from (3).

1.1.2. Physiology of the lung

The large proximal airways are composed of the trachea, the bronchi and the bronchioles, which are >2-2.5 mm in diameter [3]. The basic structure of the lining of the trachea and bronchi is a pseudostratified columnar epithelium containing ciliated cells, goblet cells, and basal and intermediate cells, among others [1]. The respiratory epithelium constitutes the interface between the external and internal environments, and as such, plays an important role in innate defence [4]. Ciliated cells are the predominant cell type within the proximal airways, accounting for over 50% of all epithelial cells [5]. Their primary role is the directional transport of mucous from the lung to the throat, facilitating clearance of inhaled environmental toxins or infectious

particles [6]. Goblet cells are involved in the production of the correct amount of mucus, of the correct viscoelasticity, which is important for efficient mucociliary clearance [7]. The presence of a mucus layer also acts as a diffusional buffer to protect the cells from noxious gases that may be inhaled. Basal cells then, are ubiquitous in the conducting epithelium, though the number of these cells decreases with airway size [8]. Basal cells are the only cells that are firmly attached to the basement membrane, and as such play a role in the attachment of more superficial cells. It is also thought that basal cells are the primary stem cell present, giving rise to goblet and ciliated epithelial cells [8]. Clara (or club) cells are located in the large bronchi and smaller bronchioles, and are thought to produce bronchiolar surfactant [9]. In addition to the production of secretions, the epithelium also produces signalling molecules and inflammatory mediators such as IL-1, IL-6, IL-8 and leukotrienes, which recruit immune cells to elicit a response in times of infection [10].

The distal airways, composed of non-cartilaginous conducting airways with an internal diameter of <2 mm, include the terminal bronchioles which end at the alveoli, the structural units responsible for gaseous exchange. This region is composed of a continuous layer of epithelial cells; descending further from the proximal region results in the continued appearance of Clara cells and neuroendocrine cells [11]. This coincides with a decrease in the presence of secretory cells and ciliated cells. The alveoli sacs themselves are lined with squamous type I pneumocytes (also known as alveolar type I epithelial cells, or AT-I cells) interspersed with cuboidal type II pneumocytes (also known as alveolar type II epithelial cells, or AT-II cells). Type I pneumocytes are responsible for carrying out gasous exchange and account for 93% of all alveolar cells. They are located at close proximity to capillaries, allowing rapid diffusion of gases to and from the bloodstream over distances of just 1 μm [12]. Type II pneumocytes produce surfactant, and account for 6% of all alveolar cells. This surfactant is essential in maintaining low surface tension at the air-liquid interface, thereby preventing collapse of the alveoli on expiration [13].

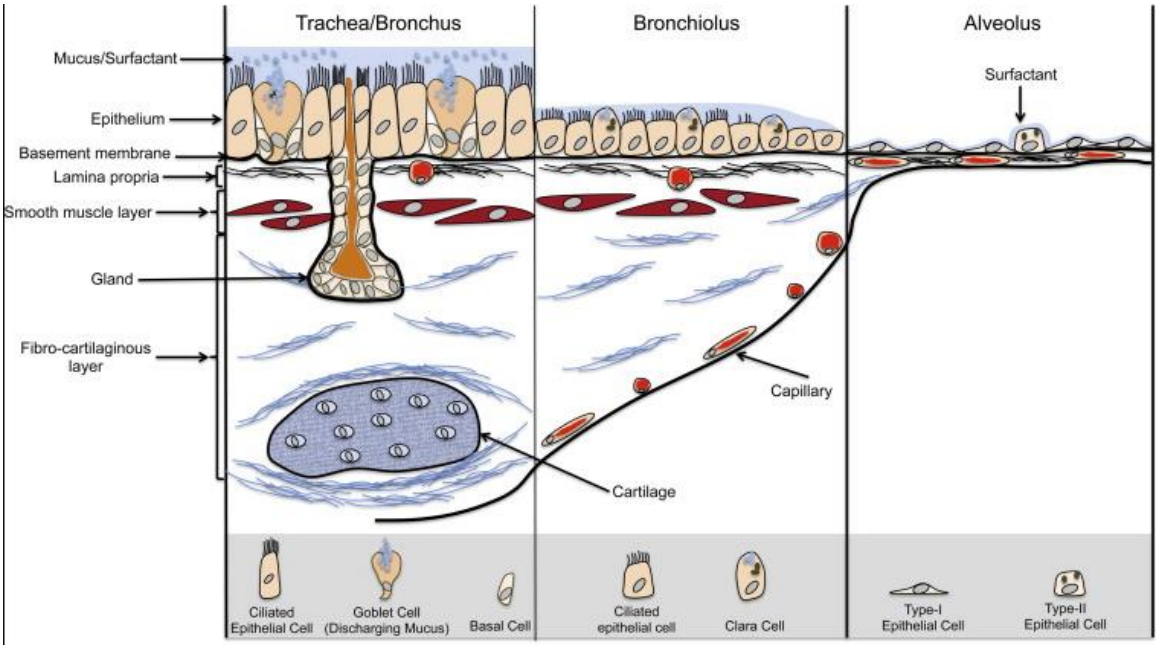

Figure 1.2. Simplified scheme of the structure of the airway wall at the three principal levels. The epithelial layer gradually becomes reduced from pseudostratified to cuboidal and then to squamous. The organization of the airway wall is mainly a mosaic of epithelial and secretory cells. In the alveoli, the smooth muscle layer is not present. The fibrous layer contains cartilage only in bronchi and gradually becomes thinner as the alveoli are approached. Adapted from [14].

1.1.3. Chronic Obstructive Pulmonary Disease and its pathophysiology

Chronic Obstructive Pulmonary Disease (COPD) is a major public health issue, affecting 64 million people worldwide, according to latest World Health Organisation (WHO) estimates (2004). More than 3 million people died of COPD in 2012, which is equal to 6% of all deaths globally that year. WHO predicts COPD will become the third leading cause of death worldwide by 2030 [15].

The WHO defines COPD as a lung disease characterised by chronic obstruction of lung airflow that interferes with normal breathing and is not fully reversible. The airflow obstruction does not change markedly over several months and is usually progressive

in the long term. The National Institute for Health and Care Excellence (NICE) in the UK define airflow obstruction as a reduced FEV_1/FVC ratio, where FEV_1 is forced expiratory volume in 1 second and the FVC is the forced vital capacity, such that FEV_1/FVC is less than 0.7 [16]. The Global Initiative for Chronic Obstructive Lung Disease (GOLD) has issued a classification system for COPD based on airflow limitation severity (Table 1.1). There is no single diagnostic test for COPD, so this is often based on clinical judgement, patient history, physical examination and confirmation using spirometry.

Table 1.1. Classification of airflow limitation severity in COPD (based on post-bronchodilator FEV1) and in patients with FEV1/FVC < 0.70. Adapted from (17).

GOLD 1	Mild	FEV_1 ≥80% predicted
GOLD 2	Moderate	50% ≤ FEV_1 < 80% predicted
GOLD 3	Severe	30% ≤ FEV_1 < 50% predicted
GOLD 4	Very Severe	FEV_1 < 30% predicted

COPD (now the preferred term for the conditions in patients previously known as chronic bronchitis and emphysema), is predominantly caused by smoking [17]. Other risk factors include exposure to air pollution and occupational dusts and irritants. The characteristic airflow obstruction is present because of a combination of airway and parenchymal damage. This damage is associated with an enhanced chronic inflammatory response in the airways and the lung to noxious particles or gases present in tobacco smoke [18].

Patients with COPD often describe symptoms of breathlessness and chronic cough which are caused by structural changes occurring with disease progression, such as loss of alveolar septation and enlargement of terminal airspaces. These changes lead to a

reduction in elastic recoil of the lungs, hyperinflation on inhalation, airflow obstruction and a loss of alveolar surface area, resulting in a reduction in gaseous exchange [19–21]. These pathological changes lead to unfavourable lung mechanics, and results in repeated cycles of exacerbation (acute worsening of symptoms), increased mucus production and infection (Figure 1.3). Exacerbations appear to accelerate the decline in lung function, with consequences such as decreased physical activity, poor quality of life, and an increased risk of death, as well as being responsible for a large proportion of healthcare costs associated with this disease [22].

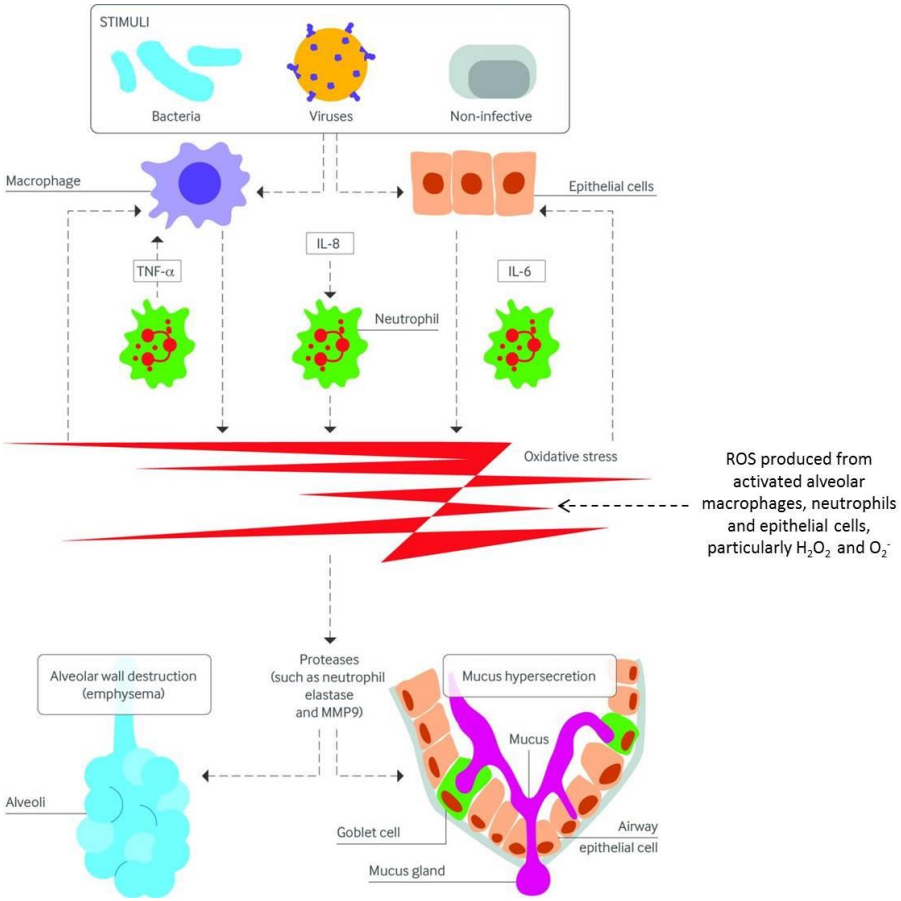

Figure 1.3. Mechanism for acute exacerbations in chronic obstructive pulmonary disease (COPD). Triggers of COPD exacerbations include infectious agents such as bacteria and viruses and non-infectious agents such as air pollution. These stimuli activate airway epithelial cells and macrophages to release inflammatory cytokines including tumour necrosis factor α (TNF-α), interleukin 6 (IL-6), and IL-8. These cytokines lead to neutrophil recruitment and the release of reactive oxidant species (ROS) and proteases from activated neutrophils, which magnify the inflammatory process. Reproduced from [23].

In this research, we will focus on the inflammatory pathogenesis of COPD. Inflammation is present in the lungs, particularly the small airways, of all people who smoke. This normal protective response to the inhaled toxins is heightened in COPD, leading to tissue destruction, impairment of the defence mechanisms which limit such destruction and disruption of the repair mechanisms. In general, the inflammatory and structural changes increase with disease severity and persist even after smoking cessation [24,25]. In terms of inflammatory cells, COPD is characterised by increased numbers of neutrophils, macrophages and T lymphocytes in the lungs [26]. Neutrophils are often increased in the sputum and distal air spaces, with increasing numbers being found on disease progression. Macrophages are increased in number in the airways, parenchyma and in bronchoalveolar lavage (BAL) fluid. T lymphocytes are increased in the airways and the lung parenchyma, with an increase in Th1 and Tc1 also being observed (which produce interferon gamma (IFN-γ)). Finally B lymphocytes are increased in the peripheral airways and within lymphoid follicles, possibly as a result of chronic infection in the airways [26]. In general, the extent of inflammation is related to the degree of airway obstruction [27]. These inflammatory cells release a variety of cytokines and mediators that participate in the disease process. Examples of such inflammatory mediators are:

(a) leukotriene B_4, a neutrophil and T cell chemoattractant which is produced by macrophages, neutrophils and epithelial cells;
(b) chemotactic factors such as the CXC chemokine interleukin 8 (IL-8), which is produced by macrophages and epithelial cells and which attracts cells from the circulation to amplify pro-inflammatory responses;
(c) pro-inflammatory cytokines such as tumour necrosis factor alpha (TNF-α), interleukin 6 (IL-6) and interleukin 1 beta (IL-1β); and finally
(d) growth factors such as transforming growth factor beta (TGF-β), which may cause fibrosis in the airways [28].

Figure 1.4. Sagittal slice of lung removed from a patient who received a lung transplant for COPD. Centrilobular lesions have coalesced to produce severe lung destruction in the upper lobe. Reproduced from [28].

1.2. Chronic Obstructive Pulmonary Disease today: management options and limitations

1.2.1. Pharmacotherapy

Despite the significant evolution of medical treatment options for COPD in the last two decades, it is still an incurable disease. Medical treatment options for non-hospitalised patients currently aim to relieve symptoms, improve exercise tolerance, improve overall health status, prevent exacerbations, and reduce mortality. Pharmacological treatment strategies usually follow a stepwise approach depending on disease severity. Treatment guidelines issued by NICE in the UK for the use of inhaled medications in COPD are set out in the algorithm shown in Figure 1.5 [29]. Initial management involves the use of bronchodilators such as short and long acting β_2-agonists (e.g. salbutamol, fomoterol) and anticholinergics (ipratropium, tiotropium) [18]. Inhaled

corticosteroids (e.g. beclometasone, budesonide) can be added in to the treatment plan, and exert an anti-inflammatory effect on the airways. Other pharmacological options which may be used in combination treatment regimens include theophylline, phosphodiesterase-4 inhibitors, and oral mucolytics. Non pharmacological treatment options include oxygen therapy, pulmonary rehabilitation, smoking cessation and vaccination against pneumonia and influenza. However, despite this range of management strategies available, no existing medications for COPD have been shown conclusively to modify the long-term decline in lung function [30].

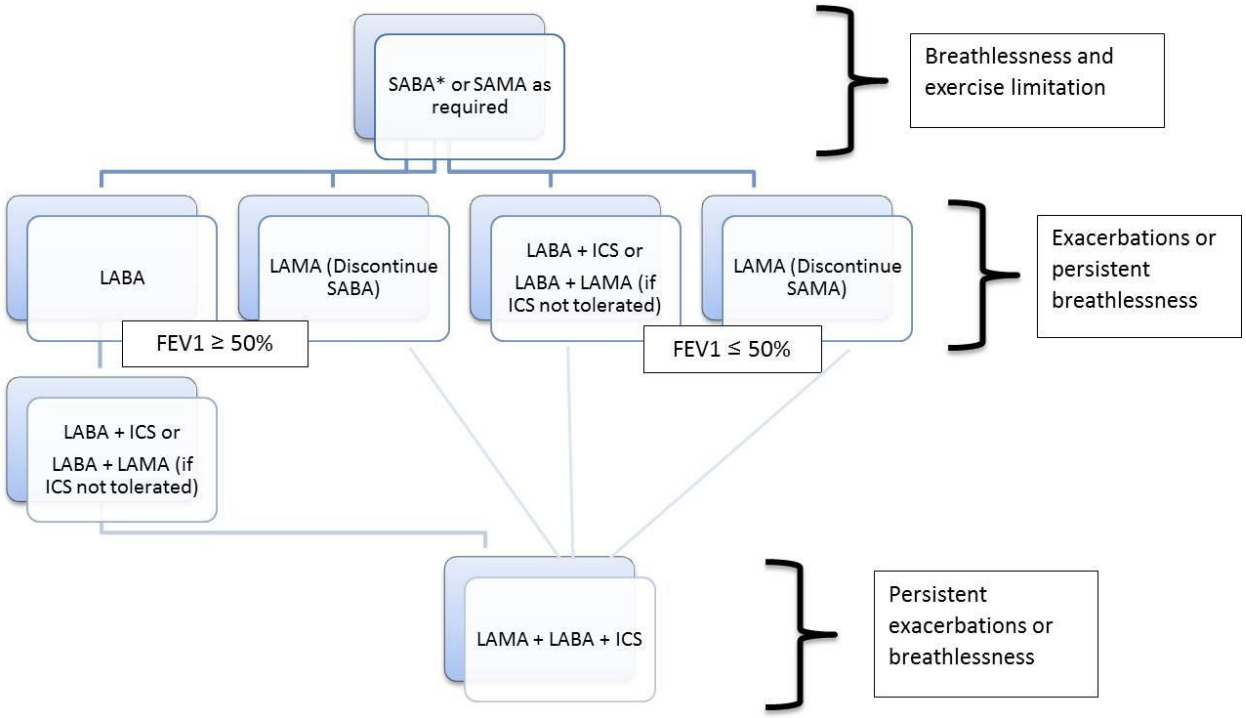

*Figure 1.5. NICE Guidelines Algorithm: inhaled therapies in COPD (SABA = short acting beta agonist, SAMA = short acting muscarinic antagonist, LABA = long acting beta agonist, LAMA = long acting muscarinic antagonist, ICS = inhaled corticosteroid, FEV = forced expiratory volume. * indicates treatment may be continued at all stages if required).*

1.2.2. Lung volume reduction strategies

One surgical option for treatment of patients in advanced COPD is lung volume reduction surgery (LVRS), which aims to reduce hyperinflation by resection of emphysematous destroyed parts of the lung [31]. LVRS has been shown to prolong survival in patients with upper lobe predominant emphysema and low functional capacity in a study carried out by the National Emphysema Treatment Trial Research Group (NETTR Group) in the USA [32]. However, in this study, the 90 day mortality rate of 7.9% following LVRS was very high, stimulating the search for other approaches with comparable physiological benefits but less attendant risk. LVRS has subsequently been associated with high morbidity, hospitalisation and operative mortality of 5-20% patients [33,34].

However, the potential benefits of LVRS are apparent in the treatment of COPD, and over the last decade several endoscopic therapeutic modalities emerged as a substantial part of advanced COPD management. These endoscopic lung volume reduction (ELVR) techniques mimic the physiological effects of LVRS. These can be either blocking or non-blocking methods, which are different in terms of reversibility and safety, and whose application is dependent on the disease distribution [35]. Endoscopic valve therapy is the only blocking and reversible ELVR technique. One way valves are placed in the bronchi of the most damaged lobe. By allowing air to escape from the lobe during expiration but preventing air from entering the blocked lobe during inspiration, volume reduction is achieved. There are two types of valves available – the endobronchial valves (EBV, Zephyr, Pulmonx Inc, Switzerland) and the intrabronchial valve (IBV, Spiration, Olympus, Japan) (Figure 1.6), which are available in different shapes but which act the same way [35]. After measurement of the airway diameter, the values are placed using a flexible delivery catheter. Since their first publication in 2003, many studies have been published evaluating the safety, efficacy and predictors for a good outcome. In the first randomised controlled trial (RCT) known as VENT (Endobronchial Valve for Emphysema Palliation Trial) [36]. The FEV1 improvement of the treatment arm was 4.3%, as compared with a decrease of 2.5% in

the control group resulting in a mean between-group difference of 6.8% (P = 0.005). A similar result was observed in the 6-min walk test.

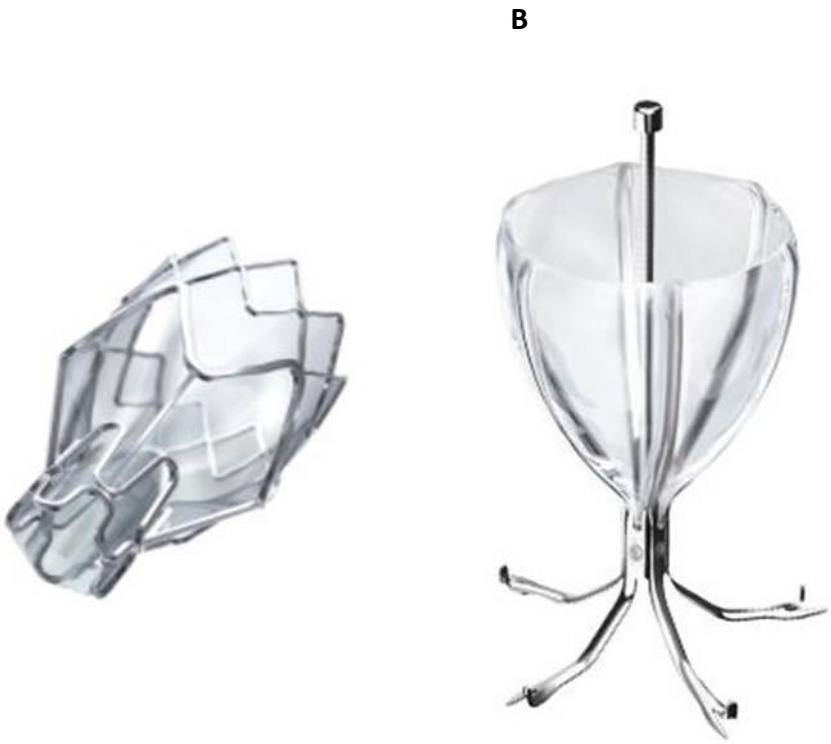

Figure 1.6. Zephyr® (A) endobronchial valve (EBV) and Spiration® (B) intrabronchial valve (IBV). Images reproduced from https://www.pulmonx.com/ous/products/zephyr-endobronchial-valve/ and http://www.spiration.com/c26/emphysema/procedure-overview

Endoscopic coil therapy is one of the non-blocking, partially irreversible ELVR techniques. The implantation of 10 LVR coils (PneumRx Inc, California, USA) in the target lobe leads to parenchymal compression resulting in target lobar volume reduction and improved elastic recoil, as determined by the first RCT, known as RESET [37]. The coil therapy is usually performed bilaterally in two bronchoscopic procedures, and is delivered using a dedicated system under fluoroscopic guidance. In the RESET trial, 23 patients received coil treatment, versus 23 patients in a control group. At 6 months, patients in the treatment group experienced significant improvement in the St

George Respiratory Questionnaire, lung function parameters (forced expiratory volume (FEV_1), residual volume, and 6 minute walk test), compared with the usual care group.

One final option is polymeric lung volume reduction (PLVR), which is a non-blocking and irreversible ELVR technique. This involves the delivery of a synthetic polymer to the emphysematous area. In 2009 results from a phase II trial of BioLVR (Biologic Lung Volume Reduction) hydrogel were published [38]. Administration of this fibrin-based hydrogel to eight sub-segmental sites initiates a localised inflammatory reaction, which collapses non-functional emphysematous lung to non-surgically produce therapeutic lung volume reduction. Results of the study found the higher volume of hydrogel (20 mL) to be more effective than low volume (10 mL), as well as showing safety and efficacy in improving physiology and functional outcomes up to six months after administration. Clinical trials for this product ended before initiation of phase III due to the emergence of a superior second-generation synthetic polymer based hydrogel product, known as the AeriSeal System (Aeris Therapeutics, Woburn, MA) [39]. The hydrogel incorporated into the AeriSeal device is delivered as a liquid foam that blocks the small airways and coats the surface of the target airway, leading to collapse – thereby promoting lung volume reduction. The AeriSeal System received CE mark of approval in 2015 for the treatment of patients with advanced upper lobe predominant and homogeneous emphysema based upon favourable results from clinical studies [40,41], and is commercially available in a select number of locations in Europe. However, one clinical trial reported two patient deaths in the treatment group [42], though these occurred some time after the procedure. One patient died of a myocardial infarction at 55 days post treatment, and the second death was as a result of pneumonia complicated by sepsis. Based on this, and the limited availability of the treatment to date, it is difficult to discern when such therapies will be fully integrated into clinical practice.

1.2.3. Lung transplantation

In the case of failure of all previously mentioned management strategies and without new drugs being successfully developed, patients in advanced COPD face the inevitable intervention of surgery and transplantation. Lung transplantation is an effective treatment for end-stage disease in appropriate candidates, but is limited for a number of reasons. One major limitation to transplantation is the reliance on acceptable donor organs, of which there is an on-going shortage. According to the Organ Donation and Transplant Ireland (ODTI) 2016 Annual Report, a total of 280 transplants were performed in Ireland that year, of which 35 were lung transplants [43]. Shortage of donor organs leads to long waiting times, which results in a substantial risk of the patient dying before transplantation. In 2015, the median waiting time for a lung transplant was eight months, with nine patients dying prior to transplantation [43]. Although survival is relatively high in the year following transplantation, rates drop to approximately 50% at 5 years post transplantation, and again to 35% at 10 years post-transplantation [44]. Aside from this, the many problems associated with lifelong immunosuppressive therapy [45], and the potential for post-operative bacterial colonisation and chronic infection at the implantation site [46], can result in life threatening complications adding to the severity of the clinical case.

1.3. Future approaches to COPD treatment – regenerative medicine (RM) and tissue engineering (TE)

Regenerative medicine (RM) and tissue engineering (TE) are rapidly evolving fields, which aim to replace or regenerate human cells, tissues, or organs in order to restore or establish normal function [47]. The process of regenerating body parts can occur *in vivo* or *ex vivo* and may require cells, natural or artificial scaffolding materials, growth factors, gene manipulation, or combinations of all the above mentioned elements.

1.3.1. Cell sources for potential use in respiratory regeneration

1.3.1.1. Endogenous stem cell populations of the respiratory tract

The possibility of utilising a regenerative approach in the treatment of chronic lung disease has been discussed in numerous publications. Airspace destruction distal to the terminal bronchioles defines the emphysema component of COPD, making restoration of functional alveoli and alveolar ducts a central goal for regenerative therapies in COPD. In order to implement a successful regenerative approach, potential treatments should include progenitor cell populations for *ex vivo* culture, or the recruitment of such populations following implantation so that a regenerative response can be recapitulated and enhanced *in vivo*.

Up until recently, the possible utility of endogenous lung stem cells for regenerative purposes had not been identified [48]. As discussed in section 1.1.2, the alveolar space is covered with alveolar type I and type II cells, and it is believed that type II cells are the progenitors for type I cells, with type II cell impairment being observed in COPD [49]. Recently alveolar epithelial progenitor cells (AEPCs) were isolated from adult human lungs for the first time [50]. In the study, carried out by Fujino *et al*, undifferentiated MSC-like cells with expression of surfactant proteins associated with ATII cells were isolated from adult human lungs. These cells were found to have the ability to self-renew and also had the capacity to generate ATII cells *in vitro*. According to a microarray analysis performed in the same study, AEPCs share many genes in common with type II cells and mesenchymal stem cells (MSCs), which suggests an overlapping phenotype with both the alveolar epithelium and the mesenchyme in these cells, prompting the thought that these cells act as lung endogenous stem cells in lung tissue repair. Mesenchymal properties, such as anti-apoptotic activity and motility, may allow a functional epithelial progenitor to become involved in alveolar repair in COPD lungs.

Other than AEPCs, only two other stem cell populations have been isolated. The first of these was lung resident MSCs which were isolated from bronchoalveolar lavage (BAL) fluid collected from lung transplant patients. These cells had the ability to self-renew and also the capacity to differentiate into a mesodermal lineage [51]. The second report [52] demonstrated that MSCs isolated from distal lung tissues have the potential to express aquaporin 5 (AQP5; a marker for ATII cells) under specific culture conditions. This lack of stem cell isolations from the distal airway, and the fact that the little progress which has been made has occurred only in the last 10-15 years, indicates that this is a new field of research, within which there is still a long way to go with regards to culturing and fully understanding such cell populations.

1.3.1.2. Exogenous stem cells for regenerative purposes: MSCs

The lung is one of the most accessible organs in which to instil exogenous cells because cells can be delivered through both the airway and circulation. In addition, most of the intravenously instilled cells are trapped within the pulmonary circulation; therefore, the efficacy of cell delivery is naturally high [49]. In terms of the choice of exogenous cell population to be utilised, current research is directed towards autologous adult stem cells. Mesenchymal Stem Cells (MSCs) are an adult bone marrow-derived stem cell population. They have a potential therapeutic advantage to other cell populations as they can be isolated from the patient's own bone marrow, circumventing issues such as immunological rejection (a potential concern with allogeneic cells or tissue), and also the ethical issue of sourcing cells (the supply of human embryos from which to obtain stem cells) [53]. When MSCs are injected intravenously, they appear to home to areas of damaged tissue in increased numbers and have been postulated to have a role in tissue repair in numerous organs including the lungs [54,55]. It is thought that on migration to the damaged lung, MSCs then exert a paracrine effect, through the release of a variety of mediators in response to a specific microenvironment that may

include the down-regulation of pro-inflammatory cytokines such as IL-6 and IL-8, and the up-regulation of anti-inflammatory cytokines such as IL-10 [56].

The immunomodulatory effects of MSCs in lung diseases have been investigated extensively in numerous animal models to date. A study carried out by Yuhgetsu *et al* [57] found improved pulmonary function, smaller alveolar airspaces and reduced cell counts in bronchoalveolar lavage (BAL) fluid, in an elastase-induced emphysema rabbit model treated with intra-tracheal bone marrow MSCs. Shigemura *et al* [58,59] investigated the use of adipose stromal cells (ASCs) seeded onto a polyglycolic acid (PGA) felt sheet as a sealant material, in the treatment of emphysema in rodent models. This treatment resulted in significantly accelerated alveolar and vascular regeneration compared with rats treated with LVRS. The limitation of these studies is that they are investigating just the emphysematous component of COPD, rather than the disease as a whole (emphysema, small airway remodelling, pulmonary hypertension and chronic bronchitis). This is due to the complexity of COPD, the mechanisms involved in the genesis of COPD being poorly defined, and the fact that it takes decades to develop. As such, none of the models of COPD reproduce the exact changes seen in humans, and this renders it difficult to translate findings to human clinical trials [60].

However, promising findings from studies investigating the effects of MSCs in acute lung injury (ALI) [61–63] have led to a collaboration with Queen's University Belfast and the Northern Ireland Clinical Trials Unit. The trial, "Repair of Acute Respiratory Distress Syndrome by Stromal Cell Administration (REALIST)", will be an open-label, dose escalation Phase 1 trial, followed by a randomised, double-blind, placebo-controlled Phase 2 trial. It is expected to begin in September 2017, and aims first to determine what dose of MSCs is safe, and will then use a placebo control to determine whether treatment with MSCs has any improvement on lung function [64]. A previous multi-centre, open-label, dose-escalation Phase 1 clinical trial, also investigating the use of MSCs in Acute Respiratory Distress Syndrome (ARDS) ("Stem cells for ARDS Treatment"

or “START”) was carried out in the United States between 2013 and 2014 [65]. It involved a single *i.v.* infusion of MSCs to 9 patients, with patients divided into three treatment groups: (i) 1 million cells/kg, (ii) 5 million cells/kg, or (iii) 10 million cells/kg. The trial found the single intravenous infusion of allogeneic, bone marrow-derived MSCs was well tolerated in nine patients with moderate to severe ARDS.

Human clinical trials investigating the use of MSCs in COPD have been few in number. One clinical trial, published by Weiss *et al* [66], involved 62 patients at six sites across the US, who were randomised to double-blind *i.v.* infusions of either allogeneic MSCs (Prochymal, Osiris Therapeutics Inc. – a product currently licensed in Canada for the treatment of graft-versus-host disease), or vehicle control. Patients in the treatment group received four monthly infusions of 100 x 10^6 cells/infusion, and were followed for two years after therapy. There were no significant differences in the overall number of adverse events, frequency of COPD exacerbations, or worsening of disease in patients treated with MSCs. There were also no significant differences in pulmonary function tests (PFTs) or quality-of-life indicators; however, an early, significant decrease in levels of circulating C-reactive protein (CRP; a marker for inflammation) was observed in patients treated with MSCs who had elevated CRP levels at study entry. This study has shown MSC therapy to be safe in patients with COPD, and provides a basis for subsequent cell therapy investigations. Following the completion of the clinical trial by Weiss *et al*, administration of MSCs for COPD treatment is being further tested in seven clinical trials (clinicaltrials.gov: NCT02645305, NCT01849159, NCT02348060, NCT02412332, NCT02161744, NCT02216630, and NCT01559051 [67]). These clinical trials were designed to further evaluate efficacy and safety of *i.v.* infusion administration of autologous or allogeneic MSCs in the treatment of COPD. It is hypothesised that MSCs will inhibit chronic inflammation in airway, alveoli and endothelium, promote tissue repair through releasing growth factors, and improve patient’s quality of life.

However, despite the many apparent advantages associated with delivery of stem cells for therapeutic purposes, there are major hurdles to their successful clinical translation. Firstly is optimising an appropriate route of administration, which is currently a choice between intratracheal and intravenous delivery. While both methods of delivery have been explored in animal studies to date (as discussed in section 1.3.1.1 and 1.3.1.2), only intravenous delivery has been utilised in human trials. The larger human airways allow greater access to the lung and therefore the intratracheal route may be valuable for airway disease. However, the barriers of innate immunity, including the mucus biofilm in several airways disease, may prevent adequate re-epithelialization of the damaged airway [68]. Other factors contributing to a lack of stem cell therapy translation are poor cell survival once delivered *in vivo* and poor cell engraftment at the intended site of action. Various factors can be attributed to this including exposure of cells to inflammatory mediators, leakage of cell suspension from injection site, and anoikis – death of adherent cells due to lack of attachment sites. In the lung in particular it has been found that, despite the fact that following *i.v.* administration, MSCs travel to the lung in the systemic circulation and become trapped in the pulmonary vasculature [69], engraftment here is low – typically less than 1% [70]. This indicates that if these low rates of engraftment are maintained, cell therapies may be ineffective in replacing damaged tissue to prompt recovery following significant injury. Coupled to this is the inflammatory environment characteristic of conditions such as COPD. Inflammation results in oxidative stress and a harsh milieu for cells within the damaged lung. It is therefore important for the cell therapies used to be resilient, as an inability to survive these circumstances would result in death of the treating cells and an ineffective outcome. Therefore, the potential for cell therapy to develop as a feasible therapeutic option is partly dependent on new strategies to enable viable cells to remain in damaged tissue and exert therapeutic benefit for extended periods [71]. Increasing retention at the site of action, should not only increase the therapeutic effect, but also reduce potential

systemic effects associated with leakage, and possibly lower the effective cellular dose, which is beneficial from both a safety and cost perspective.

1.3.2. Signalling factors for potential respiratory regeneration

An alternative strategy to the use of stem cells for regenerative applications is the delivery of other molecules to stimulate a cellular response *in vivo*. These can include growth factors (GFs), which are critical signalling molecules that instruct cells during development [72]. In the airways, the complex coordination of a range of GFs, for processes such as proliferation, differentiation and vascularisation of tissue, is required to restore functionality [73]. While not as extensively studied as in other RM applications, several GFs and other molecules have been identified that hold the potential to progress the field of respiratory TE. These include hepatocyte growth factor (HGF), bone morphogenetic protein-4 (BMP-4), keratinocyte growth factor (KGF), and *all-trans* retinoic acid (atRA).

1.3.2.1. Hepatocyte Growth Factor (HGF)

HGF is a paracrine factor produced by cells of mesenchymal origin (e.g. fibroblasts and macrophages), while the HGF receptor is expressed by epithelial and endothelial cells [74]. In adults, the primary function of HGF is tissue repair [75]. The role of HGF in lung tissue repair has been well established, and has been investigated in a number of publications [76–78]. HGF has previously shown potential for a role in the treatment of pulmonary fibrosis in rodent animal models [79,80]. Furthermore, HGF has been shown to stimulate proliferation of alveolar and airway epithelial cells following left pneumonectomy in mice, indicating its role as a pulmotrophic factor in post-pneumonectomy compensatory lung regeneration [81]. Overall, HGF has been identified as a significant signalling GF at a respiratory cellular level, and is of on-going interest from a TE perspective.

1.3.2.2. Bone Morphogenetic Protein 4 (BMP-4)

BMPs are involved in a wide variety of processes in the body. In the lung BMP-4 in particular has been identified as playing a role in development and airway healing following acute injury [82,83]. BMP-4 has been identified as a modulator of lung branching morphogenesis, and proximal-distal differentiation of ciliated and secretory epithelial cells [84]. In an *in vivo* study carried out using rhesus macaques, it was found that BMP signalling was up-regulated following asthmatic injury – indicating a potential mechanistic relationship between inflammation and BMP signalling [85]. In terms of BMP-4 action in the distal airways, it has been found that BMP-4 signalling triggers differentiation of bronchioalveolar stem cells (BASCs) down an alveolar lineage [86].

1.3.2.3. Keratinocyte Growth Factor (KGF)

KGF, also known as FGF7, has been investigated widely for its role in lung development, lung inflammation and lung repair since its discovery in 1989. Research conducted into both the addition of exogenous KGF and the blocking of KGF or KGF receptor expression resulted in disruption to normal branching morphogenesis in foetal rat lung explants [87,88]. In isolated rat foetal lung epithelial cells, alveolar type II cell maturation and surfactant synthesis could be attributed to KGF properties as a mesenchymal mediator [89]. Administration of KGF to foetal rat cells led to increased synthesis of surfactant components such as surfactant proteins A, B and C [90]. Increased transcription and translation of KGF within fibroblasts occurs in response to pro-inflammatory cytokines such as IL-1 and IL-6, and this increased expression could stimulate epithelial repair following injury via a paracrine action [91].

1.3.2.4. All-trans Retinoic Acid (atRA)

Retinoids are a family of compounds obtained from the diet, either as their parent compound retinol (Vitamin A) or as carotenoids which are oxidatively cleaved to produce retinol, or from hepatic stores [92]. The lung is second only to the liver as the largest store of retinoids in the body and retinoids are stored as retinyl esters in lipid-laden fibroblasts that are abundant in the alveolar wall often in close approximation with type II pneumocytes [17]. Lipid-laden fibroblasts generate biologically active atRA that can regulate gene transcription in pulmonary microvascular endothelial cells and atRA regulates elastin, an essential structural component of lung matrix in perinatal fibroblasts [93]. Levels of retinoid synthesising enzymes, retinoic acid receptors (RARs), and retinoid-binding proteins demonstrate dynamic patterns of regulation in whole lung during alveologenesis in the rat [94] and mouse [95]. In mice mutant for RAR genes, alveolar formation is disrupted, which has been shown in numerous studies. In research published by McGowan *et al* [96] it was found that the absence of the retinoic acid receptor-gamma (RARγ) is associated with a decrease in whole lung elastic tissue and alveolar number, and an increase in mean cord length of alveoli at postnatal day 28. They also found that additional deletion of one retinoid X receptor (RXR)α allele resulted in a decrease in alveolar surface area and alveolar number. This data suggests that RARγ is required for the formation of normal alveoli and alveolar elastic fibres in the mouse and that RAR/RXR heterodimers are involved in alveolar morphogenesis. Research carried out by Massaro *et al* [97] investigated the role of RARβ, and discovered it to be a negative regulator of alveologenesis due to its inhibition of alveolar septation. The same authors investigated the effects of atRA supplementation during alveolar septation in a separate study, and found that it results in an increase in the number of alveoli but not total surface area in normal rats. They also found that atRA prevents the reduction in both number of alveoli and low surface area corrected for body mass in rats treated with dexamethasone during septation [98]. This data provided the first experimental evidence to suggest that pharmacological regenerative

therapy might be a potential approach for human diseases characterised by too few alveoli and reduced surface area such as COPD [99].

atRA is often used as a media supplement, added to primary airway epithelial cell cultures [100]. atRA has shown potential for reversal of COPD and emphysema induced alveolar injury in animal and human trials alike [101,102]. The effect of atRA on animal subjects was studied in [103] and [104]. In the first of these studies, an elastase induced mouse model of emphysema was treated with atRA, and it was found that treatment promoted lung regeneration and increased bone marrow derived cells in the alveoli (cells which may be a source of progenitors for regeneration). The second study examined the effect on atRA on a dexamethasone treated mouse, which causes reduced lung surface area. Treatment with atRA induced alveolar repair, and increased lung surface area to volume ratio. These responses were only seen in atRA treated mice, and not in those treated with 9-*cis*-RA, 13-*cis*-RA and retinol (two metabolites of atRA and the parent compound).

In human trials, a randomised, double-blind, placebo controlled pilot study to assess the feasibility of atRA in emphysema in a clinical setting, used *i.v.* atRA at doses of 50 mg/m^2/day for 3 months, or 3 months of placebo, followed by a 3 month cross-over phase [19]. This study found that treatment with atRA was well tolerated with minimal side effects, but that physiologic and CT measurements did not change significantly over the duration of the study. It suggested that higher doses, or alternative dosage regimes be assessed in future trials. A second human trial also looked at the feasibility of atRA in emphysema and moderate to severe COPD [101]. In this study, participants received atRA at either a low dose (1 mg/kg/d) or high dose (2 mg/kg/d), 13-*cis* retinoic acid (13-cRA) (1 mg/kg/d), or placebo. This investigation found no treatment was associated with an overall improvement in pulmonary function, CT density mask score, or health-related quality of life (QOL) at the end of the 6 month study period. However, time-dependent changes in DLCO (initial decrease with delayed recovery) and St. George Respiratory Questionnaire (delayed improvement) were observed in the high

dose atRA cohort and correlated with plasma drug levels. In addition, 5 of 25 participants in the HD-atRA group had delayed improvements in their CT scores that also related to atRA levels. Retinoid-related side effects were common but generally mild. The conclusion to these findings was that there was sufficient evidence to warrant further investigation.

In the research presented in this thesis, we aim to harness alternative atRA properties, as opposed to its effects on the lung at a developmental stage. atRA has also been investigated with respect to its immunomodulatory and anti-inflammatory effects in various publications to date, though often in relation to other inflammatory conditions than those present in the lung, such as arthritis [105], acne [106] and psoriasis [107]. In arthritis for example, Nozaki *et al*, investigated the effects of atRA in improving the destruction of joints and the effect of cytokines in collagen induced disease in mice. In terms of pro-inflammatory cytokines, IL-6, IL-12 and TNF-α were found to be significantly reduced in the mice treated with atRA compared with control, indicating a potential immunomodulatory effect. A further study carried out by Ling-Jun Ho *et al* [108] investigating atRA in osteoarthritis found that atRA could reduce IL-1 induced TNF-α production in chondrocytes, again indicating an anti-inflammatory effect. In psoriasis, Balato *et al* [107] found that levels of pro-inflammatory IL-1 cytokines could be suppressed by atRA, which was supported by research carried out in other publications [109]. In terms of acne usage, atRA is licensed as a medicinal product in Ireland in topical form as Treclin 1/0.025% w/w gel (in combination with clindamycin phosphate) [110] with its anti-inflammatory activity being cited as part of the products pharmacodynamic properties. This body of previous research highlighting the immunomodulatory and anti-inflammatory activity of atRA prompted our hypothesis that this could be translated to other inflammatory conditions and specifically COPD, targeting the inflammatory pathogenic component of the disease with potential additional regenerative benefits in the clinical setting.

atRA is hydrophobic in nature, with a poor water solubility of <0.1 g/100 mL (practically insoluble), though it is soluble in DMSO and slightly soluble in ethanol. It is labile to heat (melting point = 179^{o}C [111]), light and oxygen-mediated degradation [112], presenting a challenge for use in a primarily hydrophilic biological environment. In order to overcome the hydrophobic nature of atRA, we aimed to encapsulate it in solid lipid nanoparticles (SLNs). SLNs are sub-micron sized particles made from biocompatible lipids that are solid at room and body temperature. SLNs are then coated with a layer of emulsifier molecules to facilitate their formation and enhance their long-term stability [113]. The formulation of atRA into SLNs will be discussed in detail in Chapter 4 of this thesis.

1.3.3. Investigated strategies for respiratory tissue engineering and regeneration

1.3.3.1. The use of biomaterials in respiratory tissue regeneration

Although there has not been a great deal of recent progress in the engineering of distal lung tissue for clinical applications there has been some progress in critical areas that impact the field of lung TE as a whole. TE in general aims to regenerate tissue lost due to disease or injury (instead of replacing it), by developing biological substitutes that restore, maintain or improve tissue function [114]. The manufacture of successful tissue engineered constructs utilises three main components: the biomaterial scaffold, the presence of signalling molecules such as growth factors (GFs) and the presence of cells that can grow on or within the construct, and eventually recreate the lost tissue [115] (as illustrated in Figure 1.7).

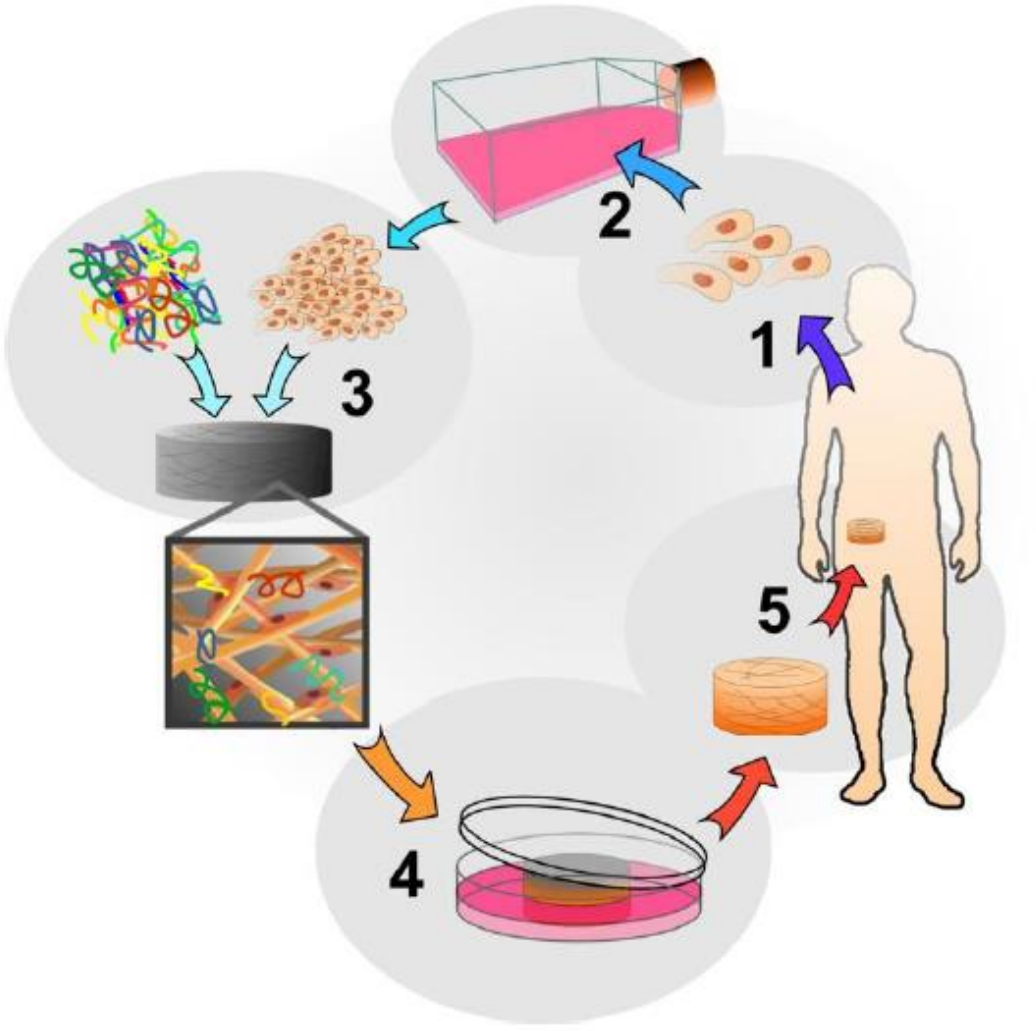

Figure 1.7. Strategies in TE [116]*: (1) Cells are harvested and, (2) expanded in culture, (3) combined with biological cues such as growth factors and a biomaterial scaffold, (4) cultured in vitro and (5) implanted at a defect site.*

1.3.3.2. Porous polymeric scaffolds

Porous polymeric scaffolds were utilised in the first reports of respiratory TE [117,118]. These studies involved the use of gelatin sponges on which foetal rat lung cells were cultured, resulting in the formation of alveolar-like structures. The alveolar-like structures were found to be composed of cells that had morphological characteristics like those of the ATII cells in intact lungs. The formation and long term maintenance of

these structures provided a unique *in vitro* model and were used to study surfactant production. Since then, further research of foetal lung cell culture on other materials including the purified gelatin product Gelfoam®, has been carried out. Gelfoam® is a compressed sponge of porcine skin gelatin, which was originally developed as a haemostatic device, but has now been explored as another natural, degradable material that supports cell proliferation [119]. This study [120], conducted by Andrade *et al* found that following injection of the Gelfoam®/foetal rat lung cell composite into lung parenchyma, the sponge showed porous structures similar to alveolar units and underwent vascularisation *in situ*. It did not induce severe local inflammatory response, and foetal lung cells in the sponge were able to survive in the adult lung for at least 35 days. Cells formed "alveolar-like structures" at the border between the sponge and the surrounding lung tissue, and the sponge was able to degrade after several months. This study suggests that cell-based tissue engineering possesses the potential to regenerate alveolar-like structures, an important step towards the ultimate goal of lung regeneration.

A polyglycolic acid (PGA) mesh and a Pluronic F127 (PF127) gel [121] has shown promise for alveolar modelling and regeneration applications. In this study, conducted by Cortiella *et al*, a population of adult-derived or somatic lung progenitor cells (SLPC) were isolated from adult mammalian lung tissue, and cultured on either the PGA mesh or the PF127 gel. When cells were combined with the synthetic scaffolds and maintained *in vitro* or implanted *in vivo*, they expressed lung-specific markers for Clara cells, pneumocytes, and respiratory epithelium and organized into identifiable pulmonary structures (including those similar to alveoli and terminal bronchi), with evidence of smooth muscle development. Although PGA has been shown to be an excellent polymer for culture of specific cell types *in vitro*, *in vivo* culture in an immunocompetent host induced a foreign body response that altered the integrity of the developing lung tissue. Use of PF127/cell constructs resulted in the development of tissue with less inflammatory reaction. This data suggest that the therapeutic use of

engineered tissues requires both the use of specific cell phenotypes, as well as the careful selection of synthetic polymers, to facilitate the assembly of functional tissue.

1.3.3.3. Decellularised tissue

In the case of TE of the airways, creation of a bioartificial lung requires engineering of viable lung architecture enabling ventilation, perfusion and gaseous exchange. This is something which has been explored as far back as the 1970s [117], though proved largely unsuccessful. A recent significant development in the field has been the use of an acellular cadaveric trachea seeded with mesenchymal stem cells (MSCs) to engineer the upper respiratory tract as a therapeutic strategy. In a landmark case in 2008, a 30 year old patient with chronic tracheitis and secondary bronchomalacia was treated with a tissue engineered tracheal segment from decellularised donor tissue which was re-seeded with autologous chondrogenic MSCs and bronchial epithelial cells to become the first recipient of a tissue engineered airway graft [122]. However, since this study, the use of tissue engineered airways grafts have been cast in doubt, due to an overall high patient mortality rate and investigations into potential misconduct and negligence [123,124]. Despite these advances and set-backs, there has been little progress in the engineering of distal lung tissue for clinical applications.

One animal study however, created a bioartificial lung via decellularisation of tissue, which was then re-seeded with epithelial and endothelial cells. This construct was subsequently perfused and ventilated using a bioreactor simulating physiological conditions, and the regenerated organs were transplanted into rats for confirmation of *in vivo* activity, showing promising results [125].

1.4.Summary

To summarise, the literature review presented in this chapter has outlined the current clinical landscape for COPD disease management and future directions, and specifically the role that RM and TE can play in overcoming the current shortcomings in treatment. The use of therapeutic agents such as stem cells and growth factors have huge potential in the management of this disease, but their direct, loco-regional delivery to the distal airways has not been fully explored or characterised to date. This leaves a void in the research which I aim to address throughout the course of the thesis.

1.5.Thesis Objectives

While effective in reducing the severity of symptoms, current strategies utilised in the management of COPD do not treat or address the underlying disease state or the progressive damage being caused. It is our view that the real potential in this field is building on these approaches, but also incorporating pro-regenerative strategies including both stem cell and small molecule delivery. The clinical potential for this approach represents a new and exciting field in the area of interventional pulmonology. However in order to achieve successful clinical translation of real benefit, it is essential that suitable vectors are available to ensure loco-regional delivery, enabling regenerative therapeutic effects directly to the damaged tissue.

The overall objective of research presented in this PhD thesis is to develop novel delivery systems suitable for minimally invasive drug and cell delivery that could have potential applications in the treatment of COPD. Our central hypothesis was that hydrogels and solid lipid nanoparticles can be used as drug and cell delivery vectors, which are then capable of exerting an anti-inflammatory effect on the local environment present in COPD. Human Mesenchymal Stem Cells (hMSCs) were utilised to exert an anti-inflammatory effect via paracrine actions, and all trans-Retinoic Acid (atRA) was utilised as an anti-inflammatory signalling molecule. Strategies such as these may provide alternatives to those currently utilised which have suboptimal effects and also enable loco-regional delivery of therapeutics, which could significantly enhance clinical outcomes. In order to test this hypothesis, the following specific objectives were pursued:

1. Investigation of the potential of the natural polymer, methylcellulose, in forming a temperature responsive hydrogel, which has the capability to support encapsulated hMSC viability and proliferation and is also able to be delivered in a minimally invasive manner (Chapter 2);

2. Investigate the potential of novel star shaped polymers in forming hydrogels which provide an alternative to natural polymer based systems for stem cell delivery (Chapter 3);
3. The formulation and development of solid lipid nanoparticles for the delivery of atRA for applications in distal airway regeneration (Chapter 4);
4. The development of an *in vitro* model for assessing the anti-inflammatory efficacy of both the hMSC/hydrogel combination therapy, and the atRA/SLN formulation, as an initial indicator of therapeutic effect (Chapter 5).

2. Chapter 2; Formulation and physicochemical characterisation of a thermoresponsive methylcellulose, collagen and beta-glycerophosphate hydrogel

The work presented in this chapter has been partially published as Payne et al., A methylcellulose and collagen based temperature responsive hydrogel promotes encapsulated stem cell viability and proliferation *in vitro.* Drug Deliv. and Transl. Res. 2017; 7(1): 132-146.

2.1.Introduction

RM is a rapidly evolving field, having the potential to overcome the shortcomings and complications associated with current treatment of chronic diseases, by replacing or regenerating human tissues through the use of cells, scaffolding materials, growth factors and other agents to achieve its intended outcomes [47].

Cell therapies using various stem cells have been extensively evaluated. MSCs have a possible therapeutic advantage over other cell populations as they can be isolated from the patient's own bone marrow, circumventing issues such as immunological rejection, and also the ethical issue of sourcing cells [53]. When MSCs are injected intravenously, they appear to home to areas of damaged tissue and have been postulated to have a role in tissue repair in numerous organs [54,55,126]. It is thought that MSCs then exert a paracrine effect through the release of a variety of mediators in response to a specific microenvironment, which may include the down-regulation of pro-inflammatory cytokines and the up-regulation of anti-inflammatory cytokines [127].

Despite the many apparent advantages associated with delivery of stem cells for therapeutic purposes, there are major hurdles to their successful clinical translation, which have been discussed in detail in Chapter 1 (section 1.3.1.2) of this thesis. Retaining cells at the site of delivery is a key issue, and one promising approach to enhancing retention and survival is the use of biomaterial scaffolds. A biomaterial scaffold can act as a surrogate extracellular matrix for encapsulated cells, to enhance cellular viability and enable physical retention at the site of action. Cell-loaded biomaterials address the issue of mechanical dispersal of cells from the injection site, and several studies have shown that biomaterial delivery vehicles can also enhance cellular retention [128–130]. However, accessibility in a minimally invasive manner is a particular challenge in delivering a biomaterial scaffold *in vivo*. Therefore, of particular interest are biomaterials that are injectable and can be easily delivered using current

medical device technology such as syringes and catheters. Hydrogels are one such biomaterial.

Hydrogels are three-dimensional, cross-linked networks which can be made from virtually any water-soluble polymer, encompassing a wide range of chemical compositions and bulk physical properties [131]. A polymer solution can be prepared and allowed to gel *in situ* after photopolymerisation, chemical crosslinking, ionic crosslinking or in response to an environmental stimulus such as temperature, pH or ionic strength of the surrounding medium ("smart hydrogels) [132]. The focus of this research is based around those that respond to a change in temperature. Temperature responsive hydrogels offer a specific advantage as the body maintains a constant temperature at 37.2°C which provides a boundary parameter for gelation to occur in, without the requirement for any other chemical or environmental agent, making their use more straightforward in a clinical environment. Thermoresponsive hydrogels have already been utilised for a wide range of applications in the biomedical field due to their tendency to maintain a liquid state at room temperature, thereby enabling administration via syringe into any tissue, organ or body cavity, with the subsequent ability to rapidly form a robust gel bolus upon heating to physiological temperature [133–138]. Formation of a gel bolus *in vivo* provides the potential to sustain the release of drugs or other therapeutic agents over time, and to allow enhanced retention and viability of cells through the provision of a 3-D architecture to support cell-matrix interactions. Due to site specific delivery and sustained release, use of such hydrogels leads to a reduction in the number of administrations, preventing damage to the molecule or cell and allowing for reduced doses compared to intravenous (*i.v.*) infusions of cells alone [139].

In the early 1960s, Wichterle and Lim were the first to report on hydrogels as we know them today, i.e. as water-swollen cross linked macromolecular networks, in their landmark paper about poly(2-hydroxyethyl methacrylate) (pHEMA) gels for use as soft contact lenses [140]. In the two decades following this discovery, hydrogel research

remained essentially focused on relatively simple, chemically cross-linked networks of synthetic polymers with applications mainly in ophthalmic and drug delivery research. In the beginning of the 1970s however, the hydrogel research focus shifted from relatively simple, water-swollen macromolecular networks to hydrogels capable of responding to a change in environmental conditions [141].

Various groups of polymers have been studied for their thermoresponsive gelling properties. Aqueous solutions of selected poly(ethylene oxide)–poly(propylene oxide)–poly(ethylene oxide) (PEO–PPO–PEO) tri-block copolymers, commercially known as Pluronics® or poloxamers, form thermoreversible gels. Pluronic® hydrogels for the controlled release of pharmaceutical agents appeared in the 1970s. Early studies evaluated Pluronic® F127 (Poloxamer 407) thermosensitive solutions for the treatment of burns [142] and for the controlled release of antimicrobials [143], among others. More recently, the release of ophthalmic drugs [144,145], antifungals [146] and hormones [147] from Pluronic® based hydrogels has been studied as well. Significant drawbacks associated with these hydrogels include their weak mechanical properties, rapid erosion and intrinsic instability, which originate from the weak hydrophobic interactions between the PPO blocks [148]. Moreover, these block copolymers are not biodegradable, which prevents the use of high molecular weight materials since they cannot pass the kidney membranes.

Table 2.1. A selection of thermoresponsive hydrogels which have undergone clinical studies.

Product Name	Thermoresponsive Polymer	Application	Manufacturer
Smart Hyd	Poloxamer-grafted-Polyacrylic Acid	Vaginal/topical drug delivery; sustained release of Luteinising Hormone-Releasing Hormone and insulin	MediSense Inc.
LeGoo™	Aqueous solution of 20% fractionated Poloxamer 407	Used intravascularly, results in occlusive plug, preventing blood flow	Pluromed
BST-CarGel™	Chitosan & combined with autologous whole blood	Improved cartilage repair when injected into microfracture bone defects	Bio Syntech
OncoGel™	ReGel™-PEG-P l PLGA)	Controlled release depot formulation of paclitaxel	Protherics Salt Lake City Inc.
InGel™	PCL-PEG-PLC triblock copolymer	Delivery of proteins and peptides	InGel

Thermogelling chitosan/glycerophosphate (CS/βGP) solutions have also been reported as a type of parenteral *in-situ* forming depot system. Chitosan is a natural linear polysaccharide, produced by the partial deacetylation of chitin, which can be found in

the outer skeleton of shrimp and insects, among others [149]. It is a biocompatible, pH-dependent cationic polymer, which is soluble in acidic aqueous solutions up to pH 6.2. An increase in pH to > 6.2 leads to the formation of a hydrated gel precipitate [150]. This means chitosan alone cannot remain a solution at physiological pH of ~7.0 – 7.4. The addition of the polyol salt, β-glycerophosphate (βGP), to chitosan dispersions however, results in a solution of neutral pH which remains liquid at or below room temperature, and forms monolithic gels at body temperature. Since CS/βGP gels were first reported on in 2000, they have been investigated for a range of drug delivery [151–156] and TE purposes. In terms of TE and RM, CS/βGP solutions have been combined with human mesenchymal stem cells (hMSCs) and desferrioxamine (DFO) as a potential multi-modal pro-angiogenic for the treatment of critical limb ischaemic (CLI) [134]. CS/βGP has also been formulated into a now licensed product "BST-CarGel™" which, when combined with autologous whole blood and injected into microfracture bone defects, leads to significantly improved cartilage repair [137].

Methylcellulose (MC) is a water soluble cellulose polysaccharide derivative, which is also biodegradable. Pure MC solutions are able to form thermoreversible gels on their own. At low temperatures, water molecules are thought to interact with MC hydrophobic methoxyl groups via hydrogen bonding, leading to the formation of a "cage-like" structure, which surrounds the methoxyl groups shielding them from the hydrophilic environment, thereby causing MC to become water-soluble. Heating of such solutions causes destruction of the hydrogen bonds and cage structure, exposing the hydrophobic regions of MC. This leads to the formation of intra- and inter-molecular chain hydrophobic associations, which ultimately results in gelation through the production of a hydrophobically cross-linked network [157]. For pure MC dispersions, gelation temperature is ~50-70^{o}C, and therefore MC alone cannot be used as an injectable product for gelation *in vivo*. As with chitosan, the addition of salts appears to alter the sol-gel transition temperature of the polymer. The combination of MC and a salt to give a thermogelling system, has been investigated for potential treatment of traumatic brain injury (TBI) [158] and spinal cord injuries [159]. In terms

of treatment of TBI, methylcellulose was combined with either phosphate buffered saline (PBS) or deionised water (dH_2O) to form hydrogels which act as a scaffold for cells, increasing adhesion and reducing the expected mechanical washout of cells from the area. This preliminary study found that it was possible to inject MC in a minimally invasive manner into the contused fronto-parietal cortex of adult rats. The formulation was found to be biocompatible, non-toxic, supportive of cell viability, and did not exacerbate the injury at time points assessed [158]. In terms of spinal cord injuries, MC was blended with hyaluronic acid (HA) to form "HAMC" – a shear-thinning gel, which allows for easy administration via intrathecal injection. The gel is formed at room temperature prior to injection and thins on the application of shear when pushed through a syringe, with a subsequent re-coil back to gel state when *in situ*. It was found that in addition to being fast gelling, HAMC is non-cell adhesive, biodegradable, and biocompatible in the intrathecal space. From the gel bolus, growth factors or drugs can be released over a sustained period of time, allowing prolongation of their therapeutic effect [159].

The relatively simple manipulation of the gelation properties of MC indicates its promise as a readily available thermoresponsive material, coupled with the fact that cellulose is the most abundant polysaccharide on earth. MC is widely used as a viscosity enhancing agent in the food and paint industries, and is recognised as an approved food additive by the U.S. Food and Drug Administration, indicating safety in humans. MC has also been previously investigated for drug delivery and regenerative applications [160,161] showing promise which has not yet resulted in clinical translation. As such, further investigation to aid and progress the use of MC is warranted. In this study, we have selected MC as a polymer with potential applicability in stem cell delivery, and βGP was selected as an appropriate catalyst for sol-gel transition at physiological pH and temperature.

In addition to MC and βGP, type I collagen has been incorporated into our formulation. Collagen is a bioactive, biocompatible, and naturally abundant protein, which has

demonstrated efficacy in regenerative therapeutic functions, both alone and as a co-polymer. Collagen gels are well documented as they support cell proliferation and adhesion [162,163]. However, despite this, collagen only gels are also associated with a lack of physical strength, potential immunogenicity issues, poor reproducibility and high costs of production [115]. Therefore, the desired outcome of this chapter was the formulation of a hydrogel that overcomes some of these issues by harnessing the advantageous properties of both MC and collagen, forming a thermoresponsive, biocompatible and bioactive delivery system for use as a drug or cell delivery vector.

Objectives

The overall objective of this Chapter was to investigate the potential of a methylcellulose, collagen and beta-glycerophosphate hydrogel to function as an injectable delivery platform for hMSCs.

- The first objective of this Chapter was to formulate a MC, collagen and beta-glycerophosphate hydrogel that exhibited a thermoresponse within the physiological temperature range.
- The second objective was to determine if the hydrogel was capable of supporting hMSC viability and proliferation.
- The third objective of this Chapter was to investigate the injectability of the hydrogel formulation, in order to ascertain whether it would be deliverable in a clinical setting.
- The final objective was to determine whether gamma irradiation of the hydrogel formulation adversely affects its thermoresponsivity and ability to support hMSC viability and proliferation.

2.2.Materials and Methods

2.2.1. Materials

For hydrogel preparation, MC high viscosity (~88 kD MW, ρ = 400 cP) and βGP were obtained from Sigma-Aldrich (Ireland) as were all chemicals and reagents used (i.e. glacial acetic acid, hydrochloric acid, and methylene blue). Bovine type I fibrillar collagen was obtained from Collagen Solutions SLB (Glasgow, UK).

2.2.2. Preparation of methylcellulose stock solution

Stock preparations of 4% w/v MC high viscosity (Sigma-Aldrich) were prepared via dispersion of MC powder gradually into heated deionised water under gentle stirring and allowed to cool. Upon reaching approximately room temperature the solution was homogenised with an Ultra Turrax Y25 Basic Homogeniser (IKA Works Inc., USA) at 6,500 RPM for 10 min. The solution was stored at 4˚C overnight.

2.2.3. Formulation of methylcellulose/collagen composite

For hydrogels containing collagen, a slurry was prepared by adding bovine tendon collagen to 0.05 M glacial acetic acid and blending at 15,000 RPM for 90 min using an overhead blender (Ultra Turrax T18 Overhead Blender, IKA Works Inc., USA) at a constant temperature of 4°C. Initial formulations used collagen slurries of 0.5% w/v, with later investigated slurries of 1% w/v being used. Degradation of the protein by heat was prevented by using a mixing vessel cooled to 4°C. To prepare the composite a known volume of stock 4% w/v MC (section 2.2.2) was removed from cold storage and placed onto a magnetic stirrer. Collagen was slowly added to this MC stock in a drop-wise fashion to prevent aggregation of protein. The MC/collagen mix was then brought to the final volume with deionised water. The resultant formulation was homogenised at 6,500 RPM in an ice bath for 10 min, and allowed to equilibrate at 4˚C overnight.

Gas was removed via centrifugation at 3,500 G and 4°C for 5 min, before transferring the mixture into a stainless steel grade 304 SS pan and freeze-drying (Advantage Genesis 25EL, VirTis Co., Gardiner NY) to a final temperature −40 °C using a previously optimised freeze-drying profile [164]. Lyophilised wafers were rehydrated in the desired salt solution, as described in Table 2.2. Following this, pH of the formulation was adjusted using 0.1 M HCl, to within a physiologically compatible range (6.8 – 7.0). Hereafter, investigated gels will be referred to as labelled in Table 2.2 i.e. gels 1 – 10. A schematic detailing the stepwise process of formulation and reconstituting gels for injection is shown in Figure 2.1.

In studies requiring sterile gel, lyophilised wafers were subjected to gamma irradiation (Section 2.2.11). After irradiation lyophilised wafers were rehydrated in sterile βGP 5.6% w/v solution under aseptic conditions (Section 2.2.11).

Table 2.2. MC formulations assessed for thermoresponsivity. MC = methylcellulose, βGP = beta glycerophosphate, PBS = phosphate buffered saline, NaCl = sodium chloride, Na_3PO_4 = trisodium phosphate.

Gel	MC (% w/v)	Collagen (% w/v)	βGP (% w/v)	Other salt – specified (% w/v)	pH	Gelation Temperature (°C)
1	2.0	-	-	Krebs Buffer	6.75	N/A
2	2.0	-	-	PBS	6.75	N/A
3	2.0	-	-	NaCl 1.0 + Na_3PO_4 1.0	6.5	50
4	2.0	-	2.75	-	6.5	47
5	2.0	-	4.0	-	6.6	44
6	2.0	-	5.6	-	6.8 - 7.0	38
7	2.0	0.1	5.6	-	6.8 - 7.0	36
8	2.5	-	5.6	-	6.8 - 7.0	39
9 "Respiragel"	**2.5**	**0.1**	**5.6**	**-**	**6.8 - 7.0**	**37**
10	2.5	0.3	5.6	-	6.8 - 7.0	39

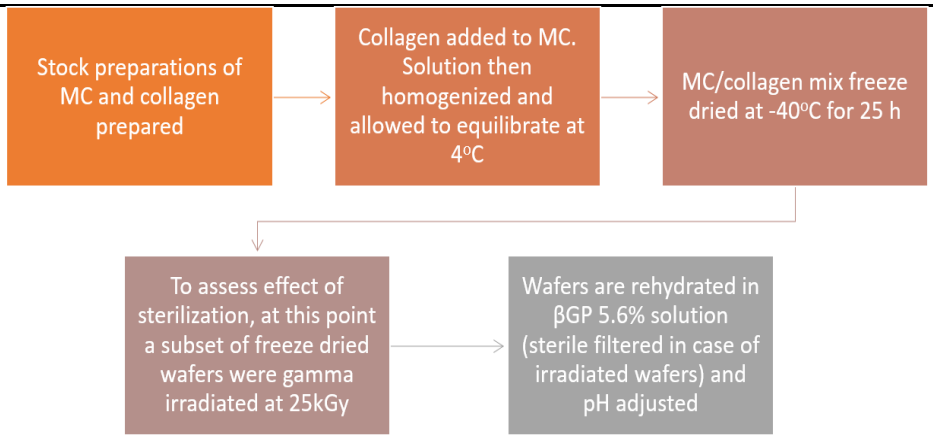

Figure 2.1. Schematic detailing the gel formulation and reconstitution process as described in Section 2.2.2 and 2.2.3.

2.2.4. Rheological testing

The rheological properties of MC formulations listed in Table 2.2 were assessed using an AR-1000 cone and plate rheometer (TA Instruments, USA) under two modes, oscillatory and flow. The thermoresponsivity was assessed using an oscillatory temperature sweep with storage modulus (G') being used as an indicator of internal gel structure. The criterion of gelation was defined at the point at which the storage modulus (G') exceeded that of the loss modulus (G''). In the case of the selected lead formulation (i.e. gel 9, "Respiragel": 2.5% methylcellulose, 0.1% collagen, 5.6% beta glycerophosphate), the polymer solution (at 25^{o}C) was also tested under a flow procedure, to measure the viscosity as a function of shear stress. Assessments at a constant temperature over time employed a solvent trap to prevent dehydration of the sample. Parameters for each rheological test are shown in Table 2.3.

Physical gelation was also observed visually via an inverted tube test. Solutions (5 mL samples) were held at 37^{o}C in a thermostatically controlled water bath, and observed at increasing time points.

Table 2.3. Rheological characterisation parameters for testing of MC formulations.

Rheological Test Type	Temperature	Frequency	Shear Stress	Time
Oscillatory temperature Sweep	25-45°C @ 1°C/min increments	1 Hz	5 Pa	N/a
Oscillatory Time Sweep	37°C	1 Hz	5 Pa	30 min
Flow Steady State	25°C	1 Hz	1 – 80 Pa	N/a

2.2.5. Gel diffusion and disintegration studies

Respiragel was selected for further evaluation in terms of robustness, due to its appropriate temperature response profile. Robustness of the gel structure was assessed by evaluating disintegration of the gel (5 mL) over time in the presence of 2 mL phosphate buffered saline (PBS) pH 7.2, when placed in a shaking water bath at 37°C and 75 RPM. At each time point the PBS was removed and gel degradation determined by weighing the tube and determining mass loss of gel.

The ability of compounds to diffuse through the formed gel over time was determined by adding 1 mL of a 0.01% w/v methylene blue solution (molecular weight (MW) = 319.85 g/mol) to 5 mL gel in a falcon tube, which had previously been allowed to equilibrate at 37°C in a thermostatically controlled water bath and shaking at 75 RPM. A visual inspection, to determine dye penetration through the gel was performed every hour up to 4 hours, and also at 24 hours.

2.2.6. Scanning Electron Microscopy (SEM) of lyophilised Respiragel

Lyophilised Respiragel samples were examined using scanning electron microscopy (SEM) in order to evaluate their architecture and internal pore size. Following

lyophilisation, samples were mounted to an aluminium stub using a carbon paste and sputter coated with gold. Imaging of the wafers and hydrogels was performed using a Zeiss Supra 35VP SEM microscope (Zeiss, Jena, Germany). Both irradiated (section 2.2.11) and non-irradiated samples were visualised, in order to determine if the irradiation process had an effect on hydrogel morphology.

2.2.7. hMSC culture

Iliac crest bone marrow aspirates were obtained from Lonza Ltd (Basel, Switzerland). Lonza use a commercial Institutional Review Board (IRB), E&I Review Services, that approves the bone marrow program (study number 00074) annually. hMSCs were isolated and cultured from this bone marrow in RCSI, using standard protocols and stringent analysis of cell phenotype (tri-lineage differentiation and a full panel of cell surface markers) as published in Duffy *et al* [165]. hMSCs were cultured in T175 tissue culture flasks (Sarstedt, Ireland) in low glucose Dulbecco's Modified Eagle Medium (DMEM), supplemented with 10% foetal bovine serum (FBS) and 1% penicillin/streptomycin (Labtech, UK) at 37°C and in a 5% carbon dioxide environment. The media was replaced every three days and the cells were passaged upon reaching 80 – 90% confluency at a ratio of 1:3.

2.2.8. Rheological assessment of cell loading concentration on Respiragel

In order to determine a cell-in-gel loading concentration that maintains a robust gel structure and thermoresponse, samples containing increasing concentrations of MSCs in hydrogel were prepared. MSCs were cultured as described in section 2.2.7. Cells were removed from the suspension via centrifugation, and on removal of the supernatant, the pellets were re-suspended in the polymer solutions at a series of concentrations via gentle pipetting at room temperature. Cell-in-gel formulation/concentration combinations investigated were:

(a) Gel 7 at cell loading concentrations of 300,000 cells/ mL, 600,000 cells/ mL and 900,000 cells/ mL; and

(b) Respiragel at cell loading concentrations of 100,000 cells/ mL, and 300,000 cells/ mL

Following loading of cells into hydrogel samples, thermoresponsivity and magnitude of G' was re-confirmed by oscillatory temperature sweep (tests as described in section 2.2.4).

2.2.9. Evaluation of encapsulated hMSC viability and proliferation

Following determination of optimal cell-in-gel loading concentration, hMSCs were suspended in Respiragel at a density of 5 x 10^5 cells/ mL. This was aspirated into a 3 mL syringe and 500 µL volumes were expelled through a 21 G needle to form droplets in Costar Transwell Inserts (Fisher Scientific, Ireland) with an 8 µm pore size and diameter of 6.5 mm, for insertion into 24 well plates. Gel 8 (containing no collagen), encapsulating the same cell concentration, was used as a control. These were allowed to gel at 37°C for 15 min before addition of 2 mL normal hMSC growth media per well. Media was replaced every two days.

Cells were cultured in gel for 7 days and the droplets were stained with a LIVE/DEAD stain (Molecular Probes, Invitrogen, Ireland) according to the manufacturer's protocol at 24 hours, day 3 and day 7, to assess cell viability over time. The droplets were visualised by fluorescence microscopy using a Leica DMIL microscope (Leica Microsystems, Switzerland). Live cells were stained green with green-fluorescent calcein-AM and dead cells were stained red with red-fluorescent ethidium homodimer-1.

In addition to LIVE/DEAD staining, samples were assessed using the Quant-iT PicoGreen dsDNA assay (Invitrogen, ThermoFisher Scientific, Ireland). Following removal of media, gel was removed from the inserts and homogenised following the addition of 1 mL 0.2 M $NaHCO_3$, 1% Triton-X lysis buffer. Lysates were stored at −80°C and underwent three

freeze–thaw cycles prior to analysis. Double-stranded DNA (dsDNA) levels within the gel lysates were measured according to the manufacturer's protocol.

All cell-in-gel assays (i.e. LIVE/DEAD and Quant-iT PicoGreen) studies were carried out in triplicate (i.e. n=3 and three independent experiments). Conditions were kept constant across replicate experiments, though different batches of hMSCs were used in each distinct repeat, in order to remove potential bias associated with one particular cell donor.

2.2.10. Assessment of polymer solution injectability at room temperature

Uniaxial compression tests were conducted to determine the force required to expel the room temperature form of Respiragel (i.e. a polymer solution) from a 3 mL syringe. All testing was carried out using a Zwick mechanical testing machine (Z050, Zwick/Roell, Germany), fitted with a 5 kN load cell. The plunger of the syringe was attached to the load cell using a custom-built adapter. This adapter was used to apply a constant feed-rate, corresponding to 8 seconds per 1 mL injection, to the plunger of the syringe.

Polymer solution samples were loaded into a 3 mL luer-lok syringe (BD, Dublin, Ireland) before compression testing. Initially, determination of the maximum force required to expel the solution through this space was performed. This was repeated following attachment of a 21 G needle (BD, Dublin, Ireland) to the syringe, and finally a custom-made catheter of internal diameter (ID) 0.514 mm attached to the syringe. A pre-load (preliminary force) of 1 N was applied for all tests and the end of test was determined to be the maximum extension (17 mm); the distance equivalent to 1 mL of solution (measured using Vernier’s callipers). The force profile per injection was recorded.

2.2.11. Assessment of gel bolus formation in *ex vivo* rat lung tissue

In order to determine whether a gel bolus would be formed *in vivo* following delivery via syringing, *ex vivo* rat lung tissue was obtained from Biomedical Research Facility (BRF) in RCSI (following ethical approval obtained from the Animal Research Ethics Committee, RCSI #REC1236bb), for gel injections. A fluorescent dye, indocyanine green (ICG; MW = 774.96 g/mol) was added to Respiragel at a concentration of 0.025% w/v. 100 µL of ICG-Respiragel was then injected directly into the lung tissue using a 1 mL syringe + 30 G needle. The lungs were then fluorescently imaged using a Xenogen IVIS imaging system 100 (Perkin Elmer, UK) with the following settings: fluorescent imaging, excitation filter 745 nm, emission filter 840 nm, binning of 8, field of view 12.4 and f stop 2. This process was repeated for 100 µL 0.025% ICG in saline as a control. Images were analysed using Living Image Software, v 4.5.4.

2.2.12. Assessment of effect of gamma irradiation on thermoresponsivity

Following the lyophilisation step detailed in section 2.2.3, Respiragel polymer wafers were sterilised (Synergy Health PLC, Westport, Ireland) using the standard gamma irradiation method specified in the European Pharmacopeia [166]. The reference absorbed dose of radiation was 25 kGy. Following gamma irradiation, lyophilised wafers were rehydrated in βGP solution filtered through a 0.22 µm filter under aseptic conditions to maintain sterility. Rheological analysis was repeated as described in section 2.2.4 in order to determine whether the sterilisation process had affected the thermoresponsivity of the formulation. Cell viability and proliferation was also repeated as described in sections 2.2.9.

In addition to cell viability fluorescent imaging, LIVE/DEAD stained samples were also imaged by confocal microscopy on a Zeiss LSM 710 confocal microscope, using Zen® 2008 software. Samples were imaged using a W N-Achroplan 10x objective (NA 0.3), to generate a 5 x 5 tile image that covered 18 mm^2. Images were acquired 100 µm below the surface to avoid inconsistencies. Image analysis and quantification were performed

using the open-source software CellProfiler (http://www.cellprofiler.org) [167]. An analysis pipeline was designed as follows: live or dead cells were identified using an automated global two class Otsu thresholding. Objects outside of defined live or dead cell diameters were then excluded before the size, shape and number of objects were measured. The open-source FIJI software [168] was then used for image preparation. Live cell counts were averaged for each sample and each group, with results being presented as % viability.

2.2.13. Statistical analysis

Two-way ANOVA followed by Sidak's post-hoc analysis was performed to determine statistical differences in cell/gel studies described in sections 2.2.9 and 2.2.12. One-way ANOVA followed by Dunnett's post-hoc analysis was used to compare forces required to perform injections of polymer solution in section 2.2.10. All statistical tests were performed using GraphPad Prism v5 (GraphPad Software Inc., CA, USA). Error is reported as standard error of the mean (SE) and significance was determined using a probability value of $p \leq 0.05$. A minimum of n=3 technical replicates and independent repeats was performed for all experiments.

2.3.Results

2.3.1. Formulation process

Ten MC formulations were assessed for thermoresponsivity, as shown in Table 2.2, section 2.2.3. Gels 1-6 were relatively simple formulations, with methylcellulose being readily soluble in the buffer or salt solution of choice. Gels including collagen (7, 9 (Respiragel) and 10) took longer to develop due to additional steps such as making the collagen slurry, addition of the collagen to the methylcellulose dispersion, freeze drying and subsequent rehydration. Rehydration of the lyophilised wafers took varying lengths of time, ranging from 2 to 5 days, and was the main rate limiting step to final formulation.

2.3.2. Thermoresponsivity of MC hydrogel formulations

A number of different parameters were investigated for their effect on the thermoresponsivity of the hydrogels. These included the effect of various salts on the formulation, the effect of concentration of the chosen salt, variation in the collagen concentration and varying the MC concentration.

Initial investigated gel formulations were varied based on inclusion of a salt component, with four salts being compared (formulations 1-4). The addition of either Krebs Buffer (gel 1) or PBS (gel 2) to MC 2.0% w/v did not result in any reduction in the gelation temperature, and as such were not continued for further evaluation. A blend of 1.0% w/v NaCl and 1.0% w/v Na_3PO_4 (gel 3) did result in a reduction in MC gelation temperature to 50^{o}C, but as the goal for sol-gel transition was 37^{o}C, this combination was also not continued further (Figure 2.2A).

Three concentrations of βGP were assessed: 2.75% w/v (gel 4), 4.0% w/v (gel 5) and 5.6% w/v (gel 6) (Figure 2.2B). Each increase in βGP concentration produced a reduction in MC gelation temperature, with 4.0% βGP gelling at 44^{o}C, and 5.6% w/v

βGP gelling at 38°C. As the 5.6% w/v βGP yielded the gelation temperature closest to that of physiological temperature (i.e. 37°C), it was concluded that this salt and concentration would be progressed for further investigation.

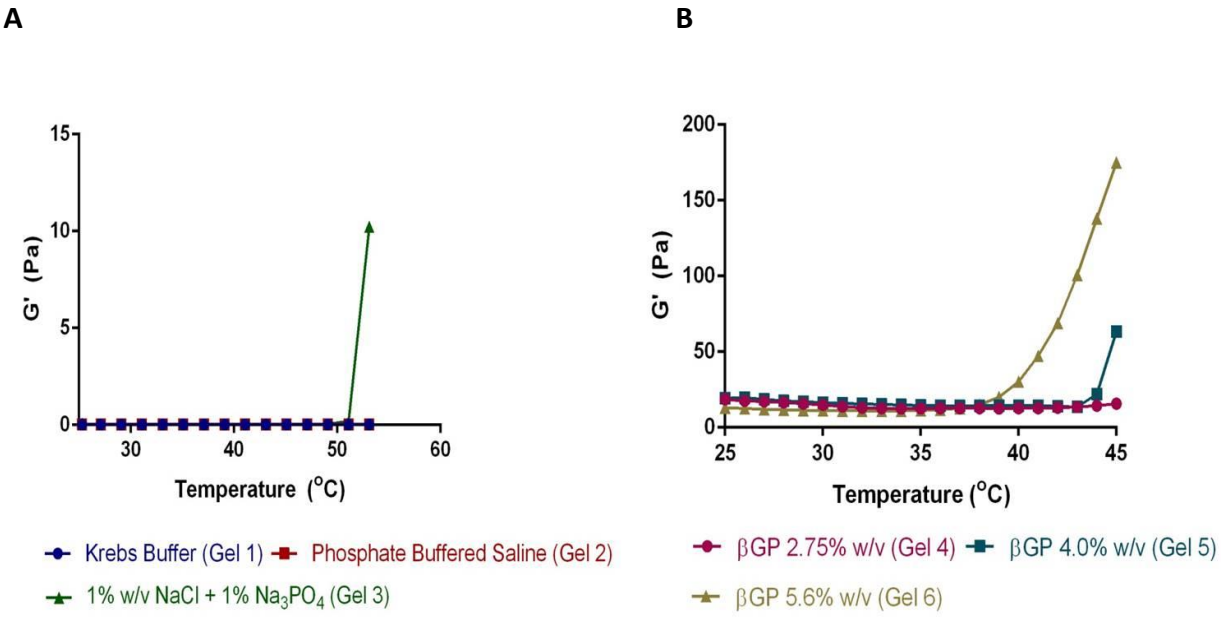

Figure 2.2. Rheological temperature response curves obtained using an AR-1000 rheometer (TA Instruments) comparing (A) 2.0% methylcellulose combined with either Krebs Buffer (gel 1), PBS (gel 2) or 1% NaCl/1% Na_3PO_4 (gel 3); (B) 2.0% methylcellulose combined with increasing concentrations of beta-glycerophosphate i.e. 2.75% (gel 4), 4% (gel 5) and 5.6% w/v (gel 6).

At this point, 0.1% w/v collagen was added to the formulation (gel 7, Table 2.2) and compared to the non-collagen containing gel. The 2.0% w/v MC formulation with no collagen present displayed a thermogelation temperature of 38°C (gel 6). The collagen containing formulation underwent sol-gel transition at the slightly lower temperature of 36°C, and this was accompanied by an increase in storage modulus (G') at this temperature (Figure 2.3A).

In order to determine whether increasing the concentration of MC would result in an increased storage modulus (G'), a further gel was developed composed of 2.5% MC and 5.6% βGP (gel 8). This formulation displayed a slightly higher gelation temperature of

39°C (Figure 2.3B). On addition of 0.1% w/v collagen to this formulation, the thermogelation temperature dropped to 37°C (gel 9). Storage moduli (G') of both 2.5% MC containing gels were observed to be higher than those resulting from the 2.0% w/v MC concentration. Similarly, in both the 2.0% and 2.5% MC formulations, the collagen containing gels consistently reached higher storage moduli than the no collagen control (Figure 2.3, A and B).

All βGP containing gel formulations were also assessed for their thermoresponsivity over time at 37°C for 30 minutes (Table 2.4). Gel 9 (hereafter referred to as "Respiragel") displayed a more rapid increase in storage modulus and achieved consistently higher storage moduli than all other formulations. Taken together with the temperature sweep results indicating sol-gel transition at 37°C, it was decided to progress with this formulation for further assessment.

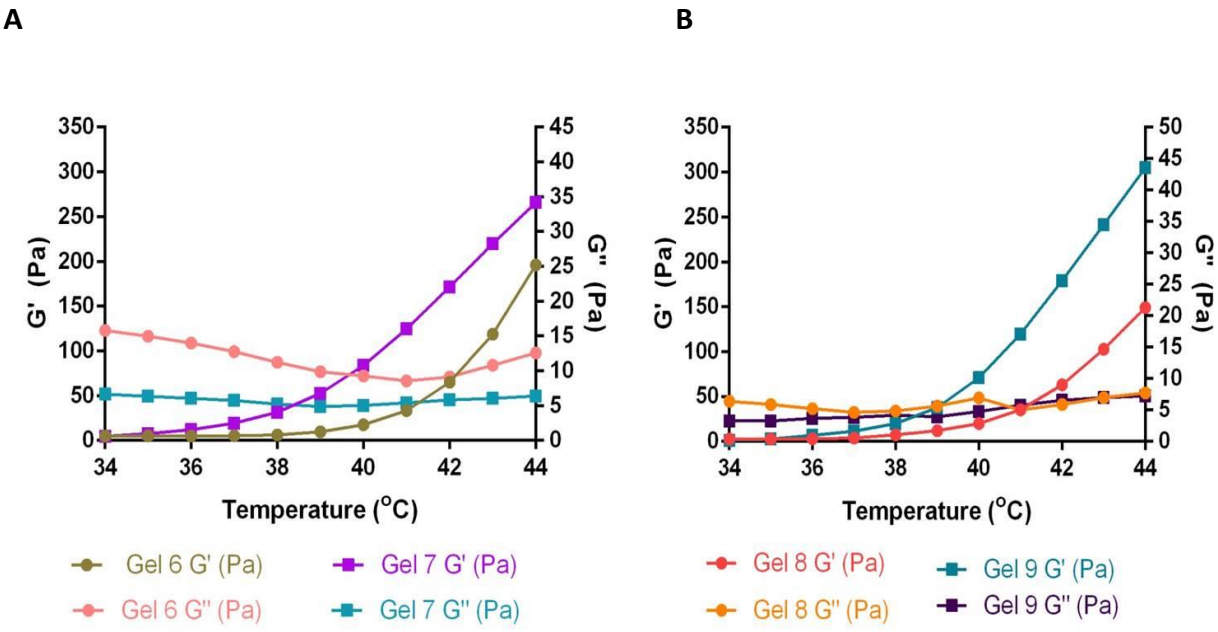

Figure 2.3. Rheological temperature response curves obtained using an AR-1000 rheometer (TA Instruments) comparing (A) 2.0% methylcellulose, 5.6% beta-glycerophosphate (gel 6) (no collagen) with 2.0% methylcellulose, 0.1% collagen, 5.6% beta-glycerophosphate (gel 7); (B) 2.5% methylcellulose, 5.6% beta-glycerophosphate (gel 8) (no collagen) with 2.5% methylcellulose, 0.1% collagen, 5.6% beta-glycerophosphate (Respiragel, i.e. gel 9). G' denotes storage modulus and G" denotes loss modulus.

Table 2.4. Comparison of storage modulus values (G') for gel formulations 6-9 (2.0% methylcellulose, 5.6% beta glycerophosphate = gel 6, 2.0% methylcellulose, 0.1% collagen, 5.6% beta glycerophosphate = gel 7, 2.5% methylcellulose, 5.6% beta glycerophosphate = gel 8, 2.5% methylcellulose, 0.1% collagen, 5.6% beta glycerophosphate = Respiragel (gel 9) at 5 minutes, 15 minutes and 30 minutes. Temperature = 37°C, shear stress = 5 Pa, frequency = 1 Hz, using an AR-1000 rheometer.

	Gel 6 (G')	**Gel 7 (G')**	**Gel 8 (G')**	**"Respiragel" (G')**
5 min	4.694 Pa	19.94 Pa	9.63 Pa	17.67 Pa
15 min	16.02 Pa	45.57 Pa	22.53 Pa	51.97 Pa
30 min	31.34 Pa	71.6 Pa	45.10 Pa	80.79 Pa

2.3.3. Hydrogel diffusion and disintegration gel properties

While the storage modulus (G') provides an indication of internal three-dimensional structure of the gel, it does not provide macroscopic evidence of the gel robustness. Assessment of diffusion of a methylene blue dye through Respiragel showed that it takes up to 24 h before substantial diffusion occurs (Figure 2.4A). Disintegration studies also showed that Respiragel does not disintegrate in the presence of PBS. This was in sharp contrast to MC 2.5% w/v alone, which begins to degrade rapidly from 24 h onwards; retaining 35% of its original weight by the final time-point (Figure 2.4B). Taken together, these results indicate that Respiragel, which forms at 37°C, is robust in nature, and has the potential to remain *in situ* for extended periods of time.

A

B

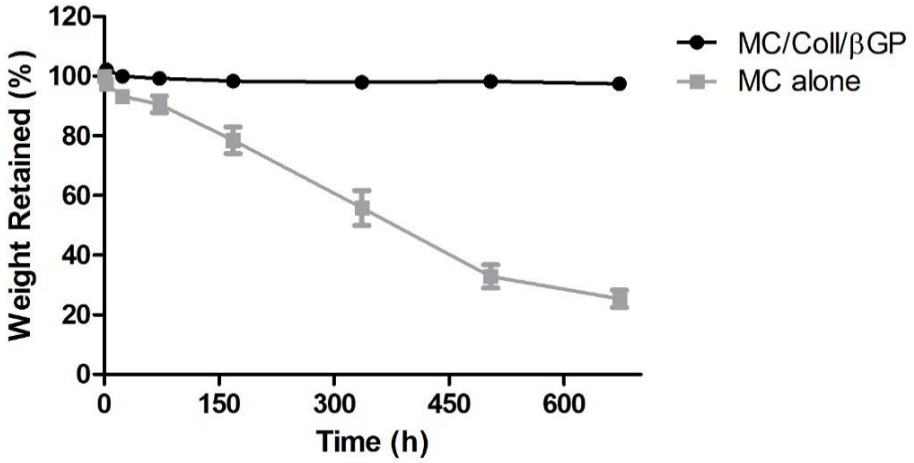

Figure 2.4(A). Penetration of methylene blue dye through 2.5% methylcellulose, 0.1% collagen, 5.6% beta-glycerophosphate gel (Respiragel) at hourly time points (@ 0, 1, 2, 3, 4, 24 hours) at 37°C; (B) Gel disintegration study of 2.5% methylcellulose, 0.1% collagen, 5.6% beta-glycerophosphate (Respiragel) compared with 2.5% methylcellulose alone over a 28-day period at 37°C and 75 RPM. Results are presented as average weights (n=3) and SE.

2.3.4. Respiragel ultrastructure

The morphology of the lyophilised Respiragel wafers was examined by scanning electron microscopy (SEM). Figure 2.5A shows the uniform porous nature of the internal wafer structure, while Figure 2.5B shows the elongated pores which appeared close to the edges of the sample. These images show a densely porous structure, with a pore size of approximately 100 nm.

A **B**

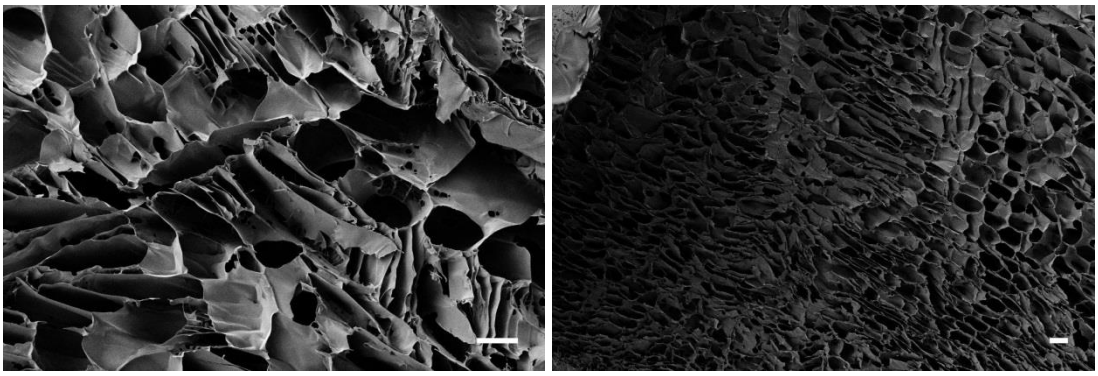

Figure 2.5 (A and B). Representative scanning electron micrographs, showing internal porous structure of lyophilised Respiragel samples. Scanning electron micrographs were obtained using a Zeiss Supra 35VP SEM microscope (Zeiss, Jena, Germany).Image A was taken at 85X magnification and 5kV accelerating voltage, and image B taken at 40X magnification and 5kV accelerating voltage. Scale bar, 100µm.

2.3.5. Effect of cell loading concentration on sol-gel transition and structure

Prior to assessing hMSC viability and proliferation in the gel, the effect of cell loading density on rheological properties of Respiragel was carried out using temperature and time sweeps. Figure 2.6 shows two temperature sweeps, comparing the 2% w/v MC gel (gel 7)(Figure 2.6A) and 2.5% w/v MC gel (Respiragel)(Figure 2.6B) in terms of increasing concentration of cells suspended within each gel respectively. From these graphs, it is evident that the inclusion of cells corresponds with a decrease in G' in both formulations (compared to a "no cells" control). The formulation of Respiragel containing a concentration of 300,000 cells/ mL, was selected for further cell in gel studies, as this combination results in the smallest decrease in G'. This data was confirmed using a time sweep of all formulations, which yielded supporting results (data not shown).

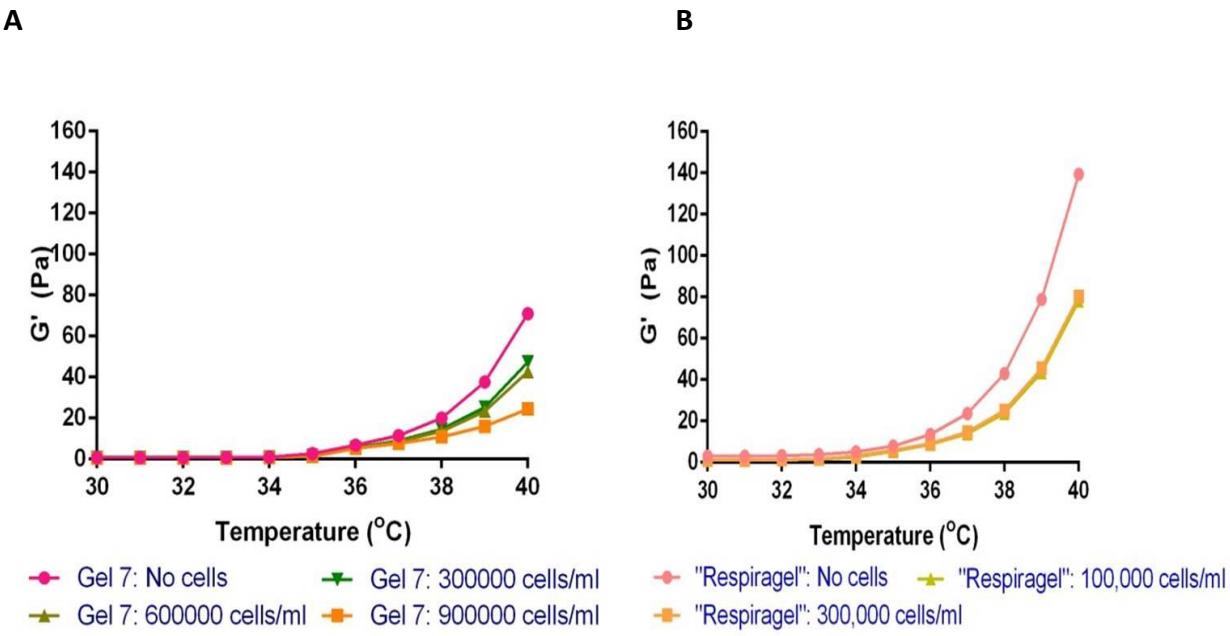

Figure 2.6. Effect on temperature response of increasing cell-in-gel loading concentrations in (A) 2% w/v methylcellulose, 0.1% collagen, 5.6% beta glycerophosphate gel (gel 7) compared with (B) 2.5% w/v methylcellulose, 0.1% collagen, 5.6% beta glycerophosphate gel (Respiragel i.e. gel 9), using an AR-1000 rheometer (TA Instruments). Shear stress = 5 Pa, frequency = 1 Hz. Gel 9 at a cell density of 300,000 cells/ mL is the most suitable combination.

2.3.6. Encapsulated hMSC viability and proliferation

Encapsulation of hMSCs indicated that cells were viable and displayed low levels of cell death up to day 7 when suspended in the collagen containing gel (Respiragel). This was in contrast to the non-collagen containing control (gel 8), in which viability decreased after day 3 (Figure 2.7A).

Measurements of double stranded DNA (dsDNA) from encapsulated hMSCs in gel 8 and Respiragel supported the viability assessment. hMSCs were shown to be capable of proliferating within the collagen containing gel up to 7 days (Respiragel), whereas proliferation is limited in the non-collagen containing control (gel 8) (Figure 2.7B).

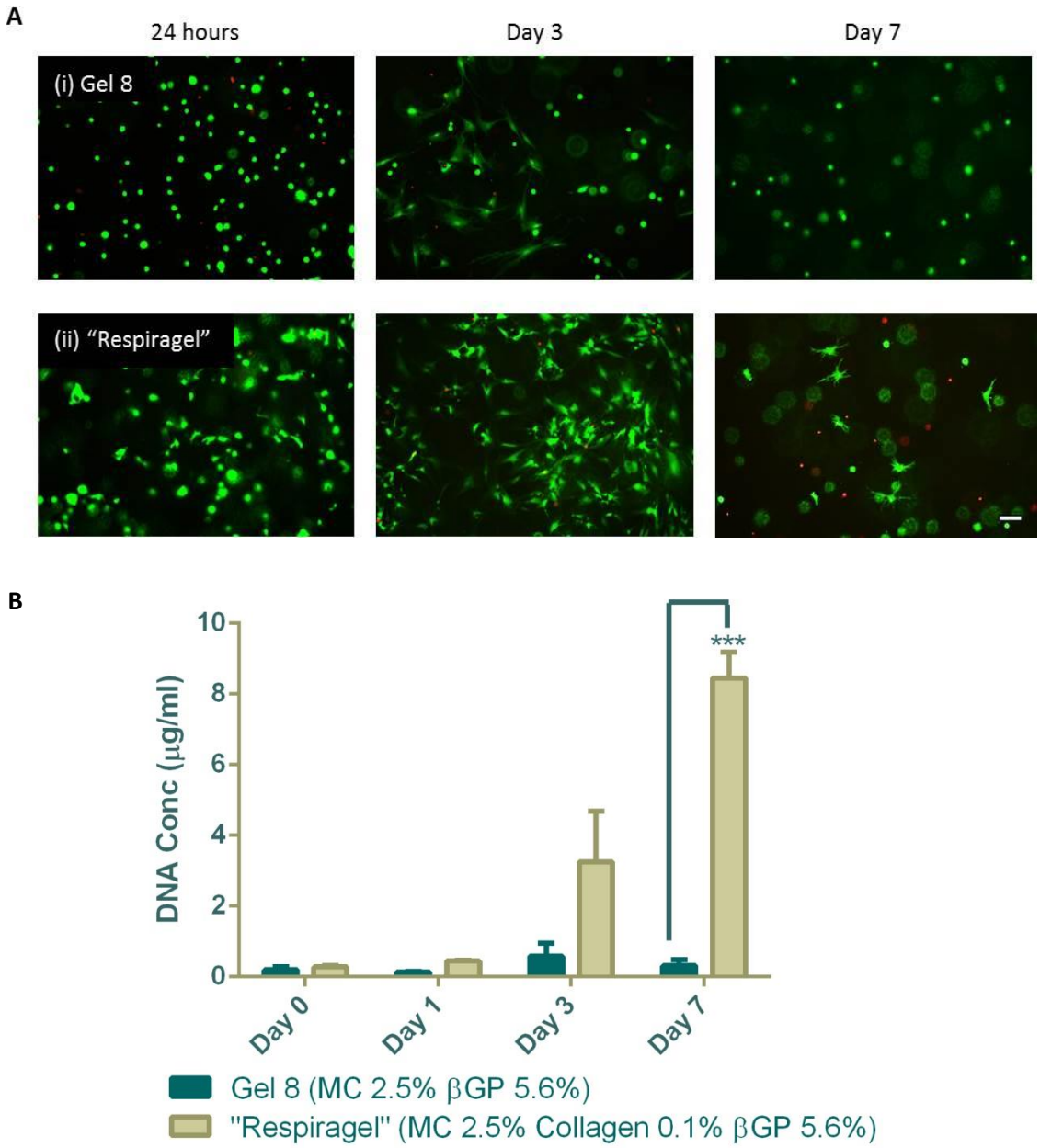

*Figure 2.7(A). LIVE/DEAD stain results: (i) 2.5% methylcellulose, 5.6% beta glycerophosphate (gel 8); (ii) 2.5% methylcellulose, 0.1% collagen, 5.6% beta glycerophosphate (Respiragel) imaged at 24 h, day 3 and day 7. Live cells are stained green, dead cells are stained red. Scale bar, 100 µm; (B) Quantification of dsDNA from hMSCs cultured in 2.5% methylcellulose, 0.1% collagen, 5.6% beta glycerophosphate (Respiragel) versus 2.5% methylcellulose, 5.6% beta glycerophosphate (gel 8) as a control. Levels of DNA are significantly higher in the collagen containing formulation. *** = P < 0.0001.*

2.3.7. Injectability of the polymer solution at room temperature

Administration of this type of delivery vehicle to a patient in a minimally invasive manner is key, and as such, it would likely be delivered using readily available medical devices such as a syringe, needle or catheter. Therefore, to determine feasibility of delivering through such devices, mechanical testing to quantify the force required to expel the formulation through them was carried out. This showed that it was possible for the polymer solution to be passed through devices including a 3 mL syringe, 3 mL syringe plus 21 G needle, and a 3 mL syringe plus catheter tubing of 0.5 m in length with an internal diameter (ID) of 0.514 mm. This diameter corresponds to the ID of a 21 G needle, which is used commonly in clinical procedures [169] (Figure 2.8A). Forces required to push the polymer solution through these devices fall below the average forces at which males can push (pinch test) [170,171] and only the catheter exceeds the force which is average for females. This result is supported by rheological flow viscosity testing of the polymer solution, which shows shear thinning properties, resulting in a rapid decrease in viscosity on application of shear stress (Figure 2.8B). On removal of the shear stress the structure recovers, indicating that this process is reversible and damage to the formulation has not occurred.

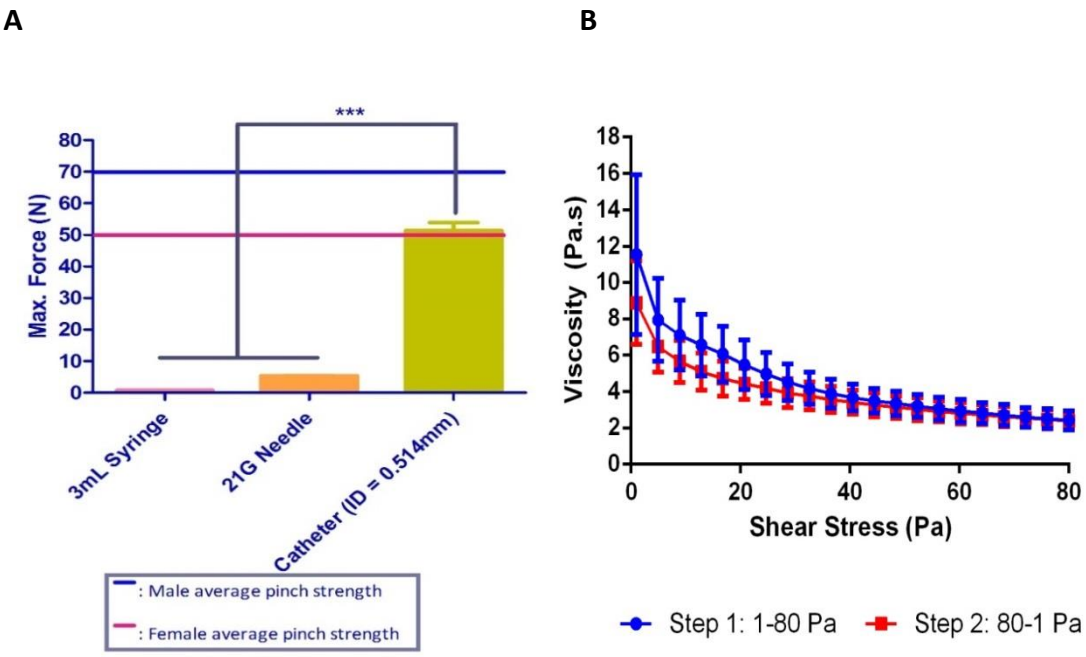

*Figure 2.8(A). Injectability study of 2.5% methylcellulose, 0.1% collagen, 5.6% beta glycerophosphate solution (Respiragel) through a 3 mL syringe, a 3 mL syringe with 21 G needle attached, and a 3 mL syringe with 21 G catheter attached, using the Zwick-Roell. Data presented shows average forces (n=6) and SE. Force required to expel polymer solution through catheter is significantly higher than that required to expel through a syringe or 21G needle. *** = P < 0.001. Male average pinch strength is 70 N, and female average pinch strength is 50 N* [170]*; (B) Assessment of viscosity of 2.5% methylcellulose, 0.1% collagen, 5.6% beta glycerophosphate solution (Respiragel), as determined by flow rheology using an AR-1000 rheometer at a constant temperature of 25°C. Results correspond with injectability data indicating that when stress is applied to the formulation, the viscosity drops; i.e. it is shear thinning in nature. Structure is recovered on removal of shear stress. Results presented as mean (n=3) and SE.*

2.3.8. Assessment of gel bolus formation in *ex vivo* rat lung tissue

In section 2.3.7, we determined that theoretically, Respiragel could be delivered through a range of clinical devices in a minimally invasive manner. We chose to confirm this through the injection of ICG-loaded Respiragel into *ex vivo* rat lung tissue. Injection of Respiragel into rat lung tissue using a 1 mL syringe with 30 G needle attached was possible using normal finger push force. On injection of the gel into the rat lung, gel can be visualised *in situ* forming a dense bolus (identified by bright yellow colouring in

Figure 2.9B. This was compared with ICG in saline (Figure 2.9C) which was observed to be delivered in a widespread manner, rather than remaining localised near the injection site. This indicates that ICG-Respiragel is able to form a gel bolus *in situ* in a superior manner to dye delivered in saline.

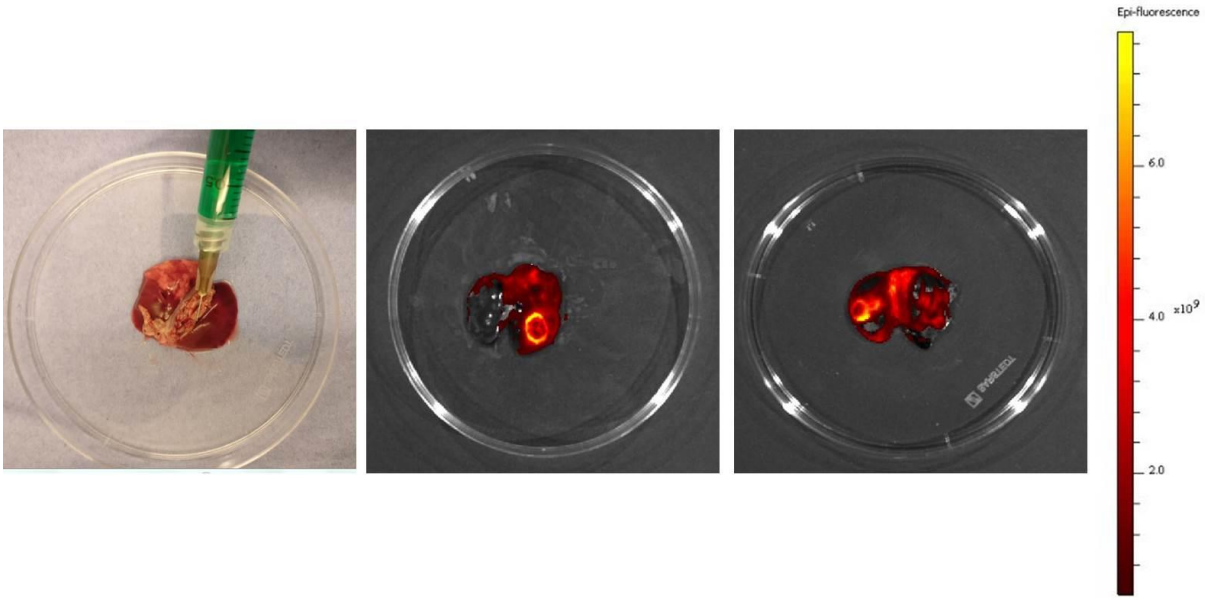

Figure 2.9(A). Injection of 0.025% ICG in Respiragel (100 µL) into ex vivo rat lung tissue using a 1 mL syringe and 30 G needle; (B) Ex vivo rat lung tissue containing ICG-Respiragel fluorescently imaged using a Xenogen IVIS imaging system 100. Highest intensity fluorescence is coloured yellow, indicating highest density of gel (or gel bolus formation); (C) Ex vivo rat lung tissue containing ICG-Saline fluorescently imaged using a Xenogen IVIS imaging system 100. Fluorescence observed in both lungs, indicating spread of dye, and lack of retention at the site of delivery.

2.3.9. Impact of sterilisation process on Respiragel formulation

2.3.9.1. Thermoresponsivity of Respiragel

In order to safely administer this type of delivery vehicle to a patient, it would need to be sterile. Therefore, with a view to the potential translatability of the formulation, Respiragel was freeze dried into a polymer wafer and subsequently sterilised using

gamma irradiation with the impact of this process being assessed. The thermoresponsivity of the irradiated Respiragel was determined as described in section 2.2.4, and was compared with the non-irradiated gel of the same composition. Rheological analysis confirmed thermoresponsivity remained at 36°C following irradiation, and storage modulus (G') was not significantly affected by this process (Figure 2.10).

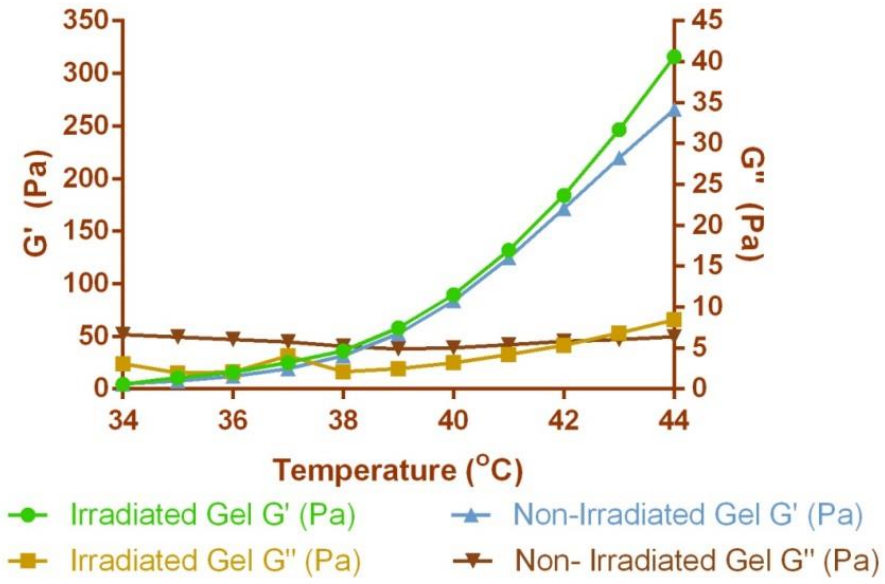

Figure 2.10. Temperature sweeps (34-45°C @ a frequency of 1 Hz and shear stress of 5 Pa) comparing irradiated 2.5% w/v methylcellulose, 0.1% collagen, 5.6% beta glycerophosphate (Respiragel) with the non-irradiated formulation of the same composition. Performed using an AR-1000 rheometer (TA Instruments).

2.3.9.2. The effect of irradiation on Respiragel ultrastructure

The morphology of the irradiated lyophilised Respiragel wafers was examined by SEM, as previously described in section 2.2.6. Image (A) in Figure 2.11 shows the uniform porous nature of the internal wafer structure, while image (B) shows the elongated pores which appeared close to the edges of the sample. These images show a densely porous structure, with a pore size of approximately 100 nm. The lyophilised polymer

structure appeared to remain intact following the irradiation process, as no difference could be observed between the irradiated and non-irradiated samples, shown in Figure 2.5 (Section 2.3.4).

A **B**

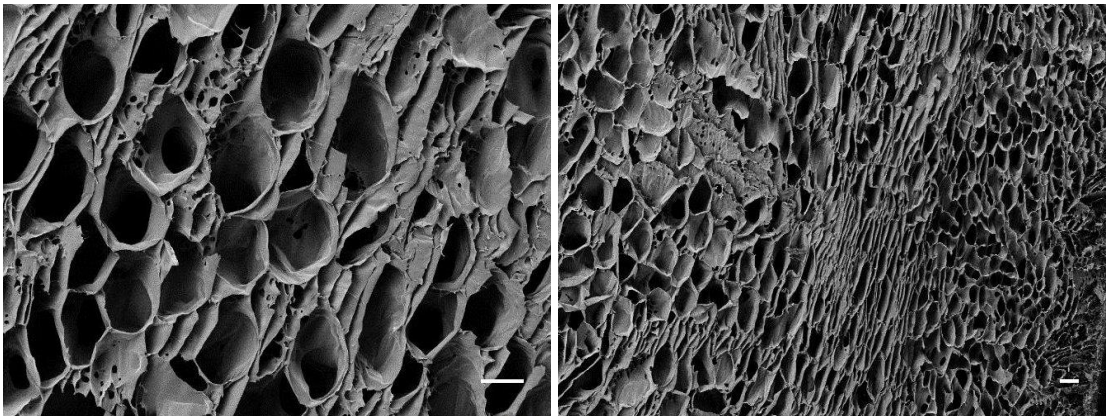

Figure 2.11. Representative scanning electron micrographs, showing internal porous structure of irradiated lyophilised Respiragel samples. SEMs were obtained using a Zeiss Supra 35VP SEM microscope (Zeiss, Jena, Germany).Image A was taken at 85X magnification and 5kV accelerating voltage, and image B taken at 40X magnification and 5kV accelerating voltage. Scale bar, 100µm.

2.3.9.3. The effect of irradiation on encapsulated hMSC viability and proliferation

The ability of the irradiated Respiragel to support encapsulated cell viability and proliferation was assessed as described in section 2.2.9, and was compared with the non-irradiated gel. LIVE/DEAD staining confirmed the presence of viable cells within the irradiated gel, with images showing a comparable spread of live cells throughout both gel formulations (Figure 2.12A). Quantification of dsDNA present in the irradiated hydrogel versus the non-irradiated hydrogel showed no significant difference between groups (Figure 2.12B). Confocal imaging was also performed on LIVE/DEAD stained hMSCs encapsulated in irradiated Respiragel versus 2.5% MC 5.6% βGP (gel 8), in order to quantify % viability of hMSCs in the hydrogel (Figure 2.12C). Respiragel shows no significant decrease in % viability up to day 8.

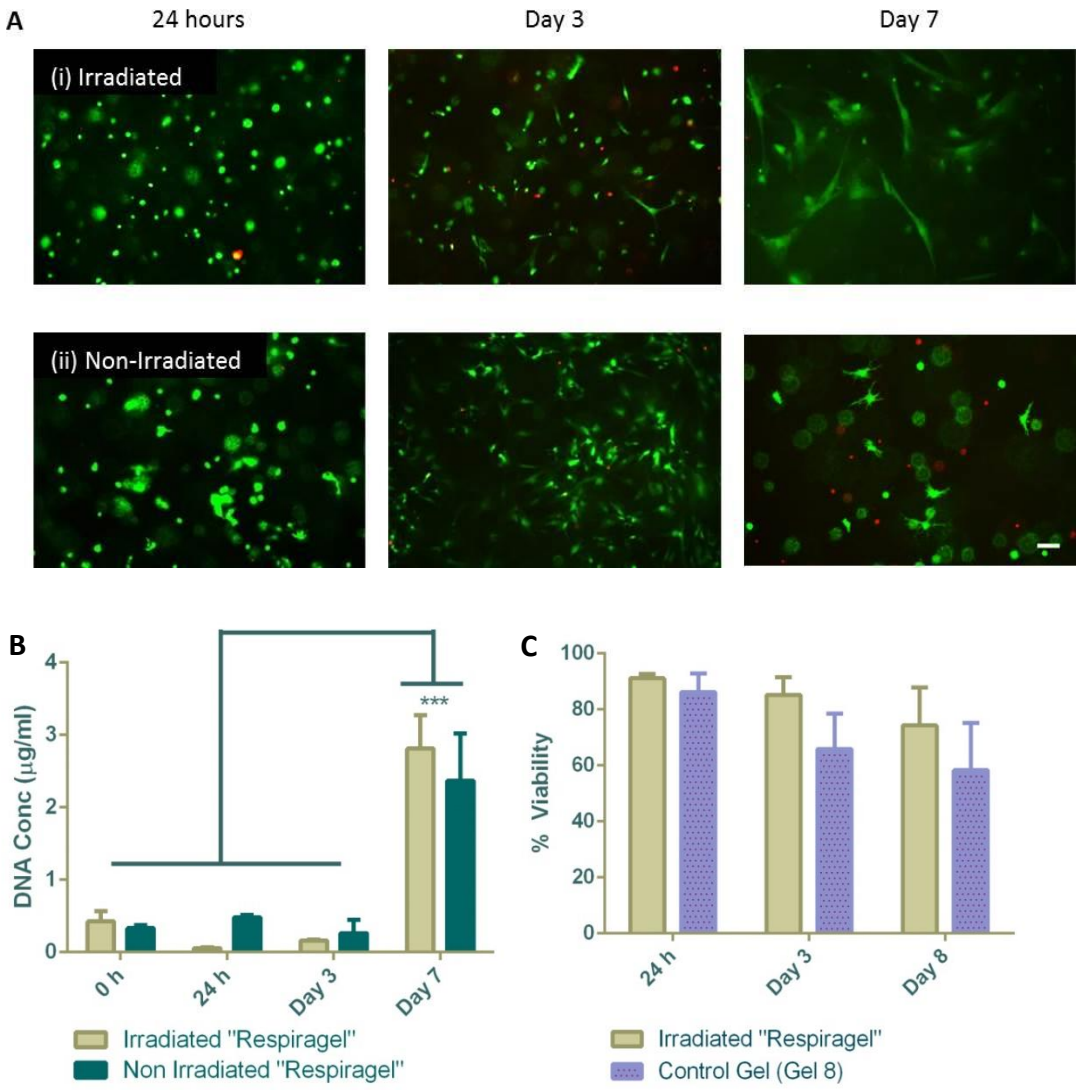

*Figure 2.12(A). LIVE/DEAD stain results of 2.5% methylcellulose, 0.1% collagen, 5.6% beta glycerophosphate (Respiragel): (i) irradiated gel; (ii) non-irradiated gel, imaged at 24 h, day 3 and day 7. Live cells are stained green, dead cells are stained red. Scale bar, 100 µm; (B) Quantification of dsDNA from hMSCs cultured in irradiated Respiragel (denoted as "Irr") versus non-irradiated gel of the same composition (denoted as "Non-Irr"). Levels of DNA are not significantly different between the irradiated and non-irradiated gels at all time points, though significantly more DNA at day 7 compared with all earlier time points for both groups. *** = P < 0.001; (C) Confocal microscopy quantification of cells using LIVE/DEAD stain. Live cells were stained green, dead cells were stained red and cells counted and quantified using a Zeiss LSM 710 confocal microscope with CellProfiler software. No significance was observed but there is a trend towards decreased viability in the control gel (gel 8) compared with irradiated Respiragel up to day 8.*

2.4.Discussion

Limitations associated with delivery of emerging cell-based therapies has resulted in the need for new and efficient systems to enable such therapies to remain in damaged tissue and exert their therapeutic benefit for extended periods. The use of biomaterial based scaffolds, which overcome these issues by behaving as a surrogate extracellular matrix, results in increased delivery of cells to the target site, helps to keep these cells localised and viable, and also enhances the production of paracrine factors, which have a role in regeneration and tissue repair [172]. This is in contrast to the injection of cells suspended in saline, the current clinical standard, which has been shown to be inferior in supporting cell retention when compared with biomaterial delivery vehicles in various studies. In research conducted by Roche *et al* [173], saline delivery of MSCs was compared with alginate or chitosan-βGP hydrogels, and collagen or alginate patches in an *in vivo* model of myocardial infarction, resulting in improved cell retention with all biomaterials above the saline control. Not only can these biomaterials support cells when *in situ*; they can also protect cells from the shearing forces associated with the injection process, which results in mechanical membrane disruption. Research published by Aguado *et al* found that injecting cells suspended in an alginate hydrogel resulted in significantly higher levels of viability post injection, when compared with delivery in a PBS control [174].

Numerous scaffolds produced from a variety of biomaterials and manufactured using a multitude of techniques have been used in the field of TE in an attempt to regenerate different tissues in the body [175–179]. There are however a number of key considerations in the selection and development of such systems. Scaffolds must be biocompatible, to prevent the possibility of an immune response in the recipient following implantation or injection. They must also be biodegradable, but equally should not degrade at a rate which causes the scaffold to collapse prematurely. In

addition to this, the scaffold should possess mechanical properties similar to those of the tissue it is being implanted into, as well as an architecture which facilitates essential processes like diffusion, the development of vasculature, and waste removal. Finally, the process must be commercially viable, and should be possible to scale-up from laboratory size to small batch production [177].

It is also important to consider the potential clinical translatability of such biomaterials. In this study, the starting materials selected are currently used in clinically available products, indicating that a formulation based on such materials could be rapidly translated – a prerequisite of the study. Delivery of the formulation in a minimally invasive manner is key, which limits the possibility of using pre-formed scaffolds, as they require surgical implantation – a significant medical procedure. Stimuli responsive hydrogels provide an alternative solution to this issue. In this study, we focused solely on temperature responsive, or thermoresponsive, hydrogels – a subsection of stimuli responsive materials. Thermoresponsive hydrogels have a number of applications in the biomedical field due to their tendency to maintain a liquid state at room temperature, thereby enabling minimally invasive administration via injection into any tissue, organ or body cavity, with the subsequent ability to rapidly form a robust gel bolus upon heating to physiological temperature [133]. Formation of a gel bolus *in vivo* allows for the potential to sustain the release of drug, stem cells or other therapeutic agents over time. Delivery of stem cells encapsulated within these hydrogels can result in protection of the cells from noxious insults in the local environment [180], and can keep cells localised and viable for extended periods, facilitating an enhanced paracrine effect. In addition to this, there is no need for surgical procedures, biological components can easily be incorporated by simple mixing and their initially flowing nature ensures proper shape adaptation resulting in a good fit with the surrounding tissue.

Development of a thermoresponsive hydrogel which exhibited specific characteristics, including a sol-gel transition temperature of approximately 37^{o}C and physiological pH,

the ability to support cell viability and proliferation, and also the ability to be delivered using standard clinical devices, was the overall goal of this study. The results presented in this chapter demonstrate that MC and collagen are able to form a thermoresponsive hydrogel in combination with βGP, and that this formulation supports encapsulated cell viability and proliferation, and can be delivered in a minimally invasive manner.

Initial formulations investigated compared the effect of various salts on the sol-gel transition temperature of 2% w/v MC (gels 1-6, Table 2.2). The sol-gel transition temperature was defined as the point at which the storage modulus (G') exceeded that of the loss modulus (G"). Of the early investigated formulations, addition of βGP produced the greatest reduction in MC gelation temperature. This is likely due to the ionic strength and anionic charge of the respective salts tested. Increasing ionic strength and higher anion charge density (i.e. 3 for phosphate present in βGP compared with 1 for chloride, present in NaCl) results in greater interaction with water molecules, thereby reducing intermolecular hydrogen bonding between water molecules and MC chains. This permits greater hydrophobic interactions between MC chains, leading to more rapid onset of gelation [157,181]. A comparison of different concentrations of βGP was undertaken (gels 4-6, Figure 2.2B), with the 5.6% w/v concentration (gel 6) resulting in the closest to optimal sol-gel transition profile (i.e. gelation at 38^{o}C).

At this point, a further gel was formulated to include 0.1% w/v collagen (gel 7, Figure 2.3A). This gel was robust, as evidenced by a high G' in temperature and time sweeps, a measure often used to indicate the internal three-dimensional structure within the gel. While this gel met our criteria in terms of sol-gel transition at physiological temperature and pH, it displayed weakened mechanical properties on advancing to cell-in-gel viability and proliferation investigations. It was hypothesised that the suspension of cells within the gel resulted in physical impediment of the gel crosslinks forming, leading to a lower observed mechanical strength. This hypothesis was confirmed on repeated rheological evaluation of the gel formulation following the

suspension of cells within it at increasing concentrations (Figure 2.6). As a result of this, a new formulation based on an increased concentration of MC to 2.5% w/v ("Respiragel") was developed and also characterised rheologically. It displayed a similar thermoresponsive profile to that of the 2% w/v gel, but reached higher storage moduli, most likely due to the increased quantity of polymer and therefore increased potential for the formation of intramolecular bonds. The results obtained from the rheological analysis of MC with βGP correspond to findings from published data, wherein a change in ionic environment lead to a lowering of the temperature at which a thermal response was observed [157,158,182]. This is believed to be due to the nature of MC gelation. MC, when dissolved in water, is thought to interact with the surrounding water molecules via hydrogen-bonding or the formation of "cage-like" structures. An increase in temperature disrupts the water-polymer forces, and allows the hydrophobic regions of the MC chains to interact. Thus, when water-polymer forces are mitigated, polymer-polymer hydrophobic forces allow the aggregation of MC molecules, which in turn subsequently allows the formation of a semi-solid. As previously mentioned, the presence of ions in solution also disrupts the water-polymer forces due to the electrostatic affinity of the ions with water molecules. This in turn allows the polymer-polymer interactions to proliferate at lower temperatures, resulting in a decrease in sol-gel transition temperature [183].

The effect of increasing concentration of MC on gelation temperature has been investigated in the literature previously [184], where it was found that a higher polymer concentration correlates with a higher sol-gel transition temperature. This is line with the results observed in our studies, where we compared two different concentrations of MC: 2.0% w/v versus 2.5% w/v, and also formulations with or without 0.1% w/v collagen present. Comparing the two formulations containing 2.5% w/v MC, the collagen containing gel (Respiragel) displayed a thermogelation temperature of 37°C, evidenced by an increase in the storage modulus at that temperature. The 2.5% MC formulation containing no collagen (gel 8) displayed a slightly higher gelation temperature of 39°C (Figure 2.3B). On comparing the two

formulations containing 2% w/v MC, the collagen containing formulation (gel 7) underwent sol-gel transition at 36°C, lower than that of the 2.5% MC formulation. In a similar manner to the 2.5% MC gel, the 2% MC formulation without collagen (gel 6) present displayed a slightly higher thermogelation temperature of 38°C (Figure 2.3A). This is likely due to a greater proportion of polymer-polymer associations to be formed, requiring more thermal energy or agitation to do so. In both the 2.5% and 2.0% MC formulations, the collagen containing gels consistently reached higher storage moduli than the no collagen control. This was expected, as previous rheological observations in the literature have indicated that the presence of increasing concentrations of collagen in gels resulted in increased storage moduli [163,185,186]. This is most likely due to the specific aggregation and cross-linking within collagen chains, which result in fibres of high strength [187]. As the storage modulus is widely reported as a measure of gel strength [188–190], this indicates improved structural integrity of the formulation when collagen is included.

While the storage modulus provides an indication of internal three-dimensional structure, it does not provide macroscopic evidence of the gel robustness. This is a key distinction to make, as some gels may reach very high storage moduli but despite this, have a tendency to dissociate within a relatively short period of time. One particular example of this behaviour is observed with Poloxamers, which can reach storage moduli in excess of 10,000 Pa [189], but due to dissociation of micelles in an excess of water, the gel integrity of Poloxamers only persists for hours to days [191,192]. In this study, assessment of diffusion of a methylene blue dye through Respiragel showed that it takes up to 24 h before diffusion occurs (Figure 2.4A). Disintegration studies also showed that Respiragel does notdisintegrate in the presence of PBS, with close to 100% of its weight retained by day 28. This was in contrast to MC 2.5% w/v alone as a control, which begins to degrade rapidly from 24 h onwards, retaining just 35% of its original weight by the final time-point (Figure 2.4B). The dye penetration and gel disintegration investigations are intended to support each other, with the disintegration study allowing for quantification of mass lost as a result of gel

breakdown; while the methylene blue dye aspect allows a visual explanation of the ability to allow for diffusion through the gel while still retaining structural integrity. These results in combination suggest that the gel formed at 37^{o}C is robust in nature, and has the potential to resist degradation in the presence of a physiologically compatible buffer system. However, further studies investigating accelerated disintegration of Respiragel using enzymes such as collagenase, would be useful to more accurately model the *in vitro* disintegration profile of the hydrogel.

hMSCs suspended within Respiragel were viable up to day 7 in culture, as assessed by LIVE/DEAD staining. In addition to this, cell proliferation was evidenced by the fact that dsDNA levels increased over the duration of the 7-day gel culture period (Figure 2.7). This is in sharp contrast to the non-collagen containing control that supported significantly lower proliferation of encapsulated cells than the collagen containing gel ($p < 0.001$). On formulating this gel, collagen was included due to its well-recognised characteristic of providing attachment sites for cells, which facilitates increased cell replication and differentiation [193]. The effect of the addition of collagen to the formulation and the consequent cell attachment is evident in the cell viability images for the collagen containing gel as stretching and spreading of the cells is clear, whereas this is not the case in the collagen free gel. The results from this study also correspond with these previous findings [163] in that cell proliferation is markedly improved in the collagen containing gel. This indicates the suitability of this material, not only as a cell delivery vector, but also as a material within which cells can remain viable and proliferate. This evidence of viability is also consistent with previous research which has shown various cell types (e.g. hBMSCs, astrocytes, and NIH-3T3 cells) being successfully cultured in gels composed of MC or collagen, or those containing βGP [158,159,162,163] highlighting the potential of this formulation as an agent of cell delivery. A useful additional experiment here would be to confirm that hMSCs remain as hMSCs following encapsulation within the gel. This could be achieved through flow cytometry, using specific hMSC markers to validate the cell type. Markers commonly

used to characterise hMSCs include the expression of CD73, CD90 and CD105, and the lack of expression of CD 14, CD34 and CD45 [194].

It should be noted here that cell seeding densities used in rheological testing of gel 7 and gel 9 (Respiragel) shown in Figure 2.6 and viability and proliferation assays shown in Figure 2.7 are substantially lower than those used previously in the literature. Much of previous research conducted into stem cell delivery focuses on their delivery *i.v.* suspended in saline which is the current clinical standard. However, as previously mentioned this leads to a huge loss of cells, with typically less than 10% cells being retained at the target site. It could be said that the large numbers of cells currently being delivered serve to overcome much of this 90% loss, and as such are far higher than may be necessary for repair. With this in mind and with the hypothesis that this hydrogel will be able to encapsulate and support cell viability and growth, it was decided that lower cell numbers would be investigated in this study.

Current medical device technology in applications such as cardiac and lung regeneration is focused on the use of novel catheter devices as a minimally invasive method of accessing damaged tissue. Catheter based methods have been used in various clinical trials such as the DREAM-HF trial (on-going), the C-CURE trial (completed) and the CHART1 and CHART2 trials [195]. In addition to this, medical device companies such as Olympus and Boston Scientific are developing advanced transbronchial needles and flexible bronchoscopes which provide access to the distal airways, showing the possibilities for delivering formulations to hard-to-reach areas. With translatability of our formulation in mind, we assessed the potential for syringing of the polymer solution in terms of force required for the gel to be expelled. Injectability testing showed that it was possible for the solution to be passed through a range of common clinical devices including a 3 mL syringe, 3 mL syringe plus 21G needle, and a 3 mL syringe plus 0.5 m catheter (Figure 2.8A). Results confirmed that the Respiragel formulation can be pushed through all three devices. Forces required fall below the average at which males can push (pinch test) [170], and only the catheter

falls at the threshold of force which is average for females, though these forces can be lowered further by slowing the speed of injection. This result is supported by flow viscosity testing of the formulation, which shows the solution has shear thinning properties, resulting in a rapid decrease in viscosity on application of shear stress. On removal of the shear force, it is able to recover its original structure, and is not adversely damaged by the shear thinning process. In addition to this, all *in vitro* cell-in-gel experiments in this study (i.e. data shown in Figure 2.7 and Figure 2.12) were carried out via syringing the cell loaded formulation through a 21G needle into inserts prior to culture and viability and proliferation assessment. This showed no adverse effects on cell viability, indicating that the gel is acting as a protective scaffold for the cells, preventing shear related damage which often occurs with cells delivered in saline [174].

Data from injectability assessment was supported by further studies in which ICG loaded Respiragel was injected into *ex vivo* rat lung tissue in order to assess depot formation and retention at the site of delivery (Figure 2.9). Injection of Respiragel into rat lung tissue could be performed manually, supporting the data presented in Figure 2.8 suggesting Respiragel could be delivered using forces falling below the male and female average push strength. Following injection of ICG Respiragel into the *ex vivo* lung tissue, fluorescent imaging using an IVIS showed the gel to remain *in situ*, with a high density of gel at the injection site (evidenced by the high fluorescent signal at this location). A lower fluorescent signal can be observed around the site of injection, which indicates some spreading of the gel (or release of the dye). It is possible that the gel did not undergo gelation as quickly as required, though in this instance, the lungs had been *ex vivo* for some time prior to injection (~ 15 mins), thus would no longer have been at 37^{o}C, possibly explaining the slight spreading from the injection site. Injection of ICG in saline however, results in a large amount of spreading from the injection site, with dye being visualised in both lungs. This data supports the hypothesis that biomaterials demonstrate improved retention at the site of delivery when

compared with saline, and also highlights the promise for this formulation for *in vivo* delivery.

Sterility of any type of delivery vehicle for administration to a patient is of utmost importance. Therefore, with a view to the potential translatability of the formulation a method for sterilisation was investigated. Autoclaving, which is the clinical standard for sterilisation, cannot be used for this formulation due to the resultant thermal denaturation of the collagen proteins [187] and therefore the lyophilised polymer wafers were sterilised using gamma irradiation. Rehydration of the wafers in sterile βGP 5.6% w/v solution under aseptic conditions maintained sterility of the formulation. Rheological assessment reconfirmed the ability of Respiragel to undergo sol-gel transition at physiological temperature post sterilisation, with no effect on the resulting storage modulus obtained (Figure 2.10). This indicates that the irradiation process does not negatively impact on the formulations physicochemical characteristics. This is supported by SEM images of the lyophilised Respiragel wafers pre- and post-irradiation, which showed no evidence of structural changes as a result of the sterilisation process (Figure 2.11). A comparative study of cell viability and proliferation in the irradiated gel versus the non-irradiated gel was also conducted, in order to establish whether the sterilisation process affects the ability of the gel to support cells suspended within the gel. Cell viability was again assessed using LIVE/DEAD staining. Results show no difference in cell viability between the two groups at all time points. This correlates with the results of the proliferation assay (Figure 2.12B), again measuring dsDNA. While there is a statistically significant increase in proliferation from day 3 to day 7 for both groups, there is no significant difference in proliferation between the two groups, supporting the hypothesis that irradiation can be used as a method to successfully sterilise this formulation without negatively impacting on its ability to support encapsulated cells.

Review of the literature surrounding gamma irradiation of polysaccharide based hydrogels indicates that sterilisation by this method can lead to degradation of the

polymer, observed previously in the case of chitosan and alginate. In the case of such materials, gamma irradiation causes degradation by free-radical induced incision of glycosidic bonds and a subsequent decrease in molecular weight [196]. Due to the structure of MC also containing repeating units linked together by glycosidic bonds, one would potentially expect it to degrade in a similar manner. However, this was not observed in this study, which may be attributed to other MC characteristics outweighing the possible degradation. In one previous study, it was found that dose of gamma irradiation applied to the chitosan and alginate (0-200 kGy) affects the degree of degradation (measured by determining molecular weight), with increased doses leading to a corresponding increase in degradation [197]. It was found that doses up to 50 kGy led to decrease in molecular weight, after which point, the degradation appears complete and no further breakdown occurs. In the research presented in this manuscript, the dose specified by the European Pharmacopoeia for sterility, i.e. 25 kGy, was used. As this is a relatively low dose of irradiation it is possible that perhaps partial rather than full degradation may be expected. The effect of varying the concentrations of polymer solution on irradiation induced degradation was also investigated in the chitosan/alginate study, with a range of 0.1-2% with chitosan and 0.5-8% with alginate being investigated. For both polymers, it was found that decreasing concentration corresponds with an increase in degradation. In our research, we use a 2.5% MC solution. Given that this is a somewhat intermediate concentration of polymer (in comparison with the alginate and chitosan concentrations), the density of glycosidic bonds may correspond with less apparent degradation effect. It is also noted in this study that the dose required to cause degradation in chitosan is lower than the dose required to cause similar degradation in alginate. This observation is linked to the initial polymer molecular weight of chitosan being lower than that of alginate. It is of worth to note here that the MC used in this study was “high viscosity” and according to the manufacturer’s literature, this corresponds to an approximate molecular weight of 88,000 g/mol, with lower viscosity alternatives ranging from 14,000-63,000 g/mol. Both alginate and chitosan have far lower molecular weights

than the MC used in our research, indicating that this density of glycosidic bonds may be sufficiently significant to resist degradation by gamma irradiation. This is not to say that no bond cleavages and degradation has occurred – however, it is possible that these bond cleavages were not so widespread as to adversely affect the observed gelation (Figure 2.10).

2.5.Conclusion

A growing body of evidence relating to the failure of stem cell delivery indicates the need for new methods to enable therapies to remain *in situ* for extended periods, in order to maximise their regenerative capabilities. The results of this chapter show the formulated hydrogel to fulfil important criteria for potential use as an injectable stem cell delivery modality. A 2.5% w/v MC, 0.1% w/v collagen, 5.6% w/v βGP gel ("Respiragel") displayed a suitable thermoresponsive profile for use as an injectable gel, which was capable of supporting hMSC viability and proliferation. This gel was structurally robust, as evidenced by a high G' in temperature sweeps, and permitted the slow diffusion of methylene blue dye through its structure. The gel also resisted disintegration in the presence of PBS, a physiologically compatible buffer system, over the course of a 28-day investigation. In an effort to ascertain the potential translatability of this formulation in a clinical setting, injectability studies confirmed the ability of the polymer solution to be delivered using a syringe, needle or catheter, findings which were supported by flow rheology; a process which also resulted in no negative impact on physicochemical characteristics or ability to support cell growth. These results indicate that devices such as these may be a possible means of delivery of this hydrogel in a clinical setting in the future, and shows the potential translatability of injectable hydrogels, such as the formulation described in this study. Finally, the freeze dried polymer wafer was subjected to sterilisation by gamma irradiation, which was shown to have no effect on the thermoresponsivity of the gel, or its ability to support hMSC viability and proliferation. This chapter represents proof of concept research for the use of a MC and collagen based hydrogel in the delivery of stem cells, while requiring further application and investigation in both *in vitro* and *in vivo* disease models in order to advance the field of stem cell therapies combined with biomaterials.

3. Chapter 3; Development and physicochemical characterisation of synthetic linear and star shaped co-polypeptide based hydrogels

3.1.Introduction

The overall goal of this thesis was to develop materials suitable for minimally invasive delivery of cells and drugs as therapeutic agents, for use in applications in which currently utilised strategies are suboptimal and in which loco-regional delivery might enable significant enhancement of clinical outcomes. In Chapter 2 of this thesis, we established that a thermoresponsive methylcellulose, collagen and beta glycerophosphate based hydrogel could support cell viability and proliferation *in vitro* and could be delivered in a minimally invasive manner. In this chapter, we aimed to replicate this process for assessment of novel synthetic hydrogels, in order to develop a catalogue of materials which could be used for cell or drug delivery applications. Bioactive synthetic hydrogels have recently emerged as promising scaffolds due to the fact that they can provide molecularly tailored biofunctions and adjustable mechanical properties, as well as an extracellular matrix-like microenvironment for cell growth and tissue formation [198].

Arguably the most well characterised and investigated synthetic polymers to date are Pluronics® or poloxamers (poly(ethylene oxide)–poly(propylene oxide)–poly(ethylene oxide) (PEO–PPO–PEO) tri-block copolymers), which have been discussed previously in section 2.1 with reference to their thermoresponsive behaviour. Limitations associated with the use of Pluronic® based hydrogels have already been mentioned, such as their weak mechanical properties, rapid erosion and intrinsic instability, which originate from the weak hydrophobic interactions between the PPO blocks [148]. In addition to this, these block copolymers are not biodegradable, which prevents the use of high molecular weight materials since they cannot pass the kidney membranes. Poly(N-isopropylacrylamide (pNiPAAm) based hydrogels are also thermoresponsive undergoing sol gel transition at approximately 30-34^{o}C [199], and can be co-polymerised through the use of other more hydrophilic monomers such as butyl methacrylate in order to tune the gelation temperature [200]. However, despite the

promise shown by thermoresponsive synthetic polymers such as these, clinical translation of pNiPAAm based hydrogels has been limited due to uncertainties surrounding the biocompatibility of the monomers and cross-linkers used in their synthesis [132]. In addition to this, the polymers of pNiPAAm and its derivatives are not biodegradable resulting in concern that a "foreign body" polymer bolus may remain *in situ* leading to potential inflammatory reactions [201]. The perception that acrylamide based polymers activate platelets on contact with blood, has also led to difficulties in securing FDA approval [202].

Disadvantages such as those associated with current synthetic polymer forming hydrogels, has resulted in a need for novel, advanced polymers capable of circumventing these issues. A promising class of materials is that of synthetic hydrogels obtained by self-assembly of amphiphilic polypeptides. Amphiphilic peptides can self-assemble into a supramolecular hydrogel matrix through non-covalent interactions such as hydrogen bonding, electrostatic interactions, pi-stacking and hydrophobic interactions when placed in an aqueous medium [203]. Such hydrogels are of interest generally, as their arrangement can be rationally designed to be highly specific, tuneable, and reversible and thereby contribute distinct and useful properties that have thus far been unrealised in traditional biomaterials [204]. In addition to this, their composition of chains of naturally occurring amino acids linked by conventional peptide bonds renders them as biologically inspired (bioinspired) and confers natural biodegradability [205]. Star shaped self-assembling co-polypeptide based polymers will be the focus of this chapter, synthesised via an N-carboxyanhydride (NCA) polymerisation reaction.

The synthesis and polymerisation of NCAs was first reported in 1906 by Hermann Leuchs [206]. NCAs are anhydrides of α-amino acids and are commonly synthesised through the use of chlorinating agents to cyclize the amino/carboxylic functionality on the α-carbon (Figure 3.1). The NCA ring is then opened through a further reaction, thus permitting the synthesis of poly(amino acids) or polypeptides [207,208].

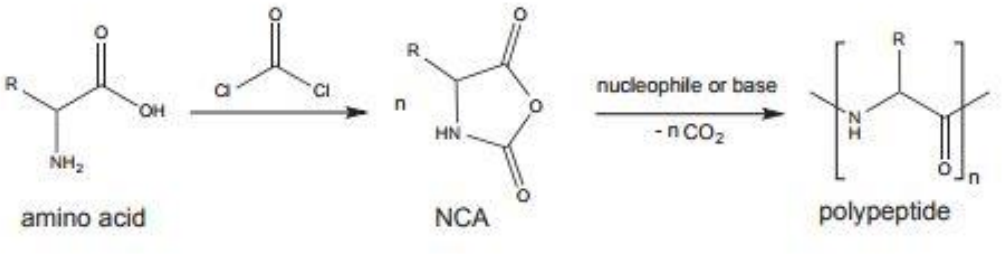

Figure 3.1. Synthesis of amino acid N-carboxyanhydrides (NCA) from phosgene and subsequent NCA polymerisation. Reproduced from [215].

Star-shaped or branched polypeptides describe a particular architectural class of polypeptides consisting of a number of linear polypeptide chains or "arms" bound to a central core. The molecular weight and number of polymeric arms can be tightly controlled by the choice of the polymerisation reaction method and the initiator (Figure 3.2) [209]. Such polypeptides can be generated via the divergent method, where arms are attached to a pre-synthesised core, or by the convergent method, whereby pre-synthesised linear polymeric arms are attached to a core via a linking agent [207]. Star-shaped hydrogels offer advantages over their linear counterparts in that their highly branched star architecture allows for superior intermolecular physical interactions between the adjacent hydrophobic moieties [210]. In this Chapter, corresponding linear polypeptide based hydrogels will be used to identify what effect, if any, star-shaped architecture has on hydrogel physicochemical characteristics.

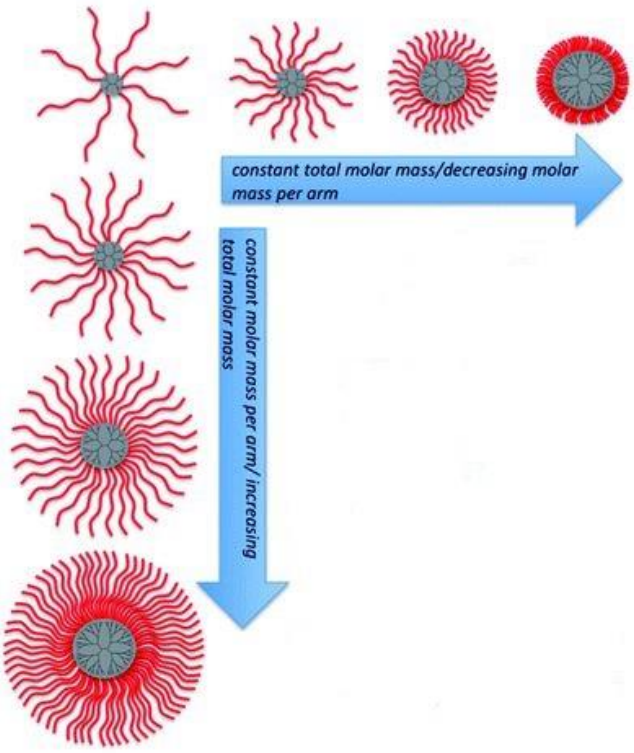

Figure 3.2. Diversity of synthesised star polypeptides resulting from NCA polymerisation reaction – number and length of "arms" and molecular weight may be varied, producing a library of polymers. Adapted from [211].

To date, star-shaped polypeptides have been investigated for numerous applications, including gene, protein and drug delivery [209][212–214]. Generally, this has been in the form of nanoparticles, due to electrostatic interaction of the star-shaped polymer with oppositely charged materials inducing nanoparticle formation. Star shaped polypeptides have been reported as particularly promising in their role as gene delivery vectors, due to their cell transfection capabilities combined with reduced associated toxicity and immunogenicity when compared with traditional viral gene vectors [209,215–217]. However, research into star-shaped polypeptide based hydrogels is still very much in its infancy, with very few instances of their development being reported in the literature [210,218,219]. Research conducted by our team in Murphy *et al* [210]

reported on the development of a range of 8-arm star-shaped diblock co-polypeptides and the investigation into their potential as self-assembling amphiphiles in aqueous media. We found the star-shaped block co-polypeptides (which were synthesised by sequential NCA polymerisation from a polypropylene imine (PPI) dendrimer core) to spontaneously self-assemble into hydrogels at a low polymer concentration of 2 wt%. The hydrogels were investigated for their viscoelastic properties revealing a strong structure dependence of the hydrogel strength. The highest gel strength was achieved with the star block co-polypeptide containing the poly(L-phenylalanine) outer blocks. We concluded that the versatile synthetic process enables straightforward modification of the hydrophobic sequence, which can be utilised to modulate the mechanical strength for various applications. Research conducted by Shen *et al* [218] also synthesised a series of star-shaped polypeptides by ring opening polymerization (ROP) of an L-glutamate based NCA. These star-shaped polymers could spontaneously form hydrogels instead of micelles in water at low concentration. They found that the critical gelation concentration (CGC) and hydrogel strength displayed a stronger dependence on arm numbers than the arm length under similar conditions, and that these properties could be easily modulated. The hydrogels showed shear thinning and rapid recovery properties. Finally, Thornton *et al* [219] reported on the generation of a range of star-shaped block copolymers composed of a biocompatible PEG core tethered to a polyalanine (PAla) shell, that possesses the capability to self-assemble in water. The hydrogels formed were able to withhold encapsulated albumin for prolonged periods before its triggered release following targeted material degradation by the proteolytic enzyme elastase. The authors concluded that the materials formed offer significant promise for the delivery of proteins, and possibly inhibitors, in response to a proteolytic enzyme overexpressed in chronic wounds, demonstrating their usefulness in biological applications.

Two polymers synthesised via NCA polymerisation will be compared in this Chapter – firstly, a star-shaped co-polypeptide based on lysine and tyrosine amino acids, denoted by PPI-G2(8)-PLL_{50}-b-PLT_{10} (or Star-PLL-PLT) and secondly the corresponding linear co-

polypeptide, also based on lysine and tyrosine, denoted by AA-PLL_{200}-b-PLT_{25} (or Linear-PLL-PLT). Lysine and tyrosine were selected as amino acids for use in these hydrogels due to their biodegradability, and also due to the promise shown from previous work conducted in this group [210], which this thesis Chapter aimed to build on. In order to clarify the nomenclature associated with such polymers, the components are explained as follows. Taking PPI-G2(8)-PLL_{50}-b-PLT_{10} as an example (Figure 3.3):

PPI	Polyproylene imine, a dendrimer, used as the core of the polypeptide. Dendrimers are nano-sized, molecules with well-defined, homogeneous, and monodisperse structure that typically have a symmetric core, an inner shell, and an outer shell [220]
G2	The generation number of the PPI dendrimer used, indicating that the branches are joined to the second nitrogen in the PPI core
(8)	The total number of arms on the dendrimer
PLL_{50}	The PLL refers to $poly_L$lysine, with the number in subscript indicating the total number of lysine units per arm – i.e. in this case, there are 50 lysine units per arm
b	Represents block, and indicates that there is a distinct block of repeating units of the first amino acid, followed by a distinct block of repeating units of the second amino acid
PLT_{10}	$Poly_L$tyrosine, of which there are 10 units per arm, the first of which is attached to the final lysine unit
AA	Allylamine, the initiator for the linear co-polypeptide

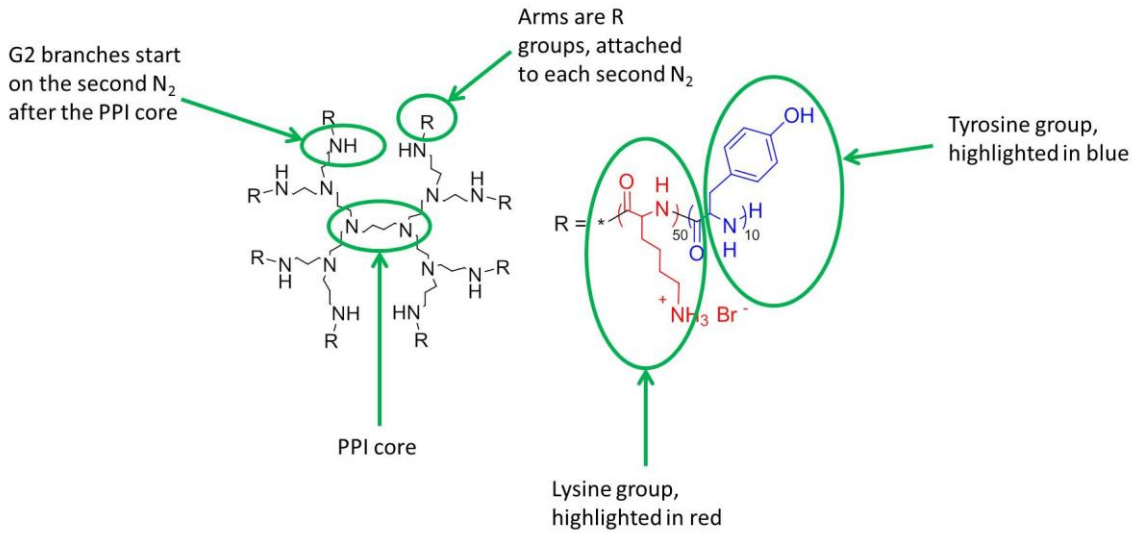

Figure 3.3. The structure of PPI-G2(8)-PLL$_{50}$-b-PLT$_{10}$, with each subgroup identified.

Objectives

The overall objective of this Chapter was to investigate the potential of star-shaped and linear co-polypeptide based hydrogels as an alternative cell delivery vector capable of supporting minimally invasive delivery.

- The first objective of this Chapter was to rheologically characterise the star-shaped and linear co-polypeptide based hydrogels.
- The second objective was to investigate the injectability of the hydrogel formulation, in order to ascertain whether it would be deliverable in a clinical setting.
- The final objective of this Chapter was to determine if the hydrogel was capable of supporting hMSC viability.

3.2.Materials and Methods

3.2.1. Materials

Star-PLL-PLT and Linear-PLL-PLT polymers were synthesised by Robert Murphy in the Translational REsearch for Nanomedical Devices (TREND) Group in RCSI. All other chemicals were obtained from Sigma Aldrich (Ireland) unless otherwise specified.

3.2.2. Polymer synthesis

Synthesis of the Star-PLL-PLT polymer followed an NCA polymerisation reaction. Specifically, ε-carbobenzyloxy-$_L$-lysine NCA (2.37 g, 7.74 mmol) was dissolved in 35 mL of anhydrous chloroform ($CHCl_3$) under a N_2 atmosphere in a Schlenk flask. It was stirred in a temperature controlled oil/water bath at 0°C. G2 poly(propylene imine) (PPI) dendrimer (14.96 mg, 1.94×10^{-2} mmol) was prepared in 2 mL of dry $CHCl_3$, and quickly charged to the flask via syringe. The solution was allowed to stir for 24 h at 0°C. Fourier Transform Infrared Spectroscopy (FT-IR) analysis was utilised to confirm consumption of NCA monomer. A sample was taken directly via syringe to monitor the molecular mass using gel permeation chromatography (GPC). The NCA of benzyl-$_L$-tyrosine (461.52 mg, 1.54 mmol) was then dissolved in 5 mL anhydrous $CHCl_3$ and charged to the flask via syringe. The solution was allowed to stir at 0°C until all of the NCA monomer was consumed as confirmed by FT-IR. The polymer was precipitated into excess diethyl ether and dried under vacuum in a dessicator (yield 89%). 1 g of the polymer was dissolved in 11 mL of trifluoroacetic acid (TFA) and allowed to stir for 1 h. 5 mL of hydrogen bromide (HBr) 33% wt in acetic acid was added drop wise to the solution in a six-fold excess with respect to the protecting groups of L-lysine and L-tyrosine and was allowed to stir for 15 h. The polymer was precipitated twice into diethyl ether (40 mL) and centrifuged. The TFA/diethyl ether waste was decanted and the precipitate was washed once more with diethyl ether. The polymer was dried under vacuum and then subsequently dissolved in deionised water. Dialysis was

performed against deionised water for 4 days using a 10,000 MWCO membrane, with frequent water replacement. The polymer was then lyophilised (yield 65%) (Figure 3.4).

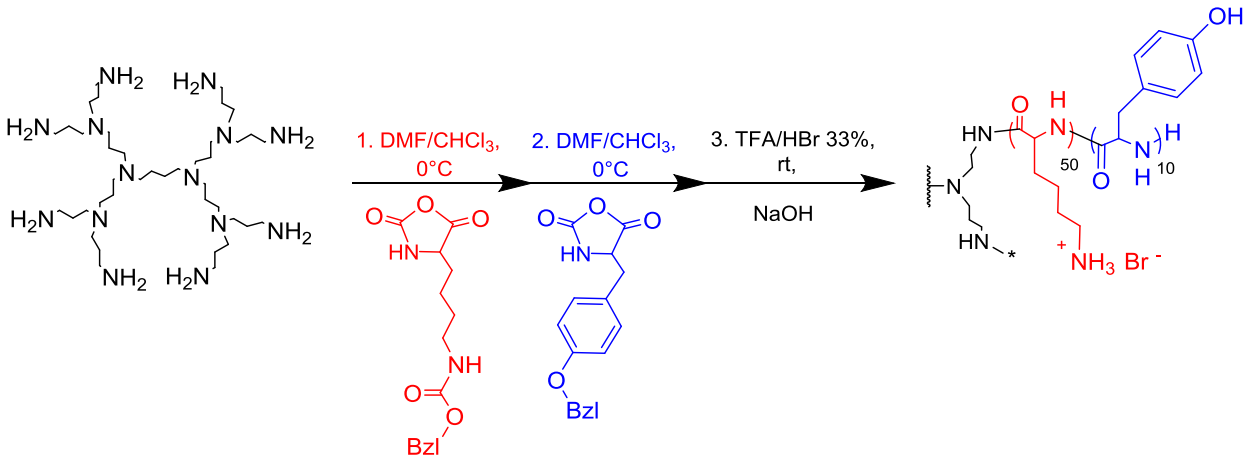

Figure 3.4. Schematic representing synthesis of the Star-PLL-PLT polymer using N-carboxyanhydride (NCA) polymerisation reaction. Initiation of reaction uses G2 PPI dendrimer (shown in black) + NCA carbobenzyloxide-L-lysine (in red) in the presence of $CHCl_3$ at 0^oC. The second step involves the addition of NCA benzyl-L-tyramine (in blue) in the presence of $CHCl_3$ at 0^oC. The final step used TFA and HBr to de-protect the amine or carboxylic acid functionalities.

The same general reaction was carried out to synthesise the Linear-PLL-PLT block co-polypeptide; however, in that case it was prepared using allylamine as an initiator (Figure 3.5).

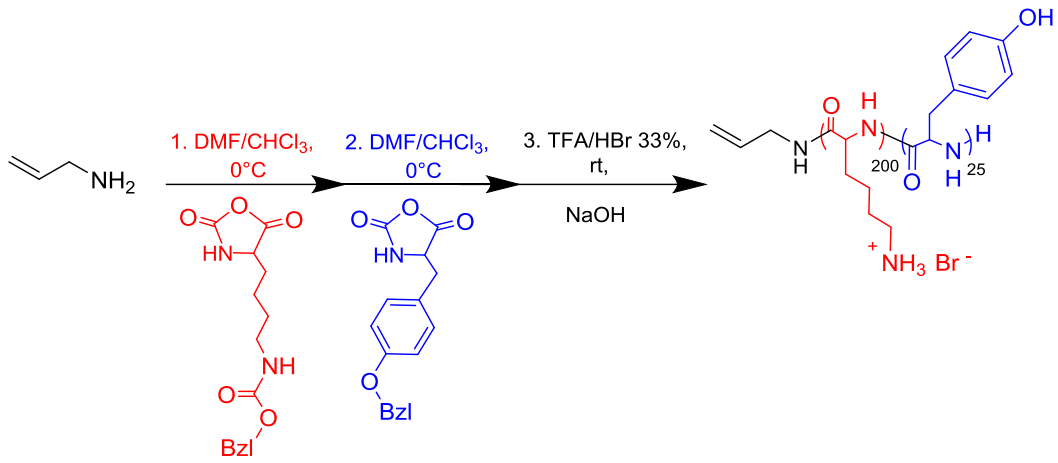

Figure 3.5. Schematic representing synthesis of the Linear-PLL-PLT polymer using N-carboxyanhydride (NCA) polymerisation reaction. Initiation of reaction uses allylamine (shown in black) + NCA carbobenzyloxide-L-lysine (in red) in the presence of $CHCl_3$ at 0°C. The second step involves the addition of NCA benzyl-L-tyramine (in blue) in the presence of $CHCl_3$ at 0°C. The final step used TFA and HBr to de-protect the amine or carboxylic acid functionalities.

3.2.3. Hydrogel formation

Gelation was performed through the addition of deionised water to the polymer in a glass beaker at a polymer concentration of 3 wt%. The mixture was left at room temperature until it appeared visually that gelation had occurred.

3.2.4. Rheological testing

The rheological properties of co-polypeptide based hydrogels were assessed using an AR-1000 cone and plate rheometer (TA Instruments, USA) under two modes, oscillatory and flow. Investigation into whether the hydrogels exhibited a thermoresponsive change in structure was assessed using an oscillatory temperature sweep with storage modulus (G') being used as an indicator of internal gel structure. Gelation was defined at the point at which the storage modulus (G') exceeded that of the loss modulus (G''). A time sweep was conducted to determine whether structural changes would occur in a time dependent manner, as were oscillatory strain sweeps (determining structure as

a function of % strain). Finally, the hydrogel was tested under a flow procedure, to measure viscosity as a function of shear stress. Assessments at increasing temperatures over time employed a solvent trap to prevent dehydration of the sample. Parameters for each rheological test are shown in Table 3.1.

Physical gelation was also observed visually (for both Star-PLL-PLT and Linear-PLL-PLT hydrogels) via an inverted tube test [221]. If the material remained in the bottom of the vial for thirty seconds following inversion, gelation was confirmed.

Table 3.1. Rheological characterisation parameters for testing of Star-PLL-PLT and Linear-PLL-PLT hydrogels.

Rheological Test Type	Temperature	Frequency	Shear Stress	Time
Oscillatory Temperature Sweep	25-45°C @ 1 °C/min increments	1 Hz	5 Pa	N/a
Oscillatory Time Sweep	37°C	1 Hz	5 Pa	30 min
Oscillatory Strain Sweep	25°C	1 Hz	5 Pa	N/a
Flow Steady State	25°C	1 Hz	1 – 80 Pa	N/a

3.2.5. Gel diffusion and disintegration testing

Robustness of the Star-PLL-PLT and Linear-PLL-PLT structures was assessed by evaluating disintegration of the gel (3 mL) over time in the presence of 1 mL phosphate buffered saline (PBS) pH 7.2, when placed in a shaking water bath at 37°C and 75 RPM. At each time point the PBS was removed and gel disintegration determined by weighing the tube and determining mass loss of gel.

The ability of compounds to diffuse through the formed gel over time was determined by adding 1 mL of a 0.01% w/v methylene blue solution (molecular weight (MW) = 319.85 g/mol) to 5 mL gel in a falcon tube, which had previously been allowed to equilibrate at 37°C in a thermostatically controlled water bath and shaking at 75 RPM. A visual inspection to determine dye penetration through the gel was performed every hour up to 4 hours, and also at 24 hours and relevant photographs taken to record each time point.

3.2.6. SEM of lyophilised polymer samples

Lyophilised Star-PLL-PLT and Linear-PLL-PLT polymer samples were examined using scanning electron microscopy (SEM) in order to evaluate their morphology and internal pore size. Following lyophilisation, samples were mounted to an aluminium stub using a carbon paste and sputter coated with gold. Imaging of the freeze dried hydrogels was performed using Hitachi S2600N Variable Pressure Scanning Electron Microscope (Hitachi, Tokyo, Japan).

3.2.7. Assessment of hydrogel injectability

Uniaxial compression tests were conducted to determine the force required to expel the Star-PLL-PLT and Linear-PLL-PLT hydrogels from a 1 mL syringe. All testing was carried out using a Zwick mechanical testing machine (Z050, Zwick/Roell, Germany), fitted with a 50 N load cell. The plunger of the syringe was attached to the load cell using a custom-built adapter. This adapter was used to apply a constant feed-rate, corresponding to 12 mm per 200 µL injection, to the plunger of the syringe.

Hydrogel samples were loaded into a 1 mL luer-lok syringe (BD, Dublin, Ireland) before injectability testing. Initially, determination of the maximum force required to expel the solution through this space was performed. This was repeated following attachment of a 21 G needle (BD, Dublin, Ireland) to the syringe, and finally a catheter of internal

diameter (ID) 0.514 mm attached to the syringe. A pre-load (preliminary force) of 1 N was applied for all tests and the end of test was determined to be the maximum extension (12 mm); the distance equivalent to 200 µL of solution (measured using Vernier's callipers). The force profile per injection was recorded.

3.2.8. hMSC culture

hMSCs were isolated and cultured as previously described in Chapter 2, section 2.2.7.

3.2.9. Evaluation of encapsulated hMSC viability

hMSCs were suspended in Star-PLL-PLT and Linear-PLL-PLT hydrogels at a density of 5 x 10^5 cells/ mL. This was aspirated into a 3 mL syringe and 300 µL volumes were expelled through a 21G needle to form droplets in Costar Transwell Inserts (Fisher Scientific, Ireland) with an 8 µm pore size and diameter of 6.5 mm, for insertion into 24 well plates. 2 mL normal hMSC growth media per well was added to each well and plates were returned to the incubator. Media was replaced every two days.

Cells were cultured in gel for 7 days and the droplets were stained with LIVE/DEAD stain (Molecular Probes, Invitrogen, Ireland) according to the manufacturer's protocol at 24 hours, day 3 and day 7, to assess cell viability over time. The droplets were visualised by fluorescence microscopy using a Leica DMIL microscope (Leica Microsystems, Switzerland). Live cells were stained green with green-fluorescent calcein-AM and dead cells were stained red with red-fluorescent ethidium homodimer-1.

At the same time points (24 h, day 3 and day 7), Cell Counting Kit 8 (CCK-8) assay was performed according to the manufacturer's instructions in order to quantify cell viability. Briefly, 10% CCK-8 reagent was added to media in each well with cells/gel still present, and plates were returned to the incubator for 2 h to react. Blank gel, containing no encapsulated cells, was used as a control. 100 µL of each sample was

plated per well, in triplicate, on a clear 96 well plate, and absorbance of the samples was measured at 450 nm using a Varioskan Flash multimode microplate reader (Fisher Scientific, Ireland). Percent viability was then calculated using the following equation:

Þ ὠ῎Ω ῶ ὦ῎Ωὰ῎Ωὸ ώ (ö ὦ ἱ ... ö ὦ ἱ ...) / (ö ὦ ... ö ὦ ἱ ...) ρ π π

Equation 3.1. Equation for calculating % cell viability using a CCK-8 assay.

3.2.10. Statistical analysis

Two-way ANOVA followed by Tukey's post-hoc analysis was used to compare forces required to perform injections within each hydrogel group in section 3.2.8, whereas Sidak's test was used to compare the differences in forces between the two hydrogels. Two-way ANOVA followed by Tukey's post-hoc analysis was also performed to determine statistical differences in cell/gel studies described in section 3.2.9. All tests were performed using GraphPad Prism v6 (GraphPad Software Inc., CA, USA). Error is reported as standard error of the mean (SE) and significance was determined using a probability value of $p < 0.05$. Due to difficulty in synthesising adequate quantities of polymer, technical repeats were performed as n=3, but experimental repeats were performed as an n=1.

3.3.Results

3.3.1. Rheological characterisation of Star-PLL-PLT and Linear-PLL-PLT hydrogels

Rheological testing was performed in order to characterise the viscoelastic properties of the Star-PLL-PLT and Linear-PLL-PLT hydrogels. As both of the polymers spontaneously gelate at room temperature on addition of dH_2O it was presumed that they were not thermosensitive. This was confirmed using a temperature sweep, assessing changes in storage (G') and loss (G") modulus from 25-45^oC, with data from the Star-PLL-PLT hydrogel shown in Figure 3.6A. At 25^oC (i.e. initiation of the test), the material had already undergone sol-gel transition, as evidenced by the high G' compared with G". No change in G' or G" was observed over the range of temperatures tested, indicating the development of a pre-formed hydrogel.

Assessment of the Star-PLL-PLT behaviour over prolonged periods of time was determined using a time sweep. No change in G' or G" was observed over the time of the test period (30 min), indicating a stable hydrogel had been formulated (Figure 3.6B).

Strain sweeps were conducted to ascertain the response of the Star-PLL-PLT to an increasing strain. Figure 3.6C shows that on increasing strain (greater than 0.928%), the Star-PLL-PLT hydrogel shows a rapid decrease in G', reverting to polymer solution form.

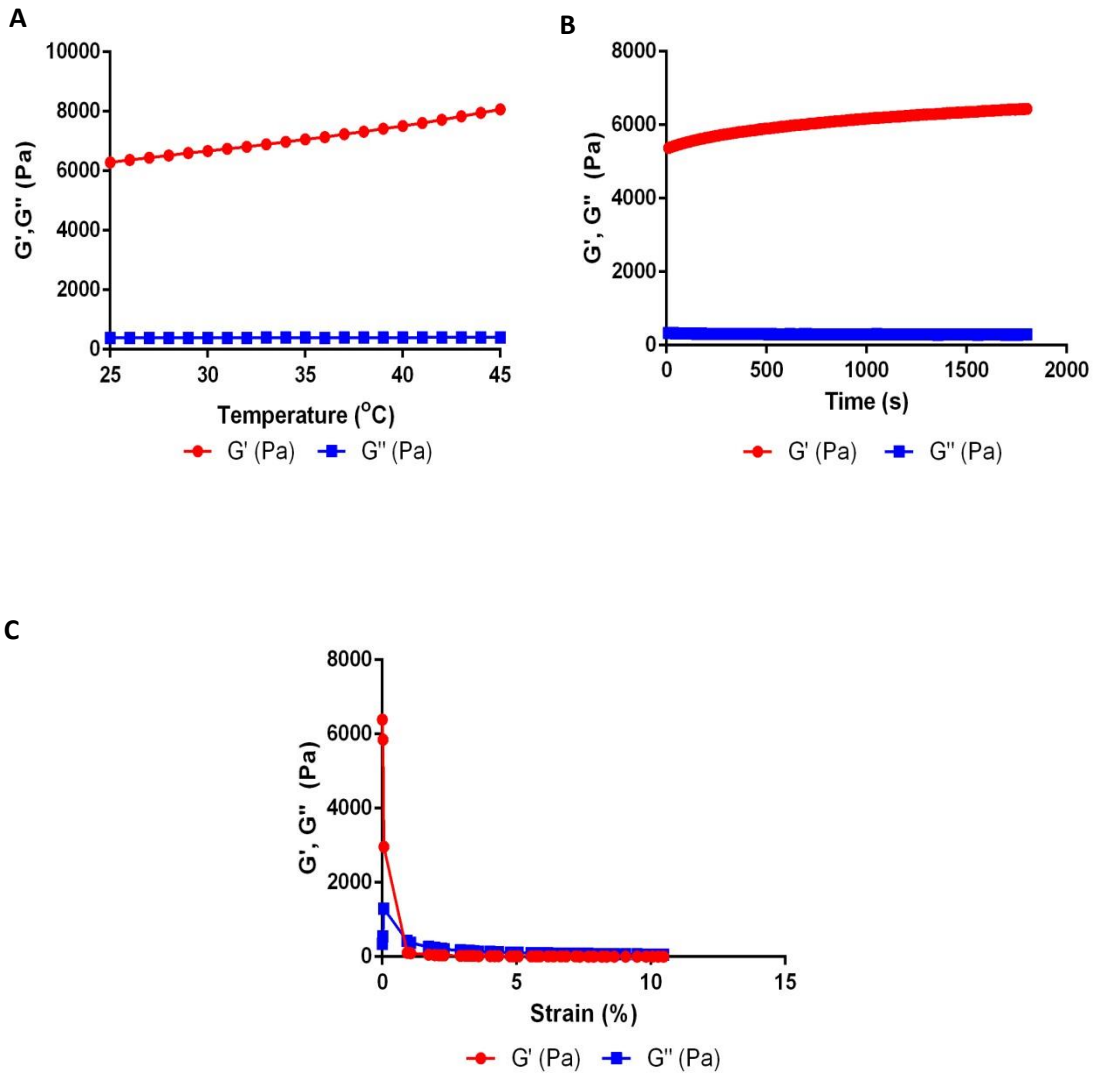

Figure 3.6. Rheological curves obtained using an AR-1000 rheometer (TA Instruments) assessing viscoelastic properties of the Star-PLL-PLT hydrogel. (A) Temperature sweep, from 25-45°C, at 1 Hz and 5 Pa – gel is not thermoresponsive in nature; (B) Time sweep, from 0-30 min at 25°C, 1 Hz and 5 Pa – gel is stable over prolonged periods of time; and (C) Strain sweep, from 0-10% strain, at 1 Hz and 5 Pa – increasing strain leads to breakdown of gel structure.

These tests were then repeated for characterisation of the Linear-PLL-PLT hydrogel. As with the Star-PLL-PLT hydrogel, a temperature sweep assessing changes in storage (G') and loss (G") modulus from 25-45°C, found that at 25°C (i.e. initiation of the test), the material had already undergone sol-gel transition, as evidenced by the high G'

compared with G". No change in G' or G" was observed over the range of temperatures tested, indicating the development of a pre-formed hydrogel (Figure 3.7A). Assessment of the Linear-PLL-PLT hydrogels behaviour over prolonged periods of time was determined using a time sweep. No change in G' or G" was observed over the time of the test period (30 min), indicating a stable hydrogel had been formulated (Figure 3.7B). Strain sweeps were conducted to ascertain the response of the Linear-PLL-PLT hydrogel to an increasing strain. Figure 3.7C shows that on increasing strain (greater than 0.234%), the Linear-PLL-PLT hydrogel shows a rapid decrease in G'.

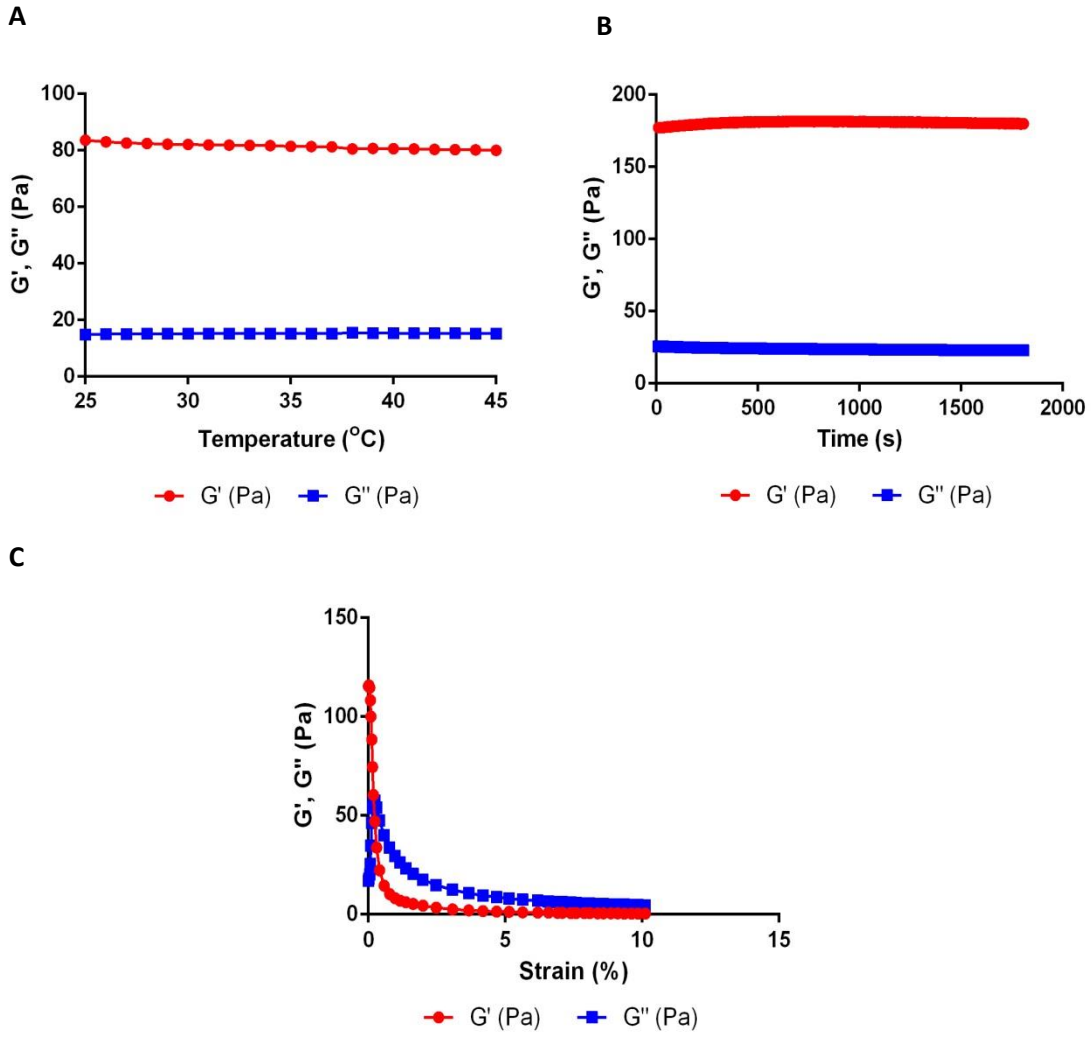

Figure 3.7. Rheological curves obtained using an AR-1000 rheometer (TA Instruments) assessing the viscoelastic properties of a Linear-PLL-PLT co-polypeptide based hydrogel. (A) Temperature sweep, from

25-45°C, at 1 Hz and 5 Pa – gel is not thermoresponsive in nature; (B) Time sweep, from 0-30 min at 25°C, 1 Hz and 5 Pa – gel is stable over prolonged periods of time; and (C) Strain sweep, from 0-10% strain, at 1 Hz and 5 Pa – increasing strain leads to breakdown of gel structure.

An inverted tube test was also utilised to confirm gelation of the polymer following addition of the aqueous media. Physical gelation was observed visually (for both Star-PLL-PLT and Linear-PLL-PLT hydrogels), and due to the resulting hydrogel remaining in the bottom of the tube for thirty seconds following inversion, gelation was confirmed (Figure 3.8).

A **B**

Figure 3.8. Inverted tube test of (A) Star-PLL-PLT hydrogel and (B) Linear-PLL-PLT hydrogel, following addition of deionised water to the polymer, to form hydrogels of 3 wt%. Gels were imaged 10 mins after addition of dH_2O. Both gels remained on the bottom of the vial for 30 s following inversion, indicating gelation had occurred.

3.3.2. Assessment of diffusion and disintegration gel properties

While the storage modulus (G') provides an indication of internal three-dimensional structure of the gel, it does not provide macroscopic evidence of the gel robustness. Assessment of diffusion of a methylene blue dye through both the Star-PLL-PLT and the Linear-PLL-PLT hydrogels showed that it takes up to 24 h before substantial diffusion occurs (Figure 3.9A), though this appears to be to a lesser extent in the Star-PLL-PLT

hydrogel compared with the Linear-PLL-PLT, which could suggest a greater structural robustness of the Star-PLL-PLT hydrogel.

Disintegration studies showed that both the Star-PLL-PLT and the Linear-PLL-PLT hydrogel disintegrated in the presence of PBS over 28 days (Figure 3.9B). However, the Star-PLL-PLT again appears to show greater structural integrity when compared with the Linear-PLL-PLT, as evidenced by the slower rate of disintegration (Figure 3.9B), with approximately 25% of the Star-PLL-PLT gel remaining at day 28, versus 0% for the Lin-PLL-PLT hydrogel.

A: Star-PLL-PLT

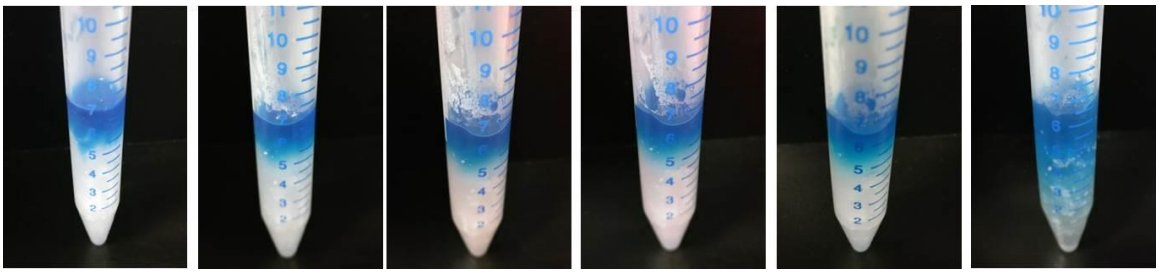

Linear-PLL-PLT

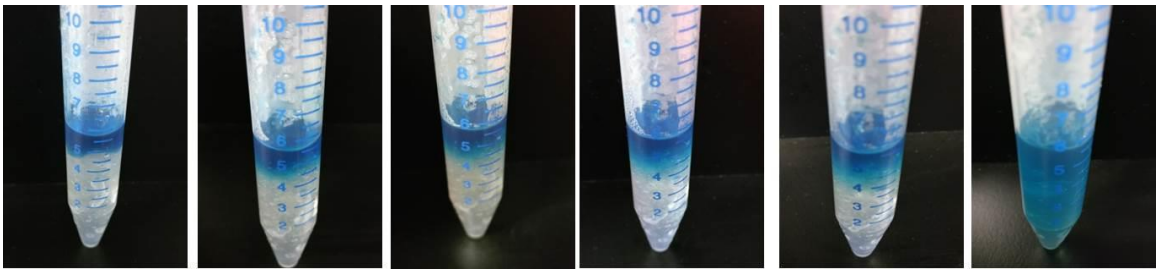

B

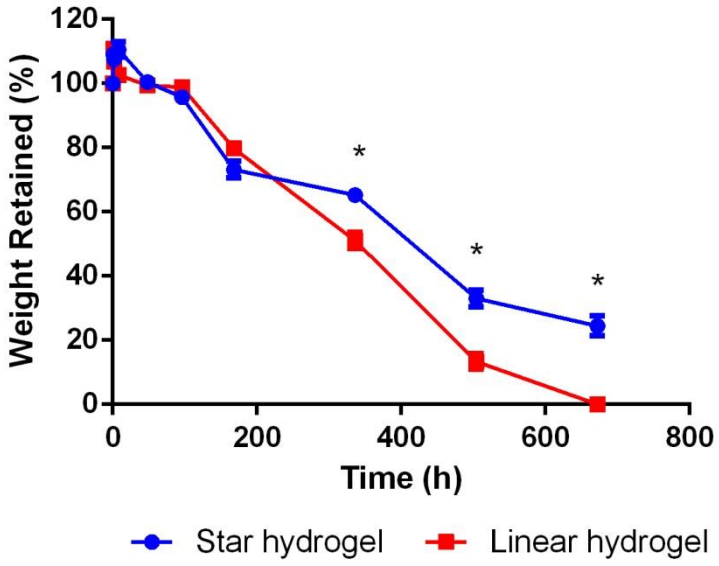

*Figure 3.9(A). Penetration of methylene blue dye through Star-PLL-PLT hydrogel and Linear-PLL-PLT hydrogel, at hourly time points (@ 0, 1, 2, 3, 4, 24 hours) at 37°C; (B) Gel disintegration study of star shaped co-polypeptide hydrogel compared with linear co-polypeptide hydrogel over a 28-day period at 37°C and 75 RPM. Results are presented as average weights (n=3) and SE. Significance determined using multiple t-tests. * = P < 0.05.*

3.3.3. Determination of Star-PLL-PLT and Linear-PLL-PLT hydrogel ultrastructure

The morphology of the lyophilised Star-PLL-PLT and Linear-PLL-PLT hydrogels was examined by scanning electron microscopy (SEM) (Figure 3.10). Image (A) shows the uniform porous nature of the Star-PLL-PLT hydrogel, and image (B) shows the internal structure of the Linear-PLL-PLT. Both hydrogels have a similar internal structure, with large, uniform pores and a cross-linked fibrous network.

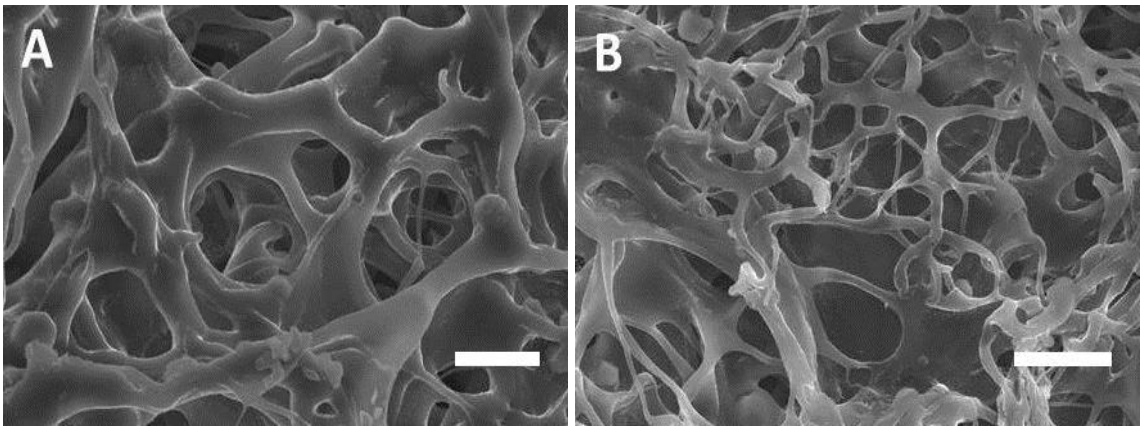

Figure 3.10. Representative scanning electron micrographs, showing internal porous structure of lyophilised co-polypeptide hydrogel samples. Scanning electron micrographs were obtained using a Zeiss Supra 35VP SEM microscope (Zeiss, Jena, Germany). Image A (Star-PLL-PLT) was taken at 85X magnification and 20kV accelerating voltage, and image B (Linear-PLL-PLT) taken at 40X magnification and 20kV accelerating voltage. Scale bar = 25 µm.

3.3.4. Injectability of Star-PLL-PLT and Linear-PLL-PLT hydrogels

Administration of this type of delivery vehicle to a patient in a minimally invasive manner is key and as such, it would likely be delivered using readily available medical devices such as a syringe, needle or catheter. Therefore, to determine feasibility of delivering through such devices, mechanical testing to determine the force required to expel the formulation through them was carried out. This testing indicated that both

hydrogels could be injected through devices including a 1 mL syringe, 1 mL syringe plus 21G needle, and a 3 mL syringe plus catheter tubing of 0.5 m in length with an internal diameter (ID) of 0.514 mm. This diameter corresponds to the ID of a 21G needle, which is used commonly in clinical procedures [169] (Figure 3.11A). Forces required to push the hydrogels through these devices fall below the average forces at which both females and males can push (i.e. 50 N and 70 N respectively) [170,171].

This result is supported by steady state flow rheology which was utilised to determine the viscosity of the Star-PLL-PLT and Linear-PLL-PLT hydrogels in response to a change in shear stress (Figure 3.11B). This showed both hydrogels to possess shear thinning properties, resulting in a rapid decrease in viscosity on application of shear stress. Interestingly, both the Star-PLL-PLT and Linear-PLL-PLT hydrogels show high, increasing viscosity values at the initiation of flow testing, after which point there is a sudden drop in viscosity, which occurs more sharply in the case of the Linear-PLL-PLT. This may indicate “plastic” rheological behaviour and the presence of a yield stress – i.e. the material does not begin to flow until a certain value or yield stress has been reached. The material behaves as an elastic gel under small stresses below its yield value [222].

A

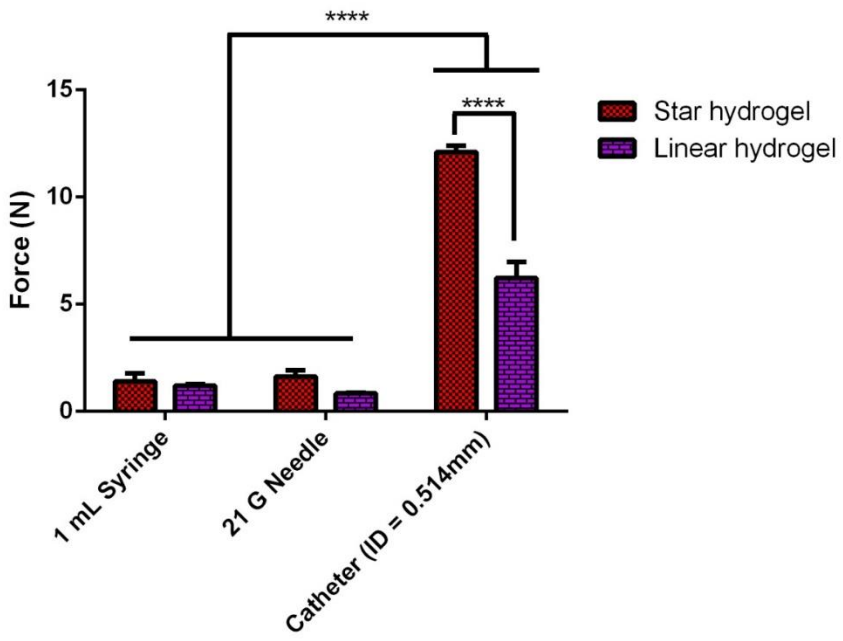

B Star-PLL-PLT

Linear-PLL-PLT

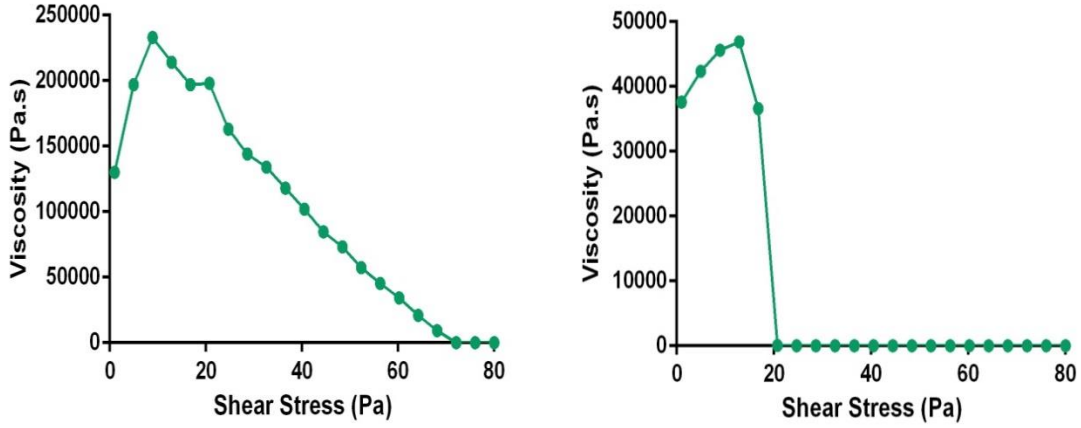

*Figure 3.11(A). Injectability study of Star-PLL-PLT and Linear-PLL-PLT hydrogels through a 1 mL syringe, a 1 mL syringe with 21G needle attached, and a 1 mL syringe with catheter of internal diameter (ID) = 0.514 mm attached, using the Zwick-Roell. Data presented shows average forces (min is n=2, max is n=10) and SE. Force required to expel hydrogels through catheter is significantly higher than that required to expel through a syringe or 21G needle. **** = P<0.0001. Significantly higher max force is required to push the Star-PLL-PLT hydrogel through the catheter than the Linear-PLL-PLT hydrogel; (B) Steady state flow, from 1-80 Pa, for Star-PLL-PLT hydrogel, and Linear-PLL-PLT hydrogel. Gels appear to be shear thinning in nature.*

3.3.5. Encapsulated hMSC viability

Based on injectability data from section 3.3.4, the Star-PLL-PLT and Linear-PLL-PLT showed potential as a means of non-invasive delivery of therapeutics. One potential therapeutic agent for which there is a significant unmet need in terms of delivery strategies is stem cells; therefore the ability of the gels to support hMSC viability was assessed. LIVE/DEAD staining of hMSC encapsulated in the gel indicated that cells were not viable and displayed high levels of cell death up to day 7 when suspended in both the Star-PLL-PLT and the Linear-PLL-PLT hydrogels (Figure 3.12A). This was determined through fluorescent imaging, which showed very few green (or live) cells, and predominantly red (or dead) cells. Fluorescent imagine was confirmed through measurement of cell metabolic activity via a CCK-8 assay, which determines % viability (Figure 3.12B). Once again, when compared with non-encapsulated hMSCs, it appears that the majority of encapsulated cells in both hydrogels are not viable after the first time point of 24 h.

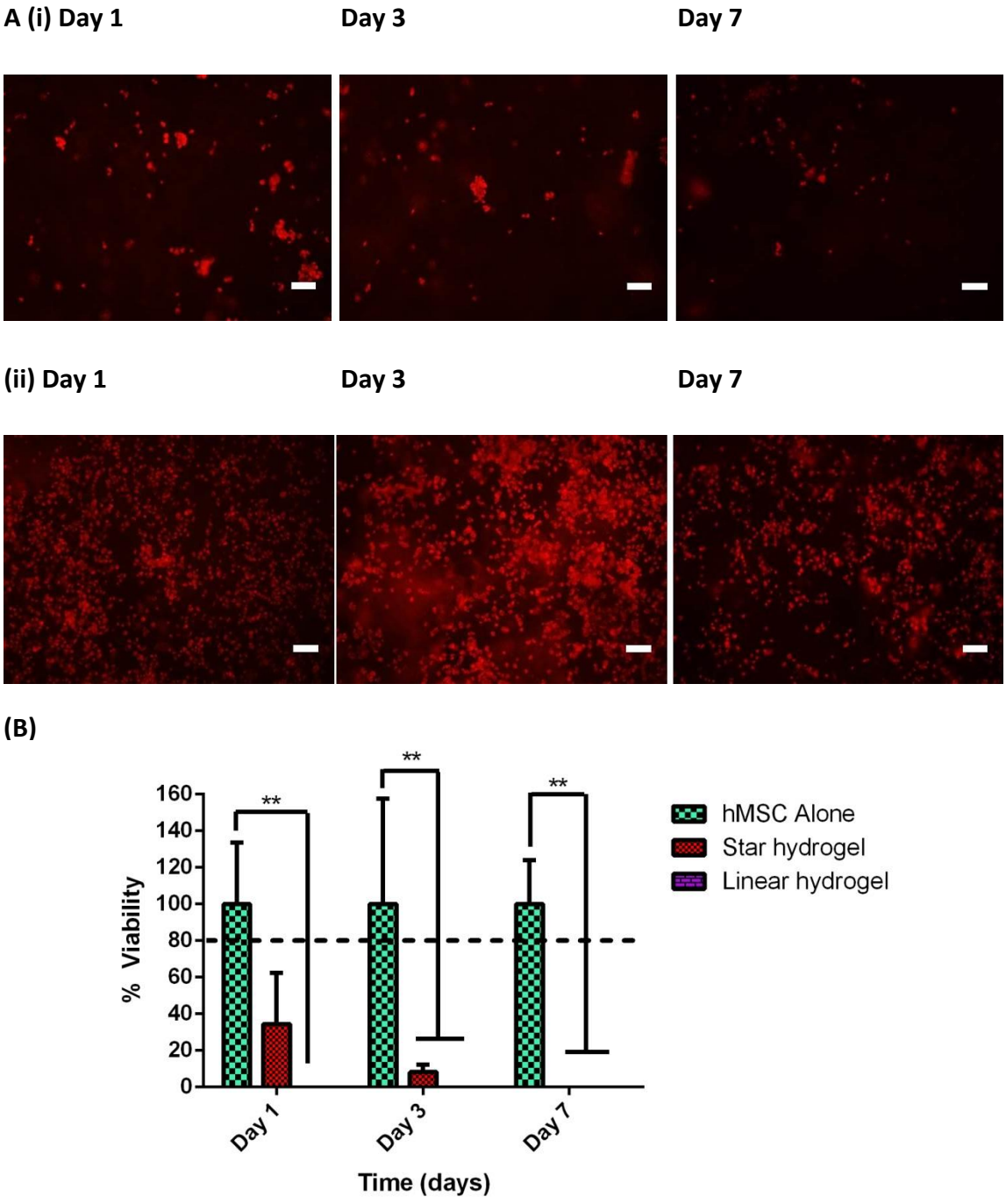

*Figure 3.12(A). LIVE/DEAD stain results for hMSCs encapsulated within either the Star-PLL-PLT hydrogel or the Linear-PLL-PLT hydrogel, imaged at 24 h, day 3 and day 7. Live cells are stained green, dead cells are stained red. Scale bar, 100 µm; (B) Average hMSC viability following supplementation encapsulation of hMSCs in hydrogels for 7 days. Non-encapsulated hMSCs were used as a control. Assay was performed using a CCK-8 viability kit. Results are presented as mean cell viability ± SE (n=3). Significance determined via two-way ANOVA, with Tukey's post hoc test. ** = P<0.001.*

3.4.Discussion

As previously discussed in the Chapters 1 and 2 of this thesis, hydrogels are promising candidates as scaffolds for TE and RM purposes. However, limitations associated with existing natural and synthetic hydrogels has resulted in the need for novel, bioinspired polymers which are capable of more accurately mimicking the extracellular matrix *in vivo* [223]. In this Chapter, synthetic Star-PLL-PLT and Linear-PLL-PLT hydrogels have been investigated in order to determine the characteristics associated with such self-assembling, amino acid based hydrogels. Experiments performed in this Chapter also provide a screening tool for such novel materials, in assessment of their potential suitability for applications in either stem cell delivery, or controlled and targeted delivery of therapeutics.

Initially, polymers were assessed for their gel forming ability, as well as their rheological properties. This is important from a therapeutic perspective, as the gel bolus will need to form rapidly *in vivo* in order to remain in place and provide appropriate retention of cells, or controlled drug release. Both the Star-PLL-PLT and Linear-PLL-PLT synthesised for use in this Chapter are "self-assembling", indicating that gelation of the polymer should occur spontaneously on coming in to contact with aqueous media, giving a preliminary indication of suitability for *in vivo* use. Self-assembly did occur for both polymers assessed here, though some minutes were required before the polymer was fully hydrated. However when this occurred, the gels were stable, as evidenced by the inverted tube test shown in Figure 3.8. As this process occurred spontaneously at room temperature, it was thought that perhaps these polymers were not thermosensitive or otherwise stimuli responsive.

Rheological characterisation confirmed that neither the Star-PLL-PLT or Linear-PLL-PLT hydrogel were thermoresponsive, as evidenced by the initial storage modulus (G') exceeding the loss modulus (G") – indicating that gelation had already occurred (Figure 3.6A and Figure 3.7A). With respect to the Star-PLL-PLT hydrogel, a slight increase in G'

modulus could be observed as temperature increased over the duration of the test, which may indicate a stronger gel being formed at higher temperatures, though ultimately, this did not trigger the gelation process. The G' associated with Linear-PLL-PLT hydrogel did not appear to change significantly over the temperature range assessed during the test, indicating no structural dependence on temperature.

Further oscillatory characterisation was utilised to determine the effects of exposing the hydrogels to one specific temperature for prolonged periods of time, and the effect that this would have on G'. Neither the Star-PLL-PLT hydrogel or the Linear-PLL-PLT hydrogel underwent any changes in terms of G' or G" over the course of this test, which was conducted at 37^{o}C. This test also gave an indication of the maximum storage modulus of each hydrogel at 37^{o}C, with the Star-PLL-PLT hydrogel reaching significantly higher values than that of the Linear-PLL-PLT hydrogel (6436 Pa versus 181.5 Pa). This would indicate a potentially greater suitability of the Star-PLL-PLT hydrogel for therapeutic delivery purposes due to its greater internal three-dimensional structure resulting in a more robust bolus formation *in situ*. This increased mechanical strength is likely due to the star-structure allowing greater possibility for intermolecular bonding between adjacent molecules strengthening the resulting 3D network, whereas the linear structure would not lend itself as well for such interactions. Previous research conducted by our group into the bonding behaviour of star-shaped co-polypeptide based hydrogels has found this to be the case [210]. This paper describes the synthesis and characterisation of a series of star and linear hydrogels, all containing PLL and combined with various other amino acids including tyrosine, phenyl alanine, alanine and valine. In such star-polypeptides, individual amphiphiles are linked to a central core thus providing a covalent core-shell nanoparticle similar to micelles. The use of the highly branched star architectures allows for superior intermolecular physical interactions between the adjacent hydrophobic moieties when compared with their linear counterparts. Examination of the conformation via spectroscopic analysis revealed that the star macromolecular architecture appears to be governed by the influence of the hydrophobic residues. Despite its polar phenol group in the side chain,

tyrosine residues are relatively hydrophobic [224] thus fulfilling this requirement in this instance. Spectroscopic analysis using FT-IR and circular dichroism (CD) in the research carried out by our group [210] and also research carried out by Huang *et al* [203] indicates that the hydrophobic residues, i.e. tyrosine moieties, form stable β-sheet assemblies through a main chain amide bond driven hydrogen bonding [225]. In addition to this, the phenolic hydroxyl groups render the tyrosine block more polar and soluble, favourably tipping the amphiphilic balance and promoting self-assembly in aqueous solution. Furthermore, the partly polar phenolic group could promote intramolecular hydrogen bonds with water molecules or main-chain carbonyls and, thus, contributes to the molecular interaction in the hydrogels [226].

Research into the mechanism of gelation for linear co-polypeptides carried out by Deming *et al* in numerous publications found self-assembly was attributed to the specific peptide secondary conformation. In their research, they utilised adjacent lysine sequences which formed long fibrous networks while poly(L-leucine) residues adopted a rigid α-helical arrangement driving spontaneous hydrogel formation in an aqueous environment [190,227–229]. The rod-like chain conformations of the hydrophobic segments were found to be crucial to hydrogel formation since they direct assembly into network structures rather than spherical micelles (as is the case with star-shaped hydrogels). Therefore, the inclusion of the hydrophobic amino acid tyrosine in the Star-PLL-PLT and Linear-PLL-PLT structures would result in gel formation via a similar mechanism.

Further rheological characterisation of these co-polypeptide hydrogels aimed to determine the effect of increasing strain on the hydrogel structure (Figure 3.6C and Figure 3.7C). Both hydrogels show a reduction in storage modulus in response to increasing strain, with the Star-PLL-PLT hydrogel appearing to revert to polymer solution form on experiencing strains greater than 0.928%, whereas the Linear-PLL-PLT reverts to polymer solution form on strains greater than 0.234%. The slightly improved resistance to strain observed with the Star-PLL-PLT hydrogel versus the Linear-PLL-PLT

hydrogel can likely be attributed to the superior intermolecular physical attractions associated with the higher degree of branching – however, these are still relatively weak forces so would not require significantly higher strain application to break them.

As previously discussed current medical device technology in applications such as cardiac and lung regeneration is focused on the use of novel catheter devices as a minimally invasive method of accessing damaged tissue. With translatability of these hydrogel formulations in mind, we assessed the potential for syringing of the hydrogel in terms of force required for the gel to be expelled. Injectability testing showed that it was possible for the hydrogels to be passed through a range of common clinical devices including a 1 mL syringe, 1 mL syringe plus 21G needle, and a 1 mL syringe plus 0.5 m catheter (Figure 3.11A). Results confirmed that both the Star-PLL-PLT and Linear-PLL-PLT hydrogel formulations could be pushed through all three devices. Forces required fall below the average at which both males and females can push (pinch test) [170]. This result is supported by rheological flow viscosity testing for both hydrogels, which shows the gels have shear thinning properties, resulting in a rapid decrease in viscosity on application of shear stress (Figure 3.11B). However, reverse flow testing to determine whether the materials regained their structure following shear thinning was not examined due to material synthesis constraints, though this would be a useful study to carry out in future work – on a visual inspection however, the Star-PLL-PLT did appear to have maintained its gel structure, whereas the Linear-PLL-PLT had reverted to polymer solution form.

While the storage modulus provides an indication of internal three-dimensional structure, it does not provide macroscopic evidence of the gel robustness. This is a key distinction to make, as some gels may reach very high storage moduli but despite this, have a tendency to dissociate within a relatively short period of time (e.g. Pluronics®, which have been discussed with respect to this phenomenon in section 2.4 [148]). In this study, assessment of diffusion of a methylene blue dye through both the Star-PLL-PLT and Linear-PLL-PLT hydrogels showed the dye readily penetrates through the

structures, with full diffusion through the depth observed by 24 h for the Linear-PLL-PLT, though some dye free gel remained at 24 h for Star-PLL-PLT (Figure 3.9A). Disintegration studies showed that the Linear-PLL-PLT hydrogel disintegrated more rapidly in the presence of PBS than the Star-PLL-PLT hydrogel, which appeared to be more robust with 24.4% of the Star-PLL-PLT remaining at 28 days (Figure 3.9B). The dye penetration and gel disintegration investigations are intended to support each other, with the disintegration study allowing for quantification of mass lost as a result of gel breakdown; while the methylene blue dye test indicates the degree of diffusion through the gel in the first 24 hours while the gel still retains its structural integrity. These results in combination suggest that while the Linear-PLL-PLT hydrogel is not sufficiently robust in nature or capable of resisting degradation in the presence of a physiologically compatible buffer system, the Star-PLL-PLT hydrogel appears to demonstrate improved structural integrity. Injectability data, dye diffusion, and disintegration testing results of the Star-PLL-PLT hydrogel all point towards a mechanically superior formulation, which has the potential to be easy delivered in a minimally invasive manner, while remaining as a durable gel bolus *in situ* for the delivery of therapeutic agents.

Assessment of hMSC viability following suspension within both the Star-PLL-PLT and Linear-PLL-PLT hydrogels showed a lack of biocompatibility from 24 h onwards in culture, as assessed by LIVE/DEAD staining and a CCK-8 viability assay (Figure 3.12). LIVE/DEAD staining shows a large proportion of red (dead) cells from 24 h onwards in both hydrogels, with very few green (live) cells present. This is confirmed with the CCK-8 viability assay which shows no viable cells present in the Linear-PLL-PLT hydrogel from 24 h onwards, indicating hydrogel toxicity compared with hMSCs alone, and a 34.48% viability at 24 h for hMSCs encapsulated in the Star-PLL-PLT hydrogel. This drops to 8.22% viability at day 3 and finally 0% viability at day 7. Viability at all time points for both gels falls significantly below the ISO guidelines for cytotoxicity *in vitro*, for which the minimum acceptable viability is 80% [230].

As previously mentioned such star-shaped polymers are novel and very little has been published on similar macromolecules to date – and what has, has been limited to synthesis and physicochemical characterisation. To the best of our knowledge, there have been no reports of previous suspension of cells (of any type) in star-shaped or linear co-polypeptide based hydrogels and their subsequent assessment as a cell delivery vector. A previous literature review on the topic of dendrimers and their future directions stated that they were not originally intended for applications in the pharmaceutical or biomedical field, and as such toxicity assessment was not initially of concern [231]. Indeed, the same review states that the number of studies evaluating biological properties of dendrimers is growing, but still more than 75% of the papers published describe purely synthetic chemistry (new concepts) or non-biological applications of dendritic systems. Therefore it is difficult to find appropriate comparisons in the literature to our own cytocompatibility studies. However, some rationalisation can be made based on the star-shaped and linear co-polypeptide chemical structures. Previous research into cytotoxicity of dendrimers has found a lack of biocompatibility and as a dendrimer (i.e. PPI in this instance) provides the central core for the Star-PLL-PLT hydrogel investigated in this Chapter, these toxicity issues may still be a cause for concern with such molecules. A review article published by Jain *et al* summarises the key issues associated with dendrimer toxicity [232]. This inherent toxicity is due to the presence of terminal -NH_2 groups and surface cationic charge present in molecules such as PPI, PLL and polyamidoamine (PAMAM) [233–235]. The presence of a cationic charge results in an interaction with negatively charged biological membranes *in vitro* and *in vivo*. This causes membrane disruption via nanohole formation, membrane thinning and erosion [236,237]. This toxicity appears to be related to core generation, with higher generation dendrimers generally being associated with higher toxicity [231,238]. Toxicity has also been postulated to be concentration dependant, with a number of publications indicating that an increased concentration results in increased toxicity [231,239]. This effect has also been identified by researchers in our group, with similar unpublished findings in relation to

star-shaped polypeptides as nanocarriers. Biocompatibility studies in this thesis may have presented an unusually high local concentration of polymer to hMSCs given that cells were encapsulated within the hydrogel, thus potentially overwhelming cells and increasing toxic effects.

One potential approach to reducing the amine termination associated toxicity is to modify the terminal -NH_2 groups of dendrimers with neutral or anionic moieties (in the literature, often through PEGylation) – which is the case with respect to these star-shaped and linear co-polypeptides, where the -NH_2 groups is linked to amino acids i.e. lysine and tyrosine blocks. It is possible that not all of the initiator (PPI or allylamine) was consumed in the NCA reactions, resulting in the presence of some toxic residues remaining – however FT-IR was performed to confirm consumption of the initiator, and indicated that this was not the case (Appendix 1.1 and 1.2). Thus the presence of these cytotoxic units may be as a result of degradation of the co-polypeptides. As previously mentioned in the introduction of this Chapter, degradation of such polypeptide based hydrogels would be expected to occur over time due to the nature of peptide bonds [205]. Degradation studies and subsequent characterisation of the degradation products was not in the scope of this Chapter and thus was not performed, but this may prove useful in ascertaining the origin of the significant polymer toxicity.

A second possible hypothesis regarding the toxicity of the Star-PLL-PLT and Linear-PLL-PLT hydrogels may be the modification of the dendrimer core through the addition of amino acids. It has been suggested in the literature that this may improve the cytocompatibility of such polymers [205,232] but conversely has also been suggested to increase their toxicity based on the choice amino acid used in the branched arms. The use of poly-$_L$-lysine (PLL) in these polypeptides could be called into question as PLL has been shown to be toxic in numerous previous studies. Research conducted by Symonds *et al* [240] found that both low and high molecular weight PLL resulted in cellular toxicity through initiating mitochondrially mediated apoptosis in three different cell types: Jurkat T cells, THLE-3 hepatocyte like cells, and hUVECs. Research published

by Kadlecova *et al* [241] compared cytotoxicity of linear, dendritic and hyper-branched PLL variants, and found linear PLL was significantly more toxic than dendritic or hyper-branched PLL. In this Chapter, Linear-PLL-PLT has been shown to be more toxic than Star-PLL-PLT, confirming the results reported by Kadlecova *et al* and indicating that modifications from a linear to star architecture may result in reduced observed toxicity. Further possible structural modification to remove the PLL blocks and replace with an alternative amino acid such as poly-$_L$-arginine (which has been thought to exhibit less toxicity than PLL [242]), may help to reduce cytotoxicity of these polymers.

3.5.Conclusion

Disadvantages associated with current synthetic polymer-based hydrogels, has resulted in a need for novel, advanced polymers capable of circumventing these issues. A promising class of materials is that of synthetic hydrogels obtained by self-assembly of amphiphilic polypeptides. In this Chapter, we have investigated the physicochemical properties of Star-PLL-PLT and Linear-PLL-PLT hydrogels, and also their ability to sustain viability of hMSCs when encapsulated within the hydrogels.

Rheological characterisation highlighted some promising features of the Star-PLL-PLT compared with the Linear-PLL-PLT hydrogel, particularly with respect to the high storage modulus obtained. This could indicate suitability of the Star-PLL-PLT in therapeutic delivery and TE applications, where high mechanical strength is required. Supporting this are results from methylene blue penetration assays and gel disintegration studies, both of which indicated improved mechanical strength of the Star-PLL-PLT compared with the Linear-PLL-PLT, due to reduced diffusion of dye throughout and slower disintegration of the hydrogel. Injectability testing combined with flow rheology showed both the Star-PLL-PLT and Linear-PLL-PLT hydrogel to have some potential for use in minimally invasive therapeutic delivery as low forces were required to push the gels through a syringe, needle and catheter.

An area in which novel hydrogels are urgently needed is in cell delivery. Neither the Star-PLL-PLT hydrogel nor the Linear-PLL-PLT hydrogel were able to support viability of encapsulated hMSCs. Their observed toxicity could be due to issues such as degradation of the polymer and toxicity of the associated degradation products, the presence of toxic side chains such as poly-$_L$-lysine (PLL), or the presence of toxic by-products of the synthesis reaction. While these materials do not appear to be suitable for cell delivery applications, with additional structural modification they could offer potential for delivery of other therapeutic molecules.

4. Chapter 4: A site-specific delivery platform for all-trans Retinoic Acid (atRA) in pulmonary regeneration applications

4.1.Introduction

As previously highlighted, current therapeutic approaches to COPD are inadequate emphasising the importance of emerging novel technologies and alternative methods to address this unmet clinical need. The possibility of utilising a regenerative approach in the treatment of chronic lung disease has been considered from two broad strategic viewpoints. First is the use of extrinsic cell therapy, in particular the use of autologous adult MSCs, which has previously been discussed in Chapters 1 and 2. A second approach is the utilisation of pharmacologically active molecules to induce lung regeneration through actions on an intrinsic population of cells [17]. These include signalling molecules and growth factors, of which a variety of molecules of interest have been identified [82,243–245].

One particular small molecule of interest in the treatment of COPD is all trans Retinoic Acid (atRA) which, as discussed in Chapter 1 (section 1.3.2.4) of this thesis, has the potential to target multiple pathologies associated with COPD. atRA belongs to the retinoid family of compounds, which are obtained from the diet. On acquisition of retinol (a fat soluble vitamin), it circulates bound to retinol binding protein and transfers to cellular retinol binding proteins upon entry into cells. Retinol is either esterified with fatty acids intracellularly and stored in lipid droplets, or if it is needed immediately, retinol is converted to retinoic acid (RA) through irreversible oxidation [92]. RA binds to retinoic acid receptors (RAR) or retinoid-X receptors (RXR), which are nuclear proteins that form stable complexes with DNA elements in RA-responsive genes, called retinoic acid responsive elements (RARE) [246]. The terpene side chain of RA can form several stereoisomers including *all-trans*, 9-*cis* and 13-*cis* RA. RARs bind atRA or 9-*cis* RA, whereas RXRs exclusively bind 9-*cis* RA. After ligand binding, one RAR and one RXR molecule form a stable heterodimer that binds with high affinity to a RARE. Once bound, the RAR–RXR heterodimer engages other factors, including histone

deacetylases that act as co-activators of the basic transcriptional machinery (Figure 4.1) [92].

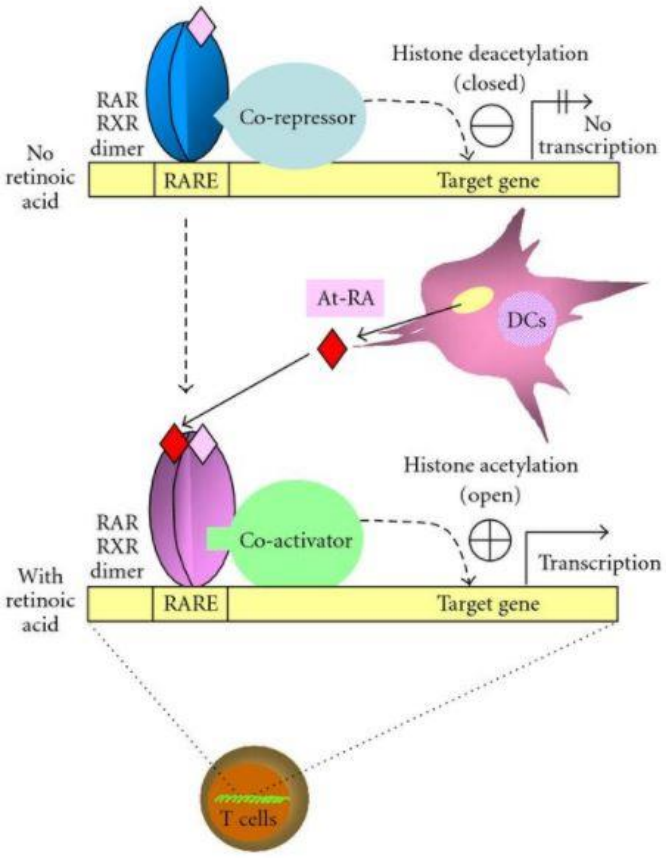

Figure 4.1. Control of gene expression by retinoic acid. RAR-RXR heterodimers serve as the nuclear receptors for retinoic acid. When RAR ligands (e.g., atRA) are not available, the RAR-RXR heterodimers attract co-repressors and histone acetyl deacetylases to the genes which are under the control of retinoic acid response elements (RARE), resulting in a closed conformation of the chromosome and blocked transcription. When RAR ligands are available in a tissue microenvironment, they would enter into T cells and activate RAR-RXR heterodimers. This is followed by the release of co-repressors and attraction of co-activators, which, in turn, recruit histone acetyl transferases, resulting in an open conformation of the chromosome and transcription of the genes. Adapted from [247].

atRA is a yellow to light-orange crystalline powder (structure shown in Figure 4.2A). It is hydrophobic in nature, with a poor water solubility of <0.1 g/100 mL (practically insoluble), though it is soluble in DMSO and slightly soluble in ethanol. It is labile to heat (melting point = 179^{o}C [111]), light and oxygen-mediated degradation [112], presenting a challenge for use in a primarily hydrophilic biological environment. In order to overcome the hydrophobic nature of atRA, we aimed to encapsulate it in solid lipid nanoparticles (SLNs). SLNs are sub-micron sized particles made from biocompatible lipids that are solid at room and body temperature. SLNs are then coated with a layer of emulsifier molecules (Figure 4.2B) to facilitate their formation and enhance their long-term stability [113].

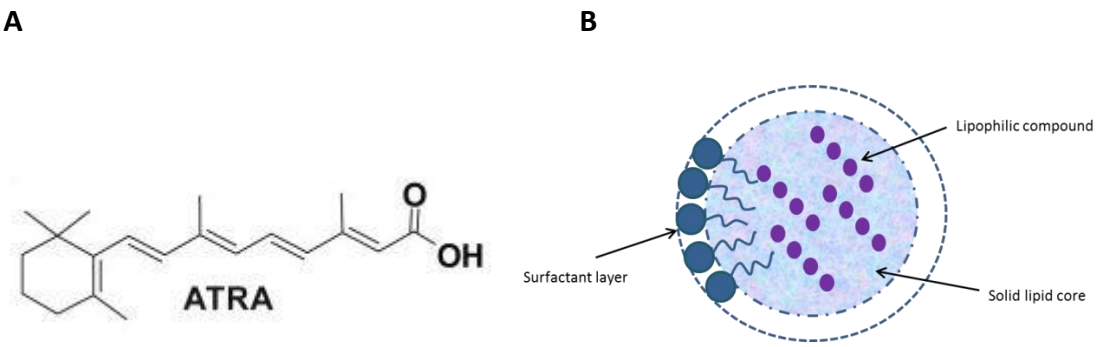

Figure 4.2(A). Chemical structure of all trans Retinoic Acid (atRA); (B) General structure of solid lipid nanoparticles (SLNs). SLNs are composed of a biocompatible solid lipid core encapsulating the lipophilic drug, coated with a layer of surfactants.

SLNs were introduced in 1991 as an alternative carrier system to traditional colloidal carriers such as emulsions, liposomes and polymeric micro- and nanoparticles [248]. The lipid matrix employed in lipid nanoparticles is usually a physiological lipid (biocompatible and biodegradable) with negligible toxicity [249]. Lipids used in the formulation of SLNs include triglycerides (such as trilaurin, trimyristin, and tripalmitin), and hard fats (such as Witepsol W35, H35 and H42, glyceryl benehate (Compritol 888 ATO) and glyceryl palmitostearate (Precirol ATO 5), and steric acid). Surfactants used in formulations include soybean lecithin (Lipoid S75), phosphatidylcholine, poloxamers

188, 182 and 407, and the polysorbates (20, 60 and 80) [250]. The choice of which lipid and which surfactant to use depends on the drug/therapeutic to be encapsulated and also on the route of administration required.

There are numerous advantages associated with the use of SLNs. These include low toxicity compared to polymeric particles due to their consisting of physiological lipids, and also the ability to encapsulate lipophilic drugs in their lipid core (as well as hydrophilic molecules) [251]. In addition to this, they have the ability to control and localise the release of the active drug [248], and it has also been reported that nanoparticles (120–200 nm) rarely undergo blood clearance by the reticuloendothelial system, allowing them to remain *in situ* for extended periods [252]. Furthermore, sufficient drug loading, long-term shelf stability [250], and easy large-scale production are advantageous [253].

To date, a large number of drugs with a great variety in lipophilicity and general structure have been studied with regard to their incorporation into SLNs [248,251,254–262]. A range of routes of administration for which such SLNs might be delivered have also been investigated, including oral [263], topical [264,265], pulmonary [266] and intravenous [260]. As part of this PhD research, we aim to investigate the utility of SLNs in encapsulating atRA, for suspension within our selected hydrogel formulation and subsequent loco-regional delivery as a potential anti-inflammatory pro-regenerative therapeutic to the distal airways. This represents an innovative use for SLNs compared with their historical application as vectors for inhaled delivery. atRA has previously been encapsulated within SLNs; however, applications have centred around the transdermal route [264,265] due to the well-recognised effects of Vitamin A on maintaining and restoring skin health in conditions such as acne, dermatitis and skin aging [267]. atRA has also been widely investigated in SLN formulations for its proposed anti-cancer activity [268–270]. However, to the best of our knowledge, atRA has never been encapsulated in SLNs for delivery to cells to elicit an anti-inflammatory

effect in COPD – and this is the strategy we aim to investigate over the course of this research.

In the current work, we demonstrate the development of atRA loaded SLNs, from initial selection of biocompatible excipients to the formulation process, post-formulation physicochemical characterisation and process optimisation. atRA SLNs were investigated for their *in vitro* biocompatibility on a lung epithelial cell line (A549s), and were subsequently suspended in Respiragel for further physicochemical and *in vitro* characterisation. atRA SLNs represent a promising small molecule delivery mechanism, which offers potential as a lung regeneration therapy. Additionally, the option to replace atRA with an alternative small molecule, growth factor or lipophilic drug remains, rendering this delivery system highly tuneable for practically any biological application of interest, thus offering immense potential for advancing drug delivery systems.

Objectives

The overall objective of this Chapter was to investigate the potential of solid lipid nanoparticles in encapsulating the lipophilic signalling molecule all-trans Retinoic Acid (atRA).

- The first objective of this Chapter was to develop a suitable SLN formulation composed of biocompatible excipients, capable of encapsulating atRA.
- The second objective was to determine the physicochemical characteristics of the formulated atRA-loaded SLNs, in terms of particle size, zeta potential, polydispersity index, drug encapsulation efficiency and drug release profile.
- The third objective was to determine the biocompatibility of atRA-loaded SLNs on a lung epithelial cell line (A549s).
- The final objective of this Chapter was to investigate whether the atRA-loaded SLNs could be suspended in Respiragel, to determine the subsequent rheological properties of this gel and to ascertain the release properties of atRA from the SLN-loaded gel.

4.2.Materials and Methods

4.2.1. Materials

Compritol® 888 ATO was generously donated by Gattefossé (France). Poloxamer 188 was purchased from BASF (Ludwigshafen, Germany). For HPLC analysis, all chemicals (methanol, acetonitrile, acetic acid and water) were of analytical grade, and were purchased from Sigma-Aldrich (Ireland). The A549 cell line was purchased from the American Type Culture Collection (ATCC, Virginia, USA). Retinoic acid, Tween® 80, dimethyl sulfoxide (DMSO), Cell Counting Kit 8 (CCK-8), and Dulbecco's Modified Eagles Medium/Nutrient Mixture F12 (DMEM/F12) media were also purchased from Sigma Aldrich (Ireland).

4.2.2. Formulation and process optimisation of blank and atRA loaded SLNs

Initial batches of SLNs were prepared using a solid lipid, Compritol® 888 ATO, and a surfactant, poloxamer 188. Preliminary characterisation of these SLNs indicated a larger particle size than desired. As a result, a second surfactant, Tween® 80, was included in the formulation. Modifications were also made to the concentrations of lipid and surfactants used. Preliminary batches of SLNs prepared are detailed in Table 4.1. Following optimisation of the blank formulation, atRA was added in at a concentration of 1% w/w of the lipid core, and batches were reassessed.

Table 4.1. Batches of SLNs prepared, detailing composition in terms of lipid, surfactant(s) and drug concentrations, and modifications in the process parameters, i.e. homogenisation time (HT) and sonication time (ST). Cells highlighted in blue indicate change made at each subsequent batch.

Batch	Compritol® 888 ATO Conc. (% w/v)	Poloxamer 188 Conc. (% w/v)	Tween® 80 Conc. (% w/v)	atRA Conc. (% w/w lipid core)	Homogenisation Time (HT)	Sonication Time (ST)
1	7.5	2.5	-	-	15	4 x 5 min cycles
2	7.5	1.5	1.5	-	15	4 x 5 min cycles
3	7	1.5	1.5	-	15	4 x 5 min cycles
4	7	1	1	-	15	4 x 5 min cycles
5	5	1	1	-	15	4 x 5 min cycles
6	5	1	1	1	15	4 x 5 min cycles
7	5	1	1	1	10	4 x 5 min cycles
8	5	1	1	1	10	3 x 5 min cycles

All SLNs prepared in this study were formulated via the emulsification-ultrasonication method (as shown in Figure 4.3) [251]. Briefly, the solid lipid, Compritol® 888 ATO, was accurately weighed and heated to above its melting point (i.e. 85^{o}C). The aqueous surfactant phase, comprising deionised water (dH_2O), Poloxamer 188 and Tween® 80 was also heated to 85^{o}C. When both the lipid phase and aqueous phase had reached the desired temperature, the lipid phase was dispersed through the aqueous phase. This was homogenised at 15,000 RPM (UltraTurrax Y25, IKA® WERKE GMBH, Germany) to form a coarse pre-emulsion. Initial batches were homogenised for 15 min, but this was subsequently reduced to 10 min following characterisation and comparison of batches. The obtained emulsion was ultrasonicated using a probe sonicator (Branson SLPt) at 70W. Initial batches were sonicated for 4 x 5 min cycles. Optimisation of the process resulted in a reduction in this time to 3 x 5 min cycles (Table 4.1). Homogenisation and sonication steps were carried out at 85^{o}C. The resulting nano-emulsion was cooled down in an ice bath to produce a nanoparticle dispersion.

For atRA SLNs, the drug (MW = 300.44 g/mol) was separately dissolved in dimethyl sulfoxide (DMSO) prior to addition to the molten lipid phase, with all subsequent steps remaining as for blank SLNs. atRA SLNs were prepared covered in tinfoil due to the light sensitivity of the drug.

Nanoparticles were then suspended in ultrapure water containing 5% w/v glucose as cryoprotectant, and were stored at -80^{o}C overnight. Frozen SLNs were lyophilised in a Labconco FreeZone Freeze Dryer and vacuum pump, at 0.023 mbar and -50^{o}C for 48 hours. Formulated blank SLNs had a MW of 9584.67 g/mol, and atRA SLNs had a MW of 9885.1 g/mol.

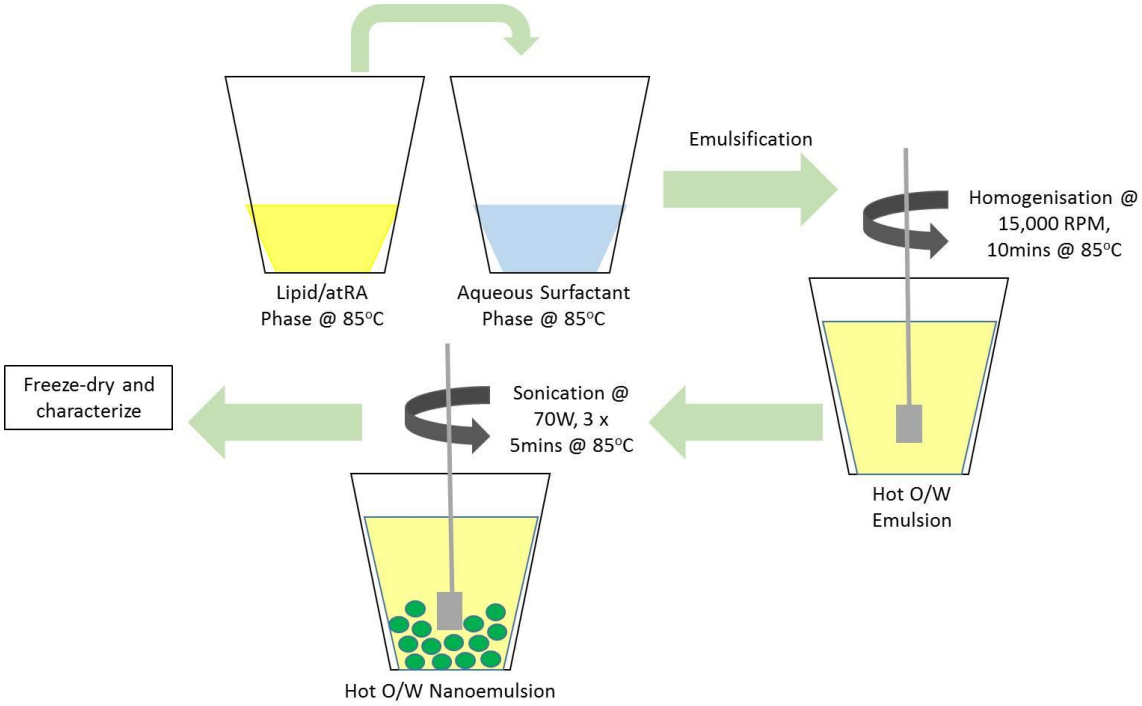

Figure 4.3. Schematic representation of SLN preparation by the emulsification-ultrasonication method. Compritol® 888 ATO is first heated to 85°C with or without atRA (depending on drug loaded or blank SLNs), as is the aqueous surfactant phase, composed of dH_2O, poloxamer 188 and Tween® 80. The oil phase is then transferred to the water phase, and homogenised at 15,000 RPM for a defined period of time (Table 4.1). This is then subjected to sonication cycles at 70 W power (Table 4.1). The resultant nano-emulsion is cooled at 4°C, mixed with glucose 5% w/v as cryoprotectant, frozen at -80°C and lyophilised.

4.2.3. Physicochemical characterisation of SLNs

4.2.3.1. Determination of particle size and polydispersity index

The average particle size distribution (Z-average size) and polydispersity index (PDI) were measured by dynamic light scattering photon correlation spectroscopy (PCS) using a Zetasizer Nano ZS (Malvern Instruments, UK) at 25°C, under a fixed angle of 173° in folded capillary cells. The measurements were obtained using a 4mW He-Ne laser operating at a wavelength of 633 nm, combined with DTS Software (v7.10). Lyophilised SLN powder was accurately weighed and dispersed in ultrapure water at a

concentration of 2 mg/mL. Measurements were performed in triplicate for three batches of nanoparticles and results are the average of three measurements.

Optimized atRA and blank SLNs were also analysed via nanoparticle tracking analysis (NTA) utilizing a Nanosight NS300 (Malvern, UK). Samples were prepared as previously described as a 2 mg/mL suspension in ultrapure water. Samples were loaded into a laser module (488 nm) sample chamber containing thermoelectric Peltier elements which allowed for temperature control at 22^{o}C. Real time video analysis of the nanoparticles was recorded via an in-built sCMOS camera with computer controlled motorized focus. Measurements were performed in triplicate for three batches of nanoparticles, and results are reported as a mean particle size عی standard deviation (nm). To prevent sample crossover, the laser module was flushed with ultrapure water between each sample until no visual nano-particulate matter could be observed via the sCMOS camera system.

4.2.3.2. Zeta potential measurement

The average zeta potential (ZP) of SLN suspensions was determined by the measurement of the electrophoretic mobility using a Malvern Zetasizer Nano ZS (Malvern Instruments, UK). Prior to the measurement, lyophilised SLN powder was weighed and dispersed in ultrapure water at a concentration of 2 mg/mL. Measurements were performed in triplicate for three batches of nanoparticles and results are the average of three measurements.

4.2.4. Transmission electron microscopy (TEM)

Shape and surface morphology of SLNs were examined by transmission electron microscopy (TEM), using a Hitachi H-7650 TEM (Hitachi High Technologies, Berkshire, UK) operating at 100kV. Lyophilised atRA-SLNs were weighed and dispersed in ultrapure water at a concentration of 1 mg/mL. A 5 µl drop of this suspension was

placed on a Silicon Monoxide/Formvar-coated copper grid (Mason Technologies, Ireland) for 1 minute after which excess sample was absorbed by filter paper. Staining was then performed with a solution of 1% uranyl acetate (negative stain) or 1% osmium tetraoxide (positive stain). Excess stain solution was absorbed by filter paper and the grids were air-dried prior to imaging.

4.2.5. High Performance Liquid Chromatography for the detection of atRA in SLNs

HPLC analysis of atRA encapsulated in SLNs was performed using an Agilent Technologies 1120 Compact LC with a Kinetex 5u C18 100Å (250 x 4.6mm) column (Phenomenex, USA). The mobile phase used in the analysis consisted of methanol : acetonitrile : water : acetic acid (8:1:1:0.05) and was set to a flow rate of 1 mL/min, as adapted from Cirpanli et al. [271], with UV detection carried out at 356 nm. Blank SLNs and a 1 µg/mL atRA solution were used as negative and positive controls respectively in HPLC analysis. The concentration of atRA in each sample was determined using an atRA calibration curve which was constructed ranging from 0.3125 µg/mL to 10 µg/mL (Appendix 2.1). A new set of standards and resulting standard curve was prepared for each new batch of atRA used in the SLN formulation.

4.2.6. Determination of nanoparticle yield, drug loading and encapsulation efficiency of atRA SLNs

The SLN yield was calculated gravimetrically from the weight of SLNs collected post lyophilisation versus the starting quantities of the lipid, surfactants and drug using the following equation:

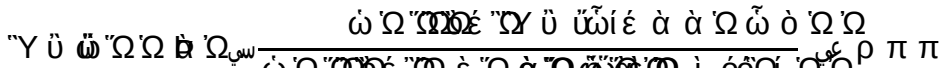

Equation 4.1. Equation used for determining % SLN particle yield post lyophilisation.

In order to extract the entrapped drug from the SLNs, lipid disruption was performed by dissolving 20 mg of atRA SLNs in 10 mL methanol, followed by vortexing for 5 min. The resulting suspension was filtered through a 0.45 µm PTFE filter (Agilent, Ireland) to remove any residual lipid and non-dissolved drug crystals. The filtrate was then transferred to amber glass vials (Agilent, Ireland) for detection by HPLC. The drug loading (DL) and encapsulation efficiency (EE) were determined using the following equations:

A

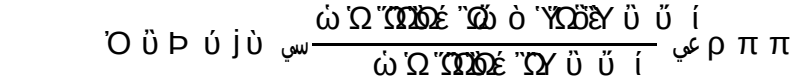

B

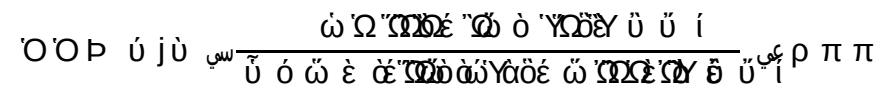

Equation 4.2(A). Equation used for determining % SLN drug loading post lyophilisation, and (B) Equation used for determining % atRA encapsulation within SLNs post lyophilisation.

4.2.7. atRA Release from SLNs using the Float-A-Lyzer® method

Release studies were performed using a Spectra/Por® Float-A-Lyzer® G2 device with a molecular weight cut off (MWCO) of 300 kD. Float-A-Lyzer® devices were first washed

with 10% v/v ethanol, followed by ultrapure water according to the manufacturer's protocol. 20 mg lyophilised atRA loaded SLN powder was weighed and suspended in 1 mL ultrapure water, before being transferred to the internal compartment of the Float-A-Lyzer®. The outer receptor compartment was filled with 5 mL of a phosphate buffered saline/ethanol/Tween® 80 release medium (8:1:1) (pH 7.4), modified from [272]. As aqueous solubility of atRA is very low, 10% w/v Tween® 80 was added to maintain sink conditions. The Float-A-Lyzer® was gently placed into the receptor fluid container, and was sealed using parafilm. This was then transferred into a 50 mL falcon tube which was covered in tin foil to protect from light. Finally, this tube was placed into a thermostatically controlled shaking water bath, at 37^{o}C and 75 RPM. Samples were taken at 30 min, then hourly up to 8 hours for the first day, followed by daily to day 7, with final time points at day 10 and day 14. The 5 mL receptor fluid was removed and replaced at each time point. Samples were subsequently analysed by HPLC using the method described in 4.2.5 and concentration of drug present calculated using the atRA calibration curve (Appendix 2.1).

4.2.8. Stability testing of blank and atRA loaded SLNs

Physical stability of blank and atRA SLNs was examined by monitoring of size, zeta potential and polydispersity index changes over a period of 3 months (Table 4.2). Blank and atRA SLNs were stored under three separate temperature conditions: -20^{o}C, 4^{o}C and 20^{o}C, with atRA SLNs being protected from light. Z-ave, ZP and PDI of SLNs stored at each temperature were measured as previously described in sections 4.2.3.1 and 4.2.3.2. Stability of atRA loaded into SLNs was also examined by monitoring encapsulation efficiency changes over a period of 3 months. EE of SLNs stored at each temperature was measured as previously described in section 4.2.5.

Table 4.2. Stability study testing performed on blank and atRA loaded SLNs at day 1, day 7, day 28, day 56 and day 84 post formulation. SLNs were evaluated for size (using both the Zetasizer Nano ZS ("Z" in Table 4.2) and the Nanosight NS300 ("N" in Table 4.2), zeta potential (ZP) and encapsulation efficiency (EE), using methods previously described.

	Blank SLNs (all temperatures)				**atRA SLNs (all temperatures)**			
	Size (Z)	Size (N)	ZP	EE	Size (Z)	Size (N)	ZP	EE
Day 1	✓	✓	✓	✗	✓	✓	✓	✓
Day 7	✓	✓	✓	✗	✓	✓	✓	✓
Day 28	✓	✓	✓	✗	✓	✓	✓	✓
Day 56	✓	✓	✓	✗	✓	✓	✓	✓
Day 84	✓	✓	✓	✗	✓	✓	✓	✓

4.2.9. A549 culture

A549 cells are a human respiratory cell line, often used in cell culture as a model for ATII cells – and as such were selected for use in this study [273]. A549 cells were obtained from the ATCC (catalogue no. CCL-185) and maintained in DMEM/Ham's F12 medium (Sigma Aldrich, Ireland) supplemented with 10% fetal bovine serum (FBS), and 1% penicillin/streptomycin (Labtech, UK), at 37°C and in a 5% CO_2 atmosphere. The cells were plated in T175 (Sarstedt, Ireland) cell culture flasks and subcultured before reaching confluency using a 0.1% trypsin solution in EDTA (Sigma). The culture medium was changed every two days. The cells were split 1:5 during each passage. The passages used for the following experiments were 80–90.

4.2.10. Evaluation of A549 viability following supplementation with atRA SLNs

A549 cells were cultured as described in section 4.2.9, and underwent expansion and three passages prior to seeding in experiments. Cells were then seeded in 24 well flat-bottom adherent plates (2 x 10^4 cells/ well in 0.5 mL DMEM/F12 media) and incubated for 24 h. After 24 h, media was removed from wells and cells were washed three times with PBS (Sigma Aldrich, Ireland). atRA SLNs were then suspended in media at two different concentrations (SLNs containing atRA equivalent to 5 µg/mL and 10 µg/mL) and pipetted gently onto cells. Non-encapsulated atRA at a concentration of 10 µg/mL in media was used as a control, as were blank SLNs (equal to the weight of 10 µg/mL atRA SLNs used), and media alone. After 4, 24, 48 and 72 h incubation, media was removed from wells and cells were washed three times with PBS, before performing a Cell Counting Kit 8 (CCK-8) assay according to the manufacturer's instructions. Briefly, media + 10% CCK-8 reagent was added to each well, and plates were returned to the incubator for 2 h to react. 100 µL of each sample was plated per well, in triplicate, on a clear 96 well plate, and absorbance of the samples was measured at 450 nm using a microplate reader. Cell viability was then calculated using the following equation:

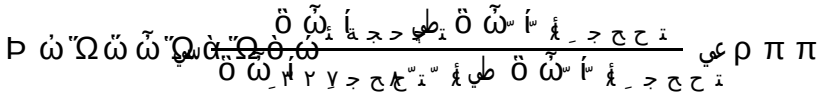

Equation 4.3. Equation used for determining % viability of A549s following supplementation with either raw atRA, atRA SLNs or blank SLNs.

4.2.11. Preparation of atRA-SLN loaded Respiragel

atRA SLNs were incorporated into the hydrogel as an additional step in the hydrogel formulation protocol (detailed in sections 2.2.2 and 2.2.3). SLNs were added in to the hydrogel following rehydration of the polymer wafer in βGP and pH adjustment. atRA

SLNs were weighed and added to the hydrogel under gentle stirring, to give a concentration of 10 µg atRA/mL gel.

4.2.11.1. Assessment of rheological properties of the atRA-SLN Respiragel

Testing was performed using an AR-1000 Rheometer (TA Instruments), as detailed in section 2.2.4, by way of temperature sweeps (25 – 40^{o}C) and time sweeps (at 37^{o}C for 30 min). Samples were tested under an oscillatory shear procedure, at 1 Hz and 5 Pa. Following this, polymer dispersions were also subjected to a flow procedure, to measure viscosity as a function of shear stress (1 – 80 Pa, at 25^{o}C). Each test was performed in triplicate, and on three distinctly separate atRA-hydrogels to ensure reproducibility of results.

4.2.11.2. SEM of lyophilised atRA-SLN Respiragel

Lyophilised atRA-SLN Respiragel samples were examined using scanning electron microscopy (SEM) in order to evaluate their architecture and internal pore size. Following lyophilisation, samples were mounted to an aluminium stub using a carbon paste and sputter coated with gold. Imaging of the wafers and hydrogels was performed using a Zeiss Supra 35VP SEM microscope (Zeiss, Jena, Germany).

4.2.11.3. atRA release from SLN-loaded Respiragel using a Float-A-Lyzer® apparatus

Release studies were performed using a Spectra/Por® Float-A-Lyzer® G2 device with a molecular weight cut off (MWCO) of 300 kD, as described in section 4.2.7. atRA SLN loaded hydrogel (1 mL) was transferred to the internal compartment of the Float-A-Lyzer®. Blank SLNs and blank hydrogel were used as controls. All subsequent apparatus set up and sampling was as previously described. Samples were analysed by HPLC using

the method described in 4.2.5 and concentration of drug present calculated using the atRA calibration curve (Appendix 2.1).

4.2.12. Statistical analysis

Two-way ANOVA followed by Bonferroni post-hoc analysis was performed to determine statistical differences in SLN/A549 viability studies described in section 4.2.10. All statistical tests were performed using GraphPad Prism v6 (GraphPad Software Inc., CA, USA). Error is reported as standard deviation (SD) for particle size data, and standard error of the mean (SE) elsewhere. Significance was determined using a probability value of $P \leq 0.05$. A minimum of n=3 independent replicates was performed for all experiments.

4.3.Results

4.3.1. Physicochemical characterisation of atRA and blank SLNs

4.3.1.1. SLN size, zeta potential and polydispersity index

Optimisation of the protocol for formulation of SLNs was required to achieve the preferred particle size (Z-ave), polydispersity index (PDI) and zeta potential (ZP). Initial formulations of blank SLNs contained Compritol® 888 ATO and poloxamer 188 only. Assessment of these particles showed a larger particle size than desired, coupled with a high PDI, indicating poor homogeneity of the nanoparticle suspension. Subsequent formulations introduced a second surfactant, Tween® 80, due to findings in the literature suggesting the combination of two surfactants results in smaller particle size [261] (Table 4.1).

In addition to these formulation changes, process variables were also modified, such as homogenisation time (HT) and sonication time (ST). Previous literature showed that HT did not have an effect on Z-ave, PDI and ZP [251], which is most likely due to the fact that the homogenisation step serves to ensure emulsification of the lipid in the aqueous phase, rather than affecting nanoparticle parameters. As a result of this, and our own findings, HT was reduced from an initial duration of 15 min to a final duration of 10 min.

ST, on the other hand, has a significant effect on Z-ave and PDI, as this is the step where nanoparticle size is determined. It was previously found that an increase in ST to as much as 10 min leads to a smaller Z-ave and PDI [251]. Based on this, initial formulation attempts in this study trialled STs of 20 min and 15 min for comparative purposes. The results from Table 4.3 show similar nanoparticle characteristics for both durations, leading to the 15 min step being selected for future formulations. On achieving consistent Z-ave, ZP and PDI values, atRA was added in to the formulation and particles were re-assessed (Table 4.3; Figure 4.4).

Table 4.3. Formulation and process optimisation and its effect on Z-ave, ZP and PDI. ST = sonication time (@ 70W), HT = homogenisation time (@ 11,000 RPM).

Batch (% = w/v)	ST	HT	Z-ave (nm)	ZP (mV)	PDI
1: 7.5% Compritol® 888 + 2.5% Poloxamer 188	4 x 5 min cycles	15 min	319.98	-29.9	0.766
2: 7.5% Compritol® 888 + 1.5% Poloxamer + 1.5% Tween® 80	4 x 5 min cycles	15 min	286.2	-25.0	0.455
3: 7% Compritol® 888 + 1.5% Poloxamer + 1.5% Tween® 80	4 x 5 min cycles	10 min	278.96	-25.2	0.438
4: 7% Compritol® 888 + 1% Poloxamer + 1% Tween® 80	4 x 5 min cycles	10 min	287.86	-25.733	0.399
5: 5% Compritol® 888 + 1% Poloxamer + 1% Tween® 80	3 x 5 min cycles	10 min	132.87	-31.24	0.359
6: 5% Compritol® 888 + 1% Poloxamer + 1% Tween® 80 + 1% atRA (freeze dried)	3 x 5 min cycles	10 min	176.85	-11.87	0.259

A

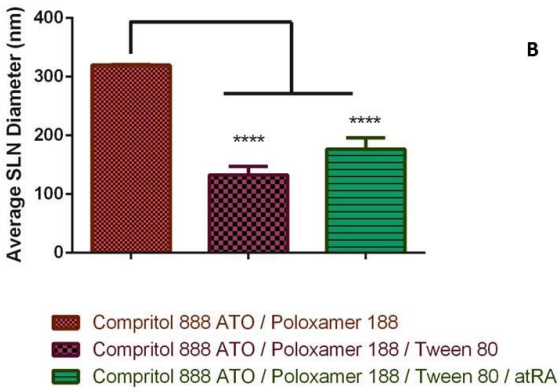

B

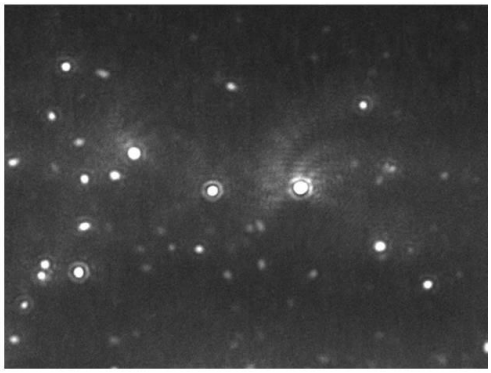

C

Formulation	Zeta Potential (mV)	Polydispersity Index	Particle Size (nm) (NANOSIGHT)
Compritol® 888 ATO / Poloxamer 188	-17	0.766	-
Compritol® 888 ATO / Poloxamer 188 / Tween® 80	-8.595	0.359	122.7
Compritol® 888 ATO / Poloxamer 188 / Tween® 80 / atRA	-11.87	0.259	126.27

*Figure 4.4(A). Average particle size data obtained using the Zetasizer Nano ZS (Malvern Instruments, UK) on assessment of three different SLN formulations. SLNs containing one surfactant (poloxamer 188) were of a large particle size. Addition of a second surfactant reduced this particle size. Inclusion of the drug molecule, atRA, resulted in a non-significant increase in size to 176.9 nm. Both blank SLNs and atRA SLNs are significantly smaller than SLNs composed of lipid + one surfactant (**** = P < 0.0001, One-way ANOVA + Tukey's post-hoc test); (B) Image of atRA SLNs obtained using a NanoSight NS300; (C) Table indicating average ZP for each SLN formulation, PDI for each formulation, and average particle size – obtained a second time, using the NanoSight ZS300.*

4.3.1.2. SLN morphology

Transmission election microscopy (TEM) of SLNs was carried out in order to assess particle morphology and confirm particle size for atRA loaded and blank SLNs. Images obtained using TEM (Figure 4.5) showed atRA SLNs to be of a spherical shape, and have also confirmed size range to be approx. 100-200 nm (supporting the results obtained using DLS and NTA).

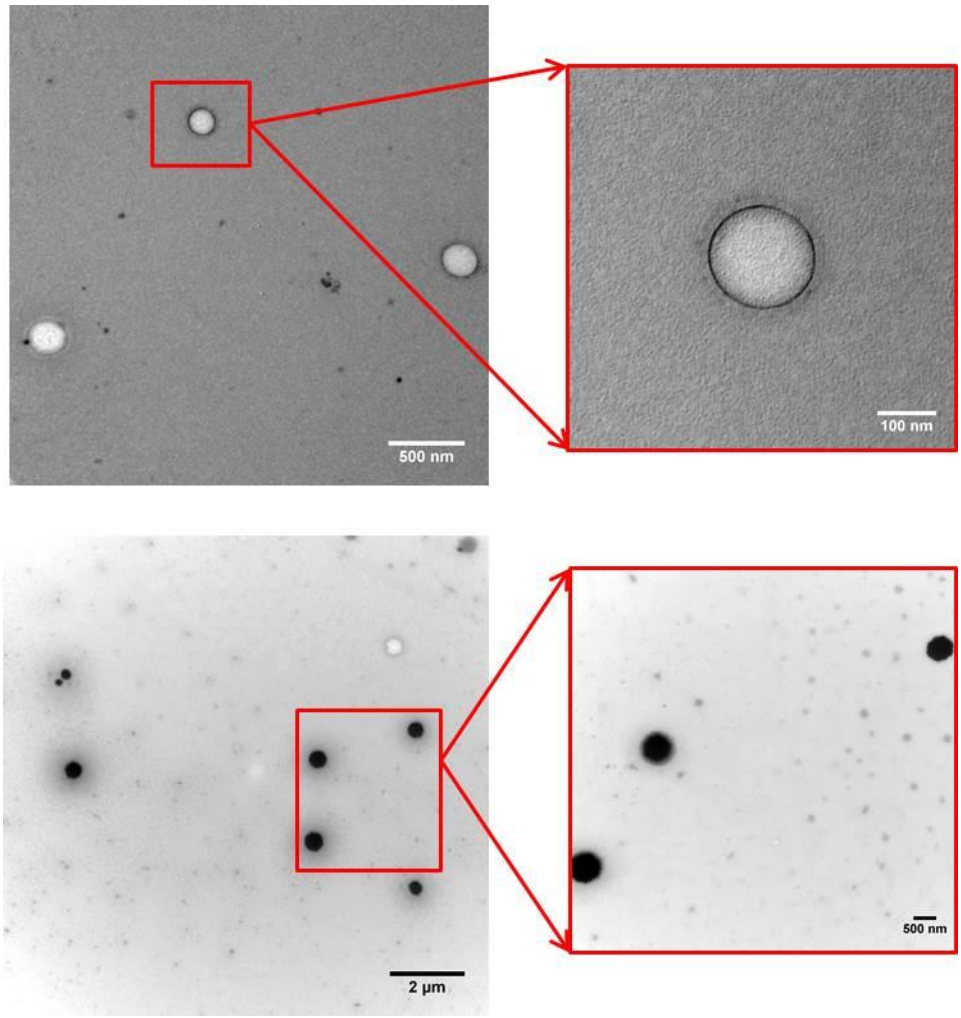

Figure 4.5. Images obtained using transmission electron microscopy (TEM) showing atRA loaded SLNs, (top) stained using 2% uranyl acetate and (bottom) stained with 2% osmium tetraoxide. All images show particles of approx. 100-400nm in size, and of a spherical shape.

4.3.2. SLN yield, drug loading and encapsulation efficiency

Average nanoparticle yield was assessed gravimetrically, with drug loading and encapsulation efficiency being assessed via HPLC (Table 4.4). Nanoparticle yield and encapsulation efficiency were found to be high, with an average yield of 92.14% and average drug encapsulation of 85.47%, suggesting very high drug entrapment in the nanoparticles. Conversely, drug loading was found to be low, on average 0.48%. This is

expected however, as lipid has a certain drug loading capacity, which if exceeded, can lead to decreased encapsulation efficiency. Therefore, finding the balance in achieving a high encapsulation without exceeding the drug loading capacity of the lipid is of critical importance in the formulation of SLNs.

Table 4.4. Average nanoparticle yield (%), drug loading and encapsulation efficiency of atRA SLNs (n=10 ± SD).

	Yield %	Drug Loading (DL) %	Encapsulation Efficiency (%)
atRA SLN	92.14 ± 2.45	0.48 ± 0.05	85.47 ± 8.77

4.3.3. atRA release from SLNs

As shown in Figure 4.6A, SLNs presented a complex *in vitro* atRA release pattern. A burst release of loaded atRA was observed for the first 8 h during which time almost 30% of the drug was released, followed by a more sustained release profile for six days. After 7 days, the average release from the particles was 43%.

The release profile obtained was analysed using the zero order, first order, Higuchi and Korsmeyer-Peppas mathematical models. Linear regression was used to calculate the coefficient values (R^2). In order to obtain the most accurate release profile, the data was split into first day release and latter release profiles. The first 8 h of release resulted in zero-order kinetics (Figure 4.6C), with the second section resulting in Korsmeyer-Peppas kinetics (Figure 4.6D).

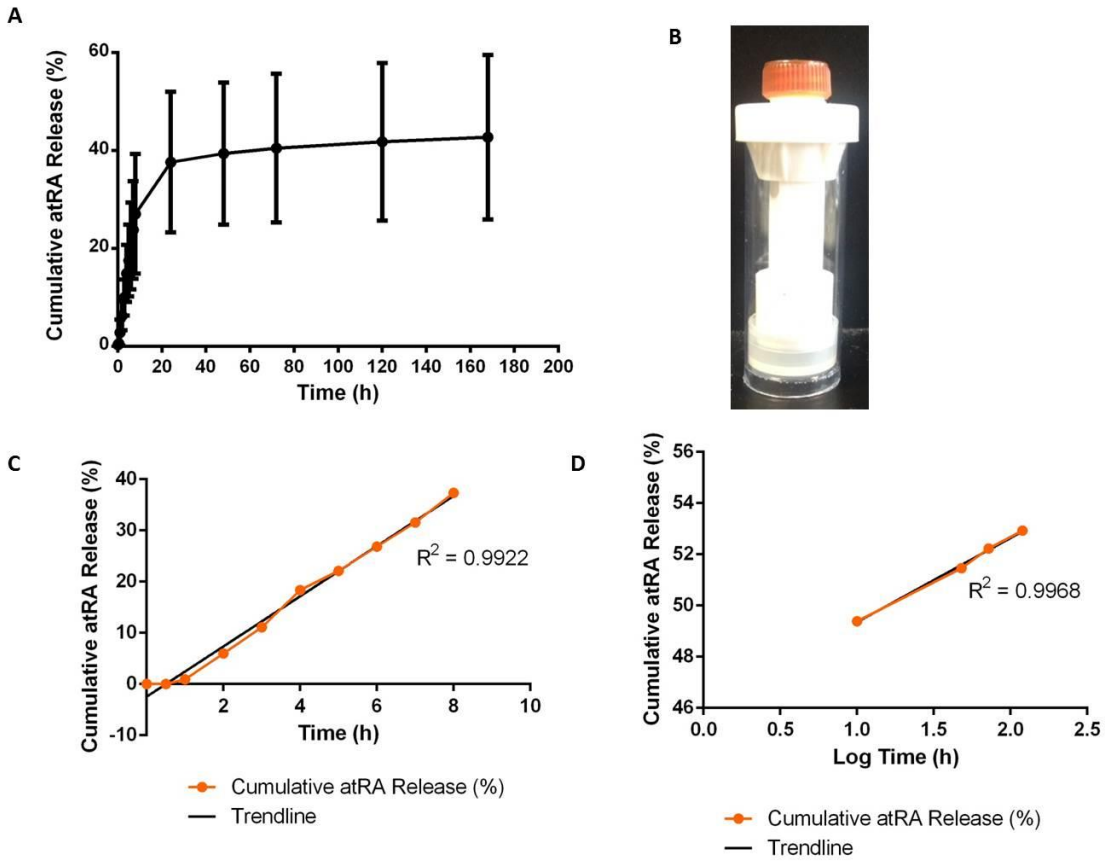

Figure 4.6(A). Cumulative release of atRA from 20 mg lyophilised SLN powder at 37°C over the space of 7 days using a Float-A-Lyzer® G2 dialysis device. Data expressed as a percentage of the total atRA loaded into 20 mg SLNs. Error bars represent mean + SE (n=4); (B) Float-A-Lyzer® G2 dialysis device; (C) Mathematical modelling of time points 0-8 h resulting in zero order release kinetics. Non-linear regression analysis applied using GraphPad v6. R^2 = 0.9922; (D) Mathematical modelling of time points 24-120 h (log time) versus cumulative atRA release (%) using non-linear regression analysis in GraphPad v6. Data follows Kors Peppas release kinetics. R^2 = 0.9968.

4.3.4. Stability studies of atRA and blank SLNs

4.3.4.1. Average particle size over time

In order to determine physical stability of atRA (Figure 4.7A) and blank SLNs (Figure 4.7B), average particle size measurements were recorded at various time points up to three months (i.e. day 1 following preparation, day 7, day 28, day 56 and day 84). SLNs

were also stored under three different storage conditions during this time, in order to determine optimal storage temperature. Particle size measurements were recorded using both the Zetasizer Nano ZS and the Nanosight NS300. On assessment with the Zetasizer, atRA SLNs stored at room temperature (i.e. 20^{o}C) experienced the most significant increase in particle size over the duration of the study. SLNs stored at 4^{o}C experienced a significant increase in particle size from day 1 to day 7, but no further changes in particle size. SLNs stored at -20^{o}C did not undergo any significant changes in particle size. However, on assessment with the Nanosight, it was found that no significant changes in particle size were observed under any temperature condition.

A

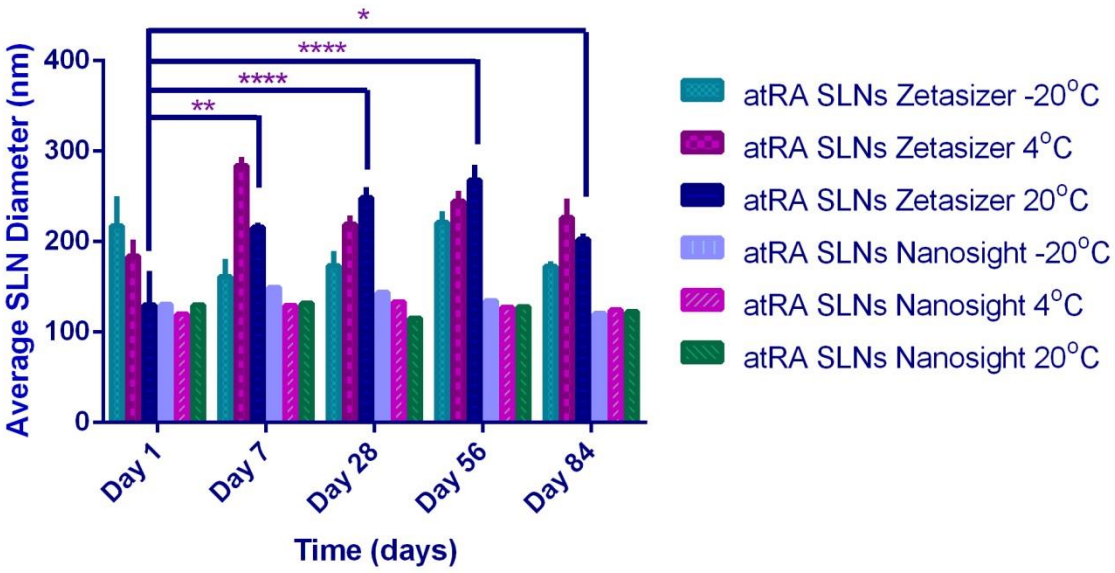

B

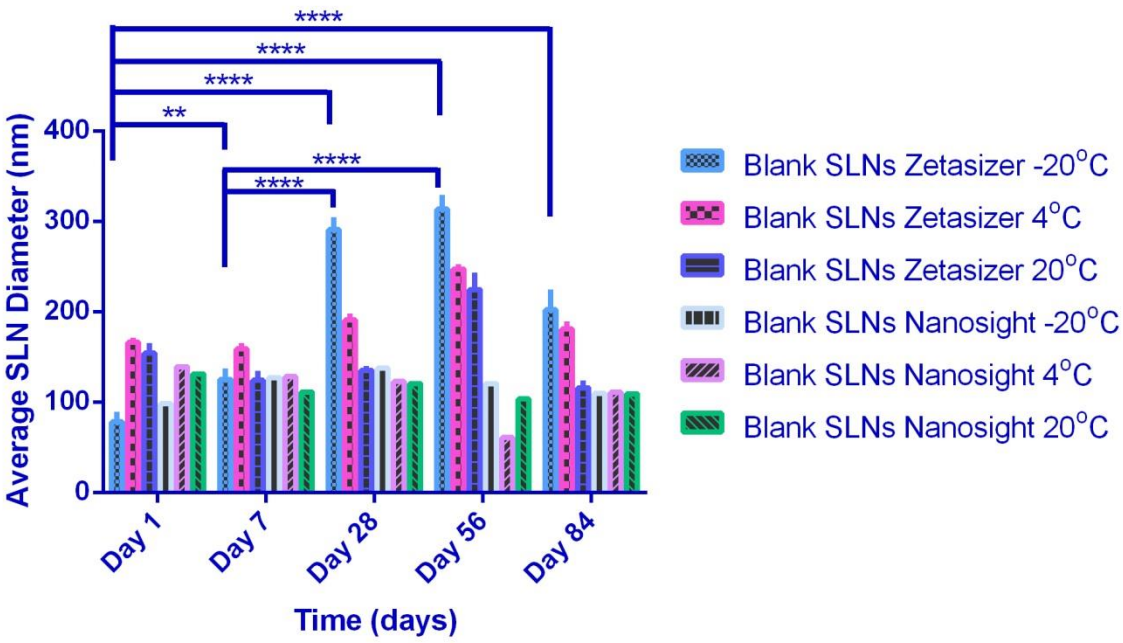

*Figure 4.7(A). Average particle size data for atRA SLNs stored at 3 temperature conditions: -20°C, 4°C and 20°C (freezer, fridge or room temperature). Particle size was measured using both a Zetasizer Nano ZS and a Nanosight NS300 (both Malvern Instruments, UK). Particle size changes appear more significant on measurement using a Zetasizer compared with the Nanosight. Storage at +20°C results in significantly larger particle size; (B) Average particle size for blank-SLNs stored at 3 temperature conditions -20°C, 4°C and 20°C. Particle size was measured using both a Zetasizer Nano ZS and a Nanosight NS300 (both Malvern Instruments, UK). Particle size changes appear more significant on measurement using a Zetasizer compared with the Nanosight. Storage at -20°C results in significantly larger particle size Results are presented as mean particle size ± SE. Significance determined via two-way ANOVA, with Tukey's post hoc test. * = P<0.01, ** = P<0.001, *** = P<0.0001 and **** = P<0.00001.*

On measurement of particle size of blank SLNs, differences in Z-ave over time and at different storage temperatures were noted when measurement was performed using the Zetasizer, but were not observed when using the Nanosight. Storage at -20°C resulted in significantly increased particle size throughout the study which was not observed with atRA SLNs (Figure 4.7). There is no significant change in blank SLN size at

4°C up to day 56, at which point a significant increase is detected. Similarly to atRA SLNs, a significantly increased size is found on storage at 20°C.

4.3.4.2. Average zeta potentiabver time

Stability studies also aimed to determine changes in zeta potential over time (Figure 4.8A). For atRA SLNs, the optimal storage temperature appears to be -20°C due to ZP remaining low at -14 mV by day 28. By day 56, ZP for all storage conditions has increased to between -10 and -5 mV, which indicates that on re-dispersion a less stable suspension may result. Storage at 4°C appears to have intermediate ZP, with storage at 20°C showing a gradual increase in ZP at each time point. For blank SLNs, ZP appears to increase consistently for all storage conditions. Storage at 4°C appears to be optimal with a low ZP at day 84 of -13 mV.

A

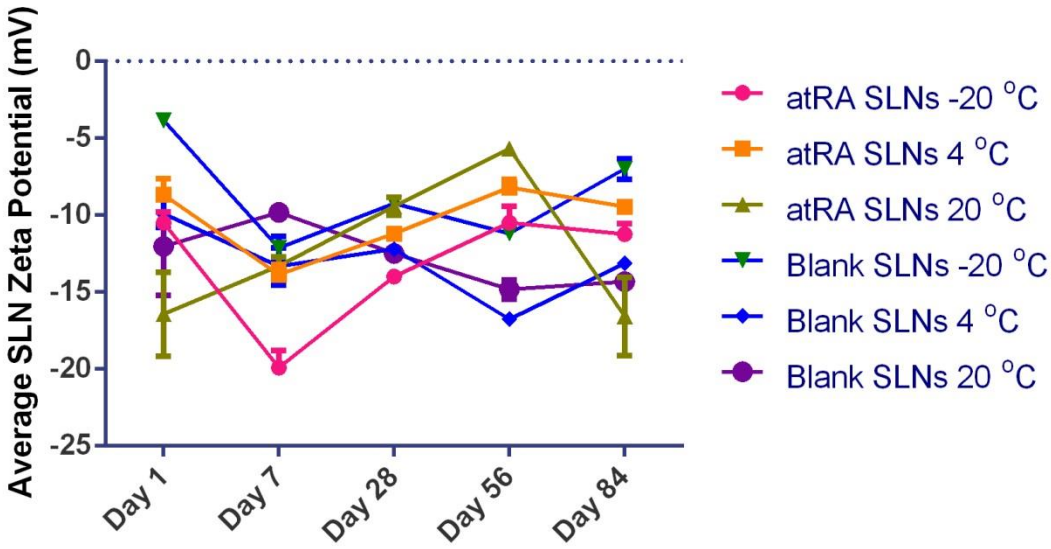

B

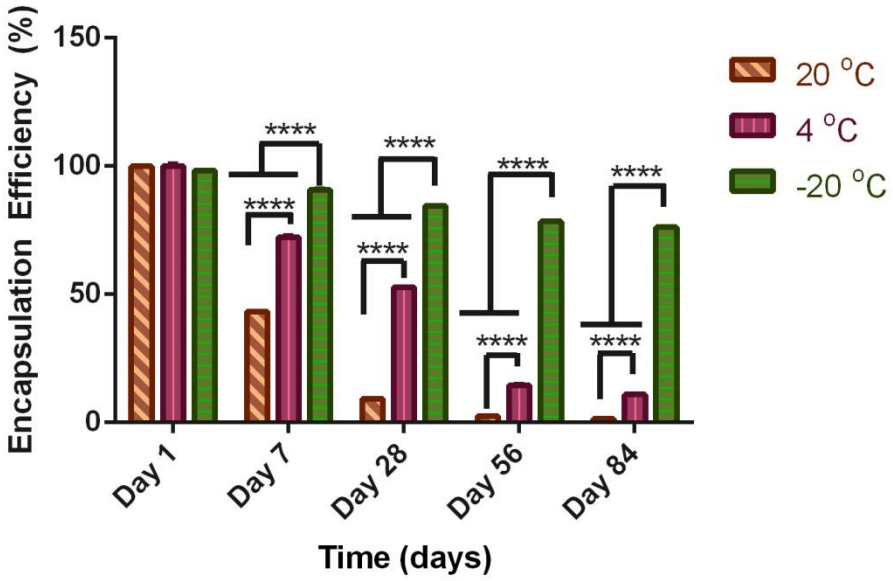

*Figure 4.8(A). Average zeta potential data for atRA and blank SLNs stored at 3 temperature conditions: -20°C, 4°C and 20°C (freezer, fridge or room temperature). Zeta potential was measured using a Zetasizer Nano ZS (Malvern Instruments, UK). Storage at +4°C appears to result in the most consistent zeta potential over time. Data is presented as mean zeta potential ± SE; (B) Average atRA encapsulation efficiency over time, on storage of SLNs at 3 different temperatures (-20°C, 4°C and 20°C).Storage at 20°C results in the most significant drop in drug encapsulation at all time points. Storage at 4°C also significantly reduces atRA encapsulation. Encapsulation is best retained at -20°C. Results are presented as mean encapsulation efficiency ± SE. Significance determined via two-way ANOVA, with Tukey's post hoc test. * = P<0.01, ** = P<0.001, *** = P<0.0001 and **** = P<0.00001.*

Repeated measurement of encapsulation efficiency was also performed via HPLC of atRA SLNs, to determine whether storage temperature affects loaded atRA stability. From Figure 4.8B, it is clear that storage at 20°C results in significant reduction in encapsulated atRA, with 1.46% encapsulation at day 84 compared with almost 100% at day 1. Storage at 4°C also results in a significant decrease in EE%, though to a lesser extent than at 20°C. Final encapsulation at day 84 is 10.94%. EE% also decreases in a time dependant manner for particles stored at -20°C, though again to a lesser extent,

with final EE of 76%. This indicates that atRA encapsulated in SLNs is most stable at -20^{o}C with higher temperatures resulting in gradual degradation of the molecule.

4.3.5. Evaluation of A549 viability post atRA SLN supplementation

Cell viability assays were carried out to determine biocompatibility of atRA SLNs (Figure 4.9). A549 lung epithelial cells were used as the *in vitro* model cell type, due to their similarity to *in situ* alveolar type II (ATII) cells [274]. Supplementation with both a low dose (LD = 5 µg/mL) and high dose (HD = 10 µg/mL) of atRA SLNs resulted in no significant reduction in cell viability over the study duration of 72 h. Both raw atRA alone and blank SLNs used as controls also showed biocompatibility with the A549 cells.

A

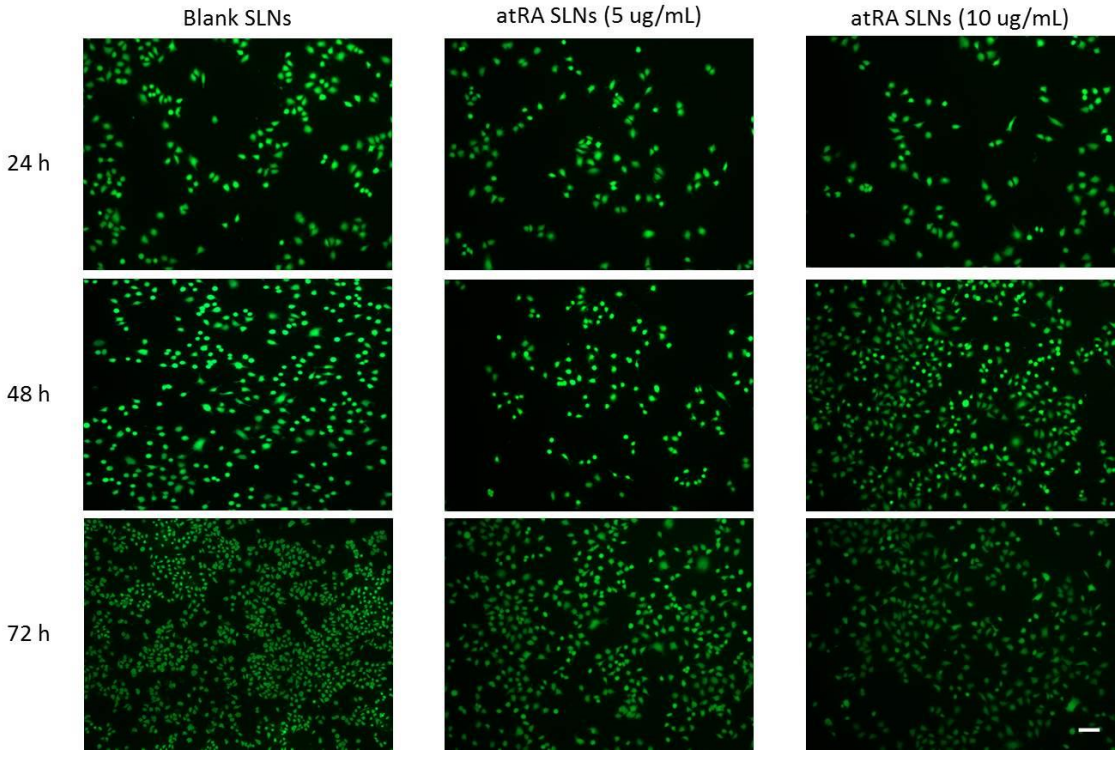

B

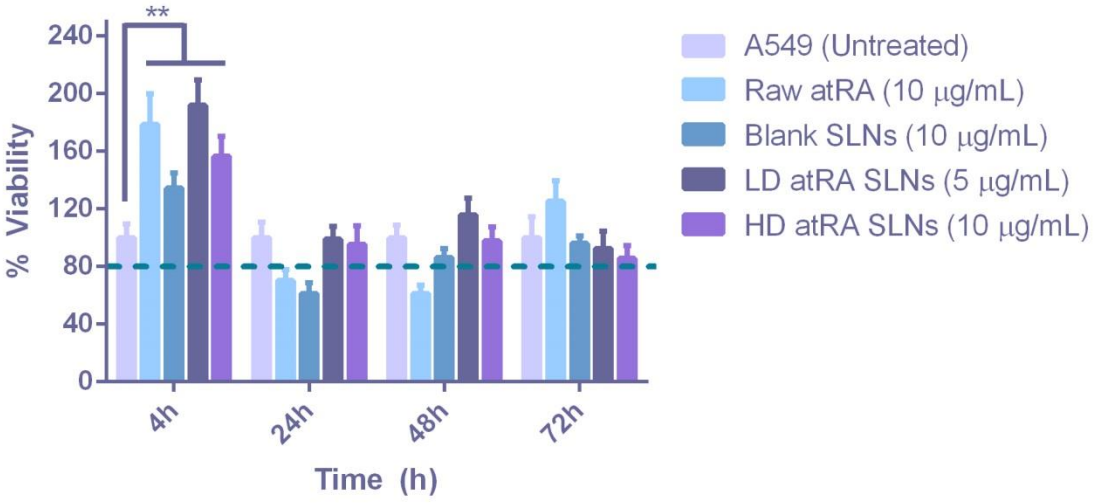

*Figure 4.9(A). LIVE/DEAD stain results for A549 cells supplemented with either blank SLNs, low dose atRA SLNs (5 µg/mL) or high dose atRA SLNs (10 µg/mL) imaged at 24 h, 48 h and 72 h. Live cells are stained green, dead cells are stained red. Scale bar, 100 µm; (B) Average A549 cell viability following supplementation with atRA and blank SLNs over a period of 72 hours. Raw atRA alone and untreated A549 cells were used as controls. Assay was performed using a CCK-8 viability kit. Results are presented as mean cell viability ± SE. Significance determined via two-way ANOVA, with Dunnett's post hoc test. ** = P<0.001.*

4.3.6. atRA loaded "Respiragel" characterisation

4.3.6.1. Assessment of rheological properties of the atRA SLN hydrogel

atRA SLNs were suspended at a conc. of 10 µg/mL in the hydrogel previously developed in Chapter 2. Repeated rheological characterisation indicated that the gel retained its thermoresponsive properties and its gelation temperature of 37°C (Figure 4.10A). Time sweeps showed that the atRA loaded Respiragel was able to maintain its structure on a prolonged hold at 37°C, and in fact increased in strength (as shown by the increasing G' in Figure 4.10B). The gel also maintained its shear thinning properties, shown by the

flow testing in Figure 4.10C, indicating a decrease in viscosity on application of increasing shear stress.

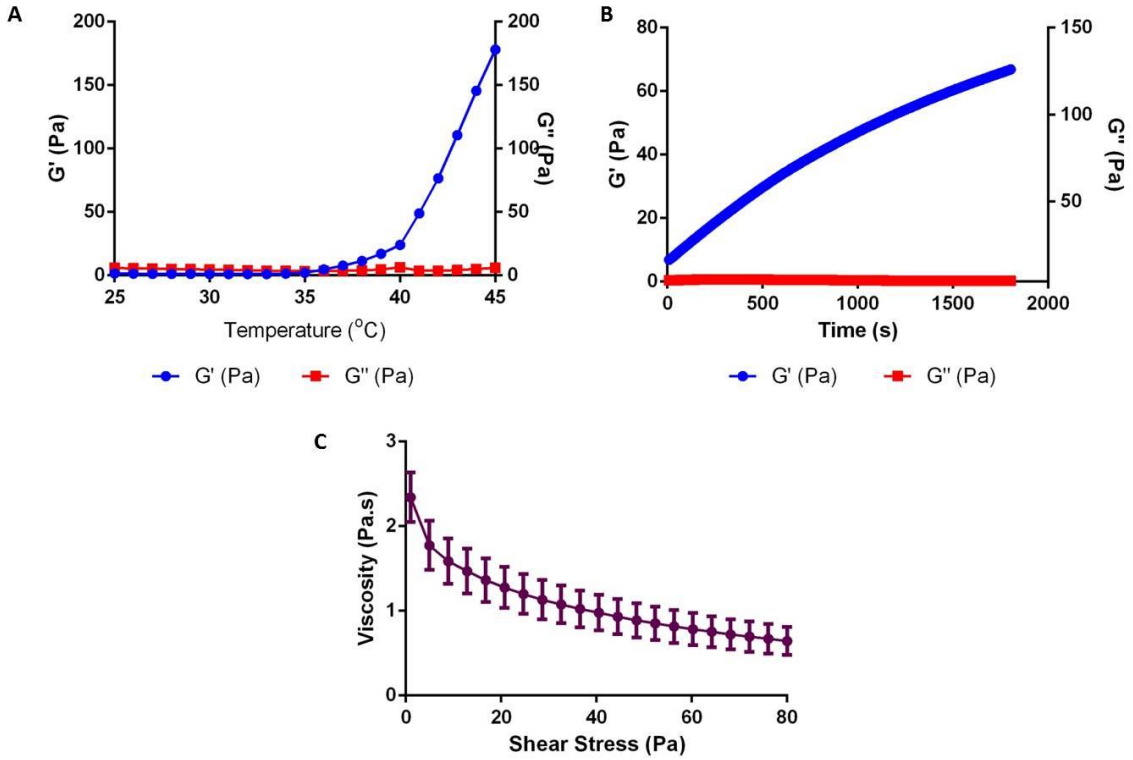

Figure 4.10 (A). A rheological temperature response curve obtained using an AR-1000 rheometer (TA Instruments) showing atRA SLN loaded Respiragel (i.e. 2.5% methylcellulose, 0.1% collagen, 5.6% beta-glycerophosphate) at a concentration of 10 µg/mL atRA in gel. G' denotes storage modulus and G" denotes loss modulus. Gelation of atRA SLN hydrogel occurs at 37°C, indicating thermoresponsivity is not affected by inclusion of SLNs; (B) Time sweep of atRA SLN loaded Respiragel, involving holding the gel at 37°C for 30 min. G' continues to increase as time increases, indicating improvement of gel strength at this temperature; (C) Flow sweep of atRA SLN loaded Respiragel, showing a decrease in viscosity with increase in shear stress (1-80 Pa) at 25°C. This indicates the gel continues to be shear thinning in nature following inclusion of atRA SLNs.

4.3.6.2. Determination of atRA SLN loaded Respiragel ultrastructure

The morphology of the lyophilised atRA SLN loaded Respiragel wafers was determined using scanning electron microscopy (SEM). Image A (Figure 4.11) shows the uniform porous nature of the internal wafer structure, while image B shows the elongated pores which appeared close to the edges of the sample. These images show a densely porous structure, with a pore size of approximately 100 µm. No structural change can be observed following inclusion of atRA SLNs in the hydrogel matrix.

A **B**

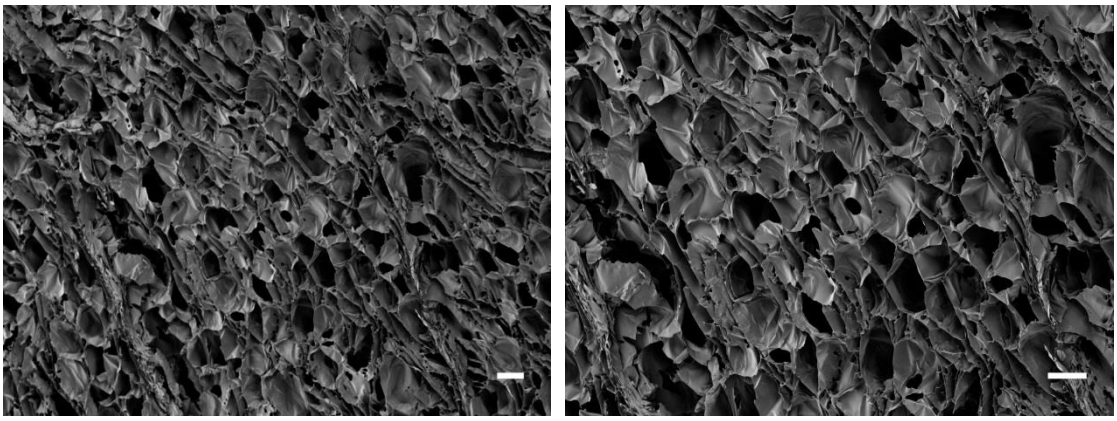

Figure 4.11. Representative scanning electron micrographs, showing internal porous structure of lyophilised atRA SLN loaded Respiragel samples. Scanning electron micrographs were obtained using a Zeiss Supra 35VP SEM microscope (Zeiss, Jena, Germany). Image (A) was taken at 55 X magnification and 5 kV accelerating voltage, and image (B) taken at 80 X magnification and 5 kV accelerating voltage. Scale bar, 100 µm.

4.3.6.3. atRA release from SLN loaded hydrogel using a Float-A-Lyzer® apparatus

Release studies performed in section 4.3.3 were repeated following suspension of atRA SLNs in Respiragel and were compared with release of atRA from SLNs alone (Figure 4.12A). A burst release was observed for the first 8 h during which time 16.4% of the drug was released. From 8 h to 24 h, a further 14% atRA was released. After 24 h a

more sustained release profile was observed for five days. After 7 days, the average release from the particles was 39.5%.

The release profile obtained was analysed using the zero order, first order, Higuchi and Korsmeyer-Peppas mathematical models. Non-linear regression was used to calculate the coefficient values (R^2). In order to obtain the most accurate release profile, the data was split into first day release and latter release profiles. The first 8 h of release resulted in zero-order kinetics (Figure 4.12B), with the second section resulting in Korsmeyer-Peppas kinetics (Figure 4.12C) – the same observation that was found with release of atRA from SLNs alone (section 4.3.3).

A

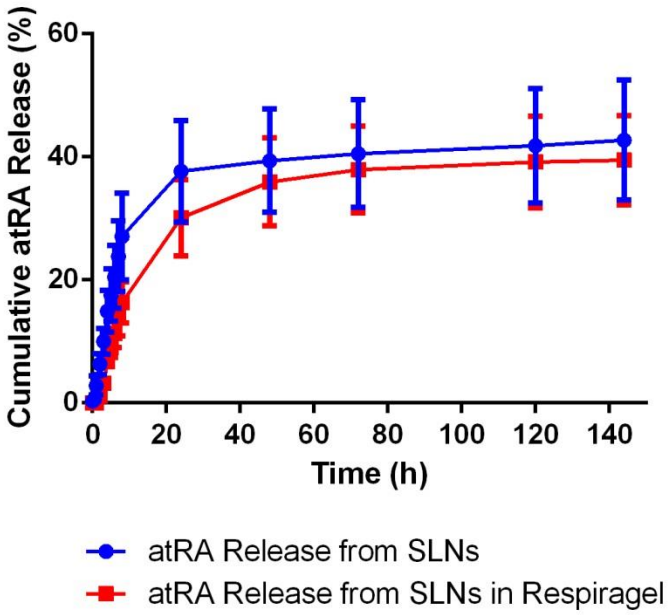

B

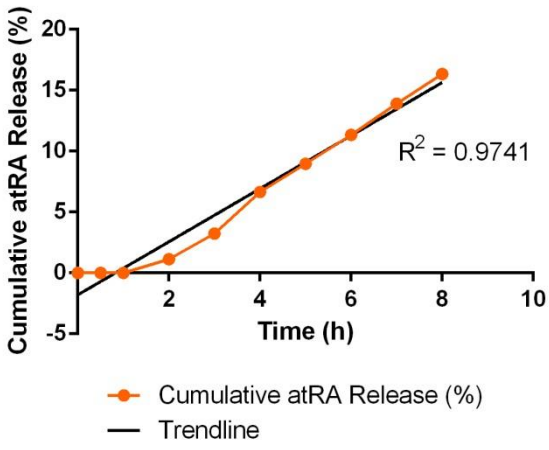

C

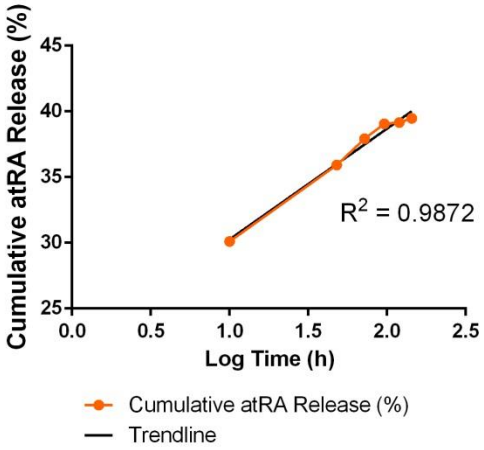

Figure 4.12(A). Cumulative release of atRA 10 µg/mL SLN loaded hydrogel at 37°C over 7 days using a Float-A-Lyzer® G2 dialysis device. Data expressed as a percentage of the total atRA loaded into SLNs loaded into hydrogel. Error bars represent mean + SE (n=3); (B) Mathematical modelling of time points 0-8 h resulting in zero order release kinetics. Non-linear regression analysis applied using GraphPad v6. R^2 = 0.9741; (C) Mathematical modelling of time points 24-144h (log time) versus cumulative atRA release (%) using non-linear regression analysis in GraphPad v6. Data follows Korsmeyer Peppas release kinetics. R^2 = 0.9872.

4.4.Discussion

While there is a large amount of literature describing the formulation and applications of SLNs (and indeed those loaded with atRA), their suspension in a hydrogel for loco-regional delivery to the distal airways has not, to the best of our knowledge, been investigated before. Therefore, the formulation of an atRA SLN loaded hydrogel for delivery and resultant anti-inflammatory activity in COPD represents a potentially novel approach in tackling the growing burden of chronic lung disease, which will be further examined in coming chapters.

Initially, a suitable SLN formulation for the encapsulation of atRA needed to be developed, which required selection of an appropriate lipid and surfactant combination. Previously, various combinations of a wide range of lipids and surfactants have been utilised in the formulation of SLNs [250]. Our preliminary formulation contained Compritol® 888 ATO as the lipid and poloxamer 188 as the surfactant. It was important from a clinical translation perspective that any excipients utilised in this formulation would have a basis of regulatory approval. Both Compritol® 888 ATO and poloxamer 188 are accepted as "inactive ingredients" by the Food and Drug Administration (FDA). Compritol® 888 ATO is a hydrophobic mixture of mono- (12 – 18% w/w), di- (45 – 54% w/w) and tri- (28 – 32% w/w) behenate of glycerol with a melting point in the range of 69 – 74^{o}C. Glyceryl behenate has been used as an excipient in marketed products manufactured by many different pharmaceutical companies (Table 4.5). A literature review also revealed Compritol® 888 ATO to be the most frequently used lipid in the formulation of SLNs [251,259,263,275–278].

Table 4.5. Internationally marketed products manufactured by different pharmaceutical companies that contain glyceryl behenate as an excipient. Reproduced from [279].

Trade name	Active pharmaceutical ingredient	Dosage forms	Manufacture	Use
Zelnorm	Tegaserod maleate	Tablets	Novartis	Treatment of irritable bowel syndrome
Aplenzin	Bupropion hydrobromide	Tablets	Sanofi-Aventis US	Antidepressant
Effient	Prasugrel	Tablets	Eli Lilly and Co.	Reduce the risk of heart-related events
Glumetza	Metformin Hcl	Extended-release tablets	Depomed	Oral antihyperglycemic drug for management of type 2 diabetes
Horizant	Gabapentin enacarbil	Extended-release tablets	GlaxoSmithKline LLC	Treat moderate-to-severe restless legs syndrome
Intuniv	Guanfacine	Extended-release tablets	Shire US Manufacturing, Inc.	Treatment of attention deficit hyperactivity disorder
Paxil-CR	Paroxetine hydrochloride	Extended-release tablets	GlaxoSmithKline LLC	Management of depression
Requip XL	Ropinirole	Extended-release tablets	GlaxoSmithKline LLC	Treatment of Parkinson's disease
Toviaz	Fesoterodine fumarate	Extended-release tablets	Pfize, Inc.	Treatment of overactive bladder
Tracleer	Bosentan	Tablets	Actelion Pharms Ltd	Managing pulmonary arterial hypertension
Wellbutrin XL	Bupropion hydrochloride	Extended-release tablets	GlaxoSmithKline	Antidepressant used for smoking cessation
Zmax	Azithromycin	Sustained-release granules for oral suspension	Pfizer, Inc.	Macrolide antibiotics for treatment of bacterial infections
Zyflo CR	Zileuton	Extended-release tablets	Cornerstone therapeutic, Inc.	Treatment of asthma
Cambia	Diclofenac potassium	Powder for oral solution	Nautilus Neurosciences, Inc.	Treatment of acute migraine attacks
Ibuprofen PM	diphenhydramine citrate, ibuprofen	Coated caplets	Dolgencorp LLC	Relief of occasional sleeplessness
Freelax	Magnesium hydroxide Saline laxative	Caplets	Wyeth	Relief of occasional constipation
Motrin PM	Diphenhydramine citrate Ibuprofen	Coated caplets	McNeil-PPC, Inc.	Relief of occasional sleeplessness

Selection of an appropriate surfactant was then required for nanoparticle formulation. When surfactants are incorporated into immiscible mixtures of oil and water, the surfactants can locate at the oil/water interface, which is thermodynamically stable, resulting in a reduction in surface tension [280]. Poloxamer 188 was selected for this formulation due to its frequent use in SLN formulations in combination with Compritol® 888 ATO [276–278,281,282]. Poloxamers, as discussed in Chapter 2, are tri-block copolymers of two ethylene oxide blocks attached to the ends of one propylene oxide polymer. Alteration of both the hydrophobe and the hydrophile allows for exceptional versatility for tailoring surfactant function and physical properties. In

general, poloxamers attach onto a particle surface via physical adsorption of the central hydrophobic region, leaving the hydrophilic region sticking out into the surrounding medium creating a "brush-like" appearance [283]. The inclusion of non-ionic surfactants such as these can also confer some steric stabilisation properties onto their associated nanoparticles, which may be of benefit [284]. Later formulations introduced a second surfactant, Tween® 80, due to larger than desired particle sizes and polydispersity indices, with findings in the literature suggesting that the combination of two surfactants results in substantially smaller particle size [285]. Tween® 80 is also FDA approved and is listed on the "inactive ingredient" database. Various concentrations of Compritol® 888 ATO, poloxamer 188 and Tween® 80 were trialled, as shown in Table 4.1.

Following this, process parameters were also optimised, by way of modifying the homogenisation time (HT) and the sonication time (ST). Starting HT was 15 min at 15,000 RPM, which was reduced to 10 min in subsequent protocols – this did not appear to have a negative effect on SLN Z-ave, ZP or PDI as no significant difference in comparative batches of SLNs was observed (Table 4.1). This corresponds with previous findings in the literature which suggest HT does not have an effect on nanoparticle size [251,286]. Following the reduction in HT, varying of ST was investigated. Initial ST was 4 x 5 min cycles, with a 1 minute pause in between. This was reduced to 3 x 5 min cycles with a 1 minute pause between – again, this change did not appear to have a significant effect on Z-ave, ZP or PDI. One previous study found a significant effect of ST on SLN size, conducted by Das *et al* [251]. However, this involves comparison of STs ranging from 1 – 10 min, compared with those investigated in this chapter (15 min and 20 min). Therefore, it is hypothesized that perhaps particle size reduction has a limit, which cannot be overcome with further sonication. Consequently, the final formulation selected was composed of Compritol® 888 ATO 5% w/v, poloxamer 188 1% w/v and Tween 80® 1% w/v, produced under 10 min homogenisation followed by 3 x 5 min sonication.

As previously mentioned in section 4.2.3, the Z-ave, or Z-average diameter, is the mean diameter of particles present in the sample. In terms of size, SLNs are defined to be < 1 µm – a condition which this SLN formulation satisfied. As one aim of this study was to suspend the SLNs in the hydrogel, we needed to determine if those produced fell within an acceptable range to permit this. On average, particles of approximately 300 nm or greater in size undergo sedimentation [287], indicating that these SLNs are sufficiently small to remain in suspension. In terms of PDI, or polydispersity index, a measure of the width of the particle size distribution, a polydisperse suspension (values close to 1) indicates that the sample has a very broad size distribution and may contain large particles or aggregates that could be slowly sedimenting. PDI values of close to 0 indicate a monodisperse suspension, where the particle sizes are distributed over a narrower range. In this case, a PDI of 0.359 indicates a relatively monodisperse suspension.

Zeta potential, then, is a measure of electrostatic charge in a dispersion. It is generally accepted in scientific literature that positively charged nanoparticles undergo cellular uptake *in vivo* to a higher extent than anionic particles [288]. Cellular uptake is not a requirement for these particles and as such, the formation of cationic particles was not of importance here. Zeta potential is also an indicator of the stability of particles in a suspension, due to the resulting attractive or repulsive forces. A highly charged dispersion indicates that the particles will experience repulsive forces, and will therefore be forced away from each other, leading to the formation of a stable dispersion. In the case of a weakly charged dispersion, particles are more likely to experience attractive forces, leading to agglomeration. In general, a ZP of greater than ± 30 mV is considered a stable suspension [289]. In this case, a resulting ZP of between -10 and -17 mV for blank SLNs may not be considered sufficiently charged to confer stability, which could indicate that particles may aggregate over time.

On achieving consistent size, zeta potential and polydispersity index values, our therapeutic signalling molecule of interest, all-trans Retinoic Acid (atRA), was added in

to the formulation and physicochemical characteristics were re-assessed. The inclusion of atRA initially led to a slight (but not significant) increase in Z-ave to 176.85 nm, a decrease in PDI to 0.259, and an increase in ZP to -11.87 mV. The increase in size of the SLNs was to be expected due to the addition of another molecule. Particle size distribution improved, as evidenced by the decreased PDI. ZP increased indicating possibly reduced stability. TEM was utilised to confirm atRA SLN shape and morphology, as it has previously been used for nanoparticle imaging in the literature [290]. Images show individual SLNs which are of rounded shape and approximately 100-200 nm in size, providing confirmation of the data generated by DLS and NTA.

atRA encapsulation within SLNs was determined via HPLC and was generally high, on average 85.47% (Table 4.4). SLNs for the delivery of atRA for various applications have been discussed in numerous previous publications, with varying success in encapsulation levels. Two previous studies found low levels of encapsulation with atRA [111,291] whereas other studies reported higher levels from a minimum of 54.49% up to a maximum of 94.60% in research conducted by Das et al [251] and averages of 96.2%, 97.4% and 95.8% respectively in further publications [261,263,292]. Encapsulation efficiency of atRA in SLNs is dependent on various factors but most importantly, on the choice of lipid selected. Compritol® 888 ATO, used in this study, is superior in terms of entrapment ability due to the resulting crystal lattice structure being less perfect in orientation when compared with homogenous glycerides, thus leaving more space for drug to be loaded [279]. The long chain length of behenic acid in Compritol® 888 ATO also enhances intermolecular entrapment of the drug by interchain intercalation [293]. It is hypothesised that a combination of these factors resulted in high encapsulation of atRA within the formed SLNs.

Release of atRA from SLNs appears to correspond with previous release data reported in the literature. A burst release was observed over the course of the first 8 h, after which point a more sustained profile became apparent (Figure 4.6A). Research conducted by Mehnert, Müller and zur Mühlen [294] found that release profile was

linked to production temperature of SLNs. The burst release was highest when producing at the highest temperature and applying the hot homogenisation method. Conversely, burst release decreases with decreasing production temperature and was almost non-existent when applying the cold homogenisation method. The same study also found that high surfactant concentration also resulted in high burst release. This was said to be due to redistribution of the active compound between the lipid and the water phase during the heating and cooling process associated with the hot homogenisation method. As a large amount of heat was used in the formulation process of these SLNs, and a relatively high concentration of surfactant was incorporated, it is likely that a combination of these findings contributed to a high initial burst release. The subsequent prolonged release profile is likely due to the release of drug entrapped within the lipid matrix [295].

Due to the observed biphasic release of atRA from SLNs, matching of the release profile to one mathematical model was not optimal. Therefore, the release profile was split into its two phases and subsequently applied to various models. The highest degree of correlation was observed with initial zero-order kinetics, followed by subsequent Korsmeyer-Peppas release (Figure 4.6, C and D). The correlation coefficient (R^2) was used as an indicator of the best fitting of the data to each model. Zero order describes release rate as being independent of drug concentration and Korsmeyer-Peppas indicates that release is a non-diffusion process [296]. Zero order release, in which a drug is released at a constant rate, is the ultimate goal of all controlled-release drug-delivery mechanisms. It leads, in principle, to the best control of plasma concentration of drug *in vivo* [297]. Korsmeyer-Peppas release on the other hand, indicates diffusion of water into the particle, subsequent swelling as water enters and the resultant dissolution of the matrix [298]. The description of this model correlates with previous discussion points relating to the second phase release being sustained due to prolonged release from the internal solid lipid phase in such nanoparticles.

It should also be noted that the final cumulative release of atRA from SLNs over the duration of the study was 43%. A terminal encapsulation efficiency assessment at the end point of the release study would have determined whether any residual atRA remained in the particles – however, by this point on visual inspection, the SLNs in suspension had turned from yellow (the colour of atRA) to white indicating no appreciable remaining drug quantity. Similar research carried out in RCSI by O'Leary *et al* investigated atRA release from an atRA collagen-hyaluronate film and also an atRA loaded bilayered collagen-hyaluronate scaffold at 37^{o}C [299]. They discovered that no atRA was found in the films at 48 h on re-testing for encapsulation. This is likely due to the short half-life of atRA, which is 0.5 – 2 h *in vivo* [300]. Taken together, this information suggests that some atRA released from SLNs into media at 37^{o}C would likely have been degraded prior to detection.

When developing a new drug delivery system, an estimation of stability is crucial as this indicates suitability for commercial applications. Stability studies of atRA and blank SLNs carried out in this work present a varied picture. Particle size across three storage conditions appears to result in an increase on measurement with the Zetasizer ZS Nano (utilising DLS or dynamic light scattering), whereas no significant change in mean particle size is observed on measurement with the Nanosight NS300 (utilising NTA, or nanoparticle tracking analysis). Average particle sizes obtained using the Nanosight also appear significantly smaller than the sizes recorded using the Zetasizer (Figure 4.7A). Various publications have addressed the discrepancies in particle size recorded from the use of DLS versus NTA [301–303]. In general, it has been found that NTA possesses clear advantages over DLS such as enabling clear visualisation of the sample, giving an approximate particle concentration and providing superior accuracy in sizing for both monodisperse and polydisperse samples. The presence of a small number of large particles in a sample has little impact on NTA accuracy, whereas this can have a large influence on data obtained using DLS [301]. Based on this, specific attention will be paid to results obtained from Nanosight assessment of particle size in the stability studies shown in Figure 4.7A and Figure 4.7B. No significant difference was observed in

particle size for particles at any storage condition when measured using the Nanosight, indicating SLN size remains consistent up to 3 months. This is a similar finding to those previously discussed in the literature indicating high stability of SLNs on prolonged storage [276,296].

Changes in ZP were observed for both atRA loaded and blank SLNs. These changes were not of a high magnitude however, with the largest difference occurring in both atRA and blank SLNs stored at -20^{o}C, showing variation of |9|mV. This may indicate that storage at this temperature leads to aggregation of particles, and could explain the changes observed in particle size measurement using the Zetasizer.

Significantly, examination of the encapsulation efficiency of atRA within SLNs showed a decrease at all storage temperatures over the course of this study. In general, encapsulation of a drug molecule within SLNs aims to improve drug stability. However, as previously discussed, atRA is extremely unstable and possesses a short half-life. Incorporation of atRA into SLNs clearly improves stability of the drug as it is still possible to detect atRA present in the samples up to 3 months (Figure 4.8B). The optimal temperature for storage with EE in mind appears to be -20^{o}C.

With a view to further *in vitro* testing of atRA and blank SLNs on a lung cell line, biocompatibility testing using A549s was carried out. Culture of A549 cells in the presence of two doses of atRA SLNs and blank SLNs showed no reduction in viability (Figure 4.9). This was anticipated due to the biocompatibility of the drug molecule used and all excipients selected, coupled with numerous previous research articles indicating the low cytotoxicity associated with similar SLNs [304–306]. This also complies with the International Organisation for Standardisation guidelines (ISO 10993-5:2009) [230], which states that samples with a cell viability larger than 80% can be considered non-cytotoxic. One potential limitation of this study, was that atRA used in SLNs had previously been dissolved in DMSO prior to formulation into particles, but blank SLNs contained no DMSO. It is thought that this is unlikely to have any significant effect on viability due to the very small amount which would be present in blank SLNs (X mg),

and also as there was no adverse effect on biocompatibility observed on assessment of atRA SLNs. However – inclusion of DMSO in blank SLNs would have been a more appropriate control.

Final assessment of atRA SLNs developed in this chapter involved incorporation of the particles in a previously developed hydrogel (see Chapter 2). Incorporation of the SLNs into the hydrogel resulted in no change to thermoresponse or shear thinning properties. This is important from a clinical translation perspective, as it indicates that flow behaviour improves when applying a stress, which is the force used when pushing through a syringe or catheter device.

Release of atRA from SLNs loaded into the hydrogel followed a similar pattern to that of atRA release from SLNs alone. A burst release was observed over the course of the first 8 h, after which point a more controlled profile became apparent (Figure 4.12A). As with release from SLNs alone, due to the biphasic release of atRA, matching of the release profile to one mathematical model was not optimal. Therefore, the release profile was split into its two phases and subsequently applied to various models. The highest degree of correlation was observed with initial zero-order kinetics, followed by subsequent Korsmeyer-Peppas release (Figure 4.12, B and C). The determination coefficient (R^2) was used as an indicator of the best fitting of the data to each model. On observation of the release models obtained, the R^2 value obtained from linear regression analysis for the first half of the dataset (zero order kinetics) is lower for atRA SLNs in hydrogel compared with SLNs alone (0.9741 versus 0.9922). Figure 4.12B also shows points from 1-3 h falling below the best fit line, indicting non-linear release at these points. This is likely due to the presence of a second matrix through which the drug is required to pass prior to detection. We hypothesize that during this time (0-3 h), atRA is releasing from SLNs within the gel, but the full amount of atRA released is not escaping the second matrix and being released from the hydrogel – therefore lower release is detected at these time points. After this point, the hydrogel may be saturated with atRA, resulting in a linear release from 4-8 h. Taken together, these

results indicate that atRA SLNs may be successfully suspended in Respiragel without alteration of gel characteristics, forming a multi-modal drug delivery system which has the potential to enable loco-regional delivery of atRA to the lung using minimally invasive devices.

4.5. Conclusion

An unmet clinical need in the treatment of chronic lung diseases such as COPD has resulted in the investigation of pro-regenerative strategies such as the delivery of stem cells and small molecules for improved patient outcomes. The results of this chapter demonstrate the feasibility of formulating a small molecule drug, all-trans Retinoic Acid, into biocompatible SLNs which can be suspended in the hydrogel developed in Chapter 2 providing sustained release on delivery. SLNs were formulated using Compritol® 888 ATO as the solid lipid, in combination with two surfactants, poloxamer 188 and Tween® 80. These SLNs were capable of high encapsulation of atRA, and subsequent prolonged release of the molecule over a period of 7 days. atRA SLNs were stable up to three months on storage at -20^{o}C. atRA SLNs were also found to be biocompatible with a relevant lung epithelial cell line, A549s, demonstrating promise for low toxicity *in vivo*. Finally, it was possible to incorporate SLNs into the hydrogel developed in Chapter 2 of this project, with no resultant effect on hydrogel rheological properties. As demonstrated in Chapter 2, the hydrogel could be delivered through a syringe, needle and catheter, and incorporation of particles into this gel indicates the potential for direct delivery of this formulation to the distal airways using current interventional pulmonology and medical device techniques. Based on this, the results presented in this chapter represent a promising formulation for delivery of small molecule drugs to the distal airways, while requiring further investigation into *in vitro* bioactivity, which will be discussed in detail in Chapter 5.

5. Chapter 5: *In vitro* assessment of anti-inflammatory activity of developed formulations: *all-trans* retinoic acid solid lipid nanoparticles and hMSC/Respiragel

5.1.Introduction

The work of previous Chapters has centred around the development of two formulation approaches with potential applications in the treatment of COPD – firstly, the use of stem cells which can be used as a cell source for repair and also for their paracrine capabilities in mounting an anti-inflammatory response; and secondly, the use of small molecule therapeutic agents – in this case all-trans Retinoic Acid, also with potential effects on inflammation. While formulation and biocompatibility studies have been described in Chapters 2 and 4 of this thesis, the potential therapeutic effect of these approaches has not yet been investigated. This Chapter focuses on assessing the anti-inflammatory effects of both the hMSC/Respiragel formulation and the atRA SLN formulation through the use of an *in vitro* model of cytokine release, with cytokines being key components of the inflammatory process observed in chronic lung diseases such as COPD.

5.1.1. Inflammatory cytokines in COPD

Results presented in this Chapter describe modulation of released IL-6 and IL-8 in an *in vitro* A549 model stimulated with IL-1β or TNF-α. The use of IL-1β and TNF-α to produce pro-inflammatory cytokines has a basis in the molecular pathogenesis of COPD. IL-1 is one of the major cytokines involved in the initiation and persistence of inflammation [307]. Enhanced production of IL-1 is documented in stable COPD, with a further increase during exacerbations of the illness [308]. BAL fluid from smokers has been shown to contain higher levels of IL-1β than BAL fluid from non-smokers, and the level of IL-1β is related to smokers lung function [309]. Research carried out by Lappalainen *et al* [310] found that induction of IL-1β expression in the lungs of a transgenic mouse caused pulmonary inflammation characterised by neutrophil and macrophage infiltrates. IL-1β resulted in distal airspace enlargement, consistent with the emphysematous component of COPD. IL-1β also caused disruption of elastin fibers

in alveolar septa, fibrosis in airway walls and in the pleura, and enhanced mucin production. TNF-α is produced by macrophages and mast cells, and has been shown to induce airway hyper-responsiveness in animals and in humans [311]. TNF-α concentrations are increased in the sputum of patients with COPD [312], again particularly during exacerbations. COPD patients who smoked were also found to have higher sputum concentrations of TNF-α when compared with ex-smoker COPD patients, and those who had never smoked [313].

IL-6 was chosen as a marker in this study due to its involvement in regulation of the immune response and inflammation, usually acting as a pro-inflammatory cytokine [314]. Increased levels of circulating IL-6 have been reported in patients with COPD compared with healthy volunteers [315], in a study which also reported increased levels of IL-8 in COPD patients. Numerous other publications have corroborated the link between up-regulation of IL-6 and inflammation in COPD including research carried out by Eid *et al* [316] which found increased levels of IL-6 and TNF-α in COPD patients with skeletal muscle depletion, and by Wedzicha *et al* [317], which found increased serum levels of IL-6 in patients experiencing COPD exacerbations. A further study carried out by Bhowmik *et al* [318] also found raised levels of IL-6 (and IL-8) in the sputum of COPD patients during exacerbations.

With respect to the selection of IL-8 as a second marker for inflammation in our *in vitro* model, once again, the pro-inflammatory characteristics of IL-8 and its relevance in COPD has been extensively investigated. IL-8 (also known as CXCL-8 or chemokine C-X-C motif ligand 8) is a chemotactic cytokine produced by alveolar macrophages, lymphocytes, epithelial cells, and neutrophils [312]. Its main actions are neutrophil recruitment and activation [319]. Research carried out by Keating *et al* [312] found that induced sputum from patients with COPD contained significantly higher levels of IL-8 (and TNF-α) than that from healthy patients, indicating a potential link between these pro-inflammatory molecules in the inflammatory pathogenesis of COPD. Publications previously cited in relation in IL-6 up-regulation have often also investigated IL-8

regulation, and have uncovered similar findings [315,318]. A further study, carried out by Pesci *et al* [320] found increased levels of IL-8 in BAL fluid from COPD patients. This summary provides examples of literature in the field linking increased levels of IL-6 and IL-8 (among other cytokines and chemokines) to the inflammatory pathogenesis of COPD – highlighting them as key markers of inflammatory processes for our *in vitro* assays.

5.1.2. *In vitro* cell culture models

In general, *in vitro* cell cultures are established to mimic tissues or microenvironments. Respiratory cell culture models incorporate a range of immortalised cell lines or primary epithelial cells for mechanistic, drug transport and toxicity studies [243]. One of the chief advantages of *in vitro* research is that, compared to animal models, cellular and subcellular functions (such as cell growth, interactions or metabolism), as well as the underlying molecular pathways, can be studied with more ease in a simplified, direct, biological model system. As is the case with cell culture models for other organ systems, immortalised cell lines are useful due to their homogenous nature, which results in better stability and more reproducibility. In addition to this cell lines are cost effective, generally easy to use, provide an unlimited supply of material, and bypass any ethical concerns associated with the use of animal and human tissue [321]. Primary cell cultures isolated from animal tissue on the other hand, more closely mimic the physiological state *in vivo*; however they represent a heterogeneous population of different cell types and each isolate will be unique and impossible to exactly reproduce. They also face limitations such as the lack of availability of normal human airway tissue from which to isolate cells, the limited number of cells that can be received from each isolation, and also certain donor variation [322].

In this Chapter, we aim to utilise an immortalised human lung epithelial cell line, A549 cells, as an *in vitro* alveolar epithelial cell model to ascertain the anti-inflammatory effects of our formulations. A549 cells were first initiated in 1972 by D. J Giard *et al*

[323] through explant culture of lung carcinomatous tissue from a 58 year old Caucasian male. Studies carried out by M Lieber *et al* [324] revealed A549 cells to contain multi-lamellar cytoplasmic inclusion bodies typical of those found in type II alveolar epithelial cells (ATII) of the lung. It was also found that at early and late passage levels, the cells synthesise lecithin with a high percentage of di-saturated fatty acids; such a pattern of phospholipid synthesis is expected for cells believed to be responsible for pulmonary surfactant synthesis (i.e. ATII cells). This indicated that the A549 cell line had the potential to act as an appropriate *in vitro* model for human ATII cells. Since these discoveries, A549s have routinely been used as a model for studying the physiology and drug metabolism of ATII cells and also as a permeability screen for substances administered via the pulmonary route [325–327].

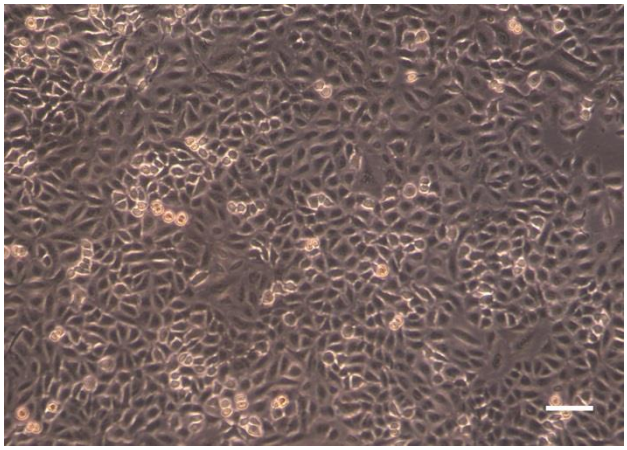

Figure 5.1. A549 cells in culture in a T175 flask two days post seeding at a density of 2 x 10^6 cells/flask. Scale bar = 100 µm.

Specifically, this body of work was interested in the application of an A549 in vitro model as a model for inflammation in COPD. The release of numerous chemokines and cytokines from both A549 cells and ATII cells following exposure to a stimulus has been investigated in various publications to date. In terms of A549s, research carried out by Standiford *et al* [328] found that IL-1β and TNF-α were able to stimulate the release of interleukin 8 (IL-8) from A549s in a dose and time dependant manner, through

induction of gene expression. A study carried out by Crestani *et al* [329] found that *in vitro* A549s produced interleukin 6 (IL-6) on stimulation with IL-1β and TNF-α. Research from a number of publications has shown a similar pattern of stimulation and subsequent cytokine release from ATII cells [330,331] which we are attempting to model, thus validating the use of A549s to achieve this.

Objectives

The overall objective of this Chapter was to investigate the anti-inflammatory effects of both the atRA SLN formulation and the hMSC/Respiragel formulation on an *in vitro* model of inflammatory lung disease, using IL-1β stimulated A549 cells.

- ¶ The first objective of this Chapter was to develop an *in vitro* model whereby A549 cells could be activated using either IL-1β or TNF-α, and to determine which pro-inflammatory cytokine elicited the greatest level of inflammation.
- ¶ The second objective was to use this *in vitro* model to assess the anti-inflammatory activity of the atRA SLN formulation with respect to its effect on IL-6 and IL-8 concentrations.
- ¶ The third objective of this Chapter was to investigate whether the atRA SLNs could be suspended in Respiragel, resulting in a similar anti-inflammatory effect with respect to IL-6 and IL-8 concentrations.
- ¶ The final objective was to use this *in vitro* model to assess the anti-inflammatory activity of the hMSC/Respiragel formulation with respect to its effect on IL-6 and IL-8 concentrations.

5.2.Materials and Methods

5.2.1. Materials

The A549 cell line was purchased from the American Type Culture Collection (ATCC, Virginia, USA). The NFκB luciferase reporter A549 stable cell line was obtained from collaborators in National University of Ireland, Galway, but was originally purchased from Signosis Inc. (Buckingham, UK). Retinoic acid, Cell Counting Kit 8 (CCK-8), and Dulbecco's Modified Eagles Medium/Nutrient Mixture F12 (DMEM/F12) media were also purchased from Sigma Aldrich (Ireland). Human recombinant IL-1β and TNF-α were purchased from Immunotools (Germany). LumiDazzle Luciferase Reporter Gene Assay Kit was purchased from Medical Supply Company Ltd (Dublin, Ireland). Human IL-6 and IL-8 Ready-Set-Go ELISA Kits were obtained from Affymetrix eBioscience (Cheshire, UK).

5.2.2. Development of a cell based assay to determine the anti-inflammatory effects of previously developed formulations

5.2.2.1. A549 culture

A549 cells were cultured as previously described in section 4.2.9. A549s were maintained in DMEM/Ham's F12 medium (Sigma Aldrich, Ireland) supplemented with 10% foetal bovine serum (FBS), and 1% penicillin/streptomycin (Labtech, UK), at 37°C and in a 5% CO_2 atmosphere. The cells were plated in T175 cell culture flasks (Sarstedt, Ireland) and subcultured before reaching confluency using a 0.1% trypsin solution in EDTA (Sigma). The culture medium was changed every two days. The cells were split 1:5 during each passage. The passages used for the following experiments were 16-21.

5.2.2.2. Activation of A549s using pro-inflammatory cytokines

A549 cells were cultured as described in section 5.2.2.1, and underwent expansion and three passages prior to seeding in experiments. Cells were then seeded in 24 well flat-bottom adherent plates (2 x 10^4 cells/ well in 0.5 mL DMEM/F12 media) and incubated for 24 h. After 24 h, media was removed from wells and cells were washed three times with PBS (Sigma Aldrich, Ireland). The pro-inflammatory cytokines, tumour necrosis factor alpha (TNF-α) or interleukin 1 beta (IL-1β), were then added to the cells diluted in media as shown in Figure 5.2. TNF-α was added at a concentration of 50 ng/mL and IL-1β was added at a concentration of 10 ng/mL as these concentrations had been previously determined as optimal for induction of inflammatory responses [332].

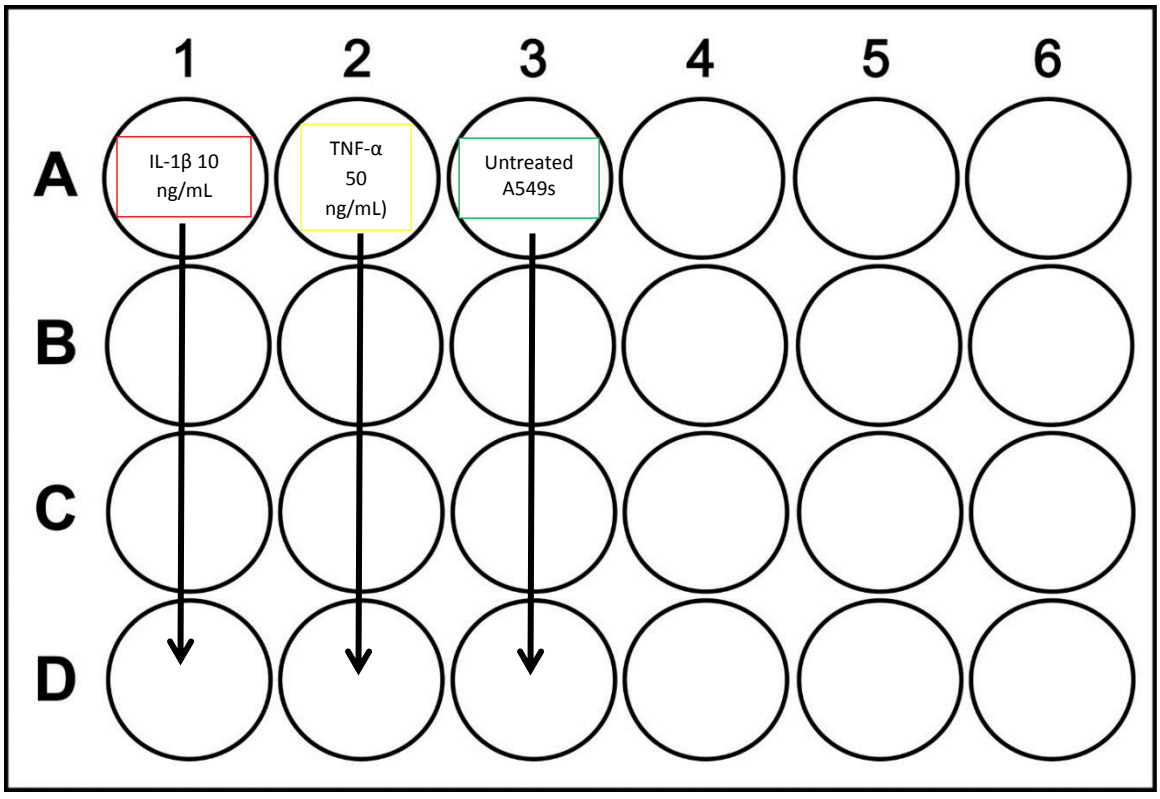

Figure 5.2. Experimental design for determination of inflammatory response of A549 lung epithelial cells at a seeding density of 2 x 10^4 cells/well in the presence of pro-inflammatory molecules IL-1β (10 ng/mL) and TNF-α (50 ng/mL). Media supernatant was removed at four time points (4 h, 24 h, 48 h and 72 h) and analysed by ELISA.

This experimental design was used to determine whether A549s would release increased levels of pro-inflammatory cytokines (i.e. IL-6 and IL-8) on supplementation with either IL-1β or TNF-α. The outcome of this experiment would direct the choice of which inflammatory cytokine to use in further studies investigating the effect of atRA SLNs on raised inflammatory cytokine levels.

5.2.3. Assessment of anti-inflammatory effect of atRA SLN formulation

5.2.3.1. Treatment of activated A549s with atRA SLN formulation

A549 cells were seeded and activated using IL-1β as described in section 5.2.2.1 and 5.2.2.2. After 24 h incubation, media was removed from wells and cells were washed three times with PBS (Sigma Aldrich, Ireland). atRA SLNs were then suspended in media at two different concentrations (SLNs containing atRA equivalent to 5 µg/mL and 10 µg/mL) and pipetted gently onto cells. Free atRA at a concentration of 10 µg/mL in media was used as a control, as were blank SLNs in media (equal to the weight of 10 µg/mL atRA SLNs used), and media alone.

5.2.3.2. Viability of A549s following treatment with atRA SLN formulation

After 4, 24, 48 and 72 h incubation, atRA SLNs and media were removed from wells and A549s were washed three times with PBS, before performing a Cell Counting Kit 8 (CCK-8) assay according to the manufacturer's instructions. Briefly, media + 10% CCK-8 reagent was added to each well, and plates were returned to the incubator for 2 h to react. 100 µL of each sample was plated per well, in triplicate, on a clear 96 well plate, and absorbance of the samples was measured at 450 nm using a Varioskan Flash multimode microplate reader (Fisher Scientific, Ireland). Percent viability was then calculated using the following equation:

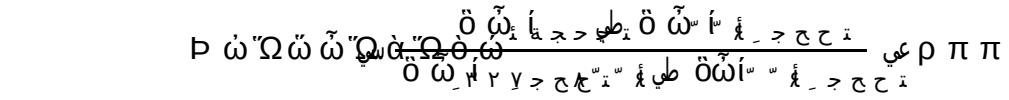

Equation 5.1. Equation used to calculate % A549 viability following supplementation with atRA, atRA SLNs or blank SLNs.

5.2.3.3. Cytokine quantification using Enzyme-linked Immunosorbent Assay (ELISA) following treatment with atRA SLN formulation

After 4, 24, 48 and 72 h incubation, media supernatant was removed from wells and stored in eppendorfs at -80^{o}C until analysis. ELISA (eBiosciences, UK) was used to quantify the levels of IL-6 and IL-8 expressed by A549s in response to treatment with the atRA SLN formulation. Assays were carried out according to the manufacturer's instructions and the absorbance of each sample was read at 450 nm and 570 nm using a Varioskan Flash multimode plate reader, whereby the quantity of IL-6 or IL-8 present was deduced by calculating against a standard curve (Appendix 3.1 and 3.2).

5.2.3.4. Treatment of activated A549s with atRA SLN/Respiragel formulation

A549 cells were cultured as described in sections 3.2.9 and 5.2.2.1, and seeded in 24 well flat-bottom adherent plates (2 x 10^4 cells/ well in 0.5 mL DMEM/F12 media) as described in section 5.2.2.2. IL-1β was then added to the cells at 24 h, diluted in media at a concentration of 10 ng/mL. A further 24 h later, media was removed from wells and cells were washed three times with PBS (Sigma Aldrich, Ireland). atRA SLNs were then suspended in the "Respiragel" polymer solution at two different concentrations (SLN hydrogel containing atRA equivalent to 5 µg/mL and 10 µg/mL). Free atRA at a concentration of 10 µg/mL in Respiragel was used as a control, as were blank SLNs in the gel (equal to the weight of 10 µg/mL atRA SLNs used), and media alone. The series

of gels were aspirated into 3 mL syringes and 500 µL volumes were expelled through a 21G needle to form droplets in Costar Transwell Inserts (Fisher Scientific, Ireland) with an 8 µm pore size and diameter of 6.5 mm. Plates were then transferred to the incubator at 37^{o}C for 15 min in order for gelation to occur. Plates were then removed and 2 mL media gently added to each well, before returning to the incubator.

After 4, 24, 48 and 72 h incubation, atRA SLNs hydrogels and media were removed from wells and A549s were washed three times with PBS, before performing a CCK-8 assay according to the manufacturer's instructions, and as described in section 5.2.2.4.

At the same time points, media supernatant was removed from wells and stored in eppendorfs at -80^{o}C until analysis. ELISA (eBiosciences, UK) was used to quantify the levels of IL-6 and IL-8 expressed by A549s in response to treatment with the atRA SLN Respiragel formulation as described in section 5.2.2.5.

5.2.4. Development of a cell based assay to determine the anti-inflammatory effects of hMSCs in Respiragel

5.2.4.1. b C ς . ! p π ϕ Ŏ dz f ű dz NJ Ŝ l· y˝ Ř -ă ndż ō ă Ŝ lj dz Ŝ y˝ ű

NFκB luciferase A549 cells were used for experiments involving hMSCs. This was due to the fact that there are two cell types used in these assays (i.e. a co-culture) meaning it is difficult to ascertain which cells are releasing the cytokines and therefore producing the detected effect. When NFκB luciferase A549s are activated, the luciferase (which is regulated by NFκB) is released, allowing the signal to be measured via a luciferase assay, thus distinguishing effects produced from A549 cells from those produced by hMSC activity.

NFκB luciferase A549 cells were cultured as previously described for A549 cells with no luciferase reporter in sections 4.2.9 and 5.2.2.1. Cells were seeded in 24 well flat-bottom adherent plates (2 x 10^4 cells/ well in 0.5 mL DMEM/F12 media) as in section

5.2.2.2 and incubated for 24 h. IL-1β was then added to the cells diluted in media at a concentration of 10 ng/mL, and plates were returned to the incubator for 24 h.

5.2.4.2. hMSC culture

hMSCs were cultured as previously described in section 2.2.7.

5.2.4.3. Treatment ž Ŧ l· Ŏ ű ǻ Ø l· ű Ŝ Ř b C ˁ . ! p π ф ă ø ǻ formulation

hMSCs were cultured as described in section 5.2.3.2. Cells were removed from the suspension via trypsinization and centrifugation, and on removal of the supernatant, the pellets were re-suspended in the Respiragel polymer solution at a density of 5 x 10^5 cells/ mL. This was aspirated into a 3 mL syringe and 500 µL volumes were expelled through a 21G needle to form droplets in Costar Transwell Inserts (Fisher Scientific, Ireland) with an 8 µm pore size and diameter of 6.5 mm. Plates containing pre-seeded and activated NFκB A549s were then removed from the incubator and inserts containing hMSC/Respiragel formulation were carefully added in on top as per the schematic shown in Figure 5.3. Plates were then returned to the incubator for culture. Samples were removed at 4 h, 24 h, 48 h and 72 h. Samples collected included media supernatant for ELISA and NFκB A549 cells for viability and luciferase assays.

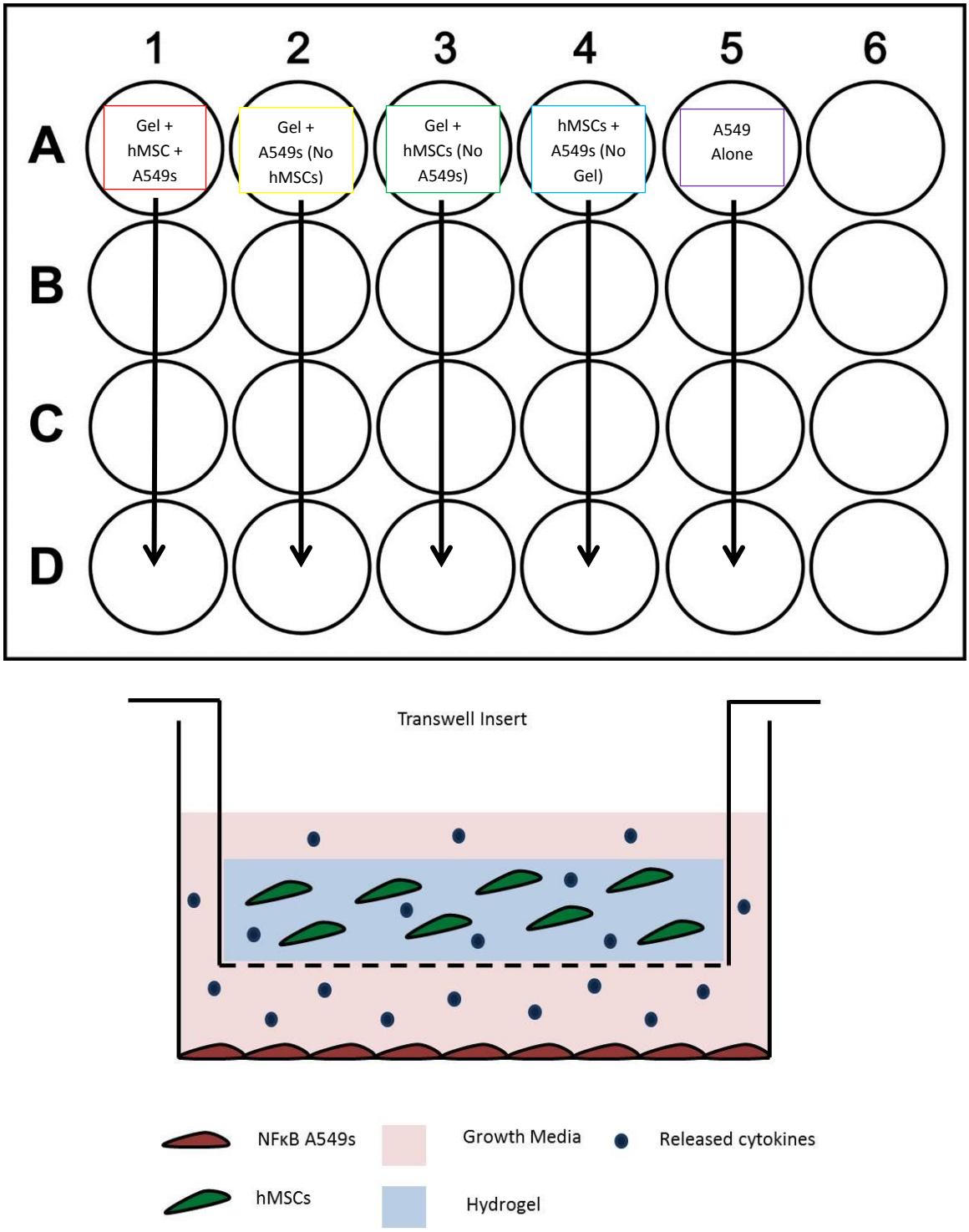

Figure 5.3. Experimental design and schematic for assessment of anti-inflammatory effect of hMSC loaded Respiragel formulation on NFκB A549 lung epithelial cells, pre-activated with IL-1β @ 10 ng/mL. Controls included a gel alone group (containing no hMSCs), gel + hMSCs without pre-activated NFκB A549s, hMSCs (not suspended in Respiragel) + NFκB A549s, and finally NFκB A549 cells alone. All NFκB

A549 cells were pre-activated using IL-1β. Media supernatant was removed at four time points (4 h, 24 h, 48 h and 72 h) and analysed by ELISA for IL-6 and IL-8 content.

5.2.4.4. 5 Ŝ ű Ŝ NJ Y ǻ y l· ű ǻ ƨ y ƨ Ŧ b C ς . ǻ y Ř dz Ŏ ű ǻ ƨ y treatment with hMSC/Respiragel formulation

As previously mentioned in 5.2.3.1, NFκB luciferase A549 cells were used due to the fact that there are two cell types used in these assays, meaning it is difficult to ascertain which cells are releasing the cytokines and producing the detected effect. When these cells are activated, the luciferase (regulated by NFκB) is released, allowing the signal to be measured via a luciferase assay.

After 4, 24, 48 and 72 h incubation, media supernatant was removed from wells and NFκB A549s were washed three times with PBS. Media was replaced and LumiDazzle Luciferase Reporter Gene Assay reagent was added according to the manufacturer's instructions. 100 µL of each sample was transferred to an opaque 96 well plate and luminescence was read for 0.1 s using a Victor Wallac multimode plate reader.

5.2.4.5. ± ǻ l· ō ǻ f ǻ ű è ƨ Ŧ b C ς . ! p п ф ă Ŧ ƨ f f hMSC/Respiragel formulation

After 4, 24, 48 and 72 h incubation, gel, inserts and media were removed from wells and NFκB A549s were washed three times with PBS, before performing a CCK-8 assay according to the manufacturer's instructions, and as described in section 5.2.2.4.

5.2.4.6. Cytokine quantification using Enzyme-linked Immunosorbent Assay (ELISA) following treatment with hMSC/Respiragel formulation

Following 4, 24, 48 and 72 h incubation, media supernatant was removed from wells and stored in eppendorfs at -80^{o}C until analysis. ELISA (eBiosciences, UK) was used to quantify the levels of IL-6 and IL-8 expressed by activated NFκB A549s in response to treatment with the hMSC loaded Respiragel formulation. Assays were carried out according to the manufacturer's instructions and the absorbance of each sample was read at 450 nm and 570 nm using a Varioskan Flash multimode plate reader, whereby the quantity of IL-6 or IL-8 present was deduced by calculating against a standard curve (Appendix 3.1 and 3.2).

5.2.5. Statistical analysis

Two-way analysis of variance (ANOVA) followed by Tukey's post-hoc analysis was performed to determine statistical differences in all studies described in this chapter, unless otherwise stated. All statistical tests were performed using GraphPad Prism v6 (GraphPad Software Inc., CA, USA). Error is reported as standard error of the mean (SE) and significance was determined using a probability value of $P \leq 0.05$. A minimum of n = 3 technical repeats and independent replicates was performed for all experiments.

5.3.Results

5.3.1. Development of a cell based assay to determine anti-inflammatory effects of the atRA SLN formulation

5.3.1.1. Determination of inflammatory response of A549s to activation with IL-м j l· y˝Ř ¢ b C h

Initial investigations aimed to ascertain whether A549s could be "activated" using the pro-inflammatory molecules IL-1β and TNF-α, and if so, which molecule would result in the greatest activation. This experimental design aimed to create a simple *in vitro* environment whereby A549 lung epithelial cells, which are often used as a model for alveolar cells, would be producing increased levels of inflammatory cytokines such as is seen in conditions like COPD. Inflammatory cytokines measured by ELISA included IL-6 and IL-8 – two prominent molecules present in COPD, as discussed in section 5.1.

Results shown in Figure 5.4 show IL-6 and IL-8 concentrations following activation of A549s using either IL-1β or TNF-α, compared with a non-activated control. Significantly higher concentrations of both IL-6 and IL-8 can be observed following activation with both molecules ($P < 0.0001$) however, IL-1β results in significantly more IL-6 and IL-8 than TNF-α from 24 h onwards. As a result of this, IL-1β was selected as our activator of choice for all subsequent *in vitro* experiments.

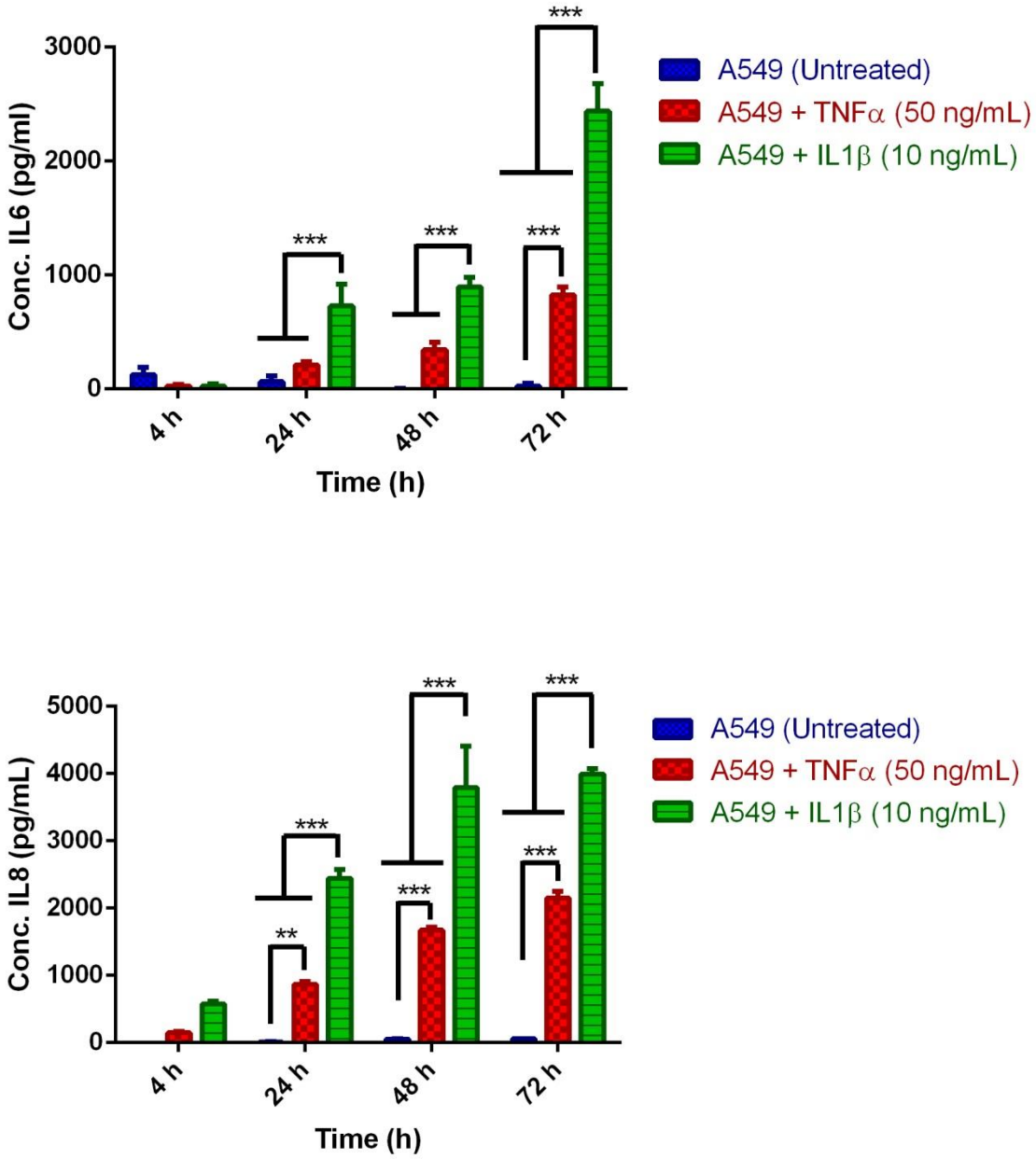

*Figure 5.4. IL-6 and IL-8 levels as determined using ELISA following activation of A549 cells with IL-1β or TNF-α, versus non-activated A549 cells as a control. Results indicate significantly higher levels of both IL-6 and IL-8 when cells are treated with IL-1β or TNF-α. However, significantly higher levels of IL-6 and IL-8 result from activation with IL-1β compared with TNF-α. Results are presented as mean cytokine concentration ± SE. Significance determined by two way ANOVA followed by Tukey's post hoc test. *** = P < 0.0001.*

5.3.1.2. Viability of A549s following treatment with atRA SLNs

A549 viability assays were carried out to determine biocompatibility of the atRA SLN formulation, and also to confirm that potential changes in inflammatory cytokine levels was not due to a drop in cell viability (Figure 5.5). A CCK-8 assay was selected which utilises a tetrazolium salt, WST-8, which is reduced by cellular dehydrogenases to an orange, water soluble formazan product [333,334]. The amount of formazan produced was directly proportional to the number of live cells. Addition of both low dose (5 µg/mL) and high dose (10 µg/mL) atRA SLNs to A549s resulted in no significant reduction in cell viability over the study duration of 72 h. Raw atRA and blank SLNs, which were used as controls, also showed biocompatibility with A549s. An increase in % viability was observed at the early time point of 4 h – it is possible that this is due a potential transient increase in cellular metabolic activity on addition of atRA and/or SLNs to the cells. As the CCK-8 assay is based on metabolic activity, an increase may result in an increase in observed viability, which then returns to expected levels at the 24 h time point.

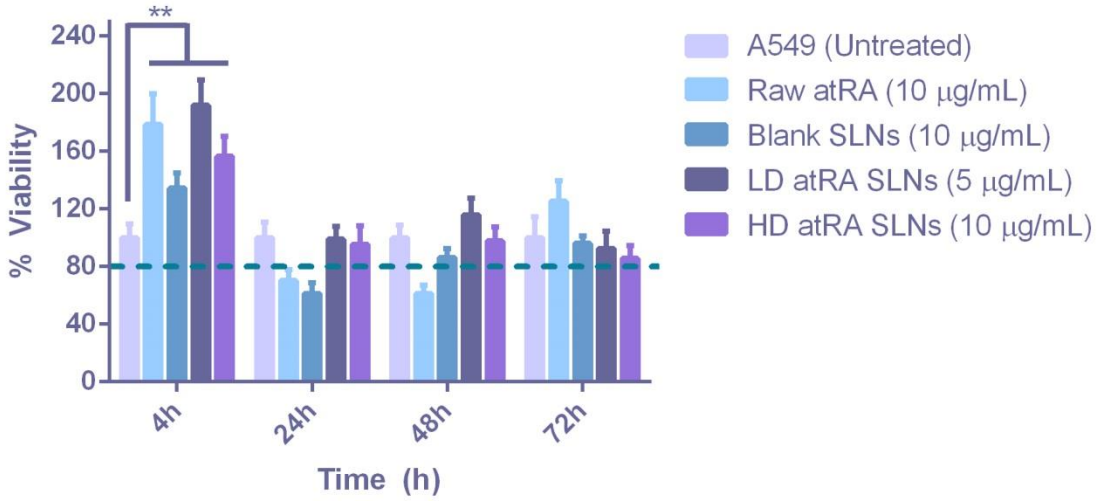

Figure 5.5. Average cell viability following addition of atRA SLN formulations to activated A549s over a period of 72 hours. Untreated A549 cells were used as a control, as were raw atRA and blank SLNs. Assay was performed using a CCK-8 viability kit, according to the manufacturer's specifications. ≥80% viability indicates biocompatibility according to ISO standards [230]*. Results are presented as mean cell viability ± SE. Significance determined via two-way ANOVA, with Dunnett's post hoc test. ** = P<0.001.*

5.3.1.3. Anti-inflammatory response of activated A549s to treatment with atRA SLNs

Quantification of the anti-inflammatory response of activated A549 cells to the atRA SLN formulation showed a similar pattern for both IL-6 and IL-8 (Figure 5.6). For both cytokines, the atRA SLN formulation results in a significant ($P < 0.001$) dose dependant reduction in concentration at both 48 h and 72 h, when compared with blank SLNs and untreated A549s. With respect to IL-8, this effect is also observed at the early time point of 24 h. The reduction in IL-6 and IL-8 is observed when A549s are treated with the high dose (HD = 10 μg/mL) atRA SLNs, though a significant reduction in IL-6 was also observed with LD atRA SLNs at the 72 h time point.

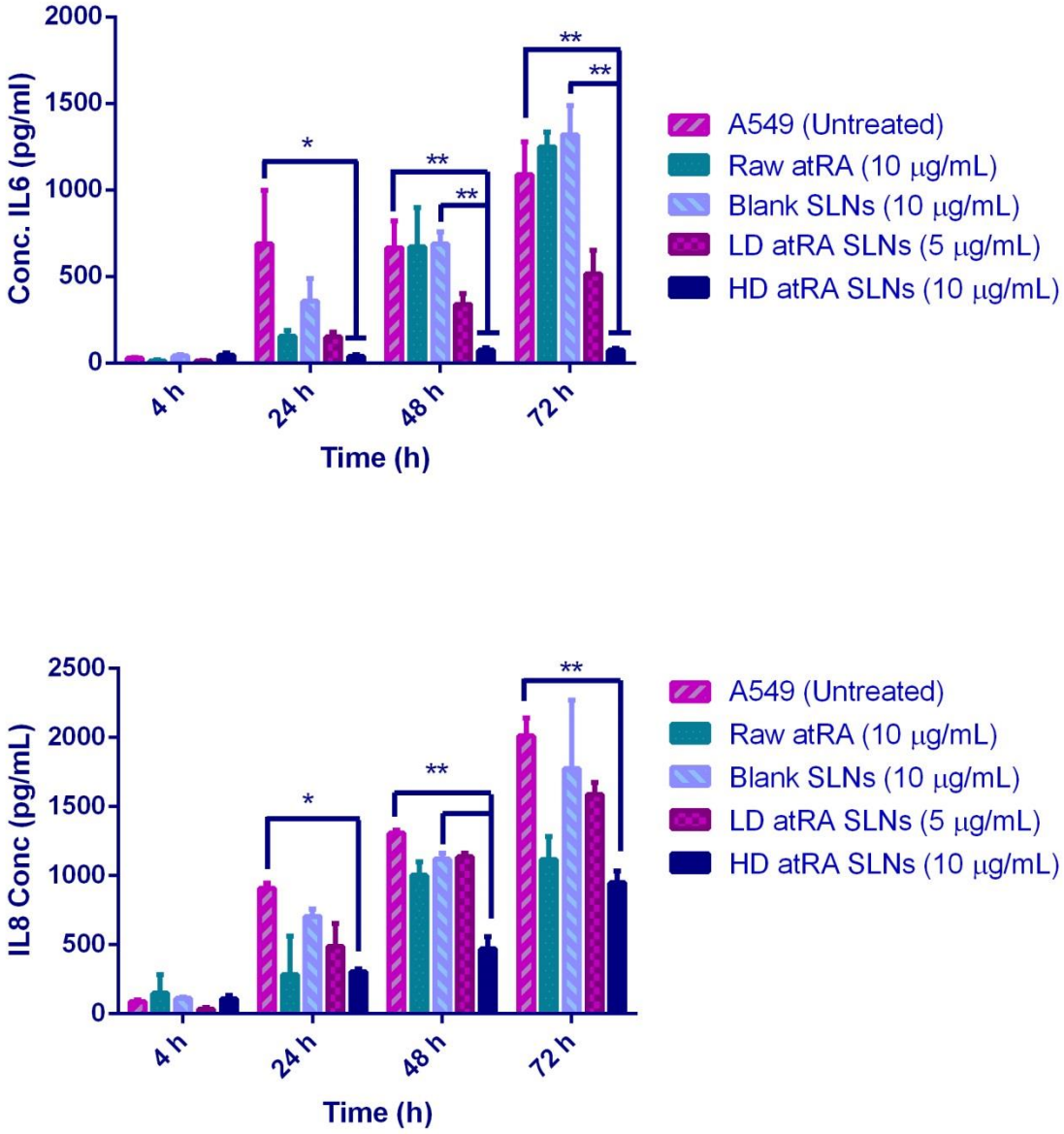

*Figure 5.6. Average IL-6 and IL-8 concentrations following treatment of IL-1β activated A549s with either raw atRA, low dose atRA SLNs (LD = 5 μg/mL), high dose atRA SLNs (HD = 10 μg/mL) or blank SLNs. Significantly reduced levels of both IL-6 and IL-8 result from addition of the HD atRA SLN formulation compared with untreated A549s alone, at 24 h, 48 h and 72 h for both cytokines. Results are presented as mean ± SE. Significance determined via two-way ANOVA, with Tukey's post hoc test. * = P<0.05, ** = P<0.001.*

5.3.2. *In vitro evaluation of* **atRA SLN/Respiragel formulation**

5.3.2.1. Viability of A549s following treatment with atRA SLN loaded Respiragel

A549 viability assays were performed to ensure that the addition of the Respiragel to the atRA SLNs did not have any adverse effect on viability. Addition of both low dose (5 µg/mL) and high dose (10 µg/mL) atRA SLN Respiragel to A549s resulted in no significant reduction in cell viability over the study duration of 72 h (Figure 5.7).

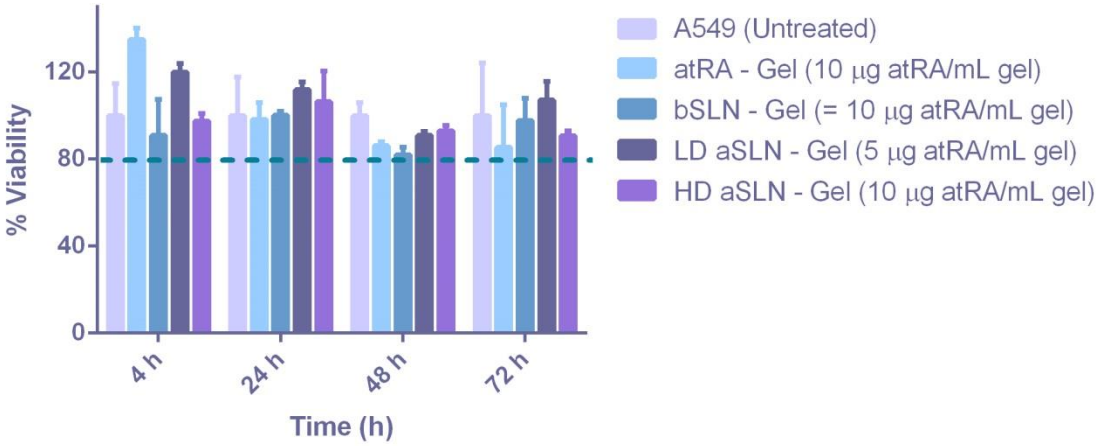

Figure 5.7. Average A549 cell viability following addition of atRA SLN loaded Respiragel formulations over a period of 72 hours. Untreated A549 cells were used as a control, as were raw atRA Respiragel and blank SLN loaded Respiragel. Assay was performed using a CCK-8 viability kit, according to the manufacturer's specifications. ≥80% viability indicates biocompatibility according to ISO standards [230]. *Results are presented as mean cell viability ± SE. Significance determined via two-way ANOVA, with Dunnett's post hoc test. No significance observed.*

5.3.2.2. Anti-inflammatory response of activated A549s to treatment with atRA SLN/Respiragel

For both cytokines, the atRA SLN/Respiragel formulation results in a significant dose dependant reduction in concentration at 72 h, when compared with untreated IL-1β

activated A549s (Figure 5.8). The reduction in IL-6 and IL-8 is observed when A549s are treated with high dose (HD = 10µg/mL) atRA SLN/Respiragel formulation, and not with the LD formulation. This is similar to what was observed for A549s treated with atRA SLNs alone (shown previously in Figure 5.6) in that the HD SLNs resulted in an anti-inflammatory effect which was observed at the 72 h time point. For atRA SLNs alone however, this effect was also seen earlier, at 48 h for IL-6 and at 24 h and 48 h for IL-8.

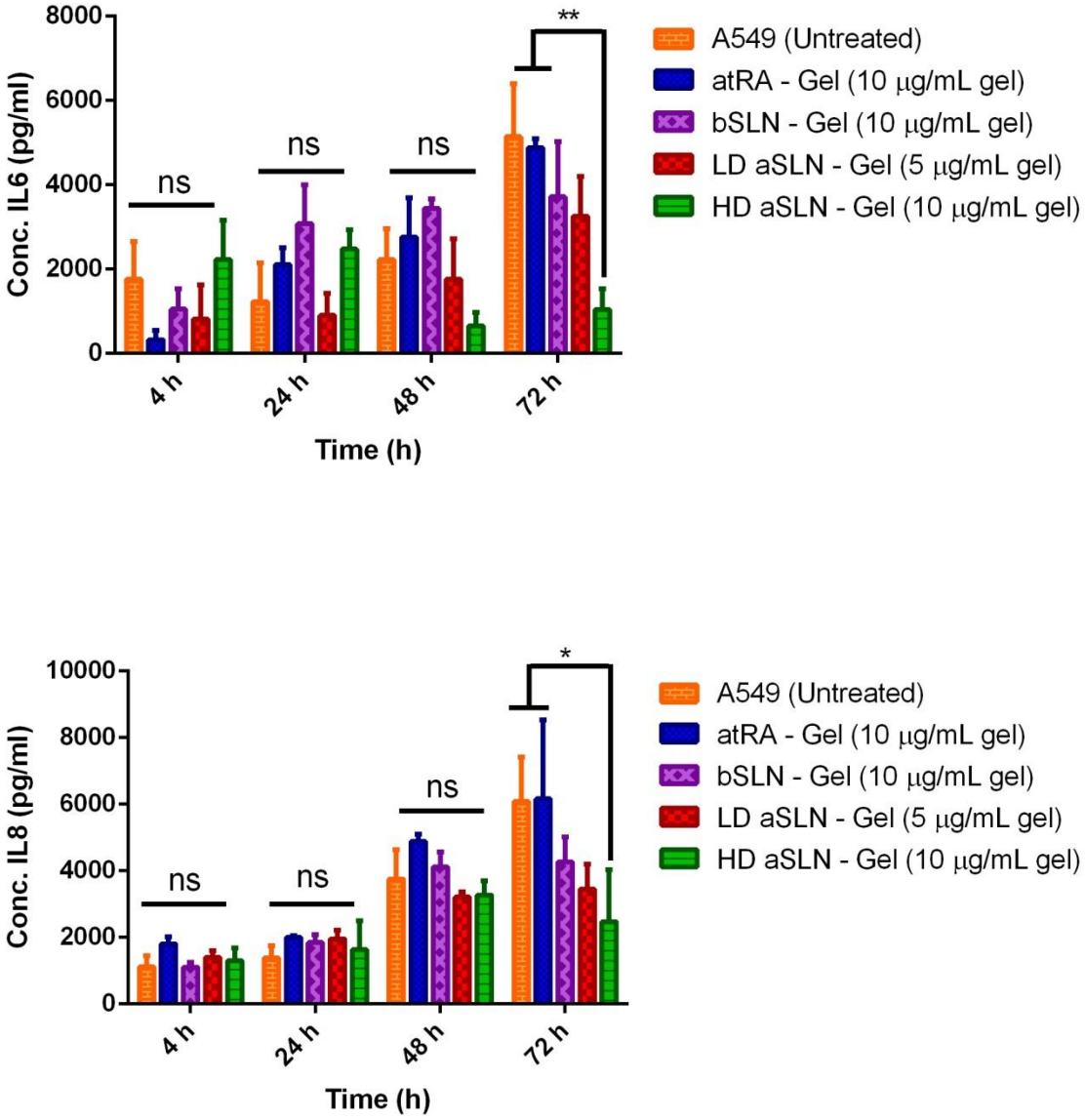

*Figure 5.8. Average IL-6 and IL-8 concentrations following treatment of IL-1β activated A549s with either raw atRA Respiragel, low dose atRA SLN Respiragel (LD = 5 μg/mL gel), high dose atRA SLN Respiragel (HD = 10 μg/mL gel) or blank SLN Respiragel. Significantly reduced levels of both IL-6 and IL-8 result from addition of the HD atRA SLN/ Respiragel formulation at 72 h compared with untreated A549s alone and also raw atRA Respiragel. Results are presented as mean ± SE. Significance determined via two-way ANOVA, with Tukey's post hoc test. * = P<0.05, ** = P<0.001.*

5.3.3. Development of a cell based assay to determine the anti-inflammatory effects of the hMSC/Respiragel formulation

5.3.3.1. ± ƛ l· ō ƛ f ƛ ű è Ƨ Ŧ b C ς . ! p п ф ă Ŧ Ƨ f f ż hMSC/Respiragel formulation

Addition of hMSC/Respiragel to NFκB A549s resulted in no significant reduction in cell viability over the study duration of 72 h (Figure 5.9). Greater than 100% viability in this group compared with A549s alone could be a result of migration of hMSCs out of the gel and into the well with A549s, resulting in both cell types being counted. As the CCK-8 assay is based on metabolic activity and is not cell type specific, the presence of both cell types in the well would likely result in an increase in observed viability. Respiragel alone also maintained viability of A549s, which was expected due to previous biocompatibility work with hMSCs presented in chapter 2 (section 2.3.6). One control group, Respiragel + MSCs should have resulted in no viability, due to no seeded A549s – however, the low viability signal here could again be attributed to some migration of hMSCs out of the gel and into the media or well.

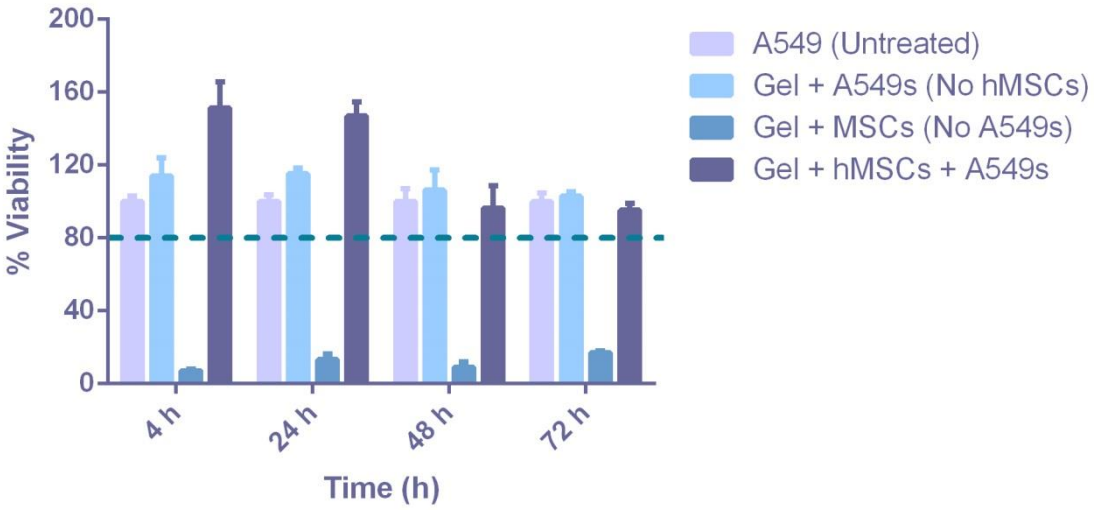

Figure 5.9. Average A549 cell viability following addition of the hMSC/Respiragel formulation over a period of 72 hours. Untreated A549 cells were used as controls. Assay was performed using a CCK-8

viability kit, according to the manufacturer's specifications. ≥80% viability indicates biocompatibility according to ISO standards [230]*. Results are presented as mean cell viability ± SE. Significance determined via two-way ANOVA, with Tukey's post hoc test.*

5.3.3.2. Anti-inflammatory response of activated NFκB A549 cells to treatment with hMSC/Respiragel formulation

Quantification of the anti-inflammatory response of activated NFκB A549 cells to the hMSC loaded Respiragel formulation was achieved using ELISA. A similar pattern is observed for both cytokines (Figure 5.10A) with no significant reduction in IL-6 or IL-8 concentrations at any time point when compared with the activated A549 alone control. In fact all treatment groups (hMSC alone, Respiragel alone, hMSC/Respiragel) showed significantly higher production of both IL-6 and IL-8 at 24, 48 and 72 h ($P < 0.0001$) relative to the A549 untreated control, with hMSCs alone showing the highest production of IL-6 and IL-8. When hMSCs alone are compared with Respiragel alone and hMSC/Respiragel combination, IL-6 and IL-8 production is again significantly higher. These results suggest that hMSCs may exert a pro-inflammatory effect rather than anti-inflammatory as had been originally hypothesised, and encapsulation within the hydrogel may dampen down this response.

As part of this study, a luciferase assay was also performed in order to ascertain which cell type in the co-culture was responsible for the modulation of cytokine levels (Figure 5.10B). As described in section 5.2.3.1, when NFκB A549s are activated, the luciferase is released, allowing the signal to be measured via a luciferase assay. Fold induction was calculated based on A549s which were not activated with IL-1β or subsequently treated with any formulation. A549s which were activated with IL-1β but not subsequently treated were used as a positive control for activation – showing a time dependant increase in NFκB induction thus confirming the pro-inflammatory activity of IL-1β on A549s. However, all treatment groups showed an immediate increase in NFκB induction at 24h followed by a reduction thereafter. The hMSC/Respiragel formulation

may be having an anti-inflammatory effect due to reduction in NFκB expression in A549 cells. This effect is also observed for the hMSC alone treatment group and also the Respiragel alone treatment group, indicating that both the hMSCs and the gel independently result in a reduction in NFκB mediated inflammation. This also indicates that, as a potential anti-inflammatory effect is observed through a reduction of NFκB in A549 cells, the corresponding increased concentrations of IL-6 and IL-8 in media may be being produced by hMSCs as opposed to the A549s. Alternatively, IL-1β may be activating another inflammatory pathway in A549s in addition to the NFκB pathway, which may not be down-regulated following addition of hMSCs.

A

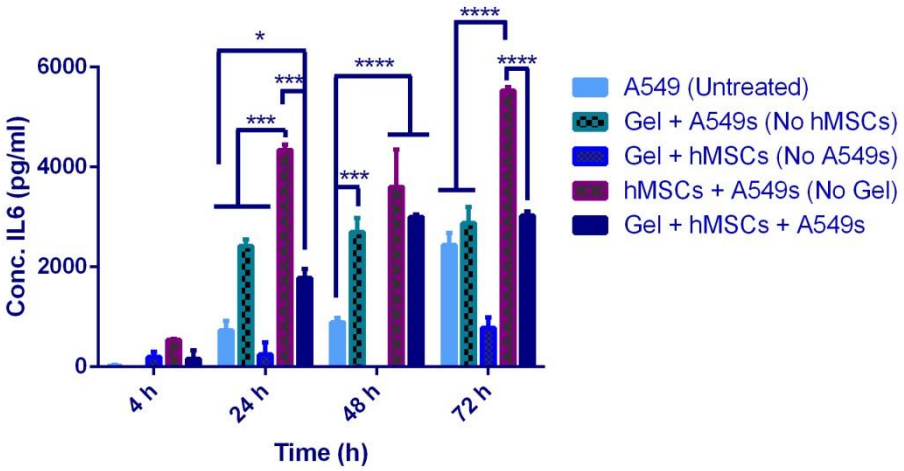
Conc. IL6 (pg/ml)
6000
4000
2000
0
4 h
24 h
48 h
72 h
Time (h)
A549 (Untreated)
Gel + A549s (No hMSCs)
Gel + hMSCs (No A549s)
hMSCs + A549s (No Gel)
Gel + hMSCs + A549s

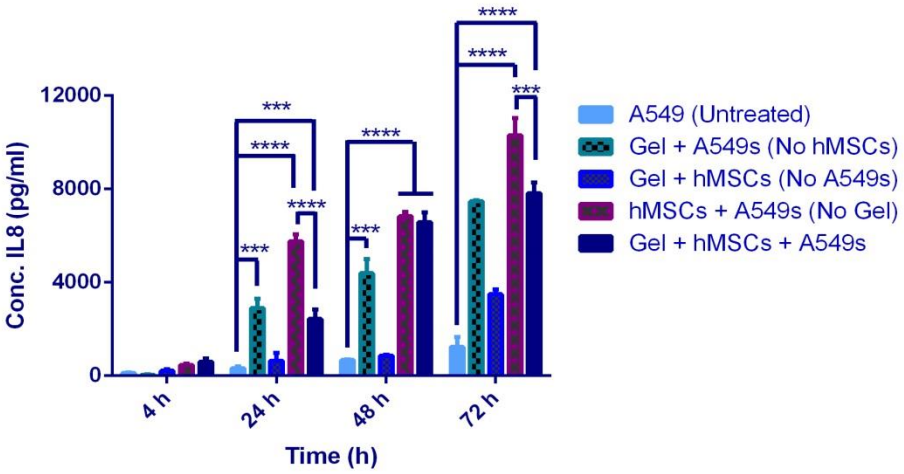
Conc. IL8 (pg/ml)
12000
8000
4000
0
4 h
24 h
48 h
72 h
Time (h)
A549 (Untreated)
Gel + A549s (No hMSCs)
Gel + hMSCs (No A549s)
hMSCs + A549s (No Gel)
Gel + hMSCs + A549s

B

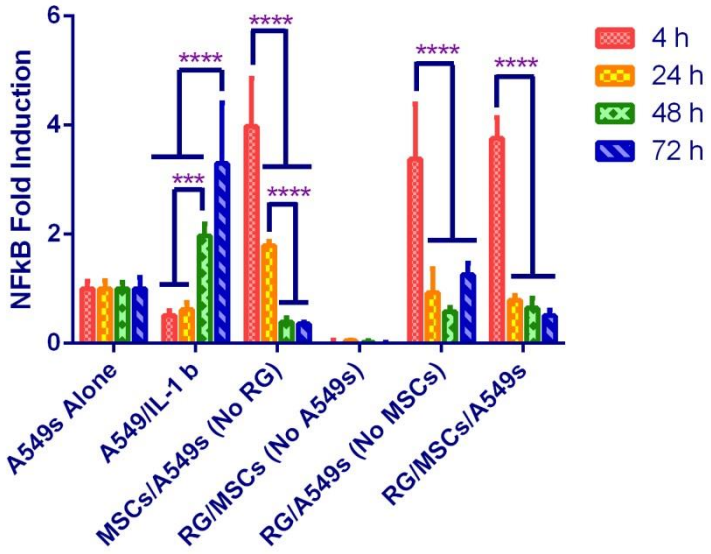
NFkB Fold Induction
6
4
2
0
A549s Alone
A549/IL-1 b
MSCs/A549s (No RG)
RG/MSCs (No A549s)
RG/A549s (No MSCs)
RG/MSCs/A549s
4 h
24 h
48 h
72 h

*Figure 5.10(A). IL-6 and IL-8 concentrations following treatment of IL-1β activated NFκB A549s with hMSC loaded Respiragel, Respiragel alone, or hMSCs alone. Significantly lower levels of both IL-6 and IL-8 result from addition of hMSC/Respiragel formulation compared with hMSCs alone, but not when compared with IL-1β activated NFκB A549s. Results are presented as mean ± SE. Significance determined via two-way ANOVA, with Tukey's post hoc test. * = P < 0.05, *** = P < 0.001,**** = P < 0.0001; (B) Fold NFκB induction obtained through detection of luciferase, integrated as a reporter in A549s. A549s treated using the Respiragel/MSC formulation experience a down-regulation in NFκB production, indicating an anti-inflammatory effect of this formulation. hMSCs alone are also anti-inflammatory due to down-regulation of NFκB, and the gel alone containing no cells also appears to have an anti-inflammatory effect at 48 h. Results are presented as mean ± SD. Significance determined via two-way ANOVA, with Tukey's post hoc test. *** = P < 0.001, **** = P < 0.0001.*

5.3.3.3. Investigation into the optimal hMSC seeding density for an anti inflammatory effect

hMSC seeding densities of 1,000,000 cells/gel and 2,000,000 cells/gel were compared with the original density of 250,000 cells/gel. Quantification of the inflammatory response of NFκB A549 cells to the increased density hMSC/Respiragel formulations was achieved using ELISA. A similar pattern is once again observed for both IL-6 and IL-8 (Figure 5.11A) with significantly increased levels of IL-6 and IL-8 in all groups when compared with the untreated A549 control, and also to the original 250,000 cells/gel group. Once again, the 250,000 hMSC/Respiragel group is not significantly different to the Respiragel alone group in terms of IL-6 and IL-8 production (as was the case in Figure 5.10A). Also of note is the fact that the 1M and 2M hMSC/Respiragel groups produce the same amount of IL-6 and IL-8 as the 250,000 hMSCs delivered alone (not suspended in hydrogel). This indicates that a much higher density of hMSCs results in the same production of cytokines as a lower density, once they are encapsulated in the hydrogel. This could possibly indicate an anti-inflammatory effect of the Respiragel, as suggested in relation to the fold NFκB induction observed in Figure 5.10B, which

showed progressive time dependant reductions in NFκB induction following treatment of IL-1β activated A549s with the Respiragel alone group.

The luciferase assay was then performed to determine the origin of the response. Figure 5.11B indicates that all three “doses” of hMSCs in the Respiragel/hMSC formulation may be having an anti-inflammatory effect due to reduction in NFκB expression, though a transient increase in NFκB induction is observed in the 250,000 hMSC group and the 1 M hMSC group at the early time point of 4 h. MSCs alone once again appear to have an anti-inflammatory effect, as seen previously in Figure 5.10B as does Respiragel alone, corroborating the findings of our previous experiments, and indicating that the inflammatory effects detected by ELISA may be due to activation of the MSCs with the IL-1β and their own subsequent production of cytokines, rather than cytokine production by A549s.

A

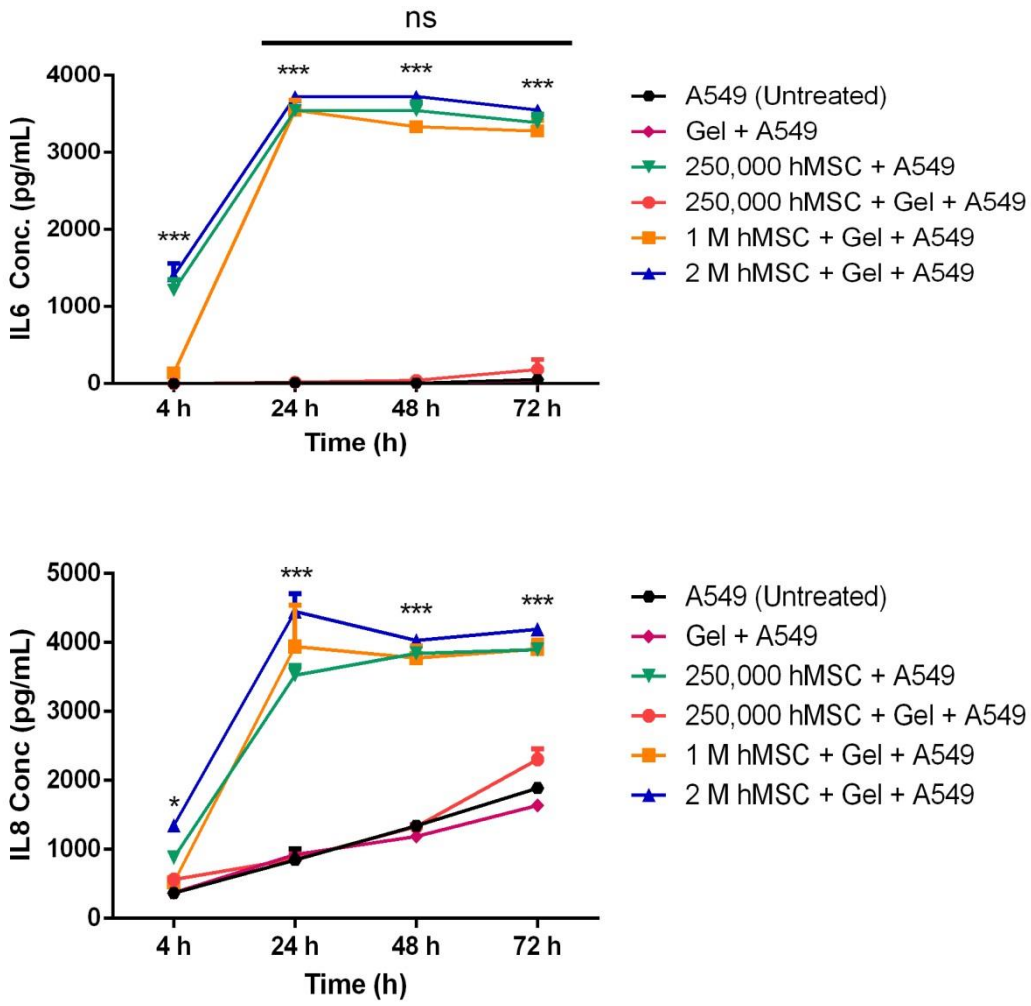
ns
***
***
***
***
IL6 Conc. (pg/mL)
4000
3000
2000
1000
0
4 h
24 h
48 h
72 h
Time (h)
A549 (Untreated)
Gel + A549
250,000 hMSC + A549
250,000 hMSC + Gel + A549
1 M hMSC + Gel + A549
2 M hMSC + Gel + A549
***
***
***
*
IL8 Conc (pg/mL)
5000
4000
3000
2000
1000
0
4 h
24 h
48 h
72 h
Time (h)
A549 (Untreated)
Gel + A549
250,000 hMSC + A549
250,000 hMSC + Gel + A549
1 M hMSC + Gel + A549
2 M hMSC + Gel + A549

B

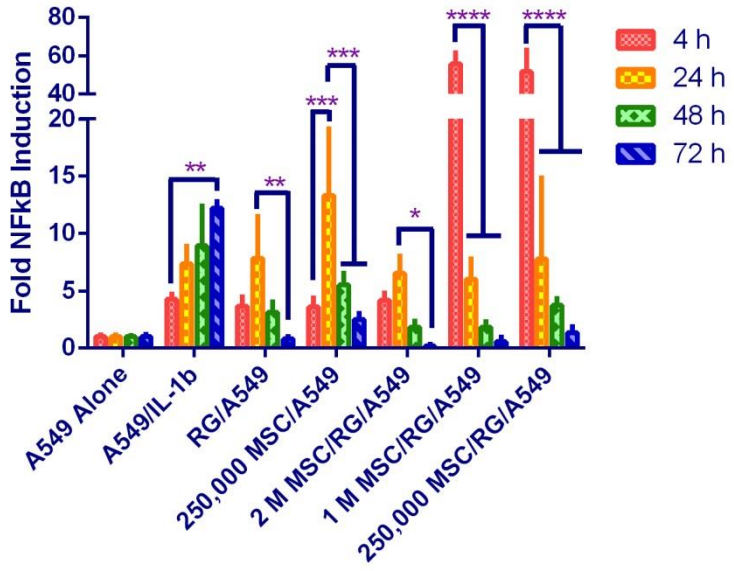
Fold NFkB Induction
80
60
40
20
15
10
5
0
**
**
***
***
*
****
****
4 h
24 h
48 h
72 h
A549 Alone
A549/IL-1b
RG/A549
250,000 MSC/A549
2 M MSC/RG/A549
1 M MSC/RG/A549
250,000 MSC/RG/A549

*Figure 5.11(A). IL-6 and IL-8 concentrations following treatment of IL-1β activated NFκB A549s with hMSC loaded Respiragel at 3 increasing seeding densities of cells: 250,000 cells/gel (usual dose), 1,000,000 cells/gel and 2,000,000 cells/gel, 250,000 hMSCs alone or Respiragel alone. The increase in cell number did not lead to an improved anti-inflammatory effect – in fact, increased hMSC numbers resulted in higher levels of IL-6 and IL-8. Results are presented as mean ± SE. Significance determined via two-way ANOVA, with Tukey's post hoc test. * = P≤0.05, ** = P<0.01 and *** = P < 0.0001; (B) Fold NFκB induction obtained through detection of luciferase, integrated as a reporter in A549s. A549s treated using the Respiragel/MSC formulation experience a down-regulation in NFκB production, indicating an anti-inflammatory effect of this formulation. This appears to be consistent with all three doses of hMSCs used, though a dose of 2 x 10^6 cells was the only dose which did not produce an increased NFκB expression at the early time point of 4 h. hMSCs alone are also anti-inflammatory due to down-regulation of NFκB, and the gel alone containing no cells also appears to have an anti-inflammatory effect at 48 h. Results are presented as mean ± SD. Significance determined via two-way ANOVA, with Tukey's post hoc test. * = P≤0.05,** = P<0.01,*** = P<0.001, **** = P<0.0001.*

5.4.Discussion

The benefits of localised therapeutic delivery to a target site are considerable, including increased efficacy and decreased toxicity [335] – benefits which are relevant and applicable across a range of clinical conditions. Therefore, the use of materials that can support the loco-regional delivery of both cells and small molecules represents a clinically appealing approach. In this thesis thus far, we have developed a solid lipid nanoparticle formulation for the delivery of all-trans Retinoic Acid and a thermoresponsive hydrogel for delivery of stem cells – formulations which represent two different approaches for the direct delivery of therapeutic agents. In this thesis chapter, we report on the effect of each of these formulations with respect to changes in cytokine levels in an *in vitro* model of inflammatory lung disease.

As previously discussed in the introduction to this chapter, A549 cells were selected as our alveolar epithelial cell line model, due to the difficulty in acquiring human alveolar epithelial cells (hAEpCs) and also their historical use as an appropriate model. Initial studies aimed to confirm that TNF-α and IL-1β were able to activate or stimulate the A549 cells, which has been previously reported on in the literature [328,329,336,337]. Activation of A549 cells using both TNF-α and IL-1β resulted in a significant increase in both IL-6 and IL-8 concentrations in cell culture supernatant (Figure 5.4). This effect is likely due to activation of NFκB signalling pathways within the cell, which is generally recognized to be one of the most important pro-inflammatory signalling pathways in the body, largely due to the role of NFκB in the expression of pro-inflammatory genes including cytokines, chemokines, and adhesion molecules (Figure 5.12) [332]. Both IL-1β and TNF-α are known to be able to initiate transcription of chemokine genes via NFκB activation, albeit employing different cellular receptors and adaptor molecules [338–340]. Five different protein sub-units constitute the NFκB family (p50, p52, p65/RelA, RelB and c-Rel) [341]. Interaction between different sub-units results in dimers that are active upon phosphorylation and in recent years, it has become evident

that there are at least two separate pathways for NFκB activation. The “canonical” pathway is triggered by microbial products and pro-inflammatory cytokines such as IL-1 and TNF-α, usually leading to activation of p50 and p65/RelA complexes resulting in regulation of expression of pro-inflammatory and cell survival genes [342]. An “alternative” NFκB pathway is activated by TNF family cytokines, but not TNF-α, and results in activation of p52/RelB complexes. This leads to the regulation of genes required for B-cell activation [343]. Based on these mechanisms, we postulate that TNF-α and IL-1β stimulate the canonical NFκB signalling pathway, resulting in increased transcription of genes related to inflammatory proteins leading to higher supernatant levels of IL-6 and IL-8 (and possibly further cytokines and chemokines which were not evaluated over the course of this study). It was also noted that significantly higher levels of IL-6 and IL-8 were achieved following activation with IL-1β when compared with the TNF-α activated A549s. Based on this finding, IL-1β was selected as our activator of choice for all subsequent *in vitro* experiments.

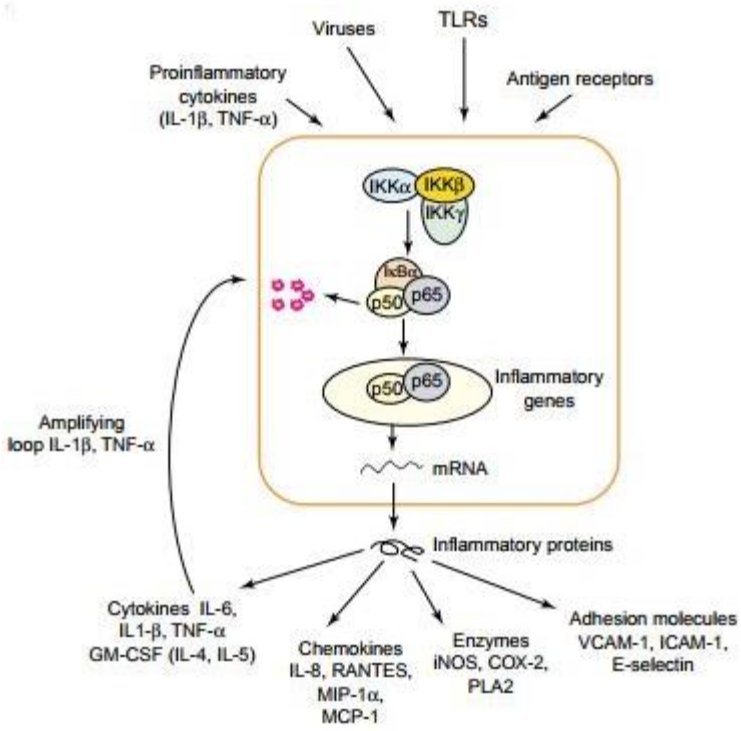

Figure 5.12. The classical NF-κB pathway is activated by a variety of inflammatory signals, resulting in coordinated expression of multiple inflammatory and innate immune genes. The pro-inflammatory cytokines IL-1β and TNF-α activate NFκB and their expression is induced in response to NFκB activation, thus forming an amplifying feed forward loop. Reproduced from [342].

The first formulation to be assessed was the atRA SLN formulation. ELISA was used to assess the effect of the atRA SLNs on IL-6 and IL-8 levels. Two different "doses" of atRA SLNs were assessed – a "low dose" of 5 µg/mL and a "high dose" of 10 µg/mL. These doses were selected based on previous reports in the literature and also within our wider research group indicating biocompatibility and a cellular response. Research in our group, carried out by O'Leary *et al*, showed a concentration of 10 µg/mL atRA loaded into a bi-layered scaffold to be optimal for enhancing gene expression for mucociliary differentiation of primary tracheobronchial cells [299]. Further research conducted outside of this group by Gray *et al* [100] also found that atRA, at a concentration of 5 x 10^{-8} M, was essential for induction of mucociliary differentiation in

in vitro normal human tracheobronchial epithelial (NHTBE) cells. The selected "doses" of 5-10 μg/mL fall within this previously investigated range [344]. A CCK-8 viability study showed atRA SLNs and blank SLNs to be non-toxic at the doses selected (Figure 5.5), confirming results found in section 4.3.5. This was anticipated due to the biocompatibility of the drug molecule used and all excipients selected, coupled with numerous previous research articles indicating the low cytotoxicity associated with similar SLNs [304–306]. This also complies with the International Organisation for Standardisation guidelines (ISO 10993-5:2009) [230], which states that samples with a cell viability larger than 80% can be considered non-cytotoxic.

Anti-inflammatory assessment of the atRA SLN formulation showed significant reduction in both investigated cytokines, when compared with untreated A549s, and also blank SLNs as controls. At 48 h, IL-6 was significantly reduced by the HD atRA SLN formulation, and at 72 h significance was achieved using both LD- and HD atRA SLNs. In terms of IL-8, concentrations were reduced at 24 h, 48 h and 72 h by HD atRA SLNs. As previously discussed in Chapter 1 of this thesis, atRA is known to possess immunomodulatory and anti-inflammatory properties, though often these effects have been investigated in relation to other inflammatory conditions than those present in the lung, such as arthritis [105], acne [106] and psoriasis [107]. These reports appear to reach similar conclusions, in that in inflammatory conditions, atRA can significantly reduce concentrations of pro-inflammatory cytokines, including IL-1β, IL-6, IL-12 and TNF-α. As previously mentioned, this body of research highlighting the immunomodulatory and anti-inflammatory activity of atRA prompted our hypothesis that this could be translated to other inflammatory conditions, and specifically COPD, targeting the inflammatory pathogenic component of the disease – which, to the best of our knowledge, is an application of atRA which has not been investigated previously. The effect of atRA on A549s in terms of immunomodulatory effects has been poorly investigated to date however it is known that atRA binds to retinoic acid receptors (RARs) and retinoid X receptors (RXRs). One previous study carried out by Kirchmeyer *et al* [345] investigating the mechanism of reduction in IL-6 in rheumatoid arthritis,

found that atRA suppresses IL-6 production through a mechanism independent of RAR, but rather through inhibition of the extracellularly regulated kinase 1/2 ($ERK_{1/2}$) pathway. Detailed further analysis would be required in order to accurately evaluate the mechanism of action of atRA however, the reduction in pro-inflammatory cytokine levels in this model is important as it indicates that atRA SLNs may have potential therapeutic applications in COPD, which is characterised by chronic inflammation.

While the more common approach for drug delivery to the lung is via aerosol devices, these are associated with issues such as deposition at areas other than the alveoli, along with mucociliary clearance and macrophage phagocytosis prior to the desired therapeutic action [346,347]. Recent advances in minimally invasive medical devices and imaging technology on the other hand, can enable loco-regional site specific delivery to diseased sites of the lung, aiding in the repair of damaged tissue through a reduction in the destructive inflammatory cytokines. The use of a thermoresponsive hydrogel as a delivery vector for atRA SLNs was considered to be of potential benefit due to its ability to form a robust bolus at the site of delivery on reaching the boundary temperature of 37^{o}C. Anti-inflammatory assessment of atRA SLN loaded Respiragel was again carried out in terms of IL-6 and IL-8 cytokine levels with the appropriate controls. In terms of both cytokines, no immunomodulatory effect was observed until 72 h, at which point a significant reduction in both IL-6 and IL-8 levels was observed as a result of treatment with the HD atRA SLN Respiragel formulation (Figure 5.8). This was a similar result to that which was observed from treatment with HD atRA SLNs alone in Figure 5.6, indicating that atRA remains bioactive following loading into the hydrogel. The difference in this instance is that the response is more delayed, which may be attributed to the differences in release profiles between atRA SLNs alone and atRA SLNs loaded in Respiragel (Figure 4.12A).

This *in vitro* model was then utilised to assess the anti-inflammatory effects of the hMSC/Respiragel formulation. Due to the presence of a second cell type in this system (i.e. hMSCs as well as A549s), it was essential that any potential immunomodulatory

effect could be attributed to one cell type or the other, rather than quantifying cytokines which could be being released from either cell type without distinction. Based on this, A549-NFκB-luciferase cells (Signosis Inc.) [348] were used. These cells have been stably transfected with a luciferase reporter vector, which contains four repeats of the NFκB binding sites – a promoter upstream of the firefly luciferase coding region. This means that when NFκB is activated, the luciferase is released and can be detected in the form of luminescence (Figure 5.13). Therefore, the cell line can be used as a reporter system for monitoring the activation of NFκB triggered by stimuli treatment, enforced gene expression and gene knockdown. In this case, we are looking at NFκB triggered by stimuli treatment using either TNF-α or IL-1β, which activate the NFκB signaling pathways, as mentioned earlier in this discussion. In these studies, the higher the luminescence signal, the more NFκB activation, or NFκB mediated inflammation.

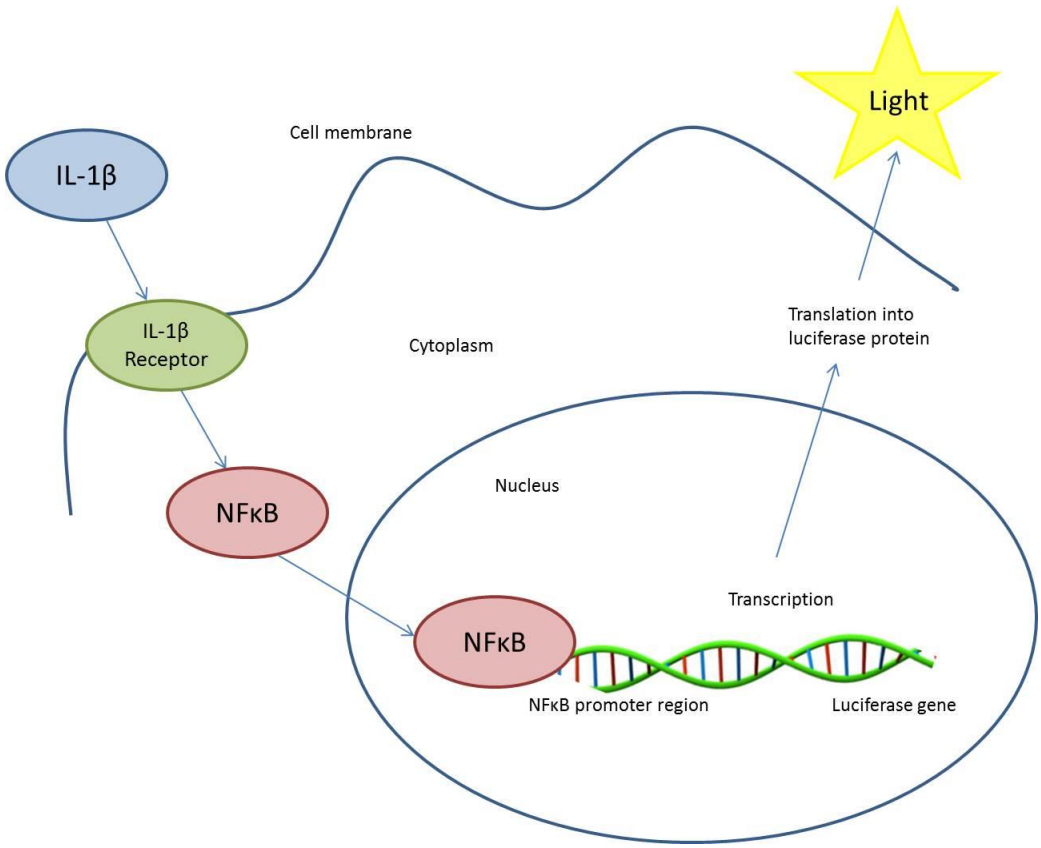

Figure 5.13. Principle behind NFκB luciferase reporter assay. Activation of the NFκB (transcription factor) through the use of an extracellular stimuli such as IL-1β results in translocation of the NFκB to the nucleus and interaction with relevant co-factors to drive gene expression. Once luciferase is expressed, it can generate light in an enzymatic assay and the amount of light measured is positively correlated with the level of NFκB activation.

Prior to assessing the anti-inflammatory effects of the hMSC/Respiragel formulation, biocompatibility with activated A549s was confirmed using a CCK-8 assay (Figure 5.9). No significant difference in viability of A549s was observed when cultured in the presence of the hMSC/Respiragel formulation, or the Respiragel alone control. This is in line with ISO standards for cytotoxicity of medical devices, which requires greater than 80% viability of cells [230]. Biocompatibility of the formulation with A549 cells was expected, due to previous assessment of biocompatibility of Respiragel with hMSCs (section 2.3.6), and the general consensus that cell lines are more robust than primary cultures, however this provided validation for future experiments.

Assessment of the potential anti-inflammatory response of NFκB A549 cells was determined via ELISA, allowing IL-6 and IL-8 media supernatant concentrations to be quantified (Figure 5.10A). It was hypothesised that treatment of activated NFκB A549s with the hMSC/Respiragel formulation would result in reduction in IL-6 and IL-8 levels due to the paracrine response elicited by hMSCs. As discussed in Chapter 1 of this thesis, MSCs are thought to release a variety of mediators in response to a specific microenvironment that may include the down-regulation of pro-inflammatory cytokines and the up-regulation of anti-inflammatory cytokines [56], which has been demonstrated in *in vitro* models of ALI to date [61]. For both cytokines however, the hMSC/Respiragel formulation on activated NFκB A549s did not result in a reduction in concentration at any time point when compared with the activated A549 alone control. In fact the opposite was observed, in that the hMSC/Respiragel/A549 group resulted in significantly higher levels of both IL-6 and IL-8 at 24, 48 and 72 h ($P < 0.0001$) indicating a potentially pro-inflammatory effect. In addition to this, the hMSC/Respiragel

combination appears to result in similar IL-6 and IL-8 concentrations as the Respiragel alone (no hMSC) group, indicating that the hMSCs encapsulated within the gel are not having any effect on detected cytokine levels. It also appears that the no Respiragel group, which involved hMSCs delivered un-encapsulated in the same well as A549s results in significantly higher levels of IL-6 and IL-8 compared with the hMSC/Respiragel/A549 formulation. As hMSCs alone appears to have the highest pro-inflammatory effect, and those encapsulated in the gel have a lesser pro-inflammatory effect, this may indicate that encapsulation of hMSCs within the gel prevents them from coming into direct contact with IL-1β in the media, resulting in less activation of hMSCs and a subsequent reduced release of IL-6 and IL-8. This theory could be compounded by findings in Chapter 2 of this thesis, where the hydrogel was shown to have a robust internal 3D structure, and also to permit only slow diffusion of dye (section 2.3.3), therefore highlighting the obstacles to movement of molecules in and out of the gel.

As part of this study, a luciferase assay was also performed in order to ascertain whether the effect was as a result of the A549 cells in culture or as a result of the hMSCs in the hydrogel (Figure 5.10B), as mentioned earlier in this discussion. Fold induction was calculated from A549s which were not activated with IL-1β or subsequently treated with any formulation. A549s which were activated with IL-1β but not subsequently treated were used as a positive control for activation – showing a time dependant increase in NFκB induction thus confirming the pro-inflammatory activity of IL-1β on A549s. Progressively decreasing levels of NFκB were observed from 24 h onwards for the hMSC/Respiragel group compared with A549s activated with IL-1β but without a subsequent treatment. This indicates that NFκB mediated production of IL-6 and IL-8 is reduced, demonstrating a potential anti-inflammatory effect of the hMSC/Respiragel formulation which is not detected using ELISA. This effect is also observed for the hMSC alone treatment group and also the Respiragel alone treatment group, indicating that both the hMSCs and the gel independently result in a reduction in NFκB mediated inflammation. This also indicates that an unknown amount of IL-6

and IL-8 being detected may be produced elsewhere, which could be attributed to hMSC production of such cytokines. Previous studies have shown that hMSCs may be stimulated with IL-1β (and indeed, TNF-α, though this was not used in combination with hMSCs in this study). Research carried out by Broekman *et al* [349], investigated the effect of IL-1β or TNF-α activated MSCs on epithelial wound healing. Among other results reported, they found that stimulation of MSCs with either IL-1β or TNF-α resulted in increased expression of IL-6 mRNA. A further study, conducted by Heo *et al* [350] found that TNF-α induced adipose derived MSCs produced IL-6 and IL-8. A review article by Bernardo *et al* [351] also discusses the enhancement of an immune response by MSCs through the production of chemokines such as CXCL-9, CXCL-10, and CXCL-11 upon stimulation with pro-inflammatory cytokines, among others. *In vitro* studies with murine and human MSCs suggest that these stimulatory effects only occur when MSCs are exposed to sufficient levels of pro-inflammatory cytokines, such as TNF-α and IFN-γ. Based on the previous literature surrounding the behaviour of MSCs, it could be concluded that, if the MSCs are indeed producing a portion of IL-6 and IL-8 quantified, this may also be in response to stimulation with the pro-inflammatory cytokine, IL-1β. The therapeutic delivery of MSCs into an inflammatory environment therefore does not necessarily mean that they will behave in an anti-inflammatory manner in order to modulate the inflammatory environment. In fact, the "plasticity" of MSCs, means that the type and intensity of inflammatory stimulus may confer the ability to suppress an immune response in some cases or in others, enhance it [352]. The papers referenced above, which discuss the activation of MSCs in wound healing, report on the benefits of MSCs being driven down a pro-inflammatory route, as this of great importance in a wound healing applications in terms of the recruitment of lymphocytes to accelerate the healing process. However, in chronic inflammatory conditions, such as COPD, where inflammation triggers repeated cycles of exacerbations, enhancement of the inflammatory environment is not the required response. Research presented in a review article by Wang *et al* discusses how the concentration of inflammatory cytokines determines the immunomodulatory effect of MSCs [352]. They hypothesise

that during times of strong inflammation (i.e. in an acute phase of disease), MSCs can be rendered immunosuppressive, whereas during times of weak inflammation (such as would be observed during a chronic or relapse phase), MSCs may enhance the immune response. Taking into account this relative lack of predictability of the behaviour of MSCs once transplanted *in vivo* and the potential for enhancement of a pro-inflammatory response, the use of MSCs as a treatment approach in chronic inflammatory conditions may be difficult to achieve in reality. As these effects are difficult to capture in standard *in vitro* assays, and due to the difficulty in adequately modelling functionally relevant behaviours for transplanted cells, further assessment would be required to confirm whether this is the case. While some additional work could be done *in vitro* by way of assessment of stimulation of MSCs alone using IL-1β, and also gene expression assays via polymerase chain reaction (PCR), *in vivo* studies would be pivotal in accurately measuring treatment and formulation efficacy. These studies are more useful for assessing the outcomes in a complex environment with the interplay of multiple factors determining effects. This will be addressed in further detail in the future work section of this thesis.

Further studies investigated whether an increased hMSC loading dose in Respiragel would lead to changes in IL-6 and IL-8 levels. As previously discussed in section 2.4 of this thesis, the loading dose of 250,000 cells/ 0.5 mL gel was selected based on rheological characterisation of the cell loaded hydrogel at varying seeding densities. At this point, the seeding density could have been revised had a reduction in inflammatory cytokine levels been achieved. From Figure 5.11A, it is evident that an increase in hMSC number resulted in further increases in IL-6 and IL-8 concentration, which is once again in contrast to the fold-NFκB induction (Figure 5.11B), where a reduction in induction is observed from 24 h onwards in all hMSC/Respiragel groups. This adds further weight to the hypothesis that the MSCs are indeed being stimulated by IL-1β in the system, resulting in increased expression of IL-6 and IL-8 from the MSCs and a heightened pro-inflammatory environment, and supports the statement

previously where further analysis of this system is required to determine gene expression from MSCs and *in vivo* effects.

5.5.Conclusion

The results presented in this Chapter indicate the promise of the atRA SLN formulation in modulating the inflammatory environment present in COPD, though simultaneously shedding some doubt on the use of hMSCs for this application. The atRA SLN formulation and the atRA SLNs suspended in Respiragel were assessed for their biocompatibility with a respiratory cell line (A549s) in this Chapter, as well as for their anti-inflammatory effects. Both investigated formulations were shown to be biocompatible with the alveolar lung cell line. HD atRA SLNs (10 µg/mL) resulted in a reduction in IL-6 and IL-8 compared with untreated A549s, indicating promise for atRA as an anti-inflammatory agent in the treatment of inflammatory lung disease. atRA SLNs retained this effect when loaded into the Respiragel formulation, though sustained release of atRA led to a delay in the observed effect to 72 h. As mentioned in Chapters 2 and 4, Respiragel could be easily and directly delivered to the distal airways using emerging medical device and interventional pulmonology techniques allowing loco-regional delivery of therapeutics, highlighting the promise of formulations such as these in what is becoming a more widely researched field. The hMSC/Respiragel formulation was also biocompatible and appeared to result in a reduction in NFκB activation when compared with untreated A549s, indicating a potential role in reducing NFκB mediated inflammation. Conversely, levels of IL-6 and IL-8 were raised on detection using ELISA. We postulate that the increase in IL-6 and IL-8 levels may be due to IL-1β mediated activation of hMSCs, resulting in up-regulated production of pro-inflammatory cytokines. It is difficult to hypothesise the effect that this might have *in vivo,* though hMSCs are known to induce both pro- and anti-inflammatory responses. Additional detailed analysis of this mechanism is required prior to furthering the use of hMSCs for chronic inflammatory conditions such as COPD.

6. Discussion

6.1.Overview

The overall objective of the research presented in this PhD thesis was to develop novel delivery systems suitable for minimally invasive drug and cell delivery, for potential applications in the treatment of COPD. Our central hypothesis was that hydrogels and solid lipid nanoparticles can be used as drug and cell delivery vectors, which are then capable of exerting an anti-inflammatory effect on the local environment present in chronic lung conditions such as COPD. Currently utilised therapeutic strategies for the treatment of COPD are suboptimal and a loco-regional delivery approach may offer the opportunity to enhance clinical outcomes in the disease.

Chronic Obstructive Pulmonary Disease (COPD) is a major public health issue, affecting 64 million people globally, and is being predicted to become the third leading cause of death worldwide by 2030 [15]. COPD is defined as a lung disease characterised by chronic obstruction of lung airflow that interferes with normal breathing and is not fully reversible. This obstruction is present due to a combination of airway and parenchymal damage, associated with an enhanced chronic inflammatory response in the airways and the lung to noxious particles or gases present in tobacco smoke [18]. Despite the significant evolution of medical treatment options for COPD in the last two decades, it is still an incurable disease. Medical treatment options for non-hospitalised patients primarily aim for symptomatic control. One surgical option for patients in advanced COPD is lung volume reduction surgery (LVRS), which involves resection of emphysematous destroyed parts of the lung [31]. However, LVRS is associated with high morbidity, hospitalisation and operative mortality [33,34] as well as limited availability of the treatment to date. In addition to this, it does not treat or address the underlying disease state or progressive damage being caused, and due to its invasive nature is only introduced at an advanced disease stage. In the case of failure of these management strategies, patients in advanced COPD face lung transplantation, which is

limited by a number of complications such as the supply of acceptable donor organs, lifelong immunosuppressive therapies and possibility of infection [45,46].

The unsatisfactory clinical outcomes associated with current treatment options for COPD has resulted in the need to investigate other advanced therapeutic options. In this thesis, we aimed to investigate the use of therapeutic approaches targeting the inflammatory component of COPD, which if treated may result in a reduction in the physical damage to lung tissue and potentially the ability to regenerate healthy tissue. Approaches investigated throughout this thesis include the use of hydrogels as a biomaterial scaffold and as a delivery vector, capable of supporting the encapsulation of stem cells; hMSCs as an encapsulated paracrine therapeutic agent; nanoparticles for drug delivery; and finally all-trans Retinoic Acid as an anti-inflammatory small molecule drug.

Development and assessment of a methylcellulose, collagen and beta-glycerophosphate based hydrogel, for its thermoresponsive properties and ability to maintain viability of encapsulated stem cells, was investigated in Chapter 2. Assessment of two alternative, synthetic, self-assembling hydrogels, Star-PLL-PLT and Linear-PLL-PLT, also for their ability to deliver cells in a minimally invasive manner was performed in Chapter 3. Formulation and characterisation of atRA loaded SLNs was performed in Chapter 4, due to previous publications supporting its anti-inflammatory effects in other chronic inflammatory conditions. Finally, *in vitro* assessment of the anti-inflammatory activity of the hMSC loaded hydrogel, the atRA SLNs and the atRA SLN loaded hydrogel formulations was carried out in Chapter 5.

The remainder of this chapter summarises the key findings and implications from each individual results chapter within this thesis and reviews outstanding questions and possible future directions which have arisen from this research.

6.2. Chapter 2: Formulation and physicochemical characterisation of a thermoresponsive methylcellulose, collagen and beta-glycerophosphate hydrogel

As mentioned throughout this thesis, loco-regional delivery of therapeutic agents has the potential to significantly enhance clinical outcomes in disease, through the targeting of treatments directly to the site of injury. The development of new materials which can enable this as well as promoting retention at the delivery site and controlled release of the therapeutic agent, are of utmost importance in furthering research in this field. Injectable hydrogels represent attractive platforms for the delivery of biotherapeutics, which can provide a depot for the controlled release of small molecule drugs and growth factor therapeutics and also provide a surrogate microenvironment for live cells, which have specific needs in order to be delivered effectively, retain viability and demonstrate therapeutic behaviour.

Chapter 1 of this thesis described current treatment strategies for COPD, with one potential option being polymeric lung volume reduction surgery (PLVR). PLVR involves the delivery of a synthetic polymer based hydrogel to emphysematous areas of the lung, initiating an inflammatory reaction which collapses emphysematous tissue. This approach provides proof of concept for the feasibility of loco-regional delivery to diseased sites of the lung in COPD. However as with all COPD treatments, bar transplantation, this approach aims to improve symptomatic control of the condition without addressing the underlying pathophysiology. The premise of Chapter 2 is to move that approach to the next stage in exploring the potential to develop a biocompatible hydrogel suitable for loco-regional delivery to the lung. Such a material could act as a carrier for drugs/cells providing the opportunity to exert a local therapeutic effect for advanced disease. A methylcellulose, collagen and beta-glycerophosphate thermoresponsive hydrogel (Respiragel) was developed to enable the encapsulation and delivery of human mesenchymal stem cells (hMSCs) to the distal

airways. It was hypothesised that this would allow for retention of hMSCs at the target site, and mediation of the local inflammatory environment through a paracrine effect.

A rheological investigation of the thermogelling behaviour of 2% w/v MC found that the inclusion of 5.6% w/v βGP resulted in a decrease of the sol-gel transition temperature from ~70^{o}C to be in line with that of physiological temperature (38^{o}C). Inclusion of collagen into the formulation and alteration of the MC concentration from 2% to 2.5% w/v resulted in an improved storage modulus and a final gelation temperature of 37^{o}C. Consequently, the formulation composed of 2.5% MC, 0.1% collagen and 5.6% βGP (Respiragel) was utilised for all further experiments.

Respiragel was shown to be biocompatible with hMSCs suspended within Respiragel, with cells remaining viable up to day 7 in culture, and observed to be stretching and spreading within the hydrogel. In addition to this, cell proliferation was evidenced by the fact that dsDNA levels increased over the duration of the 7-day gel culture period. This was in sharp contrast to the non-collagen containing control, which showed statistically less proliferation of encapsulated cells than the collagen containing gel. The results from this study also correspond with these previous findings [163] in that cell proliferation is markedly improved on inclusion of collagen, due to the availability of attachment sites. This indicates the suitability of this material not only as a cell delivery vector, but also as a material within which cells can remain viable and proliferate.

With translatability of our formulation in mind, we carried out injectability testing and showed that it was possible for the solution to be passed through a 3 mL syringe, 3 mL syringe plus 21G needle, and a 3 mL syringe plus 0.5 m catheter. Forces required fall below the average at which males can push, and only the catheter falls at the threshold of force which is average for females. This result is supported by flow rheology, which shows the solution has shear thinning properties resulting in a rapid decrease in viscosity on application of shear stress. On removal of the shear, it is able to recover its original structure and is not adversely damaged by the shear thinning process. These results in combination suggest that this hydrogel formulation is highly amenable to

delivery via a minimally invasive injection, and that its structure recovers following this process.

Sterility of any type of delivery vehicle for administration to a patient is of utmost importance. Lyophilised polymer wafers were sterilised using gamma irradiation, and no change in sol-gel transition was observed. A comparative study of hMSC viability and proliferation in the irradiated gel versus the non-irradiated gel showed no difference in viability or proliferation between the two groups at all time points.

6.3. Chapter 3: Development and physicochemical characterisation of synthetic linear and star-shaped co-polypeptide based hydrogels

While Chapter 2 established that a thermoresponsive natural polymer based hydrogel could support cell viability and proliferation *in vitro*, Chapter 3 involved the investigation of novel synthetic polymers as alternative materials that may also be capable of supporting minimally invasive cell and drug delivery. Hydrogels obtained by self-assembly of amphiphilic polypeptides represent a promising class of synthetic material for such applications. Self-assembling hydrogels are of interest as their arrangement can be rationally designed to be highly specific, tuneable, and reversible and thereby contribute distinct and useful properties [204]. In addition to this, their composition of chains of naturally occurring amino acids linked by conventional peptide bonds renders them as biologically inspired (bioinspired) and confers natural biodegradability [205].

Two synthetic self-assembling hydrogels were investigated in Chapter 3; Star-PLL-PLT and Linear-PLL-PLT. These polymers self-assembled on addition of aqueous media and readily formed hydrogels in less than 5 min. When rheologically characterised, the Star-

PLL-PLT hydrogel showed superior internal strength and robustness versus the Linear-PLL-PLT. This was evidenced by the higher storage moduli obtained from the Star-PLL-PLT (6436 Pa versus 181.5 Pa for Linear-PLL-PLT). However, on application of strain, both hydrogels appeared to revert to polymer solution form.

Injectability testing showed that both hydrogels could be passed through a range of common clinical devices including a 1 mL syringe, 1 mL syringe plus 21G needle, and a 1 mL syringe plus 0.5 m catheter with very low forces required, though significantly lower forces were required to push the Linear-PLL-PLT through the catheter compared with the Star-PLL-PLT. This again highlighted the more robust nature of the Star-PLL-PLT, possibly showing it to be the more appropriate choice over the Linear-PLL-PLT as a vector for delivery of therapeutics *in vivo*.

In order to assess the Star-PLL-PLT and Linear-PLL-PLT for their ability to act as minimally invasive cell carriers, determination of hMSC viability following suspension within the gels was performed. Both gels showed a lack of biocompatibility with hMSCs from 24 h onwards.

The results presented in this Chapter show the synthetic co-polypeptide based hydrogels to be inferior to Respiragel presented in Chapter 2 of this thesis for the application of cell delivery. The star-shaped and linear co-polypeptide based hydrogels are not stimuli responsive, which would poses challenges should they progress to clinical use. Pre-formed hydrogels require surgical implantation *in situ* which is disadvantageous due to the invasive nature of the procedure. Respiragel, on the other hand, is thermoresponsive, allowing minimally invasive delivery via syringing directly to the injection site. Both the Star-PLL-PLT and the Linear-PLL-PLT were highly susceptible to external forces, such as strain, shear stress and the presence of buffer, resulting in disintegration and reversion to polymer solution form. They are also cytotoxic for encapsulated hMSCs. Potential for these hydrogels is likely to not be in relation to cell delivery applications, however, positive characteristics such as the high storage

modulus observed with the Star-PLL-PLT, and their ease of injectability indicates that they may have a role in alternative applications such as drug delivery.

6.4.A site-specific delivery platform for all-trans Retinoic Acid (atRA) in pulmonary regeneration applications

The possibility of utilising a regenerative approach in the treatment of chronic lung disease relies on the consideration of two broad strategic viewpoints. One such approach is the utilisation of pharmacologically active molecules which can exert their effect on a population of cells at the disease site [17]. One particular small molecule of interest is all-trans Retinoic Acid (atRA) which has been shown to have both anti-inflammatory and pro-regenerative properties, and has been explored for use in COPD. In this Chapter, we aimed to formulate solid lipid nanoparticles (SLNs) encapsulating atRA, for suspension within our selected hydrogel formulation allowing for subsequent loco-regional delivery – a strategy which represents an innovative approach for pulmonary delivery compared with their historical application as vectors for inhaled delivery.

A final SLN formulation consisting of Compritol 888 ATO 5%, Poloxamer 188 1%, Tween 80 1% and atRA 1% relative to the lipid core was produced, resulting in particles with an average size of 176.85 nm, and an atRA encapsulation efficiency of 85.47%. Release of atRA from SLNs showed an initial burst which was observed from 0-8 h, after which point a more sustained profile became apparent. Final cumulative release of atRA from SLNs over the duration of the study was 43%. Stability studies conducted on atRA and blank SLNs over a period of 3 months found no significant difference in particle size at any investigated storage condition (-20^{o}C, 4^{o}C or 20^{o}C). In contrast to this, a large variance in encapsulation efficiency (EE) was observed. The optimal temperature for storage based on EE appears to be -20^{o}C, where at 3 months 76% atRA remained,

compared with 10.94% at 4°C and 1.46% at 20°C. Blank and atRA SLNs were also assessed for biocompatibility on A549 cells, which are commonly used as a model for ATII cells. Both blank and drug loaded SLNs were found to have no negative effects on A549 viability *in vitro.*

Final assessment of atRA SLNs developed in this chapter involved incorporation of the particles in a previously developed hydrogel, i.e. Respiragel, discussed in Chapter 2. Repeat rheological characterisation showed the thermoresponse to be unaffected by inclusion of the atRA SLNs. Release of atRA from SLNs loaded into the hydrogel followed a similar pattern to that of atRA release from SLNs alone. A burst release was observed from 0-8 h, after which point a more controlled profile became apparent. While this burst release appeared similar to the release of atRA from SLNs alone, the average amount of drug released was reduced at each time point compared with that from the SLNs alone. This is likely due to the presence of a second matrix through which the drug is required to pass prior to detection, resulting in a sustained release profile. However, the final amount of drug released from the SLNs in the hydrogel was not significantly different to that observed from SLNs alone, indicating that atRA release from the SLN hydrogel was more prolonged but did not result in a decrease in total drug release.

6.5.Chapter 5: In vitro characterisation of developed formulations: Respiragel and all-trans retinoic acid solid lipid nanoparticles

The work of previous Chapters has centred around the development of two formulation approaches with potential applications in the loco-regional treatment of COPD – firstly, the use of stem cells encapsulated in a hydrogel, which could be used for its paracrine capabilities in mounting an anti-inflammatory response; and secondly, the use of small molecule therapeutic agents – in this case all-trans Retinoic Acid, also

with potential effects on inflammation. This Chapter focused on assessing the anti-inflammatory effects of both the hMSC/Respiragel formulation and the atRA SLN formulation through the use of an *in vitro* model of cytokine release, with cytokines being key contributors to the inflammatory environment observed in COPD.

A549 cells were selected as our alveolar epithelial cell line model. Initial studies aimed to confirm that pro-inflammatory cytokines often raised in patients with COPD i.e. TNF-α and IL-1β, were able to stimulate A549 cells into producing increased levels of IL-6 and IL-8 – also present in increased concentrations in COPD. Activation of A549 cells using both TNF-α and IL-1β resulted in a significant increase in both IL-6 and IL-8 concentrations in cell culture supernatant. This effect is likely due to activation of NFκB signalling pathways within the cell, which is generally recognized to be one of the most important pro-inflammatory signalling pathways in the body. As IL-1β resulted in significantly higher levels of IL-6 and IL-8 compared to that observed with TNF-α, it was selected as the A549 activator for all subsequent *in vitro* experiments. For atRA SLNs, at 48 h, IL-6 was significantly reduced by the HD atRA SLN formulation (10 µg atRA/mL), and at 72 h significance was achieved using both LD- (5 µg atRA/mL) and HD atRA SLNs, when compared with cells treated with blank SLNs and also untreated A549s alone. In terms of IL-8, concentrations were reduced at 24 h, 48 h and 72 h by HD atRA SLNs. As previously discussed in Chapter 1 of this thesis, atRA is known to possess anti-inflammatory properties, though often these effects have been investigated in relation to other inflammatory diseases than those present in the lung. Thus, we postulate that the previously described anti-inflammatory effects of atRA could be translated to COPD, and results from this Chapter indicate that further investigation into these effects may be warranted.

Integration of atRA SLNs with Respiragel was performed to enable site specific delivery of the nanoparticles. Anti-inflammatory assessment was again carried out in terms of IL-6 and IL-8 cytokine levels. An anti-inflammatory effect was not observed until 72 h, at which point a significant reduction in both IL-6 and IL-8 levels resulted following

treatment of activated A549s with the HD atRA SLN Respiragel formulation. In this instance, the response is delayed compared with that observed from atRA SLNs alone where a response was detected at 48 h. This is likely due to the release kinetics previously observed, where release of atRA from the SLN loaded Respiragel is delayed compared with atRA release from SLNs alone.

This *in vitro* model was then applied to evaluate the anti-inflammatory effects of the hMSC/Respiragel formulation. NFκB-luciferase A549 cells were utilised due to the presence of a second cell type in this system (i.e. hMSCs as well as A549s), thereby allowing any potential anti-inflammatory effect to be attributed to one cell type or the other. Treatment of activated NFκB A549s with the hMSC/Respiragel formulation did not result in a reduction in IL-6 or IL-8 concentrations at any time point when compared with the activated A549 alone control, and in fact the opposite was observed as significantly higher levels of both IL-6 and IL-8 resulted at 24, 48 and 72 h ($P < 0.0001$). However, on assessing fold induction of NFκB activity of A549s, progressively decreasing levels were observed from 24 h onwards for the hMSC/Respiragel group compared with untreated IL-1β activated A549s. This seems to indicate that hMSCs are able to down-regulate the NFκB pathway in A549s, which is most likely due to a paracrine effect. However, as this down-regulation does not result in reduced IL-6 and IL-8 levels (and actually leads to increased levels of these cytokines, indicating increased inflammation), we hypothesise that the increase in IL-6 and IL-8 is a result of the hMSCs own inflammatory pathways being activated by the presence of pro-inflammatory mediators. This is representative of the *in vivo* scenario, where hMSCs would be delivered to a chronic disease site where significant inflammation is occurring.

Further studies investigated whether an increased hMSC loading dose in Respiragel would lead to improved anti-inflammatory activity of the formulation. However, an increase in hMSC number resulted in further increases in IL-6 and IL-8 concentration, which was once again in contrast to the fold-NFκB induction, which was reduced from

24 h onwards in all hMSC/Respiragel groups. This adds further weight to the hypothesis that the MSCs are indeed being stimulated by IL-1β in the system, resulting in increased release of IL-6 and IL-8 from the MSCs and a heightened pro-inflammatory environment.

6.6.Future work

The results obtained with atRA SLNs showed particular promise in relation to the specific objectives of the thesis. Future work in this area could focus on a number of areas. Multiplex ELISA may be useful to get a sense of a broader range of effects across a wider range of cytokines. However, the next step most likely required before moving to *in vivo* studies, would be to ascertain whether the anti-inflammatory effects observed using A549 cells as our model cell type would also be observed on primary alveolar cells. As the lung is composed of more than 40 cell types, the process of obtaining such cells is complex involving isolation, purification and culture of alveolar epithelial Type II (ATII) cells obtained from human tissue following lung resections [353]. Alternatively, owing to the lack of availability of human tissues in general, these studies could be performed on primary mouse or rat ATII cells. In addition to multiplex ELISA for determining concentration changes of cytokines, polymerase chain reaction (PCR) may be useful to confirm alteration of gene expression. A comparison study between primary cells and A549s would be of general interest also, to further support the use of A549s as an *in vitro* model.

Investigations into the effects of atRA SLNs on primary cells may also provide information regarding the regenerative potential of atRA as well as clarifying the possible anti-inflammatory effect. Previous publications on the pro-regenerative effects of atRA have for the most part, been conducted using *in vivo* animal models, however, some pro-regenerative effects such as increased production of surfactant proteins (B and C) [92], increased proliferation of ATII cells, and also protection against the destructive effects of elastase [354] could be assessed in an *in vitro* model using primary alveolar cells.

Ultimately an *in vivo* study of the anti-inflammatory effects of the atRA SLN and atRA SLN Respiragel formulations would be desirable, in order to validate results obtained from *in vitro* assays. COPD is notoriously difficult to model in animals due to its multi-

factorial nature, its progressive development in humans over many years and the many physiological and anatomical differences between different animal species and humans [355]. No animal model to date is able to fully encapsulate all of these requirements, so it is rather a case of choosing the most appropriate. Generally, rodents such as mice, rats and guinea pigs are used, with mice being the most common. In terms of induction of COPD lesions, common choices include the cigarette smoke induction of emphysema model, and also the elastase induced injury model [60]. The use of the cigarette smoke induced model is usually the main choice, due to the origins of COPD as a disease directly related to exposure to cigarette smoke. However, these models appear to be primarily utilised in studies assessing structural changes in the lung, which may render them to be more appropriate choices when investigating the regenerative potential of atRA. However, when investigating the anti-inflammatory effects, a model which results in elevated levels of pro-inflammatory cytokines would be the most useful, and as such we would likely choose a lipopolysachharide (LPS) induced model [60]. This model involves intra-tracheal administration of LPS (a component of gram negative bacterial cell walls), resulting in a mixed inflammatory reaction with increases in neutrophils [356] and increases in BAL TNF-α and IL-1β [357] (thus presenting a more complex but similar model to what we have created in this thesis *in vitro)*. Outcomes would be based on BAL fluid analysis of cytokine levels, again determining concentrations of IL-6 and IL-8 but also assessing for IL-10 (often detected *in vivo* but not *in vitro*) and KGF. Other markers for lung function include BAL proteins and neutrophils, to assess infiltration into the lung [61].

As a result of findings presented in Chapter 5 we hypothesise that the hMSCs present in the hMSC/Respiragel formulation may have been stimulated by IL-1β present in our *in vitro* model, resulting in increased production of IL-6 and IL-8. While not the finding that we were hoping for, this is important in that it emphasises how much is unknown regarding the behaviour of hMSCs and how they respond to stimuli under different conditions. Based on these findings, it would initially be necessary to confirm this hypothesis. This could be done by repeating the experiments presented in Chapter 5,

but without the confounding influence of co-cultured A549s. Again multiplex ELISA may be useful in assessing a wider range of cytokines. Gene expression via PCR may also be useful.

6.7.Overall conclusion

Collectively, the research presented in this thesis has resulted in the investigation of multiple formulations as potential cell or drug carriers which can be delivered in a minimally invasive manner. Both atRA SLNs and a thermoresponsive hydrogel (Respiragel), when used in combination, provide unique potential and flexibility for the loco-regional delivery of therapeutic agents in COPD where current treatment options are unsatisfactory, and where site-specific retention and controlled release could enable significant enhancements in efficacy and safety. In addition, this thesis has highlighted potential shortcomings of the use of MSCs in the treatment of inflammatory conditions, which need to be verified in further detailed studies.

7. Appendices

Appendix 1

Appendix 1.1

Supplementary data demonstrating Fourir Transform Infra-Red (FT-IR) spectra of Star-PLL-PLT in water, as described in section 3.2.2. This work was carried out by Robert Murphy (PhD student) from the Translational REsearch in Nanomedical Devices (TREND) Group in RCSI.

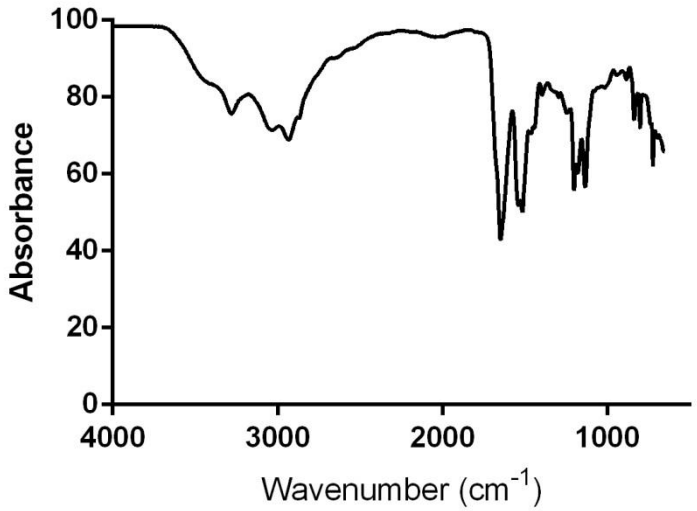

Appendix 1.2

Supplementary data demonstrating Fourir Transform Infra-Red (FT-IR) spectra of Linear-PLL-PLT in water, as described in section 3.2.2. This work was carried out by Robert Murphy (PhD student) in the Translational REsearch in Nanomedical Devices (TREND) Group in RCSI.

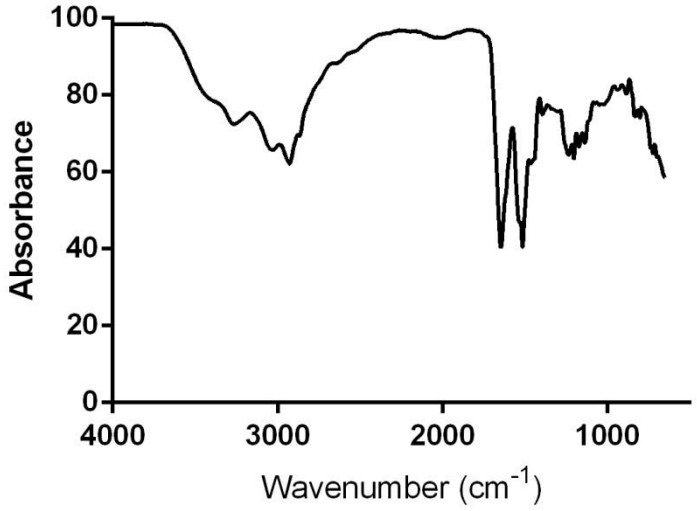

Appendix 2

Appendix 2.1

Supplementary data demonstrating a representative standard curve obtained for all-trans Retinoic Acid (0 – 10 µg/mL) using HPLC, as described in section 4.2.5.

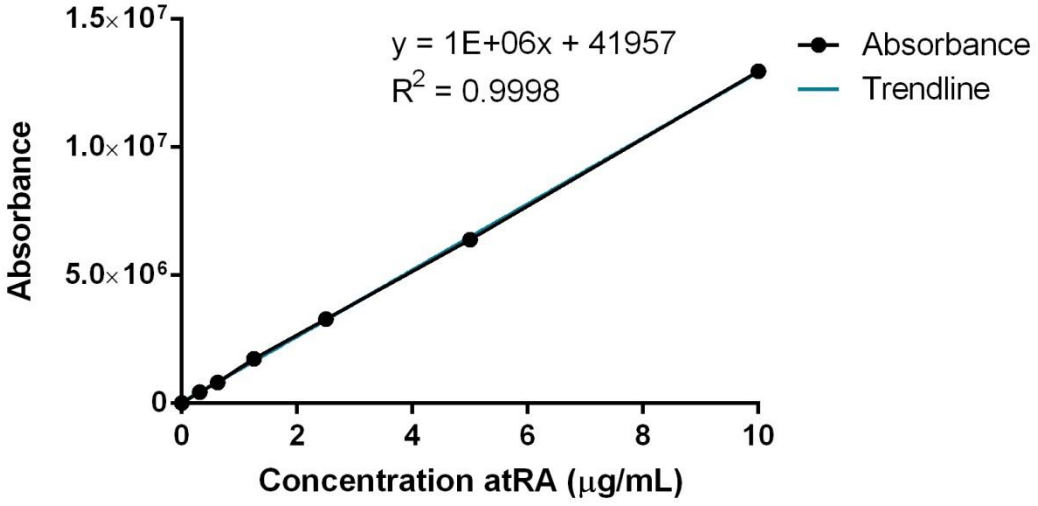

Appendix 3

Appendix 3.1

Supplementary data demonstrating a representative standard curve obtained for IL-6 (0 – 200 pg/mL) using ELISA, as described in section 5.2.2.5.

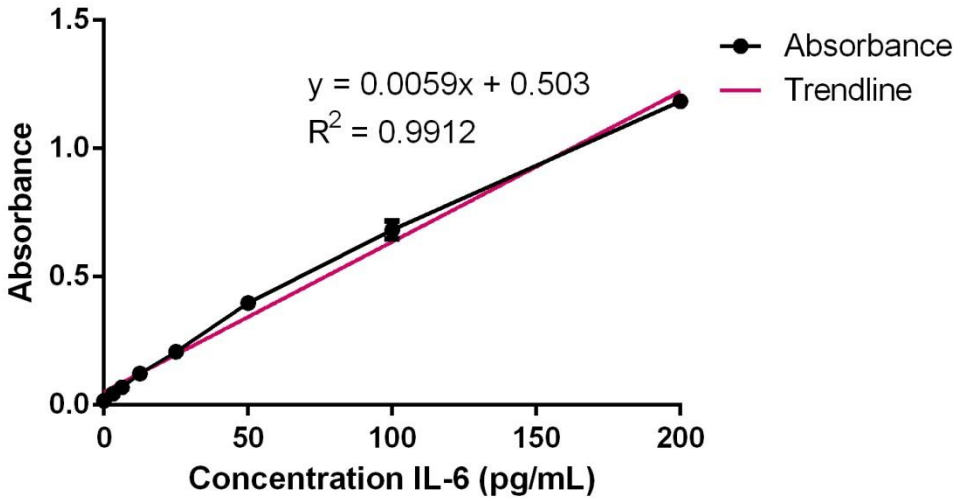

Appendix 3.2

Supplementary data demonstrating a representative standard curve obtained for IL-8 (0 – 250 pg/mL) using ELISA, as described in section 5.2.2.5.

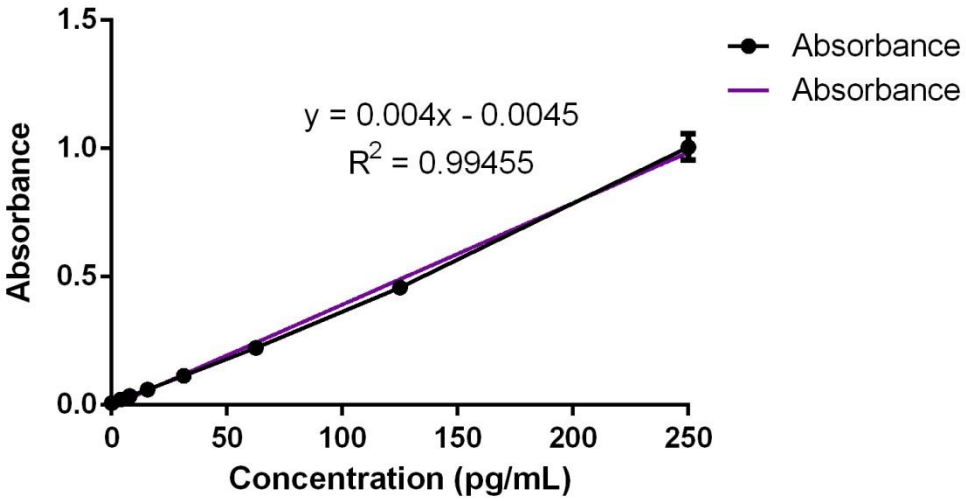

References

[1] R.G. Breeze, E.B. Wheeldon, The Cells of the Pulmonary Airways, Am. Rev. Respir. Dis. 115 (1977). http://www.atsjournals.org/doi/abs/10.1164/arrd.1977.116.4.705#.VYwTEflViko (accessed June 25, 2015).

[2] C. Kleinstreuer, Z. Zhang, J.F. Donohue, Targeted drug-aerosol delivery in the human respiratory system., Annu. Rev. Biomed. Eng. 10 (2008) 195–220. doi:10.1146/annurev.bioeng.10.061807.160544.

[3] P.-R. Burgel, The role of small airways in obstructive airway diseases., Eur. Respir. Rev. 20 (2011) 23–33. doi:10.1183/09059180.00010410.

[4] D.A. Knight, S.T. Holgate, The airway epithelium: Structural and functional properties in health and disease, Respirology. 8 (2003) 432–446. doi:10.1046/j.1440-1843.2003.00493.x.

[5] A. Tam, S. Wadsworth, D. Dorscheid, S.F.P. Man, D.D. Sin, The airway epithelium: more than just a structural barrier, Ther. Adv. Respir. Dis. 5 (2011) 255–273. doi:10.1177/1753465810396539.

[6] S.I. Rennard, D.J. Romberger, J.H. Sisson, S.G. Von Essen, I. Rubinstein, R.A. Robbins, J.R. Spurzem, Airway Epithelial Cells: Functional Roles in Airway Disease, Am. J. Respir. Crit. Care Med. 150 (1994) S27–S30. doi:10.1164/ajrccm/150.5_Pt_2.S27.

[7] D.F. Rogers, The airway goblet cell, Int. J. Biochem. Cell Biol. 35 (2003) 1–6. doi:10.1016/S1357-2725(02)00083-3.

[8] M.J. Evans, C.G. Plopper, The Role of Basal Cells in Adhesion of Columnar Epithelium to Airway Basement Membrane, Am. Rev. Respir. Dis. 138 (1988) 481–483. doi:10.1164/ajrccm/138.2.481.

[9] M. Kaliner, Z. Marom, C. Patow, J. Shelhamer, Human respiratory mucus, J. Allergy Clin. Immunol. 73 (1984) 318–323. doi:10.1016/0091-6749(84)90403-2.

[10] D. Gras, P. Chanez, I. Vachier, A. Petit, A. Bourdin, Bronchial epithelium as a target for innovative treatments in asthma, Pharmacol. Ther. 140 (2013) 290–305. doi:10.1016/j.pharmthera.2013.07.008.

[11] S.H. Randell, Airway Epithelial Stem Cells and the Pathophysiology of Chronic Obstructive Pulmonary Disease, Proc. Am. Thorac. Soc. 3 (2006) 718–725. doi:10.1513/pats.200605-117SF.

[12] J.D. Crapo, B.E. Barry, P. Gehr, M. Bachofen, E.R. Weibel, Cell number and cell characteristics of the normal human lung., Am. Rev. Respir. Dis. 126 (1982) 332–337.

[13] S.A. Rooney, S.L. Young, C.R. Mendelson, Molecular and cellular processing of lung surfactant., FASEB J. 8 (1994) 957–67. http://www.ncbi.nlm.nih.gov/pubmed/8088461 (accessed June 25, 2015).

[14] S.G. Klein, J. Hennen, T. Serchi, B. Blömeke, A.C. Gutleb, Potential of coculture in vitro models to study inflammatory and sensitizing effects of particles on the lung, Toxicol. Vitr. 25 (2011) 1516–1534. doi:10.1016/j.tiv.2011.09.006.

[15] WHO | Chronic obstructive pulmonary disease (COPD), (n.d.). http://www.who.int/mediacentre/factsheets/fs315/en/ (accessed June 24, 2015).

[16] Chronic obstructive pulmonary disease in over 16s: diagnosis and management | Guidance and guidelines | NICE, (2010). https://www.nice.org.uk/guidance/cg101/chapter/Working-definition-of-COPD

(accessed July 13, 2017).
[17] M. Hind, M. Maden, Is a regenerative approach viable for the treatment of COPD?, Br. J. Pharmacol. 163 (2011) 106–115. doi:10.1111/j.1476-5381.2011.01246.x.
[18] J. Vestbo, S.S. Hurd, A.G. Agustí, P.W. Jones, C. Vogelmeier, A. Anzueto, P.J. Barnes, L.M. Fabbri, F.J. Martinez, M. Nishimura, R. a. Stockley, D.D. Sin, R. Rodriguez-Roisin, Global strategy for the diagnosis, management, and prevention of chronic obstructive pulmonary disease GOLD executive summary, Am. J. Respir. Crit. Care Med. 187 (2013) 347–365. doi:10.1164/rccm.201204-0596PP.
[19] M.D. Roth, J.E. Connett, J.M. D'Armiento, R.F. Foronjy, P.J. Friedman, J.G. Goldin, T. a. Louis, J.T. Mao, J.R. Muindi, G.T. O'Connor, J.W. Ramsdell, A.L. Ries, S.M. Scharf, N.W. Schluger, F.C. Sciurba, M. a. Skeans, R.E. Walter, C.H. Wendt, R. a. Wise, Feasibility of retinoids for the treatment of emphysema study, Chest. 130 (2006) 1334–1345. doi:10.1378/chest.130.5.1334.
[20] E.P. Ingenito, Medical Therapy for Chronic Obstructive Pulmonary Disease in 2007, Semin. Thorac. Cardiovasc. Surg. 19 (2007) 142–150. doi:10.1053/j.semtcvs.2007.06.003.
[21] A.G.N. Agusti, COPD, a multicomponent disease: implications for management, Respir. Med. 99 (2005) 670–682. doi:10.1016/j.rmed.2004.11.006.
[22] Hurst, J. Vestbo, A. Anzueto, N. Locantore, H. Mullerova, R. Tal-Singer, B. Miller, D. Lomas, A. Agusti, W. MacNee, P. Calverley, S. Rennard, E. Wouters, J. Wedzicha, E.C. Longitudinally, Susceptibility to Exacerbation in Chronic Obstructive Pulmonary Disease., N Engl J Med. 363 (2010) 1128–1138. doi:10.1056/NEJMoa0909883.
[23] S.D. Aaron, Management and prevention of exacerbations of COPD, BMJ. 349 (2014). doi:10.1136/bmj.g5237.
[24] J.C. Hogg, Why does airway inflammation persist after the smoking stops?, Thorax. 61 (2006) 96–7. doi:10.1136/thx.2005.049502.
[25] S.R. Rutgers, D.S. Postma, N.H. ten Hacken, H.F. Kauffman, T.W. van Der Mark, G.H. Koëter, W. Timens, Ongoing airway inflammation in patients with COPD who do not currently smoke, Thorax. 55 (2000) 8–12. http://www.ncbi.nlm.nih.gov/pubmed/10607796 (accessed July 7, 2017).
[26] R. O'Donnell, D. Breen, S. Wilson, R. Djukanovic, Inflammatory cells in the airways in COPD, Thorax. 61 (2006) 448–54. doi:10.1136/thx.2004.024463.
[27] E.J.D. Oudijk, J.W.J. Lammers, L. Koenderman, Systemic inflammation in chronic obstructive pulmonary disease, Eur. Respir. J. Suppl. 46 (2003) 5–13. http://www.ncbi.nlm.nih.gov/pubmed/14621102 (accessed July 7, 2017).
[28] W. MacNee, ABC of chronic obstructive pulmonary disease: Pathology, pathogenesis, and pathophysiology, Br. Med. J. 332 (2006). http://www.bmj.com/content/bmj/332/7551/1202.full.pdf (accessed July 7, 2017).
[29] Chronic obstructive pulmonary disease: Management of chronic obstructive pulmonary disease in adults in primary and secondary care, (2010). http://www.nice.org.uk/guidance/cg101/evidence/cg101-chronic-obstructive-pulmonary-disease-update-full-guideline2 (accessed June 24, 2015).
[30] P. Montuschi, Pharmacological treatment of chronic obstructive pulmonary disease, Int. J. Chron. Obstruct. Pulmon. Dis. 1 (2006) 409–23. http://www.ncbi.nlm.nih.gov/pubmed/18044097 (accessed July 7, 2017).
[31] M. Brenner, R. Yusen, R. McKenna, F. Sciurba, A.F. Gelb, R. Fischel, J. Swain, J.C. Chen, F. Kafie, S.S. Lefrak, Lung Volume Reduction Surgery for Emphysema, Chest. 110 (1996) 205–218. doi:10.1378/chest.110.1.205.

[32] N.E.T.T.R. Group, A Randomized Trial Comparing Lung-Volume–Reduction Surgery with Medical Therapy for Severe Emphysema, N. Engl. J. Med. 348 (2003) 2059–2073. doi:10.1056/NEJMoa030287.
[33] B.F. Meyers, Complications of lung volume reduction surgery., Semin. Thorac. Cardiovasc. Surg. 14 (2002) 399–402. doi:10.1053/stcs.2002.35306.
[34] F.J. Martinez, A. Chang, Surgical therapy for chronic obstructive pulmonary disease., Semin. Respir. Crit. Care Med. 26 (2005) 167–91. doi:10.1055/s-2005-869537.
[35] D. Gompelmann, N. Sarmand, F.J.F. Herth, Interventional pulmonology in chronic obstructive pulmonary disease, Curr. Opin. Pulm. Med. (2017) 261–268. doi:10.1097/MCP.0000000000000373.
[36] F.C. Sciurba, A. Ernst, F.J.F. Herth, C. Strange, G.J. Criner, C.H. Marquette, K.L. Kovitz, R.P. Chiacchierini, J. Goldin, G. McLennan, VENT Study Research Group, A Randomized Study of Endobronchial Valves for Advanced Emphysema, N. Engl. J. Med. 363 (2010) 1233–1244. doi:10.1056/NEJMoa0900928.
[37] P.L. Shah, Z. Zoumot, S. Singh, S.R. Bicknell, E.T. Ross, J. Quiring, N.S. Hopkinson, S. V Kemp, Endobronchial coils for the treatment of severe emphysema with hyperinflation (RESET): a randomised controlled trial, Lancet Respir. Med. 1 (2013) 233–240. doi:10.1016/S2213-2600(13)70047-X.
[38] G.J. Criner, V. Pinto-Plata, C. Strange, M. Dransfield, M. Gotfried, W. Leeds, G. McLennan, Y. Refaely, S. Tewari, M. Krasna, B. Celli, Biologic lung volume reduction in advanced upper lobe emphysema: phase 2 results., Am. J. Respir. Crit. Care Med. 179 (2009) 791–8. doi:10.1164/rccm.200810-1639OC.
[39] J.P. Diaz-Jimenez, A.N. Rodriguez, Interventions in Pulmonary Medicine, Springer Science & Business Media, 2013. https://books.google.com/books?id=tZinlrg0LvIC&pgis=1 (accessed September 14, 2015).
[40] R. Fei, H. Ingerl, M. Kohlhäufl, Lung emphysema treated successfully using volume reduction with lung sealant (AeriSeal®), Open Med. 8 (2013). doi:10.2478/s11536-013-0187-0.
[41] R.F. Falkenstern-Ge, H. Ingerl, M. Kohlhäufl, Severe Emphysema Treated by Endoscopic Bronchial Volume Reduction with Lung Sealant (AeriSeal)., Case Rep. Pulmonol. 2013 (2013) 361391. doi:10.1155/2013/361391.
[42] C.E. Come, M.R. Kramer, M.T. Dransfield, M. Abu-Hijleh, D. Berkowitz, M. Bezzi, S.P. Bhatt, M.B. Boyd, E. Cases, A.C. Chen, C.B. Cooper, J. Flandes, T. Gildea, M. Gotfried, D.K. Hogarth, K. Kolandaivelu, W. Leeds, T. Liesching, N. Marchetti, C. Marquette, R.A. Mularski, V.M. Pinto-Plata, M.A. Pritchett, S. Rafeq, E.R. Rubio, D.-J. Slebos, G. Stratakos, A. Sy, L.W. Tsai, M. Wahidi, J. Walsh, J.M. Wells, P.E. Whitten, R. Yusen, J.J. Zulueta, G.J. Criner, G.R. Washko, A randomised trial of lung sealant versus medical therapy for advanced emphysema, Eur. Respir. J. 46 (2015) 651–62. doi:10.1183/09031936.00205614.
[43] J. Egan, Organ Donation and Transplant Ireland Annual Report 2015, 2015. http://www.hse.ie/eng/about/Who/organdonation/publications/ODTI-2016-Annual-Report.pdf (accessed June 4, 2017).
[44] V. Sueblinvong, D.J. Weiss, Stem cells and cell therapy approaches in lung biology and diseases., Transl. Res. 156 (2010) 188–205. doi:10.1016/j.trsl.2010.06.007.
[45] C. Knoop, a. Haverich, S. Fischer, Immunosuppressive therapy after human lung transplantation, Eur. Respir. J. 23 (2004) 159–171. doi:10.1183/09031936.03.00039203.
[46] C. Clajus, F. Blasi, T. Welte, M. Greer, T. Fuehner, M. Mantero, Therapeutic approach to

respiratory infections in lung transplantation, Pulm. Pharmacol. Ther. 32 (2015) 149–154. doi:10.1016/j.pupt.2014.07.003.
[47] G. Orlando, K.J. Wood, R.J. Stratta, J.J. Yoo, A. Atala, S. Soker, Regenerative medicine and organ transplantation: past, present, and future., Transplantation. 91 (2011) 1310–1317. doi:10.1097/TP.0b013e318219ebb5.
[48] J.L. McQualter, I. Bertoncello, Concise review: Deconstructing the lung to reveal its regenerative potential., Stem Cells. 30 (2012) 811–6. doi:10.1002/stem.1055.
[49] H. Kubo, Concise review: clinical prospects for treating chronic obstructive pulmonary disease with regenerative approaches., Stem Cells Transl. Med. 1 (2012) 627–31. doi:10.5966/sctm.2012-0065.
[50] N. Fujino, H. Kubo, T. Suzuki, C. Ota, A.E. Hegab, M. He, S. Suzuki, T. Suzuki, M. Yamada, T. Kondo, H. Kato, M. Yamaya, Isolation of alveolar epithelial type II progenitor cells from adult human lungs., Lab. Invest. 91 (2011) 363–78. doi:10.1038/labinvest.2010.187.
[51] V.N. Lama, L. Smith, L. Badri, A. Flint, A.-C. Andrei, S. Murray, Z. Wang, H. Liao, G.B. Toews, P.H. Krebsbach, M. Peters-Golden, D.J. Pinsky, F.J. Martinez, V.J. Thannickal, Evidence for tissue-resident mesenchymal stem cells in human adult lung from studies of transplanted allografts., J. Clin. Invest. 117 (2007) 989–96. doi:10.1172/JCI29713.
[52] G. Karoubi, L. Cortes-Dericks, I. Breyer, R.A. Schmid, A.E. Dutly, Identification of mesenchymal stromal cells in human lung parenchyma capable of differentiating into aquaporin 5-expressing cells, Lab. Investig. 89 (2009) 1100–1114. doi:10.1038/labinvest.2009.73.
[53] A.N. Lau, M. Goodwin, C.F. Kim, D.J. Weiss, Stem cells and regenerative medicine in lung biology and diseases., Mol. Ther. 20 (2012) 1116–30. doi:10.1038/mt.2012.37.
[54] D.S. Krause, N.D. Theise, M.I. Collector, O. Henegariu, S. Hwang, R. Gardner, S. Neutzel, S.J. Sharkis, Multi-Organ, Multi-Lineage Engraftment by a Single Bone Marrow-Derived Stem Cell, Cell. 105 (2001) 369–377. doi:10.1016/S0092-8674(01)00328-2.
[55] D.N. Kotton, B.Y. Ma, W. V Cardoso, E.A. Sanderson, R.S. Summer, M.C. Williams, A. Fine, Bone marrow-derived cells as progenitors of lung alveolar epithelium., Development. 128 (2001) 5181–8. http://www.ncbi.nlm.nih.gov/pubmed/11748153 (accessed July 17, 2015).
[56] N. Gupta, X. Su, B. Popov, J.W. Lee, V. Serikov, M.A. Matthay, Intrapulmonary delivery of bone marrow-derived mesenchymal stem cells improves survival and attenuates endotoxin-induced acute lung injury in mice., J. Immunol. 179 (2007) 1855–63. http://www.ncbi.nlm.nih.gov/pubmed/17641052 (accessed July 17, 2015).
[57] H. Yuhgetsu, Y. Ohno, N. Funaguchi, T. Asai, M. Sawada, G. Takemura, S. Minatoguchi, H. Fujiwara, T. Fujiwara, Beneficial effects of autologous bone marrow mononuclear cell transplantation against elastase-induced emphysema in rabbits, Exp. Lung Res. 32 (2006) 413–426. http://informahealthcare.com/doi/abs/10.1080/01902140601047633 (accessed July 17, 2015).
[58] N. Shigemura, M. Okumura, S. Mizuno, Y. Imanishi, A. Matsuyama, H. Shiono, T. Nakamura, Y. Sawa, Lung Tissue Engineering Technique with Adipose Stromal Cells Improves Surgical Outcome for Pulmonary Emphysema, Am. J. Respir. Crit. Care Med. 174 (2006) 1199–1205. doi:10.1164/rccm.200603-406OC.
[59] N. Shigemura, M. Okumura, S. Mizuno, Y. Imanishi, T. Nakamura, Y. Sawa, Autologous transplantation of adipose tissue-derived stromal cells ameliorates pulmonary emphysema., Am. J. Transplant. 6 (2006) 2592–600. doi:10.1111/j.1600-6143.2006.01522.x.

[60] J.L. Wright, M. Cosio, A. Churg, Animal models of chronic obstructive pulmonary disease, Am. J. Physiol. Lung Cell. Mol. Physiol. 295 (2008) 1–15. doi:10.1152/ajplung.90200.2008.
[61] J. Devaney, S. Horie, C. Masterson, S. Elliman, F. Barry, T. O'Brien, G.F. Curley, D. O'Toole, J.G. Laffey, Human mesenchymal stromal cells decrease the severity of acute lung injury induced by E. coli in the rat, Thorax. 70 (2015) 625–635. doi:10.1136/thoraxjnl-2015-206813.
[62] G.F. Curley, M. Contreras, B. Higgins, C. O'Kane, D.F. McAuley, D. O'Toole, J.G. Laffey, Evolution of the Inflammatory and Fibroproliferative Responses during Resolution and Repair after Ventilator-induced Lung Injury in the Rat, Anesthesiology. 115 (2011) 1022–1032. doi:10.1097/ALN.0b013e31823422c9.
[63] G.F. Curley, M. Hayes, B. Ansari, G. Shaw, a. Ryan, F. Barry, T. O'Brien, D. O'Toole, J.G. Laffey, Mesenchymal stem cells enhance recovery and repair following ventilator-induced lung injury in the rat, Thorax. 67 (2012) 496–501. doi:10.1136/thoraxjnl-2011-201059.
[64] Danny F McAuley, Cecelia O'Kane, Repair of Acute Respiratory Distress Syndrome by Stromal Cell Administration (REALIST): NCT03042143, (2017). https://clinicaltrials.gov/ct2/show/study/NCT03042143 (accessed June 4, 2017).
[65] J.G. Wilson, K.D. Liu, H. Zhuo, L. Caballero, M. McMillan, X. Fang, K. Cosgrove, R. Vojnik, C.S. Calfee, J.-W. Lee, A.J. Rogers, J. Levitt, J. Wiener-Kronish, E.K. Bajwa, A. Leavitt, D. McKenna, B.T. Thompson, M.A. Matthay, Mesenchymal stem (stromal) cells for treatment of ARDS: a phase 1 clinical trial, Lancet Respir. Med. 3 (2015) 24–32. doi:10.1016/S2213-2600(14)70291-7.
[66] D.J. Weiss, R. Casaburi, R. Flannery, M. LeRoux-Williams, D.P. Tashkin, A Placebo-Controlled, Randomized Trial of Mesenchymal Stem Cells in COPD, Chest. 143 (2013) 1590. doi:10.1378/chest.12-2094.
[67] X. Liu, Q. Fang, H. Kim, Preclinical Studies of Mesenchymal Stem Cell (MSC) Administration in Chronic Obstructive Pulmonary Disease (COPD): A Systematic Review and Meta-Analysis, PLoS One. 11 (2016). doi:10.1371/journal.pone.0157099.
[68] Y. Moodley, U. Manuelpillai, D.J. Weiss, Cellular therapies for lung disease: A distant horizon, Respirology. 16 (2011) 223–237. doi:10.1111/j.1440-1843.2010.01914.x.
[69] U.M. Fischer, M.T. Harting, F. Jimenez, W.O. Monzon-Posadas, H. Xue, S.I. Savitz, G.A. Laine, C.S. Cox, Jr., Pulmonary passage is a major obstacle for intravenous stem cell delivery: the pulmonary first-pass effect, Stem Cells Dev. 18 (2009) 683–92. doi:10.1089/scd.2008.0253.
[70] D.J. Weiss, I. Bertoncello, Z. Borok, C. Kim, A. Panoskaltsis-Mortari, S. Reynolds, M. Rojas, B. Stripp, D. Warburton, D.J. Prockop, Stem Cells and Cell Therapies in Lung Biology and Lung Diseases, Proc. Am. Thorac. Soc. 8 (2011) 223–72. doi:10.1513/pats.201012-071DW.
[71] Q.-D. Wang, P.-O. Sjöquist, Myocardial regeneration with stem cells: pharmacological possibilities for efficacy enhancement., Pharmacol. Res. 53 (2006) 331–40. doi:10.1016/j.phrs.2006.01.009.
[72] K. Lee, E.A. Silva, D.J. Mooney, Growth factor delivery-based tissue engineering: general approaches and a review of recent developments., J. R. Soc. Interface. 8 (2011) 153–70. doi:10.1098/rsif.2010.0223.
[73] C.J. Kirkpatrick, S. Fuchs, R.E. Unger, Co-culture systems for vascularization — Learning from nature, Adv. Drug Deliv. Rev. 63 (2011) 291–299. doi:10.1016/j.addr.2011.01.009.
[74] R.A.M. Panganiban, R.M. Day, Hepatocyte growth factor in lung repair and pulmonary

fibrosis, Acta Pharmacol. Sin. 32 (2011) 12–20. doi:10.1038/aps.2010.90.
[75] K. Matsumoto, T. Nakamura, Roles of HGF as a pleiotropic factor in organ regeneration., EXS. 65 (1993) 225–49. http://www.ncbi.nlm.nih.gov/pubmed/8422545 (accessed June 6, 2017).
[76] K. Yanagita, K. Matsumoto, K. Sekiguchi, H. Ishibashi, Y. Niho, T. Nakamura, Hepatocyte growth factor may act as a pulmotrophic factor on lung regeneration after acute lung injury., J. Biol. Chem. 268 (1993) 21212–7. http://www.ncbi.nlm.nih.gov/pubmed/8407957 (accessed June 6, 2017).
[77] H. Yamanouchi, J. Fujita, T. Yoshinouchi, S. Hojo, T. Kamei, I. Yamadori, Y. Ohtsuki, N. Ueda, J. Takahara, Measurement of hepatocyte growth factor in serum and bronchoalveolar lavage fluid in patients with pulmonary fibrosis, Respir. Med. 92 (1998) 273–278. doi:10.1016/S0954-6111(98)90108-1.
[78] L. Plantier, S. Marchand-Adam, J. Marchal-Sommé, G. Lesèche, M. Fournier, M. Dehoux, M. Aubier, B. Crestani, Defect of hepatocyte growth factor production by fibroblasts in human pulmonary emphysema, Am. J. Physiol. - Lung Cell. Mol. Physiol. 288 (2005). http://ajplung.physiology.org/content/288/4/L641.long (accessed June 6, 2017).
[79] M. Yaekashiwa, S. Nakayama, K. Ohnuma, T. Sakai, T. Abe, K. Satoh, K. Matsumoto, T. Nakamura, T. Takahashi, T. Nukiwa, Simultaneous or Delayed Administration of Hepatocyte Growth Factor Equally Represses the Fibrotic Changes in Murine Lung Injury Induced by Bleomycin, Am. J. Respir. Crit. Care Med. 156 (1997) 1937–1944. doi:10.1164/ajrccm.156.6.9611057.
[80] M. Dohi, T. Hasegawa, K. Yamamoto, B.C. Marshall, Hepatocyte Growth Factor Attenuates Collagen Accumulation in a Murine Model of Pulmonary Fibrosis, Am. J. Respir. Crit. Care Med. 162 (2000) 2302–2307. doi:10.1164/ajrccm.162.6.9908097.
[81] Y. Sakamaki, K. Matsumoto, S. Mizuno, S. Miyoshi, H. Matsuda, T. Nakamura, Hepatocyte Growth Factor Stimulates Proliferation of Respiratory Epithelial Cells during Postpneumonectomy Compensatory Lung Growth in Mice, Am. J. Respir. Cell Mol. Biol. 26 (2002) 525–533. doi:10.1165/ajrcmb.26.5.4714.
[82] D. Warburton, S. Bellusci, The molecular genetics of lung morphogenesis and injury repair., Paediatr. Respir. Rev. 5 Suppl A (2004) S283-7. http://www.ncbi.nlm.nih.gov/pubmed/14980285 (accessed September 15, 2015).
[83] J.C. Masterson, E.L. Molloy, J.L. Gilbert, N. McCormack, A. Adams, S. O'Dea, Bone morphogenetic protein signalling in airway epithelial cells during regeneration, Cell. Signal. 23 (2011) 398–406. doi:10.1016/j.cellsig.2010.10.010.
[84] M. Weaver, J.M. Yingling, N.R. Dunn, S. Bellusci, B.L. Hogan, Bmp signaling regulates proximal-distal differentiation of endoderm in mouse lung development, Development. 126 (1999). http://dev.biologists.org/content/126/18/4005.long (accessed June 6, 2017).
[85] T.M. Lynn, E.L. Molloy, J.C. Masterson, S.F. Glynn, R.W. Costello, M. V. Avdalovic, E.S. Schelegle, L.A. Miller, D.M. Hyde, S. O'Dea, SMAD Signaling in the Airways of Healthy Rhesus Macaques versus Rhesus Macaques with Asthma Highlights a Relationship Between Inflammation and Bone Morphogenetic Proteins, Am. J. Respir. Cell Mol. Biol. 54 (2016) 562–573. doi:10.1165/rcmb.2015-0210OC.
[86] J.-H. Lee, D.H. Bhang, A. Beede, T.L. Huang, B.R. Stripp, K.D. Bloch, A.J. Wagers, Y.-H. Tseng, S. Ryeom, C.F. Kim, Lung Stem Cell Differentiation in Mice Directed by Endothelial Cells via a BMP4-NFATc1-Thrombospondin-1 Axis, Cell. 156 (2014) 440–455. doi:10.1016/j.cell.2013.12.039.
[87] M. Shiratori, E. Oshika, L.P. Ung, G. Singh, H. Shinozuka, D. Warburton, G.

Michalopoulos, S.L. Katyal, Keratinocyte growth factor and embryonic rat lung morphogenesis., Am. J. Respir. Cell Mol. Biol. 15 (1996) 328–38. doi:10.1165/ajrcmb.15.3.8810636.

[88] M. Post, P. Souza, J. Liu, I. Tseu, J. Wang, M. Kuliszewski, A.K. Tanswell, Keratinocyte growth factor and its receptor are involved in regulating early lung branching, Development. 122 (1996). http://dev.biologists.org/content/122/10/3107?ijkey=5edf692f382399bb1aca6214dac9f688895f9e38&keytype2=tf_ipsecsha (accessed June 6, 2017).

[89] N. Chelly, A. Henrion, C. Pinteur, B. Chailley-Heu, J.R. Bourbon, Role of Keratinocyte Growth Factor in the Control of Surfactant Synthesis by Fetal Lung Mesenchyme, Endocrinology. 142 (2001) 1814–1819. doi:10.1210/endo.142.5.8173.

[90] N. Chelly, O.-B. Mouhieddine-Gueddiche, A.-M. Barlier-Mur, B. Chailley-Heu, J.R. Bourbon, Keratinocyte Growth Factor Enhances Maturation of Fetal Rat Lung Type II Cells, Am. J. Respir. Cell Mol. Biol. 20 (1999) 423–432. doi:10.1165/ajrcmb.20.3.3201.

[91] M. Chedid, J.S. Rubin, K.G. Csaky, S.A. Aaronson, Regulation of keratinocyte growth factor gene expression by interleukin 1., J. Biol. Chem. 269 (1994) 10753–7. http://www.ncbi.nlm.nih.gov/pubmed/7511604 (accessed June 6, 2017).

[92] S.E. McGowan, Retinoids and pulmonary alveolar regeneration: Rationale and therapeutic challenges, Drug Discov. Today Dis. Mech. 3 (2006) 77–84. doi:10.1016/j.ddmec.2006.03.005.

[93] S.E. McGowan, M.M. Doro, S.K. Jackson, Endogenous retinoids increase perinatal elastin gene expression in rat lung fibroblasts and fetal explants, Am J Physiol Lung Cell Mol Physiol. 273 (1997) L410-416. http://ajplung.physiology.org/content/273/2/L410 (accessed July 6, 2015).

[94] S.E. McGowan, C.S. Harvey, S.K. Jackson, Retinoids, retinoic acid receptors, and cytoplasmic retinoid binding proteins in perinatal rat lung fibroblasts, Am J Physiol Lung Cell Mol Physiol. 269 (1995) L463-472. http://ajplung.physiology.org/content/269/4/L463 (accessed July 6, 2015).

[95] M. Hind, J. Corcoran, M. Maden, Alveolar proliferation, retinoid synthesizing enzymes, and endogenous retinoids in the postnatal mouse lung. Different roles for Aldh-1 and Raldh-2., Am. J. Respir. Cell Mol. Biol. 26 (2002) 67–73. doi:10.1165/ajrcmb.26.1.4575.

[96] S. McGowan, S.K. Jackson, M. Jenkins-Moore, H.H. Dai, P. Chambon, J.M. Snyder, Mice bearing deletions of retinoic acid receptors demonstrate reduced lung elastin and alveolar numbers., Am. J. Respir. Cell Mol. Biol. 23 (2000) 162–7. doi:10.1165/ajrcmb.23.2.3904.

[97] G.D. Massaro, D. Massaro, W.Y. Chan, L.B. Clerch, N. Ghyselinck, P. Chambon, R.A. Chandraratna, Retinoic acid receptor-beta: an endogenous inhibitor of the perinatal formation of pulmonary alveoli., Physiol. Genomics. 4 (2000) 51–7. http://www.ncbi.nlm.nih.gov/pubmed/11074013 (accessed July 6, 2015).

[98] G.D. Massaro, D. Massaro, Postnatal treatment with retinoic acid increases the number of pulmonary alveoli in rats, Am J Physiol Lung Cell Mol Physiol. 270 (1996) L305-310. http://ajplung.physiology.org/content/270/2/L305 (accessed July 6, 2015).

[99] M. Hind, a Gilthorpe, S. Stinchcombe, M. Maden, Retinoid induction of alveolar regeneration: from mice to man?, Thorax. 64 (2009) 451–457. doi:10.1136/thx.2008.105437.

[100] T.E. Gray, K. Guzman, C.W. Davis, L.H. Abdullah, P. Nettesheim, Mucociliary differentiation of serially passaged normal human tracheobronchial epithelial cells., Am. J. Respir. Cell Mol. Biol. 14 (1996) 104–112. doi:10.1165/ajrcmb.14.1.8534481.

[101] J.T. Mao, J.G. Goldin, J. Dermand, G. Ibrahim, M.S. Brown, A. Emerick, M.F.M.C. Nitt-gray, D.W. Gjertson, F. Estrada, D.P. Tashkin, M.D. Roth, A Pilot Study of All- trans - Retinoic Acid for the Treatment of Human Emphysema, Crit. Care Med. 165 (2002) 718–723. doi:10.1164/rccm.2106123.
[102] T.H. March, P.Y. Cossey, D.C. Esparza, K.J. Dix, J.D. McDonald, L.E. Bowen, Inhalation administration of all-trans-retinoic acid for treatment of elastase-induced pulmonary emphysema in Fischer 344 rats., Exp. Lung Res. 30 (2004) 383–404. doi:10.1080/01902140490463142.
[103] K. Ishizawa, H. Kubo, M. Yamada, S. Kobayashi, M. Numasaki, S. Ueda, T. Suzuki, H. Sasaki, Bone marrow-derived cells contribute to lung regeneration after elastase-induced pulmonary emphysema, FEBS Lett. 556 (2004) 249–252. doi:10.1016/S0014-5793(03)01399-1.
[104] M. Maden, Retinoids have differing efficacies on alveolar regeneration in a dexamethasone-treated mouse, Am. J. Respir. Cell Mol. Biol. 35 (2006) 260–267. doi:10.1165/rcmb.2006-0029OC.
[105] Y. Nozaki, T. Yamagata, M. Sugiyama, S. Ikoma, K. Kinoshita, M. Funauchi, Anti-inflammatory effect of all-trans-retinoic acid in inflammatory arthritis, Clin. Immunol. 119 (2006) 272–279. doi:10.1016/j.clim.2005.11.012.
[106] J.E. Wolf, Potential anti-inflammatory effects of topical retinoids and retinoid analogues., Adv. Ther. 19 (n.d.) 109–18. http://www.ncbi.nlm.nih.gov/pubmed/12201351 (accessed July 3, 2017).
[107] A. Balato, M. Schiattarella, S. Lembo, M. Mattii, N. Prevete, N. Balato, F. Ayala, Interleukin-1 family members are enhanced in psoriasis and suppressed by vitamin D and retinoic acid, Arch. Dermatol. Res. 305 (2013) 255–262. doi:10.1007/s00403-013-1327-8.
[108] L.J. Ho, L.C. Lin, L.F. Hung, S.J. Wang, C.H. Lee, D.M. Chang, J.H. Lai, T.Y. Tai, Retinoic acid blocks pro-inflammatory cytokine-induced matrix metalloproteinase production by down-regulating JNK-AP-1 signaling in human chondrocytes, Biochem. Pharmacol. 70 (2005) 200–208. doi:10.1016/j.bcp.2005.04.039.
[109] U. Ikeda, D. Wakita, T. Ohkuri, K. Chamoto, H. Kitamura, Y. Iwakura, T. Nishimura, 1α,25-Dihydroxyvitamin D3 and all-trans retinoic acid synergistically inhibit the differentiation and expansion of Th17 cells, Immunol. Lett. 134 (2010) 7–16. doi:10.1016/j.imlet.2010.07.002.
[110] M.H.S.L. Ireland, Summary of Product Characteristics Treclin 1/0.025% w/w Gel, 2017. https://www.hpra.ie/img/uploaded/swedocuments/LicenseSPC_PA1332-043-001_10042017150040.pdf (accessed July 3, 2017).
[111] V. Jenning, S.H. Gohla, Encapsulation of retinoids in solid lipid nanoparticles (SLN), J. Microencapsul. 18 (2001) 149–158. doi:10.1080/02652040010000361.
[112] R. Blomhoff, H.K. Blomhoff, Overview of retinoid metabolism and function., J. Neurobiol. 66 (2006) 606–30. doi:10.1002/neu.20242.
[113] O.S. El Kinawy, S. Petersen, K. Bergt, J. Ulrich, Influence of emulsifiers on the formation and crystallization of solid lipid nanoparticles, Chem. Eng. Technol. 36 (2013) 2174–2178. doi:10.1002/ceat.201300490.
[114] J.E. Nichols, J.A. Niles, J. Cortiella, Design and development of tissue engineered lung: Progress and challenges., Organogenesis. 5 (2009) 57–61. http://www.pubmedcentral.nih.gov/articlerender.fcgi?artid=2710526&tool=pmcentrez&rendertype=abstract (accessed July 1, 2015).
[115] K.Y. Lee, D.J. Mooney, Hydrogels for Tissue Engineering, Chem. Rev. 101 (2001) 1869–

1880. doi:10.1021/cr000108x.
[116] Julian H George - Engineering of Fibrous Scaffolds for use in Regenerative Medicine, (n.d.). http://www.centropede.com/UKSB2006/ePoster/images/background/TE_model (accessed July 1, 2015).
[117] W.H.J. Douglas, G.W. Moorman, R.W. Teel, The formation of histotypic structures from monodisperse fetal rat lung cells cultured on a three-dimensional substrate., In Vitro. 12 (1976) 373–81. doi:10.1007/BF02796315.
[118] W.H.J. Douglas, R.W. Teel, An Organotypic in Vitro Model System for Studying Pulmonary Surfactant Production by Type II Alveolar Pneumonocytes, Am. Rev. Respir. Dis. 113 (1976) 17–23. doi:10.1164/ARRD.1976.113.1.17.
[119] S.K. (Sujata K. Bhatia, Biomaterials for clinical applications, 2nd ed., Springer, 2010. https://books.google.ie/books?id=bXtaX468LRYC&pg=PA115&lpg=PA115&dq=gelfoam+for+use+in+the+lungs&source=bl&ots=kConXmKM1U&sig=KApgBiDw0sBjguknlmwXzcl2xBo&hl=en&sa=X&ved=0ahUKEwiOs9rTr_fUAhXIJcAKHWzkByUQ6AEISDAH#v=onepage&q=gelfoam for use in the lungs&f=f (accessed July 7, 2017).
[120] C.F. Andrade, A.P. Wong, T.K. Waddell, S. Keshavjee, M. Liu, Cell-based tissue engineering for lung regeneration, Am. J. Physiol. - Lung Cell. Mol. Physiol. 292 (2007). doi:10.1152/ajplung.00175.2006.
[121] J. Cortiella, J.E. Nichols, K. Kojima, L.J. Bonassar, P. Dargon, A.K. Roy, M.P. Vacant, J.A. Niles, C.A. Vacanti, Tissue-Engineered Lung: An In Vivo and In Vitro Comparison of Polyglycolic Acid and Pluronic F-127 Hydrogel/Somatic Lung Progenitor Cell Constructs to Support Tissue Growth, Tissue Eng. 12 (2006) 1213–1225.
[122] P. Macchiarini, P. Jungebluth, T. Go, M.A. Asnaghi, L.E. Rees, T.A. Cogan, A. Dodson, J. Martorell, S. Bellini, P.P. Parnigotto, S.C. Dickinson, A.P. Hollander, S. Mantero, M.T. Conconi, M.A. Birchall, Clinical transplantation of a tissue-engineered airway., Lancet. 372 (2008) 2023–30. doi:10.1016/S0140-6736(08)61598-6.
[123] G. Vogel, Karolinska Institute has “lost confidence” in Paolo Macchiarini, says it won’t renew his contract, Science (80-.). (2016). doi:10.1126/science.aae0315.
[124] Macchiarini scandal is a valuable lesson for the Karolinska Institute, Nature. 537 (2016) 137–137. doi:10.1038/537137a.
[125] H.C. Ott, B. Clippinger, C. Conrad, C. Schuetz, I. Pomerantseva, L. Ikonomou, D. Kotton, J.P. Vacanti, Regeneration and orthotopic transplantation of a bioartificial lung., Nat. Med. 16 (2010) 927–33. doi:10.1038/nm.2193.
[126] D. Orlic, J. Kajstura, S. Chimenti, I. Jakoniuk, S.M. Anderson, B. Li, J. Pickel, R. McKay, B. Nadal-Ginard, D.M. Bodine, A. Leri, P. Anversa, Bone marrow cells regenerate infarcted myocardium., Nature. 410 (2001) 701–5. doi:10.1038/35070587.
[127] M.A. Antunes, J.G. Laffey, P. Pelosi, P.R.M. Rocco, Mesenchymal stem cell trials for pulmonary diseases, J. Cell. Biochem. 115 (2014) 1023–1032. doi:10.1002/jcb.24783.
[128] C.L. Hastings, E.T. Roche, E. Ruiz-Hernandez, K. Schenke-Layland, C.J. Walsh, G.P. Duffy, Drug and cell delivery for cardiac regeneration, Adv. Drug Deliv. Rev. 84 (2014) 85–106. doi:10.1016/j.addr.2014.08.006.
[129] Z. Liu, H. Wang, Y. Wang, Q. Lin, A. Yao, F. Cao, D. Li, J. Zhou, C. Duan, Z. Du, Y. Wang, C. Wang, The influence of chitosan hydrogel on stem cell engraftment, survival and homing in the ischemic myocardial microenvironment., Biomaterials. 33 (2012) 3093–106. doi:10.1016/j.biomaterials.2011.12.044.
[130] A.C. Gaffey, M.H. Chen, C.M. Venkataraman, A. Trubelja, C.B. Rodell, P. V Dinh, G. Hung, J.W. MacArthur, R. V Soopan, J.A. Burdick, P. Atluri, Injectable shear-thinning hydrogels used to deliver endothelial progenitor cells, enhance cell engraftment, and improve

ischemic myocardium., J. Thorac. Cardiovasc. Surg. 150 (2015) 1268–1277. doi:10.1016/j.jtcvs.2015.07.035.
[131] T.R. Hoare, D.S. Kohane, Hydrogels in drug delivery: Progress and challenges, Polymer (Guildf). 49 (2008) 1993–2007. doi:10.1016/j.polymer.2008.01.027.
[132] L. Klouda, A.G. Mikos, Thermoresponsive hydrogels in biomedical applications., Eur. J. Pharm. Biopharm. 68 (2008) 34–45. doi:10.1016/j.ejpb.2007.02.025.
[133] A. Chenite, C. Chaput, D. Wang, C. Combes, M.D. Buschmann, C.D. Hoemann, J.C. Leroux, B.L. Atkinson, F. Binette, A. Selmani, Novel injectable neutral solutions of chitosan form biodegradable gels in situ., Biomaterials. 21 (2000) 2155–61. http://www.ncbi.nlm.nih.gov/pubmed/10985488.
[134] C.L. Hastings, H.M. Kelly, M.J. Murphy, F.P. Barry, F.J. O'Brien, G.P. Duffy, Development of a thermoresponsive chitosan gel combined with human mesenchymal stem cells and desferrioxamine as a multimodal pro-angiogenic therapeutic for the treatment of critical limb ischaemia., J. Control. Release. 161 (2012) 73–80. doi:10.1016/j.jconrel.2012.04.033.
[135] Z. Zhang, J. Ni, L. Chen, L. Yu, J. Xu, J. Ding, Biodegradable and thermoreversible PCLA-PEG-PCLA hydrogel as a barrier for prevention of post-operative adhesion., Biomaterials. 32 (2011) 4725–36. doi:10.1016/j.biomaterials.2011.03.046.
[136] N.L. Elstad, K.D. Fowers, OncoGel (ReGel/paclitaxel)--clinical applications for a novel paclitaxel delivery system., Adv. Drug Deliv. Rev. 61 (2009) 785–94. doi:10.1016/j.addr.2009.04.010.
[137] M.S. Shive, C.D. Hoemann, A. Restrepo, M.B. Hurtig, N. Duval, P. Ranger, W. Stanish, M.D. Buschmann, BST-CarGel: In Situ ChondroInduction for Cartilage Repair, Oper. Tech. Orthop. 16 (2006) 271–278. doi:10.1053/j.oto.2006.08.001.
[138] J. Shalhoub, A. Thapar, A.H. Davies, The use of reverse thermosensitive polymer (LeGoo) for temporary vessel occlusion in clampless peripheral vascular surgery., Vasc. Endovascular Surg. 45 (2011) 422–5. doi:10.1177/1538574411405546.
[139] S.J. Buwalda, K.W.M. Boere, P.J. Dijkstra, J. Feijen, T. Vermonden, W.E. Hennink, Hydrogels in a historical perspective: From simple networks to smart materials, J. Control. Release. 190 (2014) 254–273. doi:10.1016/j.jconrel.2014.03.052.
[140] O. Wichterle, D. Lim, Hydrophilic Gels for Biological Use, Nature. 185 (1960) 117–118. http://dx.doi.org/10.1038/185117a0.
[141] J. Kopecek, Hydrogels : From Soft Contact Lenses and Implants to, J. Polym. Sci. 47 (2009) 5929–5946. doi:10.1002/pola.
[142] I.R. Schmolka, Artificial skin. I. Preparation and properties of pluronic F-127 gels for treatment of burns., J. Biomed. Mater. Res. 6 (1972) 571–82. doi:10.1002/jbm.820060609.
[143] R.M. Nalbandian, R.L. Henry, H.S. Wilks, Artificial skin. II. Pluronic F-127 Silver nitrate or silver lactate gel in the treatment of thermal burns., J. Biomed. Mater. Res. 6 (1972) 583–90. doi:10.1002/jbm.820060610.
[144] S.D. Desai, J. Blanchard, In vitro evaluation of pluronic F127-based controlled-release ocular delivery systems for pilocarpine., J. Pharm. Sci. 87 (1998) 226–30. doi:10.1021/js970090e.
[145] A.. El-Kamel, In vitro and in vivo evaluation of Pluronic F127-based ocular delivery system for timolol maleate, Int. J. Pharm. 241 (2002) 47–55. doi:10.1016/S0378-5173(02)00234-X.
[146] J. Yun Chang, Y.-K. Oh, H. Soo Kong, E. Jung Kim, D. Deuk Jang, K. Taek Nam, C.-K. Kim, Prolonged antifungal effects of clotrimazole-containing mucoadhesive thermosensitive

gels on vaginitis, J. Control. Release. 82 (2002) 39–50. doi:10.1016/S0168-3659(02)00086-X.
[147] M. Katakam, W.R. Ravis, A.K. Banga, Controlled release of human growth hormone in rats following parenteral administration of poloxamer gels, J. Control. Release. 49 (1997) 21–26. doi:10.1016/S0168-3659(97)01648-9.
[148] E. Ruel-Gariépy, J.-C. Leroux, In situ-forming hydrogels--review of temperature-sensitive systems., Eur. J. Pharm. Biopharm. 58 (2004) 409–26. doi:10.1016/j.ejpb.2004.03.019.
[149] S. Supper, N. Anton, N. Seidel, M. Riemenschnitter, C. Curdy, T. Vandamme, Thermosensitive chitosan/glycerophosphate-based hydrogel and its derivatives in pharmaceutical and biomedical applications., Expert Opin. Drug Deliv. 11 (2014) 249–67. doi:10.1517/17425247.2014.867326.
[150] A. Chenite, M. Buschmann, D. Wang, C. Chaput, N. Kandani, Rheological characterisation of thermogelling chitosan / glycerol-phosphate solutions, Carbohydr. Polym. 46 (2001) 39–47.
[151] E. Ruel-Gariépy, A. Chenite, C. Chaput, S. Guirguis, J.-C. Leroux, Characterization of thermosensitive chitosan gels for the sustained delivery of drugs, Int. J. Pharm. 203 (2000) 89–98. doi:10.1016/S0378-5173(00)00428-2.
[152] H.Y. Zhou, X.G. Chen, M. Kong, C.S. Liu, D.S. Cha, J.F. Kennedy, Effect of molecular weight and degree of chitosan deacetylation on the preparation and characteristics of chitosan thermosensitive hydrogel as a delivery system, Carbohydr. Polym. 73 (2008) 265–273. doi:10.1016/j.carbpol.2007.11.026.
[153] Y. Peng, J. Li, J. Li, Y. Fei, J. Dong, W. Pan, Optimization of thermosensitive chitosan hydrogels for the sustained delivery of venlafaxine hydrochloride., Int. J. Pharm. 441 (2013) 482–90. doi:10.1016/j.ijpharm.2012.11.005.
[154] E. Ruel-Gariépy, M. Shive, A. Bichara, M. Berrada, D. Le Garrec, A. Chenite, J.-C. Leroux, A thermosensitive chitosan-based hydrogel for the local delivery of paclitaxel, Eur. J. Pharm. Biopharm. 57 (2004) 53–63. doi:10.1016/S0939-6411(03)00095-X.
[155] H.D. Han, C.K. Song, Y.S. Park, K.H. Noh, J.H. Kim, T. Hwang, T.W. Kim, B.C. Shin, A chitosan hydrogel-based cancer drug delivery system exhibits synergistic antitumor effects by combining with a vaccinia viral vaccine., Int. J. Pharm. 350 (2008) 27–34. doi:10.1016/j.ijpharm.2007.08.014.
[156] E. Khodaverdi, M. Tafaghodi, F. Ganji, K. Abnoos, H. Naghizadeh, In vitro insulin release from thermosensitive chitosan hydrogel., AAPS PharmSciTech. 13 (2012) 460–6. doi:10.1208/s12249-012-9764-9.
[157] Y. Tang, X. Wang, Y. Li, M. Lei, Y. Du, J.F. Kennedy, C.J. Knill, Production and characterisation of novel injectable chitosan/methylcellulose/salt blend hydrogels with potential application as tissue engineering scaffolds, Carbohydr. Polym. 82 (2010) 833–841. doi:10.1016/j.carbpol.2010.06.003.
[158] M.C. Tate, D. a Shear, S.W. Hoffman, D.G. Stein, M.C. LaPlaca, Biocompatibility of methylcellulose-based constructs designed for intracerebral gelation following experimental traumatic brain injury., Biomaterials. 22 (2001) 1113–23. http://www.ncbi.nlm.nih.gov/pubmed/11352091.
[159] D. Gupta, C.H. Tator, M.S. Shoichet, Fast-gelling injectable blend of hyaluronan and methylcellulose for intrathecal, localized delivery to the injured spinal cord., Biomaterials. 27 (2006) 2370–9. doi:10.1016/j.biomaterials.2005.11.015.
[160] C.C. Huang, Z.X. Liao, D.Y. Chen, C.W. Hsiao, Y. Chang, H.W. Sung, Injectable cell constructs fabricated via culture on a thermoresponsive methylcellulose hydrogel system for the treatment of ischemic diseases, Adv. Healthc. Mater. 3 (2014) 1133–

1148. doi:10.1002/adhm.201300605.
[161] S. Thirumala, J. Gimble, R. Devireddy, Methylcellulose Based Thermally Reversible Hydrogel System for Tissue Engineering Applications, Cells. 2 (2013) 460–475. doi:10.3390/cells2030460.
[162] D. Wallace, Collagen gel systems for sustained delivery and tissue engineering, Adv. Drug Deliv. Rev. 55 (2003) 1631–1649. doi:10.1016/j.addr.2003.08.004.
[163] L. Wang, J.P. Stegemann, Thermogelling chitosan and collagen composite hydrogels initiated with beta-glycerophosphate for bone tissue engineering., Biomaterials. 31 (2010) 3976–85. doi:10.1016/j.biomaterials.2010.01.131.
[164] F. O'Brien, Influence of freezing rate on pore structure in freeze-dried collagen-GAG scaffolds, Biomaterials. 25 (2004) 1077–1086. doi:10.1016/S0142-9612(03)00630-6.
[165] G.P. Duffy, T. Ahsan, T. O'Brien, F. Barry, R.M. Nerem, Bone marrow-derived mesenchymal stem cells promote angiogenic processes in a time- and dose-dependent manner in vitro., Tissue Eng. Part A. 15 (2009) 2459–70. doi:10.1089/ten.TEA.2008.0341.
[166] C. of Europe, European Pharmacopoeia, 5.0, Strasbourg, 2005.
[167] M.R. Lamprecht, D.M. Sabatini, A.E. Carpenter, CellProfiler: Free, versatile software for automated biological image analysis, Biotechniques. 42 (2007) 71–75. doi:10.2144/000112257.
[168] J. Schindelin, I. Arganda-Carreras, E. Frise, V. Kaynig, M. Longair, T. Pietzsch, S. Preibisch, C. Rueden, S. Saalfeld, B. Schmid, J.-Y. Tinevez, D.J. White, V. Hartenstein, K. Eliceiri, P. Tomancak, A. Cardona, Fiji: an open-source platform for biological-image analysis., Nat. Methods. 9 (2012) 676–82. doi:10.1038/nmeth.2019.
[169] K. Bramley, M.A. Pisani, T.E. Murphy, K.L. Araujo, R.J. Homer, J.T. Puchalski, Endobronchial Ultrasound-Guided Cautery-Assisted Transbronchial Forceps Biopsies: Safety and Sensitivity Relative to Transbronchial Needle Aspiration, Ann. Thorac. Surg. 101 (2016) 1870–1876. doi:10.1016/j.athoracsur.2015.11.051.
[170] T. Nilsen, M. Hermann, C.S. Eriksen, H. Dagfinrud, P. Mowinckel, I. Kjeken, Grip force and pinch grip in an adult population: Reference values and factors associated with grip force, Scand. J. Occup. Ther. 19 (2012) 288–296. doi:10.3109/11038128.2011.553687.
[171] W. Rungseevijitprapa, R. Bodmeier, Injectability of biodegradable in situ forming microparticle systems (ISM), Eur. J. Pharm. Sci. 36 (2009) 524–531. doi:10.1016/j.ejps.2008.12.003.
[172] M.P. Lutolf, Biomaterials: Spotlight on hydrogels., Nat. Mater. 8 (2009) 451–3. doi:10.1038/nmat2458.
[173] E.T. Roche, C.L. Hastings, S.A. Lewin, D.E. Shvartsman, Y. Brudno, N. V Vasilyev, F.J. O'Brien, C.J. Walsh, G.P. Duffy, D.J. Mooney, Comparison of biomaterial delivery vehicles for improving acute retention of stem cells in the infarcted heart., Biomaterials. 35 (2014) 6850–8. doi:10.1016/j.biomaterials.2014.04.114.
[174] B.A. Aguado, W. Mulyasasmita, J. Su, K.J. Lampe, S.C. Heilshorn, Improving viability of stem cells during syringe needle flow through the design of hydrogel cell carriers., Tissue Eng. Part A. 18 (2012) 806–15. doi:10.1089/ten.TEA.2011.0391.
[175] D.W. Hutmacher, Scaffolds in tissue engineering bone and cartilage, Biomaterials. 21 (2000) 2529–2543. http://158.110.32.35/download/CURCIO/Hurtmacher-BIO-2000.pdf (accessed June 22, 2017).
[176] L.E. Freed, G. Vunjak-Novakovic, R.J. Biron, D.B. Eagles, D.C. Lesnoy, S.K. Barlow, R. Langer, Biodegradable Polymer Scaffolds for Tissue Engineering, Nat. Biotechnol. 12 (1994) 689–693. doi:10.1038/nbt0794-689.

[177] F.J. O'Brien, Biomaterials & scaffolds for tissue engineering, Mater. Today. 14 (2011) 88–95. doi:10.1016/S1369-7021(11)70058-X.
[178] B. Dhandayuthapani, Y. Yoshida, T. Maekawa, D.S. Kumar, Polymeric Scaffolds in Tissue Engineering Application: A Review, Int. J. Polym. Sci. 2011 (2011) 1–19. doi:10.1155/2011/290602.
[179] B.P. Chan, K.W. Leong, Scaffolding in tissue engineering: general approaches and tissue-specific considerations., Eur. Spine J. 17 (2008) 467–79. doi:10.1007/s00586-008-0745-3.
[180] J.A. Burdick, R.L. Mauck, S. Gerecht, To Serve and Protect: Hydrogels to Improve Stem Cell-Based Therapies., Cell Stem Cell. 18 (2016) 13–5. doi:10.1016/j.stem.2015.12.004.
[181] Y. Xu, L. Li, Thermoreversible and salt-sensitive turbidity of methylcellulose in aqueous solution, Polymer (Guildf). 46 (2005) 7410–7417. doi:10.1016/j.polymer.2005.05.128.
[182] Y. Xu, C. Wang, K.C. Tam, L. Li, Salt-assisted and salt-suppressed sol-gel transitions of methylcellulose in water., Langmuir. 20 (2004) 646–52. http://www.ncbi.nlm.nih.gov/pubmed/15773087.
[183] K. Kobayashi, C. Huang, T.P. Lodge, Thermoreversible Gelation of Aqueous Methylcellulose Solutions, Macromolecules. 32 (1999) 7070–7077. doi:10.1021/ma990242n.
[184] K. Chen, A.N. Baker, S. Vyazovkin, Concentration Effect on Temperature Dependence of Gelation Rate in Aqueous Solutions of Methylcellulose, Macromol. Chem. Phys. 210 (2009) 211–216. doi:10.1002/macp.200800518.
[185] Y.-L. Yang, L.M. Leone, L.J. Kaufman, Elastic moduli of collagen gels can be predicted from two-dimensional confocal microscopy., Biophys. J. 97 (2009) 2051–60. doi:10.1016/j.bpj.2009.07.035.
[186] C. Helary, I. Bataille, A. Abed, C. Illoul, A. Anglo, L. Louedec, D. Letourneur, A. Meddahi-Pellé, M.M. Giraud-Guille, Concentrated collagen hydrogels as dermal substitutes., Biomaterials. 31 (2010) 481–90. doi:10.1016/j.biomaterials.2009.09.073.
[187] W. Friess, Collagen--biomaterial for drug delivery., Eur. J. Pharm. Biopharm. 45 (1998) 113–36. http://www.ncbi.nlm.nih.gov/pubmed/9704909.
[188] Y.-F. Tang, Y.-M. Du, X.-W. Hu, X.-W. Shi, J.F. Kennedy, Rheological characterisation of a novel thermosensitive chitosan/poly(vinyl alcohol) blend hydrogel, Carbohydr. Polym. 67 (2007) 491–499. doi:10.1016/j.carbpol.2006.06.015.
[189] K. Edsman, J. Carlfors, R. Petersson, Rheological evaluation of poloxamer as an in situ gel for ophthalmic use, Eur. J. Pharm. Sci. 6 (1998) 105–112. doi:10.1016/S0928-0987(97)00075-4.
[190] A.P. Nowak, V. Breedveld, L. Pakstis, B. Ozbas, D.J. Pine, D. Pochan, T.J. Deming, Rapidly recovering hydrogel scaffolds from self-assembling diblock copolypeptide amphiphiles, Nature. 417 (2002) 424–428. doi:10.1038/417424a.
[191] H.-R. Lin, K.. Sung, Carbopol/pluronic phase change solutions for ophthalmic drug delivery, J. Control. Release. 69 (2000) 379–388. doi:10.1016/S0168-3659(00)00329-1.
[192] B. Jeong, S.W. Kim, Y.H. Bae, Thermosensitive sol–gel reversible hydrogels, Adv. Drug Deliv. Rev. 54 (2002) 37–51. doi:10.1016/S0169-409X(01)00242-3.
[193] H.K. Kleinman, R.J. Klebe, G.R. Martin, Role of collagenous matrices in the adhesion and growth of cells., J. Cell Biol. 88 (1981) 473–85. http://www.pubmedcentral.nih.gov/articlerender.fcgi?artid=2112752&tool=pmcentrez&rendertype=abstract (accessed May 6, 2016).
[194] M. Dominici, K. Le Blanc, I. Mueller, I. Slaper-Cortenbach, F. Marini, D. Krause, R. Deans, A. Keating, D. Prockop, E. Horwitz, Minimal criteria for defining multipotent

mesenchymal stromal cells. The International Society for Cellular Therapy position statement., Cytotherapy. 8 (2006) 315–7. doi:10.1080/14653240600855905.
[195] C. Sanina, J.M. Hare, Mesenchymal Stem Cells as a Biological Drug for Heart Disease: Where Are We With Cardiac Cell-Based Therapy?, Circ. Res. 117 (2015) 229–33. doi:10.1161/CIRCRESAHA.117.306306.
[196] D.W. Lee, W.S. Choi, M.W. Byun, H.J. Park, Y.-M. Yu, C.M. Lee, Effect of gamma-irradiation on degradation of alginate., J. Agric. Food Chem. 51 (2003) 4819–4823. doi:10.1021/jf021053y.
[197] J.M. Wasikiewicz, F. Yoshii, N. Nagasawa, R.A. Wach, H. Mitomo, Degradation of chitosan and sodium alginate by gamma radiation, sonochemical and ultraviolet methods, Radiat. Phys. Chem. 73 (2005) 287–295. doi:10.1016/j.radphyschem.2004.09.021.
[198] J. Zhu, R.E. Marchant, Design properties of hydrogel tissue-engineering scaffolds, Expert Rev. Med. Devices. 8 (2011) 607–26. doi:10.1586/erd.11.27.
[199] A. Gandhi, A. Paul, S.O. Sen, K.K. Sen, Studies on thermoresponsive polymers: Phase behaviour, drug delivery and biomedical applications, Asian J. Pharm. Sci. 10 (2015) 99–107. doi:10.1016/j.ajps.2014.08.010.
[200] Y. Qiu, K. Park, Environment-sensitive hydrogels for drug delivery, Adv. Drug Deliv. Rev. 53 (2001) 321–339. doi:10.1016/S0169-409X(01)00203-4.
[201] N. Bertrand, J.G. Fleischer, K.M. Wasan, J.-C. Leroux, Pharmacokinetics and biodistribution of N-isopropylacrylamide copolymers for the design of pH-sensitive liposomes, Biomaterials. 30 (2009) 2598–2605. doi:10.1016/j.biomaterials.2008.12.082.
[202] L.E. Bromberg, E.S. Ron, Temperature - responsive gels and thermogelling polymer matrices for protein and peptide delivery, Adv. Drug Deliv. Rev. 31 (1998) 197–221. doi:10.1016/S0169-409X(97)00121-X.
[203] J. Huang, C.L. Hastings, G.P. Duffy, H.M. Kelly, J. Raeburn, D.J. Adams, A. Heise, Supramolecular hydrogels with reverse thermal gelation properties from (oligo)tyrosine containing block copolymers., Biomacromolecules. 14 (2013) 200–206. doi:10.1021/bm301629f.
[204] M.J. Webber, E.A. Appel, E.W. Meijer, R. Langer, Supramolecular biomaterials, Nat. Mater. 15 (2015) 13–26. doi:10.1038/nmat4474.
[205] C.-Y. Yang, B. Song, Y. Ao, A.P. Nowak, R.B. Abelowitz, R.A. Korsak, L.A. Havton, T.J. Deming, M. V. Sofroniew, Biocompatibility of amphiphilic diblock copolypeptide hydrogels in the central nervous system, Biomaterials. 30 (2009) 2881–2898. doi:10.1016/j.biomaterials.2009.01.056.
[206] H.R. Kricheldorf, Polypeptides and 100 Years of Chemistry of α-Amino Acid N-Carboxyanhydrides, Angew. Chemie Int. Ed. 45 (2006) 5752–5784. doi:10.1002/anie.200600693.
[207] M. Byrne, R. Murphy, A. Kapetanakis, J. Ramsey, S.-A. Cryan, A. Heise, Star-Shaped Polypeptides: Synthesis and Opportunities for Delivery of Therapeutics, Macromol. Rapid Commun. 36 (2015) 1862–1876. doi:10.1002/marc.201500300.
[208] J. Huang, A. Heise, A. Kapetanakis, S. Roche, R. O'Connor, C. Kerskens, A. Heise, D.F. Brougham, J.S. Shin, J.S. Suh, J. Cheon, K. Kataoka, I. Luzinov, S. Minko, Stimuli responsive synthetic polypeptides derived from N-carboxyanhydride (NCA) polymerisation, Chem. Soc. Rev. 42 (2013) 7373. doi:10.1039/c3cs60063g.
[209] M. Byrne, D. Victory, A. Hibbitts, M. Lanigan, A. Heise, S.-A. Cryan, C.Y. Yeh, P.S. Lai, J. Cheng, Molecular weight and architectural dependence of well-defined star-shaped poly(lysine) as a gene delivery vector, Biomater. Sci. 1 (2013) 1223.

doi:10.1039/c3bm60123d.
[210] R. Murphy, T. Borase, C. Payne, J. O'Dwyer, S.-A. Cryan, A. Heise, L. Cubero-Ponce, M.S. Hahn, X.Z. Zhang, Hydrogels from amphiphilic star block copolypeptides, RSC Adv. 6 (2016) 23370–23376. doi:10.1039/C6RA01190J.
[211] M. Byrne, P.D. Thornton, S.-A. Cryan, A. Heise, Star polypeptides by NCA polymerisation from dendritic initiators: synthesis and enzyme controlled payload release, Polym. Chem. 3 (2012) 2825. doi:10.1039/c2py20327h.
[212] K. Wang, H.-Q. Dong, H.-Y. Wen, M. Xu, C. Li, Y.-Y. Li, H.N. Jones, D.-L. Shi, X.-Z. Zhang, Novel Vesicles Self-Assembled From Amphiphilic Star-Armed PEG/Polypeptide Hybrid Copolymers for Drug Delivery, Macromol. Biosci. 11 (2011) 65–71. doi:10.1002/mabi.201000247.
[213] Y. Yan, D. Wei, J. Li, J. Zheng, G. Shi, W. Luo, Y. Pan, J. Wang, L. Zhang, X. He, D. Liu, A poly(l-lysine)-based hydrophilic star block co-polymer as a protein nanocarrier with facile encapsulation and pH-responsive release, Acta Biomater. 8 (2012) 2113–2120. doi:10.1016/j.actbio.2012.02.016.
[214] L.Y. Qiu, R.J. Wang, C. Zheng, Y. Jin, L.Q. Jin, β-cyclodextrin-centered star-shaped amphiphilic polymers for doxorubicin delivery, Nanomedicine. 5 (2010) 193–208. doi:10.2217/nnm.09.108.
[215] T.K. Georgiou, Star polymers for gene delivery, Polym. Int. 63 (2014) 1130–1133. doi:10.1002/pi.4718.
[216] Y. Zhang, Y. Wang, C. Zhang, J. Wang, D. Pan, J. Liu, F. Feng, Targeted Gene Delivery to Macrophages by Biodegradable Star-Shaped Polymers, ACS Appl. Mater. Interfaces. 8 (2016) 3719–3724. doi:10.1021/acsami.5b08119.
[217] D. Ma, Y. Zhao, X.-Y. Zhou, Q.-M. Lin, Y. Zhang, J.-T. Lin, W. Xue, Photoenhanced Gene Transfection by a Star-Shaped Polymer Consisting of a Porphyrin Core and Poly(L -lysine) Dendron Arms, Macromol. Biosci. 13 (2013) 1221–1227. doi:10.1002/mabi.201300139.
[218] Y. Shen, S. Zhang, Y. Wan, W. Fu, Z. Li, Hydrogels assembled from star-shaped polypeptides with a dendrimer as the core, Soft Matter. 11 (2015) 2945–51. doi:10.1039/c5sm00083a.
[219] P.D. Thornton, S.M.R. Billah, N.R. Cameron, Enzyme-degradable self-assembled hydrogels from polyalanine-modified poly(ethylene glycol) star polymers, Macromol. Rapid Commun. 34 (2013) 257–262. doi:10.1002/marc.201200649.
[220] E. Abbasi, S.F. Aval, A. Akbarzadeh, M. Milani, H.T. Nasrabadi, S.W. Joo, Y. Hanifehpour, K. Nejati-Koshki, R. Pashaei-Asl, Dendrimers: synthesis, applications, and properties, Nanoscale Res. Lett. 9 (2014) 247. doi:10.1186/1556-276X-9-247.
[221] S.R. Raghavan, B.H. Cipriano, Gel Formation: Phase Diagrams Using Tabletop Rheology and Calorimetry, in: Mol. Gels, Springer-Verlag, Berlin/Heidelberg, 2006: pp. 241–252. doi:10.1007/1-4020-3689-2_9.
[222] V.S. Rudraraju, C.M. Wyandt, Rheological characterization of Microcrystalline Cellulose/Sodiumcarboxymethyl cellulose hydrogels using a controlled stress rheometer: part I, Int. J. Pharm. 292 (2005) 53–61. doi:10.1016/j.ijpharm.2004.10.011.
[223] M.P. Lutolf, J.A. Hubbell, Synthetic biomaterials as instructive extracellular microenvironments for morphogenesis in tissue engineering, Nat. Biotechnol. 23 (2005) 47–55. doi:10.1038/nbt1055.
[224] G.J. Lesser, G.D. Rose, Hydrophobicity of amino acid subgroups in proteins, Proteins Struct. Funct. Genet. 8 (1990) 6–13. doi:10.1002/prot.340080104.
[225] R. V. Rughani, D.A. Salick, M.S. Lamm, T. Yucel, D.J. Pochan, J.P. Schneider, Folding, Self-

Assembly, and Bulk Material Properties of a *De Novo* Designed Three-Stranded β-Sheet Hydrogel, Biomacromolecules. 10 (2009) 1295–1304. doi:10.1021/bm900113z.
[226] E.N. Baker, R.E. Hubbard, Hydrogen bonding in globular proteins, Prog. Biophys. Mol. Biol. 44 (1984) 97–179. doi:10.1016/0079-6107(84)90007-5.
[227] † Andrew P. Nowak, ‡ Victor Breedveld, § and David J. Pine, † Timothy J. Deming*, A.P. Nowak, V. Breedveld, D.J. Pine, T.J. Deming, Unusual Salt Stability in Highly Charged Diblock Co-polypeptide Hydrogels, J. Am. Chem. Soc. 125 (2003) 15666–15670. doi:10.1021/JA0381050.
[228] Darrin J. Pochan, A. Lisa Pakstis, B. Ozbas, A.P.N. And, T.J. Deming, SANS and Cryo-TEM Study of Self-Assembled Diblock Copolypeptide Hydrogels with Rich Nano- through Microscale Morphology, Macromolecules. 35 (2002) 5358–5360. doi:10.1021/MA025526D.
[229] T.J. Deming, R. Cromartie, D.A. Gabriel, B. Senger, J.-F. Stoltz, P. Schaaf, J.-C. Voegel, C. Picart, Polypeptide hydrogels via a unique assembly mechanism, Soft Matter. 1 (2005) 28. doi:10.1039/b500307e.
[230] International Organisation for Standardisation, ISO 10993-5: Biological evaluation of medical devices. Part 5: Tests for in vitro cytotoxicity, (2009) 34. https://www.iso.org/standard/36406.html (accessed July 5, 2017).
[231] R. Duncan, L. Izzo, Dendrimer biocompatibility and toxicity, Adv. Drug Deliv. Rev. 57 (2005) 2215–2237. doi:10.1016/j.addr.2005.09.019.
[232] K. Jain, P. Kesharwani, U. Gupta, N.K. Jain, Dendrimer toxicity: Let's meet the challenge, Int. J. Pharm. 394 (2010) 122–142. doi:10.1016/j.ijpharm.2010.04.027.
[233] N. Malik, R. Wiwattanapatapee, R. Klopsch, K. Lorenz, H. Frey, J.. Weener, E.. Meijer, W. Paulus, R. Duncan, Dendrimers: Relationship between structure and biocompatibility in vitro, and preliminary studies on the biodistribution of 125I-labelled polyamidoamine dendrimers in vivo, J. Control. Release. 65 (2000) 133–148. doi:10.1016/S0168-3659(99)00246-1.
[234] G.A. Brazeau, S. Attia, S. Poxon, J.A. Hughes, In vitro myotoxicity of selected cationic macromolecules used in non-viral gene delivery, Pharm. Res. 15 (1998) 680–4. http://www.ncbi.nlm.nih.gov/pubmed/9619774 (accessed August 21, 2017).
[235] B. Ziemba, A. Janaszewska, K. Ciepluch, M. Krotewicz, W.A. Fogel, D. Appelhans, B. Voit, M. Bryszewska, B. Klajnert, In vivo toxicity of poly(propyleneimine) dendrimers, J. Biomed. Mater. Res. - Part A. 99 A (2011) 261–268. doi:10.1002/jbm.a.33196.
[236] S. Hong, P.R. Leroueil, E.K. Janus, J.L. Peters, M.-M. Kober, M.T. Islam, B.G. Orr, J.R. Baker, M.M. Banaszak Holl, Interaction of Polycationic Polymers with Supported Lipid Bilayers and Cells: Nanoscale Hole Formation and Enhanced Membrane Permeability, Bioconjug. Chem. 17 (2006) 728–734. doi:10.1021/bc060077y.
[237] P.R. Leroueil, S. Hong, A. Mecke, J.R. Baker, B.G. Orr, M.M. Banaszak Holl, M.M.B. Holl, Nanoparticle interaction with biological membranes: does nanotechnology present a Janus face?, Acc. Chem. Res. 40 (2007) 335–42. doi:10.1021/ar600012y.
[238] C.C. Lee, J.A. Mackay, J.M.J. Fréchet, F.C. Szoka, Designing dendrimers for biological applications, Nat. Biotechnol. 23 (2005) 1517–1526. doi:10.1038/nbt1171.
[239] D.P. Walsh, A. Heise, F.J. O'Brien, S.-A. Cryan, An efficient, non-viral dendritic vector for gene delivery in tissue engineering, Gene Ther. (2017). doi:10.1038/gt.2017.58.
[240] P. Symonds, J.C. Murray, A.C. Hunter, G. Debska, A. Szewczyk, S.M. Moghimi, Low and high molecular weight poly(l -lysine)s/poly(l -lysine)-DNA complexes initiate mitochondrial-mediated apoptosis differently, FEBS Lett. 579 (2005) 6191–6198. doi:10.1016/j.febslet.2005.09.092.

[241] Z. Kadlecova, L. Baldi, D. Hacker, F.M. Wurm, H.-A. Klok, Comparative Study on the In Vitro Cytotoxicity of Linear, Dendritic, and Hyperbranched Polylysine Analogues, Biomacromolecules. 13 (2012) 3127–3137. doi:10.1021/bm300930j.
[242] H.O. McCarthy, J. McCaffrey, C.M. McCrudden, A. Zholobenko, A.A. Alia, J.W. McBride, A.S. Massey, S. Pentlavalli, K.-H. Chen, G. Cole, S.P. Loughran, N.J. Dunne, R.F. Donnelly, V.L. Kett, T. Robson, Development and characterization of self-assembling nanoparticles using a bio-inspired amphipathic peptide for gene delivery, J. Control. Release. 189 (2014) 141–149. doi:10.1016/J.JCONREL.2014.06.048.
[243] C. O'Leary, J.L. Gilbert, S. O'Dea, F.J. O'Brien, S.-A. Cryan, Respiratory Tissue Engineering: Current Status and Opportunities for the Future., Tissue Eng. Part B. Rev. (2015). doi:10.1089/ten.TEB.2014.0525.
[244] B. Crestani, S. Marchand-Adam, C. Quesnel, L. Plantier, K. Borensztajn, J. Marchal, A. Mailleux, P. Soler, M. Dehoux, Hepatocyte Growth Factor and Lung Fibrosis, Proc. Am. Thorac. Soc. (2012). http://www.atsjournals.org/doi/abs/10.1513/pats.201202-018AW#.VffoFvlViko (accessed September 15, 2015).
[245] A. Gazdhar, A. Temuri, L. Knudsen, M. Gugger, R.A. Schmid, M. Ochs, T. Geiser, Targeted gene transfer of hepatocyte growth factor to alveolar type II epithelial cells reduces lung fibrosis in rats., Hum. Gene Ther. 24 (2013) 105–16. doi:10.1089/hum.2012.098.
[246] L. Altucci, M.D. Leibowitz, K.M. Ogilvie, A.R. de Lera, H. Gronemeyer, RAR and RXR modulation in cancer and metabolic disease., Nat. Rev. Drug Discov. 6 (2007) 793–810. doi:10.1038/nrd2397.
[247] C.H. Kim, Regulation of FoxP3+ Regulatory T Cells and Th17 Cells by Retinoids, Clin. Dev. Immunol. 2008 (2008) 1–12. doi:10.1155/2008/416910.
[248] R.H. Müller, K. Mäder, S. Gohla, Solid lipid nanoparticles (SLN) for controlled drug delivery - A review of the state of the art, Eur. J. Pharm. Biopharm. 50 (2000) 161–177. doi:10.1016/S0939-6411(00)00087-4.
[249] R.H. Müller, S. Maassen, H. Weyhers, W. Mehnert, Phagocytic uptake and cytotoxicity of solid lipid nanoparticles (SLN) sterically stabilized with poloxamine 908 and poloxamer 407., J. Drug Target. 4 (1996) 161–70. doi:10.3109/10611869609015973.
[250] K. Mäder, W. Mehnert, Solid lipid nanoparticles: production, characterization and applications., Adv. Drug Deliv. Rev. 47 (2001) 165–96. doi:10.1016/S0169-409X(01)00105-3.
[251] S. Das, W.K. Ng, P. Kanaujia, S. Kim, R.B.H. Tan, Formulation design, preparation and physicochemical characterizations of solid lipid nanoparticles containing a hydrophobic drug: Effects of process variables, Colloids Surfaces B Biointerfaces. 88 (2011) 483–489. doi:10.1016/j.colsurfb.2011.07.036.
[252] I.P. Kaur, R. Bhandari, S. Bhandari, V. Kakkar, Potential of solid lipid nanoparticles in brain targeting., J. Control. Release. 127 (2008) 97–109. doi:10.1016/j.jconrel.2007.12.018.
[253] A. Dingler, S. Gohla, Production of solid lipid nanoparticles (SLN): scaling up feasibilities, (2008). http://informahealthcare.com/doi/abs/10.1080/02652040010018056 (accessed July 5, 2015).
[254] K. Westesen, H. Bunjes, M.H.. Koch, Physicochemical characterization of lipid nanoparticles and evaluation of their drug loading capacity and sustained release potential, J. Control. Release. 48 (1997) 223–236. doi:10.1016/S0168-3659(97)00046-1.
[255] R. Cavalli, M.R. Gasco, S. Morel, Behaviour of timolol incorporated in lipospheres in the presence of a series of phosphate esters, STP Pharma Sci. 2 (n.d.) 514–518. http://cat.inist.fr/?aModele=afficheN&cpsidt=4431458 (accessed July 5, 2015).

[256] R. Cavalli, S. Morel, M.R. Gasco, P. Chetoni, m. F. Saettone, Preparation and evaluation in vitro of colloidal lipospheres containing pilocarpine as ion pair, Int. J. Pharm. 117 (1995) 243–246. doi:10.1016/0378-5173(94)00339-7.
[257] R. Cavalli, Solid lipid nanoparticles as carriers of hydrocortisone and progesterone complexes with β-cyclodextrins, Int. J. Pharm. 182 (1999) 59–69. doi:10.1016/S0378-5173(99)00066-6.
[258] R. Cavalli, O. Caputo, M.R. Gasco, Solid lipospheres of doxorubicin and idarubicin, Int. J. Pharm. 89 (1993) R9–R12. doi:10.1016/0378-5173(93)90313-5.
[259] Y.C. Kuo, C.Y. Chung, Solid lipid nanoparticles comprising internal Compritol 888 ATO, tripalmitin and cacao butter for encapsulating and releasing stavudine, delavirdine and saquinavir, Colloids Surfaces B Biointerfaces. 88 (2011) 682–690. doi:10.1016/j.colsurfb.2011.07.060.
[260] S.J. Lim, M.K. Lee, C.K. Kim, Altered chemical and biological activities of all-trans retinoic acid incorporated in solid lipid nanoparticle powders, J. Control. Release. 100 (2004) 53–61. doi:10.1016/j.jconrel.2004.07.032.
[261] S.-J. Lim, C.-K. Kim, Formulation parameters determining the physicochemical characteristics of solid lipid nanoparticles loaded with all-trans retinoic acid., Int. J. Pharm. 243 (2002) 135–146. doi:10.1016/S0378-5173(02)00269-7.
[262] L.G. Souza, E.J. Silva, a. L.L. Martins, M.F. Mota, R.C. Braga, E.M. Lima, M.C. Valadares, S.F. Taveira, R.N. Marreto, Development of topotecan loaded lipid nanoparticles for chemical stabilization and prolonged release, Eur. J. Pharm. Biopharm. 79 (2011) 189–196. doi:10.1016/j.ejpb.2011.02.012.
[263] L. Hu, X. Tang, F. Cui, Solid lipid nanoparticles (SLNs) to improve oral bioavailability of poorly soluble drugs., J. Pharm. Pharmacol. 56 (2004) 1527–1535. doi:10.1211/0022357044959.
[264] V. Jenning, M. Schäfer-Korting, S. Gohla, Vitamin A-loaded solid lipid nanoparticles for topical use: Drug release properties, J. Control. Release. 66 (2000) 115–126. doi:10.1016/S0168-3659(99)00223-0.
[265] V. Jenning, A. Gysler, M. Schäfer-Korting, S.H. Gohla, Vitamin A loaded solid lipid nanoparticles for topical use: Occlusive properties and drug targeting to the upper skin, Eur. J. Pharm. Biopharm. 49 (2000) 211–218. doi:10.1016/S0939-6411(99)00075-2.
[266] S. Weber, a. Zimmer, J. Pardeike, Solid Lipid Nanoparticles (SLN) and Nanostructured Lipid Carriers (NLC) for pulmonary application: A review of the state of the art, Eur. J. Pharm. Biopharm. 86 (2014) 7–22. doi:10.1016/j.ejpb.2013.08.013.
[267] J.P. Jee, S.J. Lim, J.S. Park, C.K. Kim, Stabilization of all-trans retinol by loading lipophilic antioxidants in solid lipid nanoparticles, Eur. J. Pharm. Biopharm. 63 (2006) 134–139. doi:10.1016/j.ejpb.2005.12.007.
[268] R. Gatti, M.G. Gioia, V. Cavrini, Analysis and stability study of retinoids in pharmaceuticals by LC with fluorescence detection, J. Pharm. Biomed. Anal. 23 (2000) 147–159. doi:10.1016/S0731-7085(00)00285-5.
[269] M.H. Akanda, R. Rai, I.J. Slipper, B.Z. Chowdhry, D. Lamprou, G. Getti, D. Douroumis, Delivery of retinoic acid to LNCap human prostate cancer cells using solid lipid nanoparticles, Int. J. Pharm. 493 (2015) 161–171. doi:10.1016/j.ijpharm.2015.07.042.
[270] A.D. Brooks, W. Tong, F. Benedetti, Y. Kaneda, V. Miller, R.P. Warrell, Inhaled aerosolization of all-trans-retinoic acid for targeted pulmonary delivery., Cancer Chemother. Pharmacol. 46 (2000) 313–8. http://www.ncbi.nlm.nih.gov/pubmed/11052629 (accessed June 12, 2017).
[271] Y. Cirpanli, N. Unlü, S. Caliş, a A. Hincal, Formulation and in-vitro characterization of

retinoic acid loaded poly (lactic-co-glycolic acid) microspheres., J. Microencapsul. 22 (2005) 877–889. doi:10.1080/02652040500273878.
[272] E. Almouazen, S. Bourgeois, A. Boussaïd, P. Valot, C. Malleval, H. Fessi, S. Nataf, S. Briançon, Development of a nanoparticle-based system for the delivery of retinoic acid into macrophages, Int. J. Pharm. 430 (2012) 207–215. doi:10.1016/j.ijpharm.2012.03.025.
[273] R.J. Swain, S.J. Kemp, P. Goldstraw, T.D. Tetley, M.M. Stevens, Assessment of cell line models of primary human cells by Raman spectral phenotyping, Biophys. J. 98 (2010) 1703–11. doi:10.1016/j.bpj.2009.12.4289.
[274] L.L. Nardone, S.B. Andrews, Cell line A549 as a model of the type II pneumocyte, Biochim. Biophys. Acta - Lipids Lipid Metab. 573 (1979) 276–295. doi:10.1016/0005-2760(79)90061-4.
[275] a zur Mühlen, C. Schwarz, W. Mehnert, Solid lipid nanoparticles (SLN) for controlled drug delivery--drug release and release mechanism., Eur. J. Pharm. Biopharm. 45 (1998) 149–155. doi:10.1016/S0939-6411(97)00150-1.
[276] C. Freitas, R.H. Müller, Correlation between long-term stability of solid lipid nanoparticles (SLN) and crystallinity of the lipid phase., Eur. J. Pharm. Biopharm. 47 (1999) 125–132. doi:10.1016/S0939-6411(98)00074-5.
[277] C. Freitas, R.H. Müller, Effect of light and temperature on zeta potential and physical stability in solid lipid nanoparticle (SLN®) dispersions, Int. J. Pharm. 168 (1998) 221–229. doi:10.1016/S0378-5173(98)00092-1.
[278] C. Freitas, R.H. Mu, Stability determination of solid lipid nanoparticles (SLN) in aqueous dispersion after addition of electrolyte, J. Microencapsul. 16 (1999) 59–71.
[279] M.H. Aburahma, S.M. Badr-Eldin, Compritol 888 ATO: a multifunctional lipid excipient in drug delivery systems and nanopharmaceuticals, Expert Opin. Drug Deliv. 11 (2014) 1865–1883. doi:10.1517/17425247.2014.935335.
[280] M.J. Lawrence, G.D. Rees, Microemulsion-based media as novel drug delivery systems, Adv. Drug Deliv. Rev. 64 (2012) 175–193. doi:10.1016/j.addr.2012.09.018.
[281] C. Freitas, R.H. Müller, Spray-drying of solid lipid nanoparticles (SLN(TM)), Eur. J. Pharm. Biopharm. 46 (1998) 145–151. doi:10.1016/S0939-6411(97)00172-0.
[282] C. Schwarz, W. Mehnert, Freeze-drying of drug-free and drug-loaded solid lipid nanoparticles (SLN), 157 (1997) 171–179.
[283] G. Storm, S.O. Belliot, T. Daemen, D.D. Lasic, Surface modification of nanoparticles to oppose uptake by the mononuclear phagocyte system, Adv. Drug Deliv. Rev. 17 (1995) 31–48. doi:10.1016/0169-409X(95)00039-A.
[284] C. Lourenco, Steric stabilization of nanoparticles: Size and surface properties, Int. J. Pharm. 138 (1996) 1–12. doi:10.1016/0378-5173(96)04486-9.
[285] H.D.C. Smyth, A.J. Hickey, Controlled Pulmonary Drug Delivery, 2011. doi:10.1007/978-1-4419-9745-6.
[286] R. Thatipamula, C. Palem, R. Gannu, S. Mudragada, M. Yamsani, Formulation and in vitro characterization of domperidone loaded solid lipid nanoparticles and nanostructured lipid carriers., Daru. 19 (2011) 23–32. http://www.ncbi.nlm.nih.gov/pubmed/22615636 (accessed May 16, 2017).
[287] P. Gehr, C. Mühlfeld, B. Rothen-Rutishauser, F. Blank, Particle-Lung Interactions, Second Edition, CRC Press, 2009. https://books.google.com/books?id=YozLBQAAQBAJ&pgis=1 (accessed July 23, 2015).
[288] E. Fröhlich, The role of surface charge in cellular uptake and cytotoxicity of medical nanoparticles., Int. J. Nanomedicine. 7 (2012) 5577–91. doi:10.2147/IJN.S36111.

[289] M. Larsson, A. Hill, J. Duffy, Suspension Stability: Why Particle Size, Zeta Potential and rheology are Important, Annu. Trans. Nord. Rheol. Soc. 20 (2012) 209–214. http://rheology-esr.net/member/Transactions/2012/26 Larsson Suspension Stability Why Particle Size Zeta Potential and Rheology are Important.pdf (accessed July 23, 2015).
[290] H. Singh, S. Jindal, M. Singh, G. Sharma, I.P. Kaur, Nano-formulation of rifampicin with enhanced bioavailability: Development, characterization and in-vivo safety, Int. J. Pharm. 485 (2015) 138–151. doi:10.1016/j.ijpharm.2015.02.050.
[291] K.A. Shah, A.A. Date, M.D. Joshi, V.B. Patravale, Solid lipid nanoparticles (SLN) of tretinoin: Potential in topical delivery, Int. J. Pharm. 345 (2007) 163–171. doi:10.1016/j.ijpharm.2007.05.061.
[292] C.-M. Lee, H.-J. Jeong, J.-W. Park, J. Kim, K.-Y. Lee, Temperature-induced release of all-trans-retinoic acid loaded in solid lipid nanoparticles for topical delivery, Macromol. Res. 16 (2008) 682–685. doi:10.1007/BF03218581.
[293] S. Cai, Q. Yang, T.R. Bagby, Lymphatic drug delivery using engineered liposomes and solid lipid nanoparticles, Adv. Drug Deliv. Rev. 63 (2011) 901–908. doi:10.1016/j.addr.2011.05.017.
[294] R.H. Müller, M. Radtke, S.A. Wissing, Solid lipid nanoparticles (SLN) and nanostructured lipid carriers (NLC) in cosmetic and dermatological preparations, Adv. Drug Deliv. Rev. 54 (2002) S131–S155. doi:10.1016/S0169-409X(02)00118-7.
[295] K. Vivek, H. Reddy, R.S.R. Murthy, Investigations of the effect of the lipid matrix on drug entrapment, in vitro release, and physical stability of olanzapine-loaded solid lipid nanoparticles, AAPS PharmSciTech. 8 (2007) 16–24. doi:10.1208/pt0804083.
[296] A.C. Silva, A. Kumar, W. Wild, D. Ferreira, D. Santos, B. Forbes, Long-term stability, biocompatibility and oral delivery potential of risperidone-loaded solid lipid nanoparticles, Int. J. Pharm. 436 (2012) 798–805. doi:10.1016/j.ijpharm.2012.07.058.
[297] A. Gokhale, Achieving Zero-Order Release Kinetics Using Multi-Step Diffusion-Based Drug Delivery, (n.d.). http://www.pharmtech.com/achieving-zero-order-release-kinetics-using-multi-step-diffusion-based-drug-delivery?pageID=3 (accessed May 17, 2017).
[298] G. Singhvi, M. Singh, Review: In Vitro Drug Release Characterization Models, Int. J. Pharm. Stud. Res. 2 (2011) 77–84. http://www.technicaljournalsonline.com/ijpsr/VOL II/IJPSR VOL II ISSUE I JANUARY MARCH 2011/IJPSR VOL II ISSUE I Article 13.pdf (accessed May 17, 2017).
[299] C. O'Leary, F.J. O'Brien, S.-A. Cryan, Retinoic Acid-Loaded Collagen-Hyaluronate Scaffolds: A Bioactive Material for Respiratory Tissue Regeneration, ACS Biomater. Sci. Eng. (2017) acsbiomaterials.6b00561. doi:10.1021/acsbiomaterials.6b00561.
[300] J.P. Van Wauwe, M.C. Coene, J. Goossens, W. Cools, J. Monbaliu, Effects of cytochrome P-450 inhibitors on the in vivo metabolism of all-trans-retinoic acid in rats., J. Pharmacol. Exp. Ther. 252 (1990) 365–9. http://www.ncbi.nlm.nih.gov/pubmed/2299598 (accessed May 17, 2017).
[301] V. Filipe, A. Hawe, W. Jiskoot, Critical evaluation of nanoparticle tracking analysis (NTA) by NanoSight for the measurement of nanoparticles and protein aggregates, Pharm. Res. 27 (2010) 796–810. doi:10.1007/s11095-010-0073-2.
[302] W. Anderson, D. Kozak, V.A. Coleman, Å.K. Jämting, M. Trau, A comparative study of submicron particle sizing platforms: Accuracy, precision and resolution analysis of polydisperse particle size distributions, J. Colloid Interface Sci. 405 (2013) 322–330. doi:10.1016/j.jcis.2013.02.030.

[303] M. Gaumet, A. Vargas, R. Gurny, F. Delie, Nanoparticles for drug delivery: The need for precision in reporting particle size parameters, Eur. J. Pharm. Biopharm. 69 (2008) 1–9. doi:10.1016/j.ejpb.2007.08.001.
[304] R.H. Müller, D. Rühl, S. Runge, K. Schulze-Forster, W. Mehnert, Cytotoxicity of solid lipid nanoparticles as a function of the lipid matrix and the surfactant, Pharm. Res. 14 (1997) 458–62. http://www.ncbi.nlm.nih.gov/pubmed/9144731 (accessed July 5, 2017).
[305] M. Nassimi, C. Schleh, H.-D. Lauenstein, R. Hussein, K. L?bbers, G. Pohlmann, S. Switalla, K. Sewald, M. M?ller, N. Krug, C.C. M?ller-Goymann, A. Braun, Low cytotoxicity of solid lipid nanoparticles in *in vitro* and *ex vivo* lung models, Inhal. Toxicol. 21 (2009) 104–109. doi:10.1080/08958370903005769.
[306] D.M. Ridolfi, P.D. Marcato, D. Machado, R.A. Silva, G.Z. Justo, N. Durán, In vitro cytotoxicity assays of solid lipid nanoparticles in epithelial and dermal cells, J. Phys. Conf. Ser. 304 (2011) 12032. doi:10.1088/1742-6596/304/1/012032.
[307] C. Dinarello, Biologic basis for interleukin-1 in disease, Blood. 87 (1996). http://www.bloodjournal.org/content/87/6/2095.long?sso-checked=true (accessed July 26, 2017).
[308] K.F. Chung, Cytokines in chronic obstructive pulmonary disease, Eur. Respir. J. Suppl. 34 (2001) 50s–59s. http://www.ncbi.nlm.nih.gov/pubmed/12392035 (accessed July 28, 2017).
[309] A. Ekberg-Jansson, B. Andersson, B. Bake, M. Boijsen, I. Enanden, A. Rosengren, B.E. Skoogh, U. Tylén, P. Venge, C.G. Lofdahl, Neutrophil-associated activation markers in healthy smokers relates to a fall in DLCO and to emphysematous changes on high resolution CT, Respir. Med. 95 (2001) 363–373. doi:10.1053/rmed.2001.1050.
[310] U. Lappalainen, J.A. Whitsett, S.E. Wert, J.W. Tichelaar, K. Bry, Interleukin-1β Causes Pulmonary Inflammation, Emphysema, and Airway Remodeling in the Adult Murine Lung, Am. J. Respir. Cell Mol. Biol. 32 (2005) 311–318. doi:10.1165/rcmb.2004-0309OC.
[311] J.C. Kips, J. Tavernier, R.A. Pauwels, Tumor Necrosis Factor Causes Bronchial Hyperresponsiveness in Rats, Am. Rev. Respir. Dis. 145 (1992) 332–336. doi:10.1164/ajrccm/145.2_Pt_1.332.
[312] V.M. Keatings, P.D. Collins, D.M. Scott, P.J. Barnes, Differences in interleukin-8 and tumor necrosis factor-alpha in induced sputum from patients with chronic obstructive pulmonary disease or asthma, Am. J. Respir. Crit. Care Med. 153 (1996) 530–534. doi:10.1164/ajrccm.153.2.8564092.
[313] S.E. Tanni, N.R. Pelegrino, A.Y. Angeleli, C. Correa, I. Godoy, Smoking status and tumor necrosis factor-alpha mediated systemic inflammation in COPD patients, J. Inflamm. (Lond). 7 (2010) 29. doi:10.1186/1476-9255-7-29.
[314] S. Akira, T. Hirano, T. Taga, T. Kishimoto, Biology of multifunctional cytokines: IL 6 and related molecules (IL 1 and TNF), FASEB J. 4 (1990) 2860–7. http://www.ncbi.nlm.nih.gov/pubmed/2199284 (accessed July 28, 2017).
[315] G.J. Hageman, I. Larik, H.-J. Pennings, G.R.M.M. Haenen, E.F.M. Wouters, B. Aalt, Systemic poly(ADP-ribose) polymerase-1 activation, chronic inflammation, and oxidative stress in COPD patients, Free Radic. Biol. Med. 35 (2003) 140–148. doi:10.1016/S0891-5849(03)00237-5.
[316] A.A. Eid, A.A. Ionescu, L.S. Nixon, V. Lewis-Jenkins, S.B. Matthews, T.L. Griffiths, D.J. Shale, Inflammatory Response and Body Composition in Chronic Obstructive Pulmonary Disease, Am. J. Respir. Crit. Care Med. 164 (2001) 1414–1418. doi:10.1164/ajrccm.164.8.2008109.
[317] J.A. Wedzicha, T.A.R. Seemungal, P.K. MacCallum, E.A. Paul, G.C. Donaldson, A.

Bhowmik, D.J. Jeffries, T.W. Meade, Acute Exacerbations of Chronic Obstructive Pulmonary Disease Are Accompanied by Elevations of Plasma Fibrinogen and Serum IL-6 Levels, Thromb. Haemost. 84 (2000) 210–215. https://th.schattauer.de/en/contents/archive/issue/888/manuscript/2494.html (accessed July 28, 2017).

[318] A. Bhowmik, T.A. Seemungal, R.J. Sapsford, J.A. Wedzicha, Relation of sputum inflammatory markers to symptoms and lung function changes in COPD exacerbations, Thorax. 55 (2000) 114–20. http://www.ncbi.nlm.nih.gov/pubmed/10639527 (accessed July 28, 2017).

[319] W.B. Smith, J.R. Gamble, I. Clark-Lewis, M.A. Vadas, Interleukin-8 induces neutrophil transendothelial migration, Immunology. 72 (1991) 65–72. http://www.ncbi.nlm.nih.gov/pubmed/1997402 (accessed July 28, 2017).

[320] A. Pesci, B. Balbi, M. Majori, G. Cacciani, S. Bertacco, P. Alciato, C. Donner, Inflammatory cells and mediators in bronchial lavage of patients with chronic obstructive pulmonary disease, Eur. Respir. J. 12 (1998). http://erj.ersjournals.com/content/12/2/380.long (accessed July 28, 2017).

[321] G. Kaur, J.M. Dufour, Cell lines: Valuable tools or useless artifacts, Spermatogenesis. 2 (2012) 1–5. doi:10.4161/spmg.19885.

[322] B. Rothen-Rutishauser, F. Blank, C. Mühlfeld, P. Gehr, *In vitro* models of the human epithelial airway barrier to study the toxic potential of particulate matter, Expert Opin. Drug Metab. Toxicol. 4 (2008) 1075–1089. doi:10.1517/17425255.4.8.1075.

[323] D.J. Giard, S.A. Aaronson, G.J. Todaro, P. Arnstein, J.H. Kersey, H. Dosik, W.P. Parks, In Vitro Cultivation of Human Tumors: Establishment of Cell Lines Derived From a Series of Solid Tumors, JNCI J. Natl. Cancer Inst. 51 (1973) 1417–1423. doi:10.1093/jnci/51.5.1417.

[324] M. Lieber, G. Todaro, B. Smith, A. Szakal, W. Nelson-Rees, A continuous tumor-cell line from a human lung carcinoma with properties of type II alveolar epithelial cells, Int. J. Cancer. 17 (1976) 62–70. doi:10.1002/ijc.2910170110.

[325] S. Kobayashi, S. Kondo, K. Juni, Permeability of Peptides and Proteins in Human Cultured Alveolar A549 Cell Monolayer, Pharm. Res. 12 (1995) 1115–1119. doi:10.1023/A:1016295406473.

[326] Z. Wang, Q. Zhang, Transport of proteins and peptides across human cultured alveolar A549 cell monolayer, Int. J. Pharm. 269 (2004) 451–6. http://www.ncbi.nlm.nih.gov/pubmed/14706256 (accessed July 25, 2017).

[327] K.A. Foster, C.G. Oster, M.M. Mayer, M.L. Avery, K.L. Audus, Characterization of the A549 Cell Line as a Type II Pulmonary Epithelial Cell Model for Drug Metabolism, Exp. Cell Res. 243 (1998) 359–366. doi:10.1006/excr.1998.4172.

[328] T.J. Standiford, S.L. Kunkel, M.A. Basha, S.W. Chensue, J.P. Lynch, G.B. Toews, J. Westwick, R.M. Strieter, Interleukin-8 gene expression by a pulmonary epithelial cell line. A model for cytokine networks in the lung, J. Clin. Invest. 86 (1990) 1945–1953. doi:10.1172/JCI114928.

[329] B. Crestani, P. Cornillet, M. Dehoux, C. Rolland, M. Guenounou, M. Aubier, Alveolar type II epithelial cells produce interleukin-6 in vitro and in vivo. Regulation by alveolar macrophage secretory products, J. Clin. Invest. 94 (1994) 731–740. doi:10.1172/JCI117392.

[330] P. Mao, S. Wu, J. Li, W. Fu, W. He, X. Liu, A.S. Slutsky, H. Zhang, Y. Li, Human alveolar epithelial type II cells in primary culture, Physiol. Rep. 3 (2015). doi:10.14814/phy2.12288.

[331] S.L. Kunkel, T. Standiford, K. Kasahara, R.M. Strieter, Interleukin-8 (IL-8): The Major Neutrophil Chemotactic Factor in the Lung, Exp. Lung Res. 17 (1991) 17–23. doi:10.3109/01902149109063278.
[332] M.T. O'Gorman, N.A. Jatoi, S.J. Lane, B.P. Mahon, IL-1b and TNF-a induce increased expression of CCL28 by airway epithelial cells via an NFkB-dependent pathway, Cell. Immunol. 238 (2005) 87–96. doi:10.1016/j.cellimm.2006.02.003.
[333] H. Tominaga, M. Ishiyama, F. Ohseto, K. Sasamoto, T. Hamamoto, K. Suzuki, M. Watanabe, A water-soluble tetrazolium salt useful for colorimetric cell viability assay, Anal. Commun. 36 (1999) 47–50. doi:10.1039/a809656b.
[334] M. Kwolek-Mirek, R. Zadrag-Tecza, Comparison of methods used for assessing the viability and vitality of yeast cells, FEMS Yeast Res. 14 (2014). doi:10.1111/1567-1364.12202.
[335] S. Mitragotri, P.A. Burke, R. Langer, Overcoming the challenges in administering biopharmaceuticals: formulation and delivery strategies, Nat. Rev. Drug Discov. 13 (2014) 655–72. doi:10.1038/nrd4363.
[336] T.J. Standiford, S.L. Kunkel, S.H. Phan, B.J. Rollins, R.M. Strieter, Alveolar macrophage-derived cytokines induce monocyte chemoattractant protein-1 expression from human pulmonary type II-like epithelial cells, J. Biol. Chem. 266 (1991) 9912–8. http://www.ncbi.nlm.nih.gov/pubmed/2033076 (accessed July 26, 2017).
[337] S. Koyama, E. Sato, H. Nomura, K. Kubo, M. Miura, T. Yamashita, S. Nagai, T. Izumi, Monocyte chemotactic factors released from type II pneumocyte-like cells in response to TNF-alpha and IL-1alpha, Eur. Respir. J. 13 (1999). http://erj.ersjournals.com/content/13/4/820 (accessed July 26, 2017).
[338] J. Tschopp, K. Burns, J. Clatworthy, L. Martin, F. Martinon, C. Plumpton, B. Maschera, A. Lewis, K. Ray, F. Volpe, TOLLIP, a new component of the IL-1RI pathway, links IRAK to the IL-1 receptor, Nat. Cell Biol. 2 (2000) 346–351. doi:10.1038/35014038.
[339] E.L. Cooke, I.J. Uings, C.L. Xia, P. Woo, K.P. Ray, Functional analysis of the interleukin-1-receptor-associated kinase (IRAK-1) in interleukin-1 beta-stimulated nuclear factor kappa B (NF-kappa B) pathway activation: IRAK-1 associates with the NF-kappa B essential modulator (NEMO) upon receptor stimulatio, Biochem. J. 359 (2001) 403–10. http://www.ncbi.nlm.nih.gov/pubmed/11583588 (accessed August 8, 2017).
[340] G. Chen, D. V Goeddel, TNF-R1 Signaling: A Beautiful Pathway, Science (80-.). 296 (2002) 1634–1635. doi:10.1126/science.1071924.
[341] L.A.J. O'Neill, Signal transduction pathways activated by the IL-1 receptor/toll-like receptor superfamily, Curr. Top. Microbiol. Immunol. 270 (2002) 47–61. http://www.ncbi.nlm.nih.gov/pubmed/12467243 (accessed August 8, 2017).
[342] G. Bonizzi, M. Karin, The two NF-κB activation pathways and their role in innate and adaptive immunity, Trends Immunol. 25 (2004) 280–288. doi:10.1016/j.it.2004.03.008.
[343] T. Lawrence, The Nuclear Factor NFkB Pathway in Inflammation, Cold Spring Harb. Perspect. Biol. 1 (2009) 1–10.
[344] M. Nakajoh, T. Fukushima, T. Suzuki, M. Yamaya, K. Nakayama, K. Sekizawa, H. Sasaki, Retinoic Acid Inhibits Elastase-Induced Injury in Human Lung Epithelial Cell Lines, Am. J. Respir. Cell Mol. Biol. 28 (2003) 296–304. doi:10.1165/rcmb.4845.
[345] M. Kirchmeyer, M. Koufany, S. Sebillaud, P. Netter, J.-Y. Jouzeau, A. Bianchi, All-trans retinoic acid suppresses interleukin-6 expression in interleukin-1-stimulated synovial fibroblasts by inhibition of ERK1/2 pathway independently of RAR activation, Arthritis Res. Ther. 10 (2008). doi:10.1186/ar2569.
[346] J. Du, P. Du, H. Smyth, Hydrogels for controlled pulmonary delivery, Ther. Deliv. (2013)

1293–1305. doi:10.4155/tde.13.90.
[347] A. Hibbitts, N. Lieggi, O. McCabe, W. Thomas, J. Barlow, F. O'Brien, S.-A. Cryan, Screening of siRNA nanoparticles for delivery to airway epithelial cells using high-content analysis, Ther. Deliv. 2 (2011) 987–99. http://www.ncbi.nlm.nih.gov/pubmed/22826866 (accessed September 14, 2017).
[348] A. Dey, E.T. Wong, C.F. Cheok, V. Tergaonkar, D.P. Lane, R-Roscovitine simultaneously targets both the p53 and NF-κB pathways and causes potentiation of apoptosis: implications in cancer therapy, Cell Death Differ. 15 (2008) 263–273. doi:10.1038/sj.cdd.4402257.
[349] W. Broekman, G.D. Amatngalim, Y. de Mooij-Eijk, J. Oostendorp, H. Roelofs, C. Taube, J. Stolk, P.S. Hiemstra, TNF-α and IL-1β-activated human mesenchymal stromal cells increase airway epithelial wound healing in vitro via activation of the epidermal growth factor receptor, Respir. Res. 17 (2016) 3. doi:10.1186/s12931-015-0316-1.
[350] S.C. Heo, E.S. Jeon, I.H. Lee, H.S. Kim, M.B. Kim, J.H. Kim, Tumor Necrosis Factor-α-Activated Human Adipose Tissue–Derived Mesenchymal Stem Cells Accelerate Cutaneous Wound Healing through Paracrine Mechanisms, J. Invest. Dermatol. 131 (2011) 1559–1567. doi:10.1038/jid.2011.64.
[351] M.E. Bernardo, W.E. Fibbe, Mesenchymal Stromal Cells: Sensors and Switchers of Inflammation, Cell Stem Cell. 13 (2013) 392–402. doi:10.1016/j.stem.2013.09.006.
[352] Y. Wang, X. Chen, W. Cao, Y. Shi, Plasticity of mesenchymal stem cells in immunomodulation: pathological and therapeutic implications, Nat. Immunol. 15 (2014) 1009–1016. doi:10.1038/ni.3002.
[353] C. Ehrhardt, K.-J. Kim, C.-M. Lehr, Isolation and Culture of Human Alveolar Epithelial Cells, in: Hum. Cell Cult. Protoc., Humana Press, New Jersey, 2005: pp. 207–216. doi:10.1385/1-59259-861-7:207.
[354] J. Lenssen, J. Stolk, Pulmonary stem cells and the induction of tissue regeneration in the treatment of emphysema, Int. J. Chron. Obstruct. Pulmon. Dis. 2 (2007) 131–9. http://www.ncbi.nlm.nih.gov/pubmed/18044685 (accessed September 11, 2017).
[355] D.A. Groneberg, K.F. Chung, Models of chronic obstructive pulmonary disease, Respir. Res. 5 (2004) 18. doi:10.1186/1465-9921-5-18.
[356] M.A. Birrell, S. Wong, A. Dekkak, J. De Alba, S. Haj-Yahia, M.G. Belvisi, Role of Matrix Metalloproteinases in the Inflammatory Response in Human Airway Cell-Based Assays and in Rodent Models of Airway Disease, J. Pharmacol. Exp. Ther. 318 (2006) 741–750. doi:10.1124/jpet.106.105544.
[357] K.M. Lee, R.A. Renne, S.J. Harbo, M.L. Clark, R.E. Johnson, K.M. Gideon, 3-Week Inhalation Exposure to Cigarette Smoke and/or Lipopolysaccharide in AKR/J Mice, Inhal. Toxicol. 19 (2007) 23–35. doi:10.1080/08958370600985784.